UNIVERSITY OF READING

Department of Meteorology

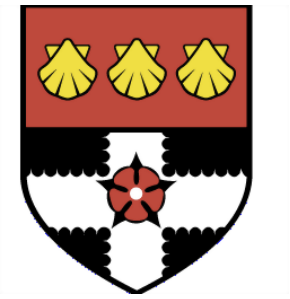

Climate model systematic biases in the Maritime Continent: mean state, interannual variability and teleconnections

Ying Ying Toh

A thesis submitted for the degree of Doctor of Philosophy

April 2018

Declaration

I confirm that this is my own work and the use of all material from other sources has been properly and fully acknowledged.

Ying Ying Toh

Abstract

Societies in the Maritime Continent depend on monsoon rainfall for their water supply. Large spatio-temporal variability of the rains has a significant socio-economic impact and affects the global circulation. However, the Maritime Continent remains a major modelling challenge.

In this thesis, the fidelity of the fifth Coupled Model Intercomparison Project (CMIP5) models at simulating mean climate and its variability over the Maritime Continent is assessed. We find that model horizontal resolution is not a good indicator of performance in atmosphere-only models. Instead, a given model's local Maritime Continent biases are somewhat related to biases in the local Hadley circulation and global monsoon. Cluster analysis on Maritime Continent annual cycle precipitation results in two distinct clusters: Cluster I models are able to capture both the winter monsoon and summer monsoon shift, whereas Cluster II models simulate weaker seasonal migration than observed.

A model's Maritime Continent climatological mean-state precipitation is shown to be negatively correlated with sea-surface temperature (SST) biases in central tropical Pacific Ocean (CTPO) and western tropical Indian Ocean (WTIO) regions in coupled CMIP5 models. On interannual timescales, the El Niño-Southern Oscillation (ENSO) and Indian Ocean Dipole (IOD) teleconnections to Maritime Continent precipitation are well simulated by both uncoupled and coupled CMIP5 models. However, the spatial pattern of these teleconnections is not well captured, especially in coupled models.

Idealized Maritime Continent SST-perturbation experiments are performed using the HadGEM3-GA6 atmospheric model in the CPTO and WTIO regions. These result in remote responses of Maritime Continent mean precipitation, somewhat comparable with the signals related to biases found in the CMIP5 coupled models. This suggests that remote Indo-Pacific SST biases in the CMIP5 coupled models could plausibly cause the precipitation biases over the Maritime Continent, and thus highlights the importance of reducing these biases to improve Maritime Continent mean state and climate variability.

Acknowledgements

I would like to express my gratitude to my supervisors, Andy Turner and Chris Holloway for their guidance and constant support throughout my PhD study, as well as to Stephanie Johnson who had transitioned into a mentorship role.

I am grateful to my Monitoring Committee, Pete Inness and Steve Woolnough for assessing my work and academic progress. To members of the Tropical Weather Group, thank you for the discussions and feedback on my research.

I am thankful to the Malaysian Government for funding my PhD studies at the University of Reading under the Malaysian Public Service Department Training (HLP) scholarship and Malaysian Meteorological Department (MET Malaysia) for endorsing my application for scholarship and study leave.

I greatly appreciate the assistance that I received from Andy Heaps for help in using Python cf-plot to produce publication-quality figures, Mike Wong for helping to set up my first MetUM run, and Archer and NCAS helpdesk for computing support related to MetUM.

I would like to thank my family and friends for their encouragement, in particular, my parents for supporting my decision to further study abroad in UK and my PhD office mates, who had provided a pleasant working environment in Harry Pitt 179.

Lastly, additional thanks go to my friends: Jemima, Tom, Noel and Michael who had helped to proofread my thesis.

Contents

List of Figures

List of Tables

Chapter 1

Introduction

1.1 Motivation

The Maritime Continent is the largest archipelago on Earth, consisting of thousands of large and small islands. Literature commonly refers the Maritime Continent to the groups of islands of Indonesia, Borneo, New Guinea and the surrounding seas. In this thesis, our study area covers the Maritime Continent domain from 20°S to 20°N and 80°E to 160°E as shown in Figure 1.1. This includes the islands of Indonesia, Malaysia, Brunei, Singapore, Philippines, Papua New Guinea and the Solomon islands as well as northern Australia and parts of mainland Southeast Asia including Thailand, Laos, Cambodia, Vietnam and Myanmar.

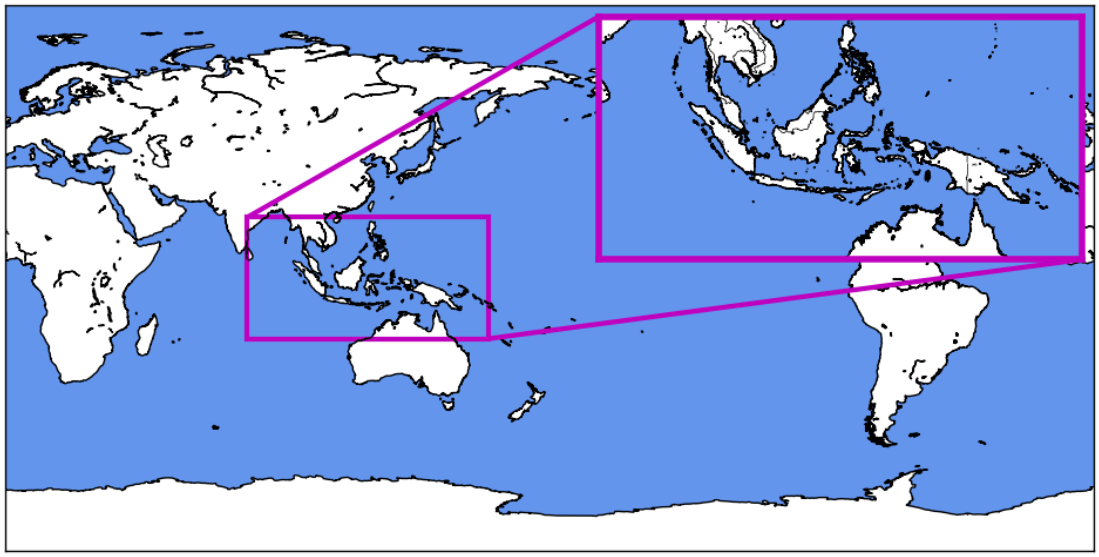

Figure 1.1: Location and spatial cover of the Maritime Continent domain in this study.

More than 600 million people live in this region, for which rainfall serves as the primary water source for agriculture, drinking, and sanitation. The agricultural sector, which relies heavily on rainfall, is one of the key sectors for countries in this region. Variations in rainfall

not only have significant implications for agriculture but also on the overall economies of these countries. The drought events, for example in 1997/98 and 2015/16 in Indonesia, have resulted in huge losses in the agricultural sector and to the overall economy. Forest fires induced by dry weather and biomass burning to clear the land for agricultural purposes lead to haze events during the drought events. Such haze pollution has detrimental effects on human health. Figure 1.2 shows hot spots (land fires) in Sumatra and widespread smoke haze on 31 August 2015 from the NOAA-18 satellite. The World Bank estimated that 2.6 million hectares areas are burned in 2015 and resulted in total damages and losses of IDR 221 trillion (USD 16.1 billion), which is equivalent to 1.9 percent of Indonesia's 2015 gross domestic product (GDP) (Glauber et al., 2016).

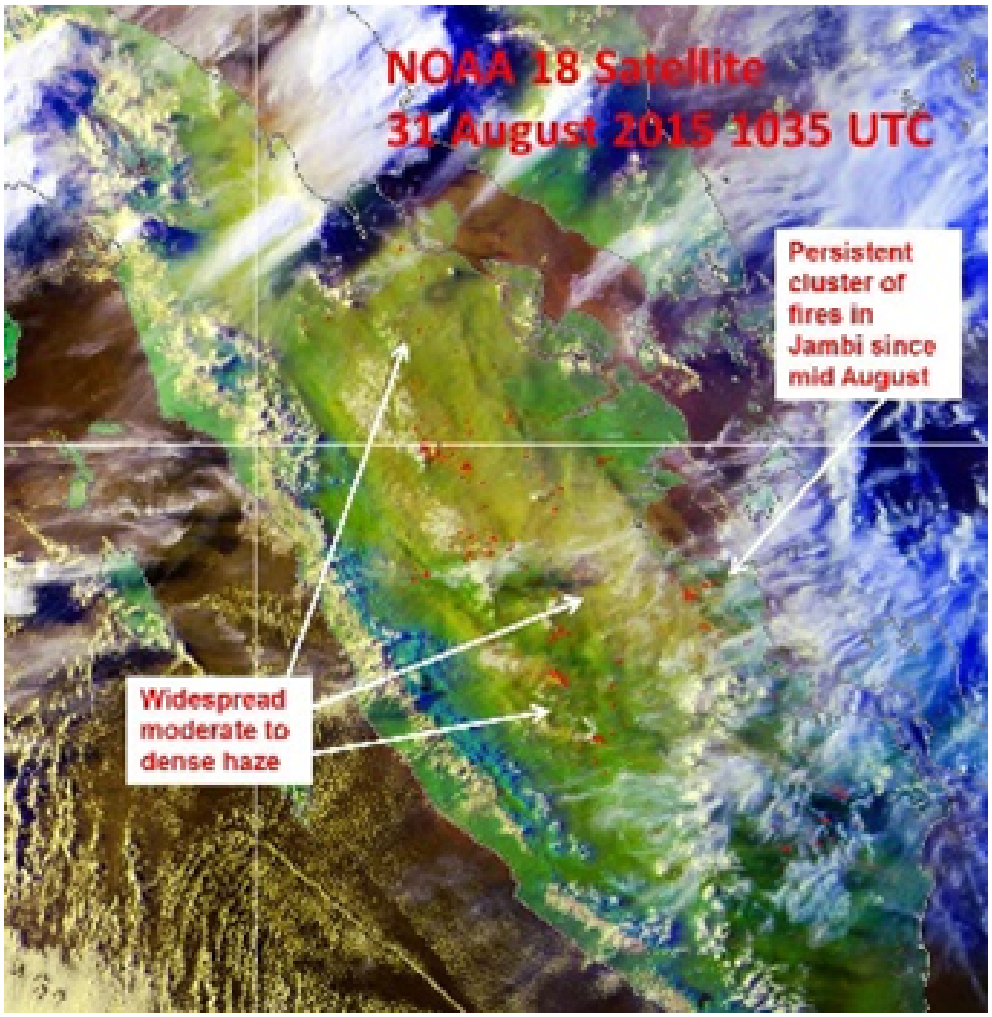

Figure 1.2: Satellite imagery from NOAA-18 showing the hot spots (land fires) in Sumatra and smoke haze on 31 August 2015, taken from `http://asmc.asean.org/home/`

On the other hand, severe flooding events cause frequent loss of human life, damage infrastructure and cause displacement of people. For example, one of the most severe floods occurred in Thailand during 2011 (Fig. 1.3), inundating more than 29,000 km^2 of land area

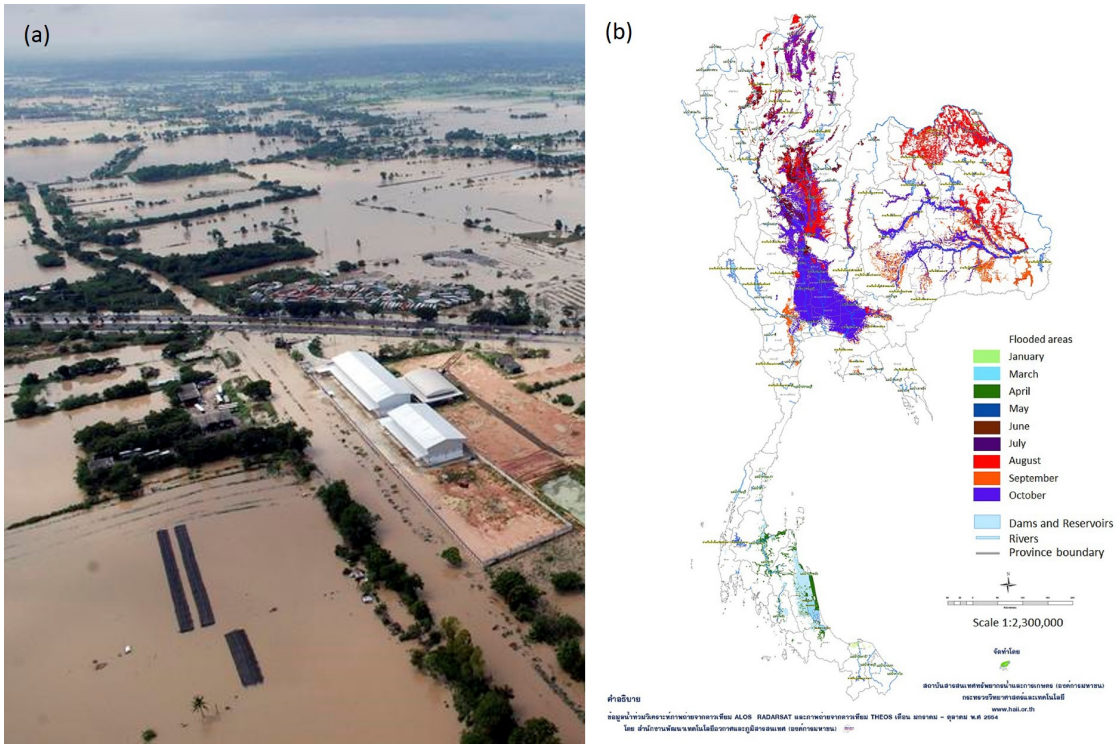

Figure 1.3: (a) An aerial view of the flooded area in Nakhon Ratchasima province, Thailand on October 2011, taken from `http://www.chiangraitimes.com` (b) Diagram of 2011 flooded areas in Thailand, taken from `http://www.thaiwater.net/web/index.php`

and affecting 13.4 million people, while 657 people were killed (HAII, 2011). The World Bank estimated total damages and losses of THB 1.43 trillion (USD 46.5 billion).

However, General Circulation Models (GCMs) struggle to correctly simulate the mean climate and its variability over the Maritime Continent. Better understanding of the climate mean state and its variability in the Maritime Continent region and its representation in GCMs are crucial from both a socio-economic and climate perspective.

1.2 General climate of the Maritime Continent

The Maritime Continent is characterized by pronounced seasonal variations in precipitation and wind patterns. To illustrate the variations in the annual cycles of rainfall and low-level wind over the Maritime Continent region (20°S to 20°N and 80°E to 160°E), we show the monthly mean precipitation from observational datasets of Global Precipitation Climatology Project (GPCP) rainfall and 850hPa wind from the ERA-Interim reanalysis datasets in Fig. 1.4. In general, the Maritime Continent receives abundant rainfall throughout the year. However, most parts of the region experience a dry season during certain months. For example, the mainland of Southeast Asia in the northern Maritime Continent receives little rainfall from December to March, while the southern Maritime Continent, particularly Sulawesi, northern

Australia and Java, receive less rainfall from July to October. For convenience, the areas north and south of 10°N in the Maritime Continent are called the northern and southern Maritime Continent respectively, in this thesis. The year is divided into four seasons of 3 months each: winter (DJF, December-January-February) corresponding to the Australian summer monsoon; summer (JJA, June-July-August) represents the Asian summer monsoon; while spring (MAM, March-April-May) and autumn (SON, September-October-November) represent the monsoon transitions, also known as the intermonsoons.

The annual cycle of rainfall (Fig. 1.4) shows that maximum rainfall is observed over the southern Maritime Continent in boreal winter and gradually shifts north in boreal summer and back, as previously discussed by Meehl (1987); Chang et al. (2005); As-Syakur et al. (2016) and Zhang et al. (2016). Meehl (1987) also showed that the seasonal shift of rainfall is not only a north-south seesaw pattern, but rainfall also shifts from east to west and back. During the intermonsoon seasons, the dominant convective activity is located near the equator. There is a pronounced reversal of the wind direction from northeasterly in winter to southwesterly in summer over the northern Maritime Continent along with the rainfall migration; whereas, over the southern Maritime Continent, northwesterly winds in winter change to southeasterlies in summer. Cross-equatorial flows are observed from winter hemisphere towards the summer hemisphere in the low-level wind. Cold surges from mid-latitudes also affect convection in the Maritime Continent, in which cold air is advected from the Siberian High towards the equator. During boreal winter, the strengthening of the northeasterly wind associated with cold surges enhances the Hadley cell and precipitation over the Maritime Continent (Ooi et al., 2011).

Convection in the Maritime Continent is strongly organized in space and time by the presence of island and their topography, consisting of thousands of kilometres of coastline and mountains with elevations over 2000m above sea level (Chang et al., 2005). The interactions across scales, ranging from diurnal to long-term time-scales modulates the precipitation and wind patterns over the Maritime Continent. Next, we will briefly outline the diurnal and intraseasonal time scales variability, which have been shown to interact with seasonal and interannual times scales (Moron et al., 2015; Slingo et al., 2003).

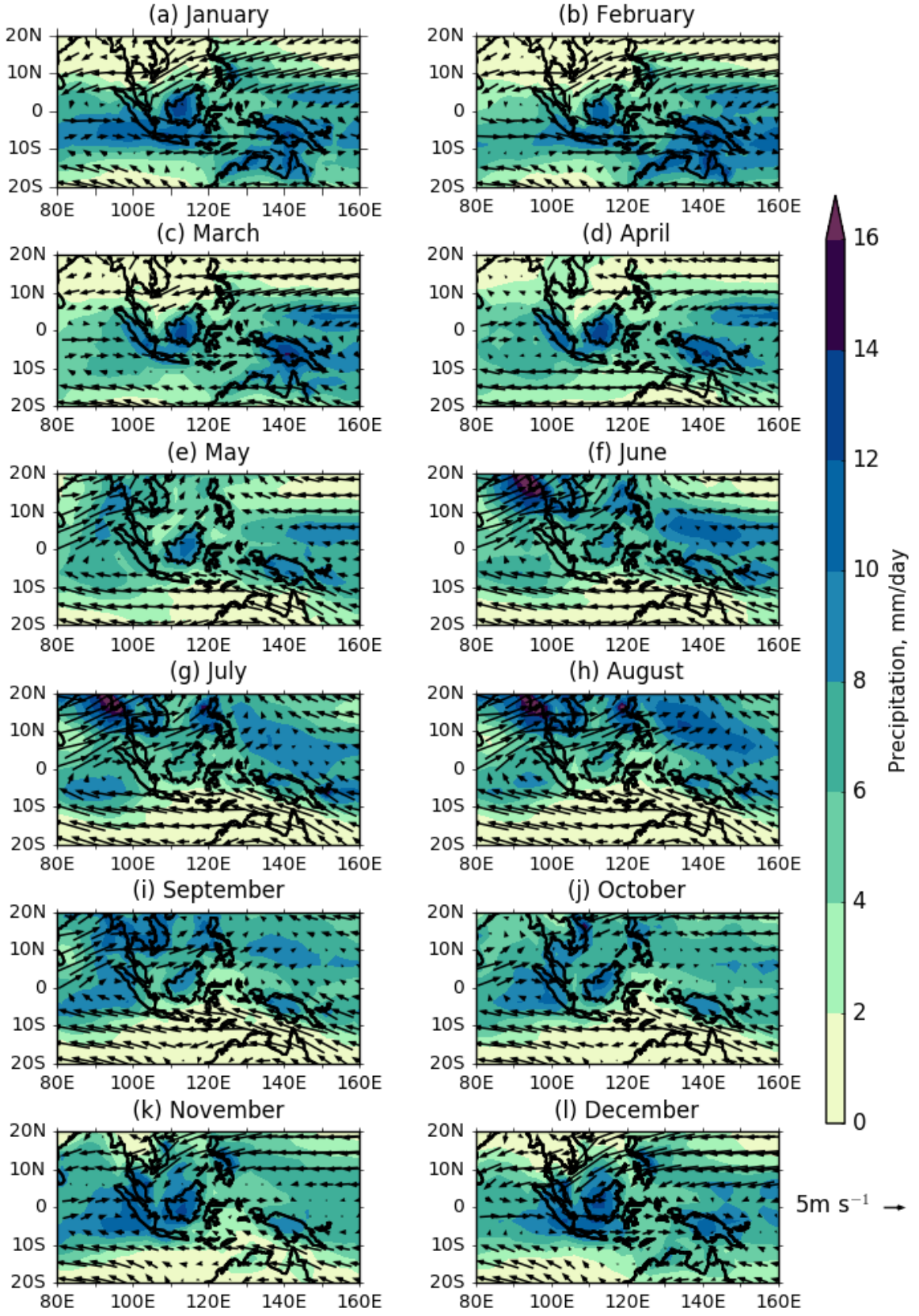

Figure 1.4: Monthly mean precipitation (shading, mm day^{-1}) from GPCP and 850 hPa wind (vectors, m s^{-1}) from ERA-Interim for (a) January to (l) December for 1979-2008 over the Maritime Continent region (20°S-20°N, 80°E-160°E).

1.3 Diurnal cycle

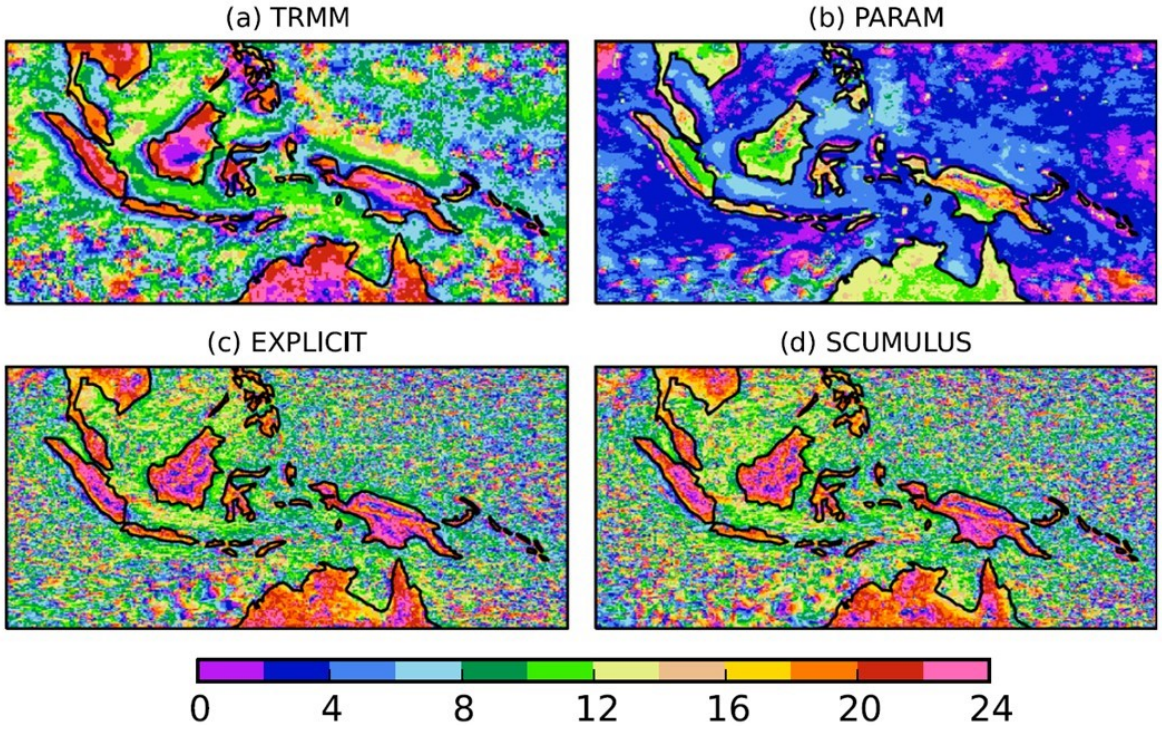

Figure 1.5: Local time of the maximum precipitation from March 2009 to February 2010 in (a) Tropical Rainfall Measuring Mission (TRMM) observations and three model simulations: (b) PARAM (standard Global Atmosphere/Global Land (GA4) MetUM parameterization schemes), (c) EXPLICIT (explicit convection), and (d) SCUMULUS (switching off only the deep convective parameterization). Figure taken from Birch et al. (2015).

The diurnal variations of convection the Maritime Continent are associated with land-sea breezes and complex topography over this region. Precipitation maximums occur in the early morning over the oceans and in the evening over the land (Yang and Slingo, 2001; Arakawa and Kitoh, 2005; Ichikawa and Yasunari, 2006; Wu et al., 2009; Birch et al., 2015). Figure 1.5(a) taken from Birch et al. (2015) illustrates the distinct features of the diurnal cycle of Maritime Continent precipitation peaking over the land in the evening between 18 to 00 local time, and propagating offshore from 00 to 06 local time towards the ocean in the morning. The other panels in Fig. 1.5 will be discussed in Section 1.8.2. Wu et al. (2009) showed that the nighttime precipitation that occurs offshore of Sumatra is caused by the the mountainous topography of the island and induced local circulations. Qian et al. (2013) showed that local diurnal cycle of land-sea breeze in the Maritime Continent is also modulated by the monsoonal wind.

1.4 Intraseasonal variability

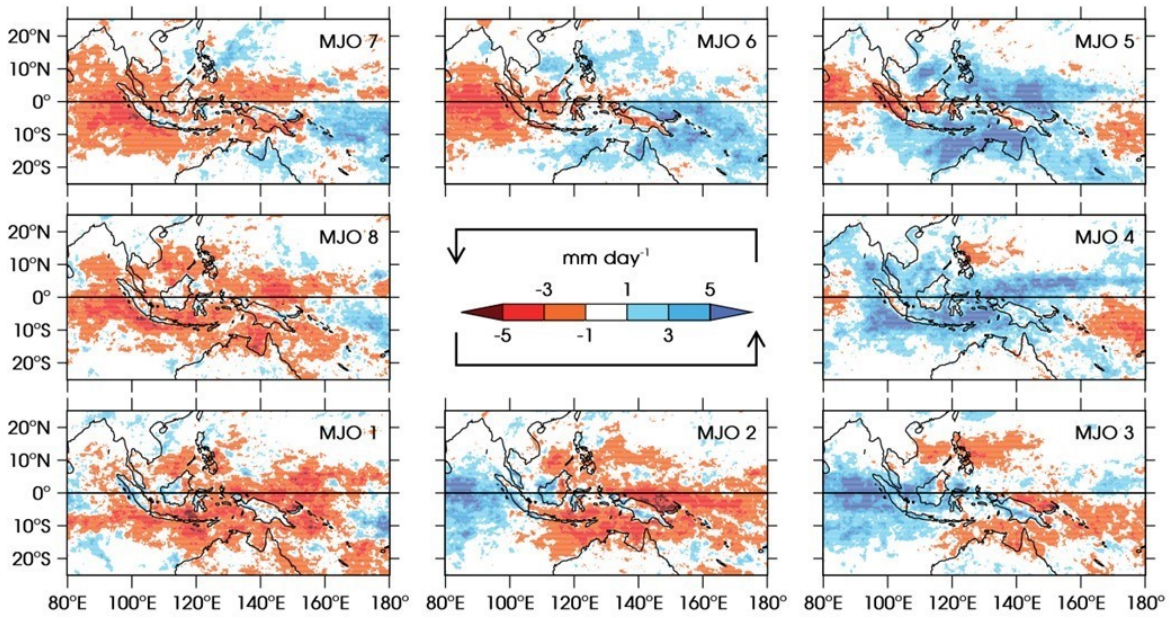

Figure 1.6: Precipitation anomalies (mm day^{-1}) over the Maritime Continent region from TRMM for the MJO phases, taken from Peatman et al. (2014). The MJO phases move in an anti-clockwise direction from Phase 1 to Phase 8.

The Madden-Julian Oscillation (MJO) is the dominant mode of tropical intraseasonal variability and exerts significant influence on the Maritime Continent climate. The MJO is named after Madden and Julian (1972), who identified a 40-50 day oscillation in time series of sea-level pressure and upper air data at tropical stations. Most MJO events begin in the western Indian Ocean and are more active during the boreal winter. The eastward propagation of the MJO from the Indian Ocean to the Pacific influences rainfall variations over the Maritime Continent. The westerly anomaly associated with the passage of the MJO converges with the easterly anomaly over the Maritime Continent and enhances the convection. On the other hand, topography in the Maritime Continent, the elongated and higher mountains, in particular, has a blocking effect on the westerly flows, shifting the westerly anomaly and the convection southward from the path of MJO (Wu and Hsu, 2009). Figure 1.6 shows the precipitation anomaly from TRMM over the Maritime Continent during the eight phases of MJO, taken from Peatman et al. (2014). The MJO phases are defined following the Wheeler and Hendon (2004) definition and move in an anti-clockwise (eastward) direction from Phase 1 to Phase 8. Enhancement of convection is strongest over the Maritime Continent during phases 3 to 5 (last column of Fig. 1.6). MJO is also linked with the initiation of El Niño events and we will discuss this in Section 1.7.1.

1.5 Monsoon

The word "monsoon" comes from the Arabic word "mausim", meaning season. A monsoon is a pronounced seasonal change of the prevailing wind direction and precipitation patterns. Monsoons are driven by land-ocean temperature contrasts in the summer hemisphere. There are a number of monsoons occurring over different parts of the world such as over Asia, Australia, South America, the West Africa and East Africa. These various regional monsoons can be viewed as components of an integrated global monsoon system.

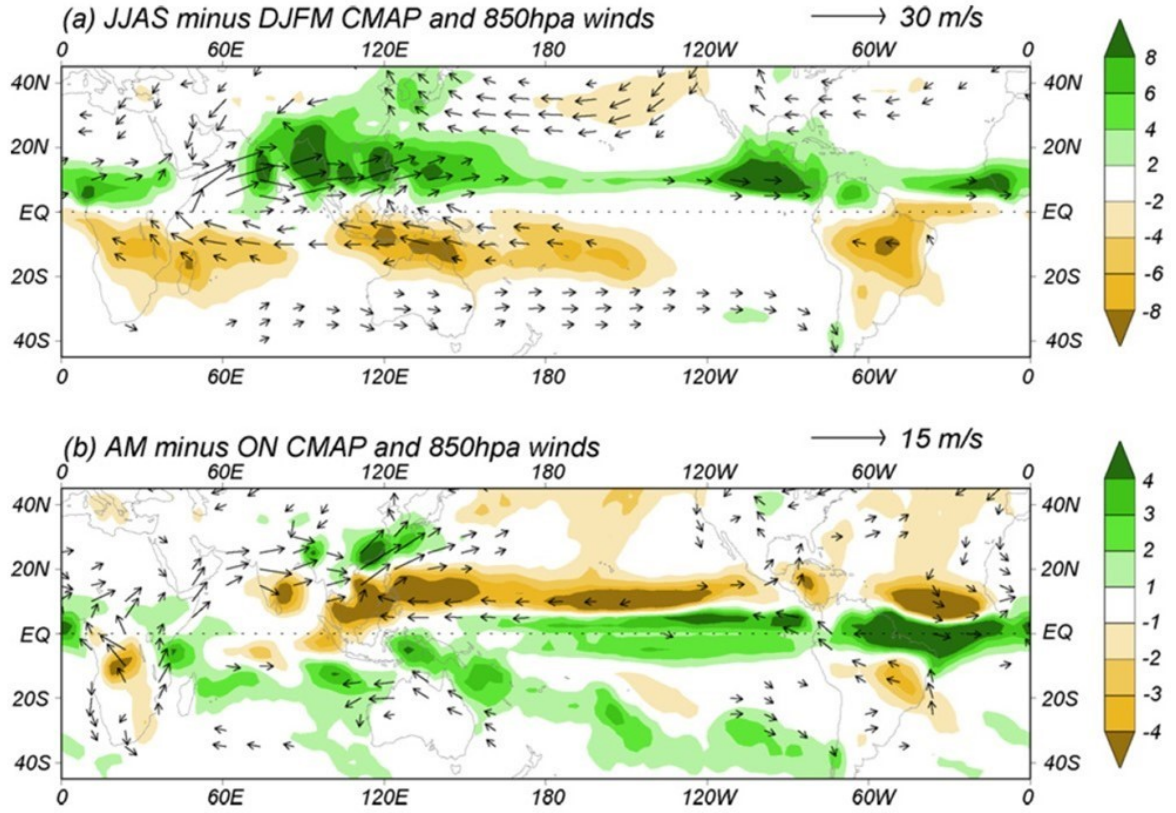

Figure 1.7: Precipitation (shading, mm day^{-1}) and 850 hPa winds (arrows, m s^{-1}) of (a) the Solsticial mode (JJAS minus DJFM) and (b) the Equinoctial mode (AM minus ON), taken from Wang and Ding (2008).

Wang and Ding (2008) identified two leading modes from empirical orthogonal function (EOF) analysis that can represent the global monsoon and annual cycle of tropical precipitation. The first EOF is in phase with the annual cycle and shows the boreal summer and winter monsoon rainfall regimes (off-equatorial ITCZ positions) while the second EOF represents the location of the spring and autumn ITCZ, closer to the equator. They further showed that the first EOF (solsticial mode) is equivalent to the difference between solsticial seasons (JJAS minus DJFM) and the second EOF (equinoctial mode) can be depicted by the difference between equinoctial seasons (AM minus ON). Figure 1.7 shows the global monsoon (solsticial

and equinoctial modes) calculated based on these seasonal differences of precipitation (Wang and Ding, 2008).

The differences in land distribution and topography contribute to the asymmetric structure of winds and precipitation over the two hemispheres. Meehl (1987) suggests that the unequal distribution of land and sea over the northern and southern hemispheres, and the differential heating of land and sea creates a stronger monsoon over the northern hemisphere, i.e the Asian summer monsoon.

A marked seasonal cycle is observed over the Maritime Continent following the transition from the Asian to the Australian summer monsoons associated with the migration of the Intertropical Convergence Zone (ITCZ) (Moron et al., 2015).

1.6 Intertropical Convergence Zone (ITCZ)

The ITCZ is the low pressure area near the equator where the Northern Hemisphere trade winds converge with those from the Southern Hemisphere. The location of the ITCZ varies throughout the year following the movement of the sun. The ITCZ over the ocean remains closer to the equator most of the time, while over the land it can move further south and north. Figure 1.8(a) shows the zonally averaged mean precipitation from the Tropical Rainfall Measuring Mission (TRMM) Multisatellite Precipitation Analysis (TMPA) and surface winds from the European Centre for Medium-Range Weather Forecasts (ECMWF) interim reanalysis over the Pacific Ocean (160°E - 100°W). The surface winds remain easterly throughout the year and the seasonal shift in the latitudinal position of the ITCZ (red line in Fig. 1.8a) is less, between 9°N in boreal summer and 2°N in boreal winter (Schneider et al., 2014). On the other hand, ITCZ in the South Asian monsoon region (65°E - 95°E) has larger seasonal migration (between 20°N in boreal summer and 8°S in boreal winter) and moves abruptly into the summer hemisphere, while surface winds turn westerly north of the Equator (Fig. 1.8b).

During boreal summer, the sun heats the Northern Hemisphere more strongly, thus the ITCZ is located north of the equator and winds blow from the Southern Hemisphere to the Northern Hemisphere. The reverse happens during boreal winter, although the annual mean ITCZ is around 6 °N. The position of the annual mean ITCZ is associated with the Atlantic Ocean's meridional overturning circulation transporting energy northward across the Equator and resulting in a warmer northern hemisphere. This ocean energy transport is compensated by atmospheric energy transported southwards across the equator from the warmer to cooler hemisphere through meridional Hadley circulation, with the ascending branch and ITCZ displaced north of the Equator (Schneider et al., 2014).

The ITCZ is collocated with the rising branch of the Hadley Circulation. The Hadley Circulation is a meridional overturning circulation where the air masses rise over the equatorial region, diverge at upper levels, descend in the subtropics, and flow back towards the equator.

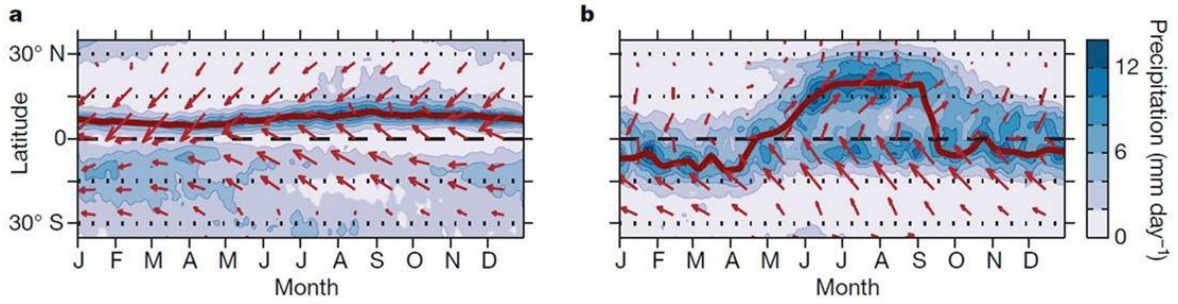

Figure 1.8: Latitude-time plot of mean precipitation from TRMM Multisatellite Precipitation Analysis (shading, mm day^{-1}) and surface winds from the ECMWF interim reanalysis (vectors, m s^{-1}) zonally averaged over (a) the Pacific (160°E - 100°W) and (b) the South Asian monsoon sector (65°E - 95°E) during 1998-2012. Red line shows the ITCZ (position of the maximum precipitation each month). Figure taken from Schneider et al. (2014).

The Hadley Circulation features a seasonally varying distribution associated with seasonal shift of the ITCZ.

The warm sea surface temperature (SST) in the Maritime Continent Indo-Pacific Warm Pool (IPWP) region provides ample moisture for convection. The latent heat release from the precipitation over the Maritime Continent is one of the major heat sources that drive the weather and climate patterns of the Indo-Pacific and across the globe (Ramage, 1968; Neale and Slingo, 2003; Zhang et al., 2016). Fig. 1.9 shows the linearised solution of heat induced tropical circulation, with symmetric heating centred on the equator, proposed by Gill (1980). The westerly winds from the west (Indian Ocean) flow towards the Maritime Continent as a result of a Rossby wave response. The easterly winds flow towards the heating source (the Maritime Continent) as a result of a Kelvin wave response over the Pacific Ocean. These lead to rising motion over the Maritime Continent and subsidence further east (over the Pacific), forming the Walker circulation. The excitation of the two cyclonic circulations straddling the equator, induced by the Rossby wave, with the flow at the suface directed poleward from the heat source region, corresponds to the Hadley circulation (Gill, 1980).

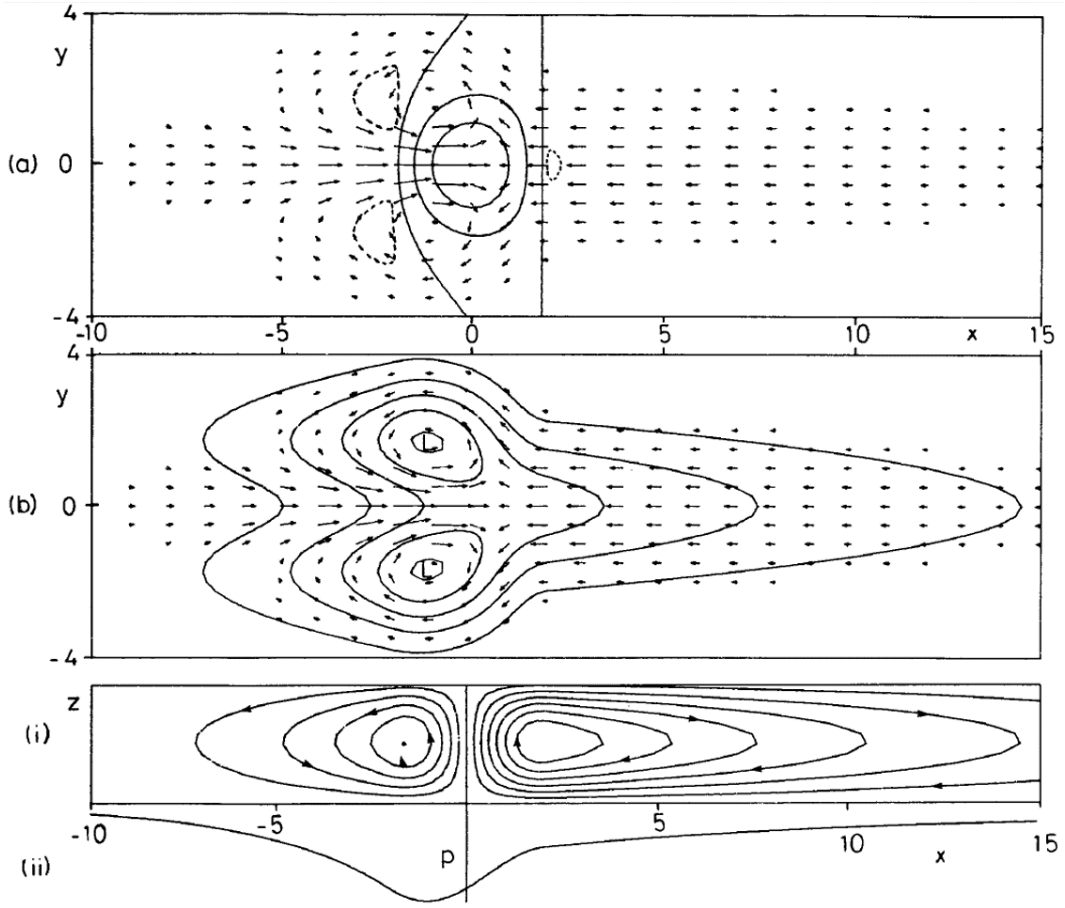

Figure 1.9: The Gill (1980) solution of heat induced tropical circulation, with symmetric heating centred on the equator: (a) contours of vertical velocity and low-level wind velocity (vectors), (b) contours of perturbation pressure and low-level wind velocity (vectors), (c) meridional mean of (i) stream-function and (ii) perturbation pressure, taken from Gill (1980).

1.7 Interannual variability

The Maritime Continent rainfall has large interannual variability associated with El Niño-Southern Oscillation (ENSO) and Indian Ocean Dipole (IOD) via modulation of the ascending branch of Walker circulation.

1.7.1 El Niño-Southern Oscillation (ENSO)

ENSO affects the climate over a large part of the world, beyond the tropical Pacific, and is one of the most studied modes of variability. El Niño was first discovered by Peruvian fishermen in the 19th century. They refer to the warm waters off of the South American coast that appear every few years around Christmas as El Niño, which means the “Christ Child” or “the little boy” in Spanish. Conversely, La Niña (“the little girl”) is the opposite phase of El Niño and refers to colder than average sea surface temperatures over the same region, i.e. the

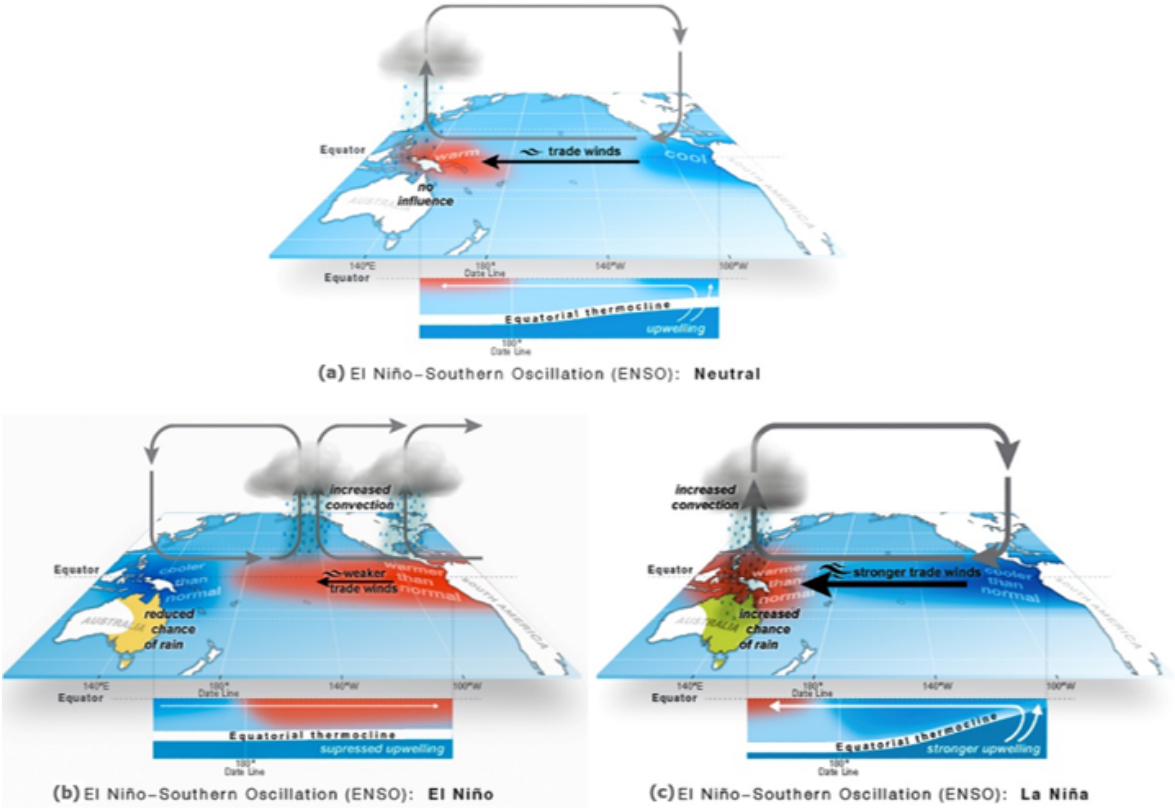

Figure 1.10: Schematic diagram for ENSO: (a) neutral phase; (b) El Niño phase and (c) La Niña phase. Figure taken from `http://www.bom.gov.au/climate/iod/`

east-central Equatorial Pacific.

The Southern Oscillation refers to atmospheric pressure changes between the western (Darwin, north Australia) and eastern (Tahiti, French Polynesia) tropical Pacific. Sir Gilbert Walker first identified the east-west components of large-scale circulations, while Bjerknes (1969) linked the Southern Oscillation and SST variations in the equatorial Pacific Ocean as ENSO. Bjerknes (1969) showed that ENSO is a coupled ocean and atmosphere phenomenon, where fluctuations in Pacific SST drive changes in the atmosphere, which in turn impact the ocean in a positive feedback through the Walker circulation, known as the Bjerknes feedback.

Figure 1.10 shows a schematic diagram of ENSO in neutral, El Niño and La Niña phases. During neutral conditions (Fig. 1.10a), the easterly trade winds blow from the eastern Pacific towards the west, driving warm SST towards the west Pacific and allowing for upwelling of cooler water towards the surface layer in the eastern Pacific. The thermocline is deeper in the west than the east. This leads to convective heating and upward motion over the warmer western Pacific, with eastward upper-level return flow across the Pacific and descent over the eastern Pacific completing the Walker circulation.

El Niño is the warm phase of ENSO events when unusually warm SST anomalies observed over the central and eastern Equatorial Pacific. El Niño events occur approximately every

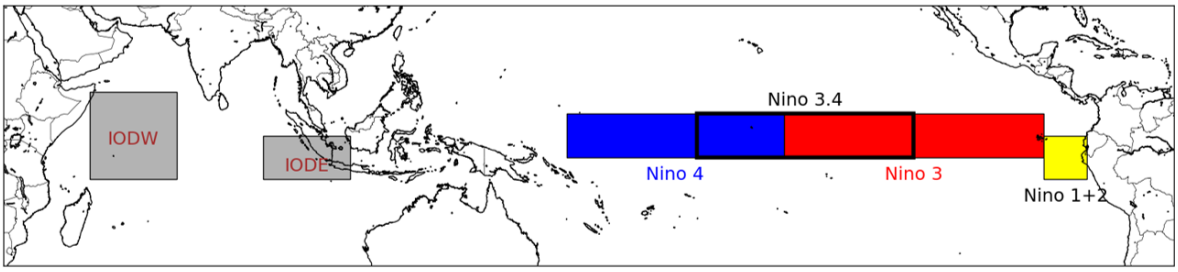

Figure 1.11: Definition of the Niño regions in the equatorial Pacific and Indian Ocean Dipole eastern (IODE) and western (IODW) poles.

two to seven years and are generally initiated in boreal spring or summer and peak in winter. During El Niño the trade winds weaken or even reverse direction, initiated by atmospheric disturbances such as MJO or Westerly Wind Bursts (WWB), which generate an eastward propagating downwelling oceanic Kelvin wave on the thermocline and result in warmer SST over the central and eastern Pacific. The warmer SST over the central and eastern Equatorial Pacific leads to anomalous convective heating, shifting the convection and Walker circulation ascending branch from western Pacific and Maritime Continent towards the central and eastern equatorial Pacific. The opposite occurs during La Niña also known as the cold phase of ENSO.

Figure 1.11 shows the four Niño regions that are used to classify ENSO based on the area-averaged SST anomalies, computed from a base period over these Niño regions. These regions are: Niño 1+2 (0°-10°S, 80°W-90°W), Niño 3 (5°S-5°N, 90°W-150°W), Niño 3.4 (5°S-5°N, 120°W-170°W) and Niño 4 (10°S-10°N, 160°E-150°W)(Bamston et al., 1997).

A number of studies (Hendon, 2003; Kubota et al., 2011; As-syakur et al., 2014; McBride et al., 2003) showed that the Maritime Continent receives below normal rainfall during El Niño while La Niña enhances the precipitation. However, Hendon (2003) and As-syakur et al. (2014) also pointed out that the Maritime Continent-Indonesia precipitation is highly correlated with ENSO in the dry season (JJA and SON) but not during the wet season (DJF and MAM) when precipitation variations are not spatially coherent (McBride et al., 2003). Kubota et al. (2011) found that there is spatial and temporal variability of dry conditions over the Maritime Continent during El Niño years, where dry conditions first occur over the equatorial region in boreal summer and spread to the off-equatorial region in autumn, and continue into winter and spring. Qian et al. (2013) showed that the southwestern Borneo experienced increase of rainfall while the rest of the region experienced reduced rainfall during the El Niño events in DJF. They then showed that this is related to the inverse relationship between monsoonal wind speed and diurnal cycle of land-sea breeze. During El Niño, the easterly wind anomalies weakens monsoonal northwesterly wind and enhance sea breeze convergence, which increase the rainfall over southwestern Borneo in DJF.

1.7.2 Indian Ocean Dipole (IOD)

IOD is a coupled ocean-atmosphere phenomenon, similar to ENSO but in the equatorial Indian Ocean. Saji et al. (1999); Webster et al. (1999) identified this dipole mode in the Indian Ocean which has a significant influence on precipitation from eastern Africa to Indonesia.

Figure 1.12 shows the schematic diagram of IOD (BOM, 2017) during neutral, positive and negative phases. During the IOD positive phase, low-level westerly winds weaken over the equatorial Indian Ocean and easterly anomalies blow from the IODE towards the warmer IODW, generating upwelling in the IODE. The Indian Ocean Walker circulation weakens and is in reverse direction (Fig. 1.12b) compared to the IOD neutral phase (Fig. 1.12a). The ascending branch of the Walker circulation is located over the IODW and precipitation increases over the IODW and east Africa. Subsidence occurs over the IODE and rainfall is reduced over the Maritime Continent. Opposite conditions occur during a negative IOD phase (Fig. 1.12c). Warmer SST conditions are observed over the IODE, accompanied by strengthening of low-level westerlies and upper level easterlies, bringing more rainfall over the Maritime Continent.

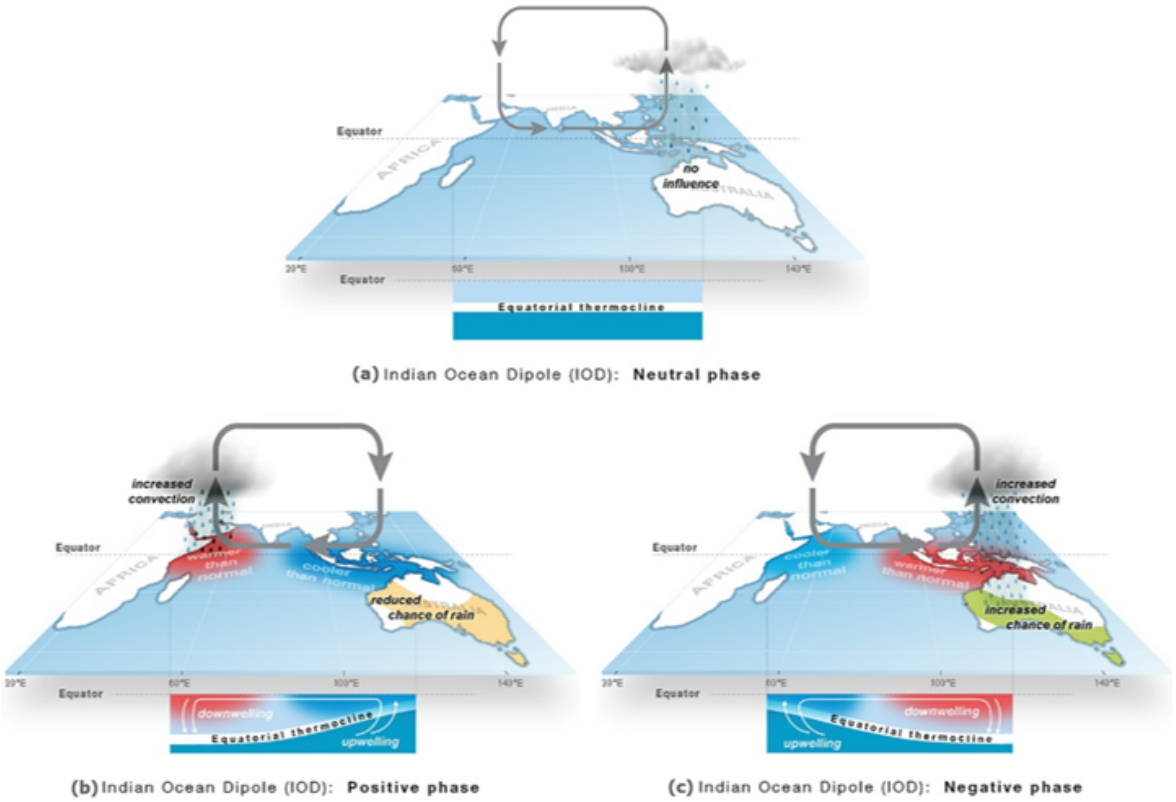

Figure 1.12: Schematic diagram of the IOD: (a) neutral phase; (b) positive phase and (c) negative phase. From `http://www.bom.gov.au/climate/enso/history/ln-2010-12/three-phases-of-ENSO.shtml`

This study uses the Dipole Mode Index (DMI) as defined in Saji et al. (1999) to represent the IOD. DMI is the difference between western Indian Ocean (IODW, 10°S-10°N, 50°E-70°E) and eastern Indian Ocean (IODE, 0°S-10°S, 90°E-110°E) SST anomalies as shown in Fig. 1.11. An IOD event usually starts to develop in boreal summer (JJA) and reaches its peak in boreal autumn (SON). IOD events typically last for several months and there are zero to three occurrences in a decade.

While previous studies (Saji et al., 1999; Webster et al., 1999) showed that the IOD is an independent mode of variability in the Indian Ocean, Allan et al. (2001) argued that the IOD is related to the ENSO. Nur'utami and Hidayat (2016) showed that an individual IOD event, individual ENSO event and combinations of both ENSO and IOD events have different impacts on Indonesian rainfall variability. Indonesian rainfall is more significantly increased when negative IOD and La Niña concurrently occur as both of the ascending branches of Pacific and Indian Ocean Walker cells are located over the Maritime Continent, than as a result of a single event of negative IOD or La Niña. Meanwhile, the magnitude of rainfall decrease when a positive IOD and El Niño occur together is greater than when a single event of either positive IOD or El Niño occurs. As-syakur et al. (2014) investigate the rainfall relationship with IOD and ENSO in Indonesia using satellite data. They concluded that both ENSO and the IOD result in fairly similar temporal patterns of rainfall anomalies in Indonesia, especially during the dry season. During El Niño and positive IOD events, the Indonesian SST is cooler than normal. This leads to reduced rainfall over Indonesia. The opposite happens during La Niña and a negative IOD.

In the following section, we will discuss the climate model characteristic and biases, in particular on aspects that are important to correctly represent the climate of the Maritime Continent.

1.8 Modelling the Maritime Continent

With the development of General Circulation Models (GCMs), there has been a lot of improvement in simulating observed features of global and regional mean climate and its variability. One noteworthy effort is the establishment of the Coupled Model Intercomparison Project (CMIP) under the World Climate Research Program (WCRP) to study the GCM simulations of present climate and projections of future climate change under standardized boundary conditions (Meehl et al., 2000).

Comparison studies between different phases of the CMIP multi-model ensemble found that generally there are improvements in the performance of CMIP5 over CMIP3 in the simulations of monsoon features (Sperber et al., 2013; Jourdain et al., 2013) possibly due to increased horizontal and vertical resolution in the atmosphere and ocean, parameterization development and improved representation of various processes in CMIP5 models. However,

considerable systematic errors still exist, suggesting that the state-of-art of climate models are still lacking good representations of the necessary physical mechanisms. Next, we highlight the climate model characteristic and potential sources of bias that previous literature has found important for correctly representing the present-day climate of the Maritime Continent.

1.8.1 Model resolution

The Maritime Continent includes large islands with length larger than 1000km (e.g. Sumatra, Java, Borneo, New Guinea) and small islands with length less than 1km. The complex topography over the Maritime Continent affects the spatial variability of rainfall over this region (Chang et al., 2005) and this also impact on the large-scale circulation. However, current GCMs have typically a too coarse resolution with grid size between 100 to 500 km due to limitations in computational resources, hence only large islands in the Maritime Continent are represented in most GCMs. Studies have shown that the inadequate representation of land-sea breeze circulations associated with insufficient representation of islands and mountains in coarse-resolution models impacts on the simulation of precipitation in this region (Qian, 2008).

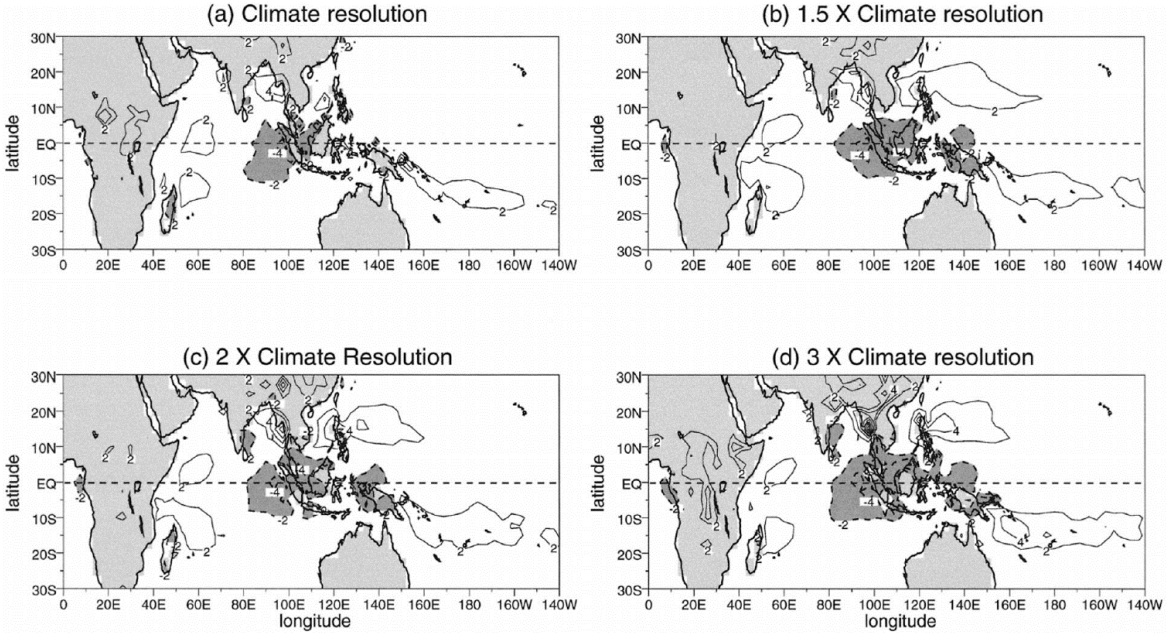

Figure 1.13: Annual mean precipitation bias (mm day^{-1}) from horizontal resolution sensitivity experiments using the MetUM HadAM3 model: (a) climate resolution (2.5°$\times$ 3.75°); (b) 1.5 $\times$ climate resolution (1.67°$\times$ 2.5°); (c) 2 $\times$ climate resolution (1.25°$\times$ 1.875°); (d) 3 $\times$ climate resolution (0.83°$\times$ 1.25°). Contour interval for precipitation anomalies is 2 mm day^{-1}, shaded below -2 mm day^{-1} and zero contour omitted. Figure taken from Neale and Slingo (2003).

In the MetUM, Neale and Slingo (2003) found that a decrease in grid spacing from 350

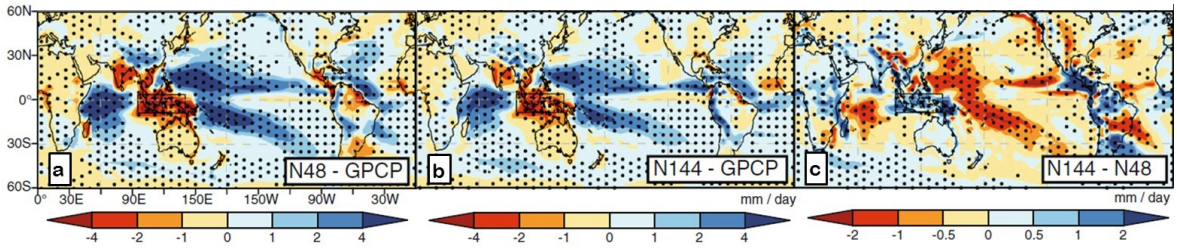

Figure 1.14: Annual mean precipitation bias (mm day^{-1}) with respect to GPCP in the (a) N48 (2.5°× 3.75°) and (b) N144 (0.83°× 1.25°) MetUM HadGAM1 resolution experiments. (c) N144 minus N48. Stippling indicates grid points where a paired t-test rejects the null hypothesis of equal means at the 95% confidence level. Black box shows the central part of the Maritime Continent between 95.625° to 140.625 °E and -8.75° to 3.75 °N. Figure taken from Schiemann et al. (2014).

to 110 km does not reduce dry biases in the Maritime Continent (Figure 1.13). Instead, they showed that biases in simulating the diurnal cycle over the islands of Maritime Continent (related to land-sea breeze circulation) can impact on the simulation of seasonal mean climate. The errors in land sea breezes resulted in troposheric flow biases that affects the surface fluxes and convection initiation. Other more recent studies (Schiemann et al., 2014; Johnson et al., 2015) suggest increasing resolution improves the precipitation simulation in the newer version of the MetUM. Schiemann et al. (2014) attributed the improvement of the Maritime Continent precipitation to the better-resolved boundary conditions (land-sea mask, soil and vegetation parameters) when the grid spacing decreased from approximately 350 to 110 km. They also highlighted that increasing resolution resulted in an increase of rainfall over most parts of the Maritime Continent but the model still exhibits dry biases over the central part of the Maritime Continent (95.625° to 140.625 °E and -8.75° to 3.75 °N, depicted in a black box in Fig. 1.14) in all resolution. Johnson et al. (2015) showed that better representation of orography over the Maritime Continent at a finer resolution (approximately 40 km) improved precipitation over the islands compared to coarse resolution (approximately 200 km). Despite different conclusions, these studies highlight the Maritime Continent as one of the region where the simulated mean climate has some sensitivity to resolution. These results also suggest that models still lack a good representation of the necessary physical mechanisms, which we will discuss in next section.

1.8.2 Parameterization

Current coupled and atmosphere-only climate models still rely on parameterizations as models cannot resolve most of the atmospheric processes due to limited resolution. Complex physical processes such as cloud, land-surface and radiation occur at scales finer than the coarse model's grid. They are approximated by the parameterization in order to be represented in the models.

Studies have shown that the simulation of tropical precipitation is highly sensitive to the choice of the convection parameterization scheme (Sherwood et al., 2014; Bush et al., 2015). Parameterizations allow the inclusion of these important subgrid scale processes in the GCMs. However, parameterization's deficiencies can also lead to significant biases in climate models. Both coupled and uncoupled model simulations fail to reproduce the observed seasonal cycle of the western Pacific monsoon, suggesting that the representation of convection is likely to be a key source of error (Brown et al., 2013). Ackerley et al. (2015) suggest precipitation and circulation biases over Australia to be related to parameterization of convection in the CMIP5 models. They proposed that the inclusion of the prognostic cloud fraction and prognostic condensate scheme (PC2) scheme in ACCESS1.3 resulted in higher rainfall simulated over Australia than the ACCESS1.0, which does not use PC2 scheme.

Models using convective parameterization fail to simulate the distinct diurnal cycle over the Maritime Continent and tend to simulate the maximum precipitation a few hours earlier than observed (Birch et al., 2015; Yang and Slingo, 2001) possibly due inadequate parameterization of physical processes in the convection scheme and land surface scheme. The interaction between these two schemes and also the radiation scheme may also result in errors in the diurnal cycle. Recent advancement in computer resources allow us to conduct high resolution model simulations with the convective parameterization switched off, and permits the convection to develop explicitly. Figure 1.5 showed the local time of the maximum precipitation in TRMM observations and three model simulations: PARAM (standard Global Atmosphere/Global Land (GA4) MetUMs parameterization schemes), EXPLICIT (explicit convection, switching off deep and convective parameterization), and SCUMULUS (switching off only the deep convective parameterization) in Birch et al. (2015) study. This figure indicates that the local time of maximum precipitation simulated by explicit resolved convection experiment (Fig. 1.5c) is closer to observation than the parameterized convection experiment. Holloway et al. (2012) showed that Indo-Pacific precipitation distribution simulated in an limited area experiment of the MetUM with explicit convection is in better agreement with observations compared to a parameterized convection experiment simulation which tends to produce relatively too much light rainfall. Biases in diurnal time scales can impact on seasonal climate simulations over the Maritime Continent (Slingo et al., 2003).

Although explicitly resolving convection leads to a better simulation of precipitation than the parameterization, current GCMs still have to rely on parameterization due to continued limitations to computational resources. Improving parameterization schemes is crucial for better simulated tropical precipitation.

1.8.3 Impact of ocean-atmosphere coupling

Atmosphere-only models are forced by prescribed SSTs. Atmosphere-only models are lacking SST biases hence can provide insights into deficiencies of the atmospheric model that are unaffected by the systematic SST biases present in coupled models. However, atmosphere-only models are missing the one-way atmosphere to ocean interactions, which may introduce different biases. Coupled ocean-atmosphere models, on the other hand, are able to simulate two-way air-sea interactions. However, SST biases and poorly represented air-sea interactions in the coupled models produce other errors when simulating mean climate and its variability.

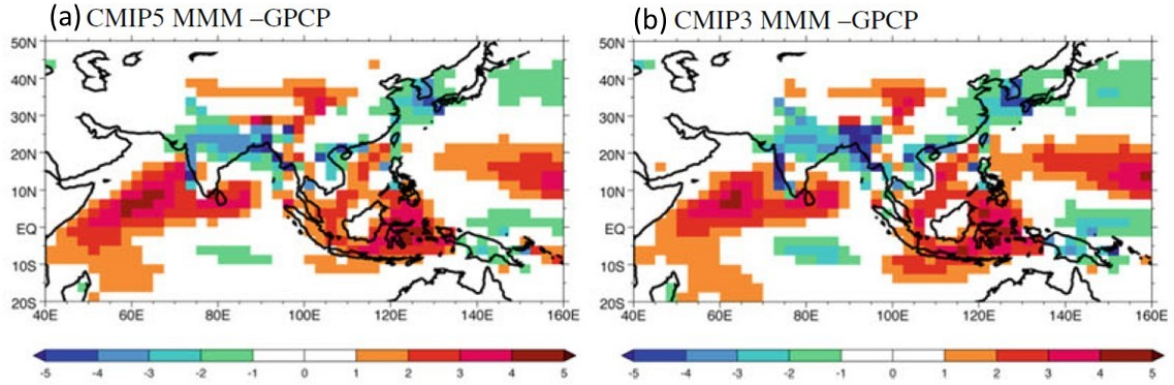

Figure 1.15: JJAS precipitation bias (mm day^{-1}) with respect to GPCP for (a) CMIP5 MMM and (b) CMIP3 MMM, taken from Sperber et al. (2013). CMIP5 MMM consists of 25 models, while the CMIP3 MMM consists of 22 models.

Most GCMs have difficulty capturing the climate mean state and its variability over the Maritime Continent. In atmosphere-only models, one common error is the underestimation of the mean precipitation over the Maritime Continent (Neale and Slingo, 2003; Schiemann et al., 2014) which is attributed to a poor representation of the diurnal cycle and lack of strong organized MJO events in the model (Slingo et al., 2003). On the other hand, coupled models overestimate the mean precipitation in the Maritime Continent, which is associated with cold SST biases over the Pacific Ocean (Inness and Slingo, 2003; Sperber et al., 2013). Figure 1.15 shows that CMIP5 MMM still exhibits similar spatial pattern and magnitude of biases over the Maritime Continent to CMIP3 MMM.

The SST biases such as excessive cold tongue biases (in which the equatorial cold tongue is too cold and extends too far west in the Pacific Ocean) are a major and continuing issue in the CMIP models (Cai et al., 2009; Li and Xie, 2014), despite some improvement in the simulation of the equatorial Pacific cold tongue from CMIP3 to CMIP5 (Song et al., 2014). Li and Xie (2012) found that the dry biases and surface easterly biases over the Pacific cold tongue are not present in CMIP5 atmosphere-only models, suggesting that these biases in coupled models arise from misrepresentation of ocean-atmosphere interactions via the Bjerknes feedback in coupled models. On the other hand, the double ITCZ problem in

CMIP models which is characterized by two excessive precipitation bands straddling the equator is associated with local SST biases in the ocean models and a poor representation of precipitation and large-scale circulation interactions in the atmospheric models (Oueslati and Bellon, 2015).

Wang et al. (2005) showed that ECMWF (European Centre for Medium-range Weather Forecast)-Hamburg (ECHAM4) coupled model is able to capture the negative correlation between rainfall anomalies and SST anomalies in the Asia-Pacific region (5°N - 30°N, 70°E - 150°E) during the boreal summer. Whereas, the corresponding atmospheric model forced by prescribed SST failed to simulate this negative relationship due to the lack of air-sea interactions in the AMIP model that leads to a poor simulation of the Asian-Pacific summer monsoon rainfall variability.

In terms of ENSO simulation, Jha and Kumar (2009) found that seasonal atmospheric response to ENSO SST in the National Centers for Environmental Prediction (NCEP) Climate Forecast System (CFS) atmosphere-only and coupled models are identical despite the extra degrees of freedom in coupled models. Studies (Cai et al., 2009; Jourdain et al., 2013) showed that the Pacific cold tongue biases that extend too far west produce a significant positive correlation with rainfall over Papua in DJF season, opposite to observations, which show a negative correlation and thus affect the ENSO-rainfall teleconnection simulated by the coupled CMIP models. Turner et al. (2005) showed that the improved mean state of the tropical Pacific in heat flux-adjustments experiment in the coupled HadCM3 model, led to improved ENSO simulation, that in turn also improved the Asian summer monsoon-ENSO teleconnection. The analysis by Annamalai et al. (2007) in the CMIP3 models arrives at the same conclusion, that models with better representation of the basic state, accompanied by associated changes in the Walker circulation, capture the ENSO-Asian summer monsoon teleconnection better. On the other hand, Langenbrunner and Neelin (2013) showed that an AMIP model with specified observed SSTs, also struggles to simulate ENSO precipitation teleconnections and there is only slight improvement of the ENSO-precipitation teleconnection in atmosphere-only runs of CMIP5 compared to CMIP3.

For the IOD simulation, Saji et al. (2006) showed that most of the CMIP5 models simulate the IOD spatial pattern and temporal evolution well. However, Weller and Cai (2013) found that CMIP3 and CMIP5 models tend to simulate IOD amplitude larger than observed and there are no significant improvements between the two phases of CMIP. Li et al. (2015b) showed that the weak southwest summer monsoon over the Arabian Sea in coupled CMIP5 models induced warm SST biases over the western equatorial Indian Ocean, which resulted in an overly large amplitude of interannual IOD variability simulated in CMIP5 models.

This study investigates the Maritime Continent mean state biases and their impact on teleconnections with the Indian and Pacific Oceans in both uncoupled and coupled CMIP5 models, and in new experiments using the Met UM HadGEM3-GA6 (Met Office Unified Model,

Hadley Centre Global Environment Model version 3, Global Atmosphere 6.0) atmosphere-only model.

1.9 Thesis aims and outline

Chapter 1.1 outlines the motivation behind this study. The remainder of Chapter 1 provides an overview of the characteristics of the Maritime Continent climate and its variability, focusing on the annual cycle and monsoon seasonality, followed by the two major modes of interannual variability affecting this region, i.e ENSO and IOD. Furthermore, this chapter also discusses the climate model characteristic and biases, in particular on aspects that are important to correctly represent the climate of the Maritime Continent.

This thesis has three main aims and more specific questions based around the main aims will be addressed in each of the subsequent chapters. The principal aims of this thesis are:

1. To investigate the fidelity of current state-of-the-art climate models at simulating the climate mean state and its variability in the Maritime Continent;

2. To explore the impact of model biases in the Maritime Continent on tropical variability and teleconnections;

3. To determine the relationship between SSTs in the tropics and climate variability within the Maritime Continent.

Chapter 2 assesses mean state biases in the Atmospheric Model Intercomparison Project (AMIP) experiments of the Coupled Model Intercomparison Project Phase 5 (CMIP5) for the Maritime Continent region. AMIP experiments that are forced by prescribed SSTs enable the identification of atmospheric model deficiencies and common features in isolation; these are unaffected by the systematic SST biases present in coupled models. The results from Chapter 3 have previously been published in Toh et al. (2018). Adjustment has been made to the Introduction section in this chapter to avoid redundancy with Chapter 1. Additional analysis and figures are included in this Chapter compared with the published article. Specific questions addressed in this chapter are:

- How well do CMIP5 models simulate the mean seasonal climate over the Maritime Continent?

- What are the model systematic biases in the Maritime Continent?

- What are the possible sources of model systematic biases?

Chapter 3 investigates the impacts of air-sea interactions in the tropical oceans on Maritime Continent precipitation in CMIP5 models. This chapter will also focus on the relationship

between the Maritime Continent and ENSO as well as with the IOD in both atmosphere-only and coupled CMIP5 models. We will use a variety of composite analyses, multimodel regression and correlation techniques to address the following questions:

- How well do CMIP5 coupled models simulate the tropical ocean SSTs?
- What is the relationship between Maritime Continent mean state precipitation biases and tropical SST biases?
- How well do CMIP5 atmosphere-only and coupled models simulate teleconnections between ENSO/IOD and the Maritime Continent?
- Does ocean-atmosphere coupling improve these teleconnections?
- How are these teleconnections influenced by the mean state SST biases?

Chapter 4 describes a suite of sensitivity experiments performed using the MetUM HadGEM3-GA6 model. These experiments are performed to test causality in the relationships between SST anomalies and precipitation anomalies by removing the ocean feedbacks and to better understand the mechanisms underlying these relationships. The Maritime Continent SST perturbation sensitivity experiments will assess the importance of the Maritime Continent region SST on the tropical variability and teleconnections. The second series of experiments will determine the influence of SST perturbations elsewhere in the tropics (i.e. Pacific and Indian Oceans) on climate variability within the Maritime Continent. Chapter 5 addresses the following questions:

- What are the systematic biases in HadGEM3-GA6?
- How sensitive is the tropical Indo-Pacific circulation and precipitation in the model to SST changes in the Maritime Continent, the Pacific Ocean and the Indian Ocean?
- How do these sensitivity experiments alter the atmospheric response to ENSO and IOD?
- How does the sensitivity of the seasonal mean climate and climate variability in the tropics to SST perturbations compare to the relationships found in the coupled models in Chapter 4?

The last chapter presents the conclusions of the thesis, summarizing the key findings in this study. This includes a discussion on the limitations of this study and suggestions for future work.

Chapter 2

Maritime Continent seasonal climate biases in AMIP experiments of the CMIP5 multimodel ensemble

Preamble

This chapter has been published in Climate Dynamics in February 2018 with the same title by Ying Ying Toh, Andrew G. Turner, Stephanie J. Johnson and Christopher E. Holloway. Adjustment has been made to the Introduction section in this chapter to avoid redundancy with Chapter 1. Additional analysis and figures are included in this Chapter compared with the published article (Toh et al., 2018).

2.1 Introduction

The fidelity of 28 CMIP5 models in simulating mean climate over the Maritime Continent in the AMIP experiment is evaluated in this chapter. The CMIP5 simulations are used in the IPCC Fifth Assessment Report for future climate projection (Flato et al., 2013). In order to have confidence in the future projections made by models, the models should be able to correctly simulate characteristics of the current climate on regional (Maritime Continent) and global scales. Thus, this thesis focuses only on present-day climate simulations.

Previous studies mentioning the Maritime Continent in CMIP5 are largely focussed on the topic of nearby monsoon regions. Several studies have evaluated the fidelity of CMIP5 models in simulating the Australian monsoon (Jourdain et al., 2013; Ackerley et al., 2015), the western Pacific monsoon (Brown et al., 2013) and the Asian summer monsoon (Sperber et al., 2013). These studies found that different models show varying ability at each aspect of monsoon simulation. However, no single model in the CMIP5 ensemble best represents all aspects of the monsoon, either in an individual subregion or when considering all characteristics of the

monsoon as a whole. Comparison studies between different phases of the CMIP multi-model ensemble found that generally there are improvements in the performance of CMIP5 over CMIP3 (Sperber et al., 2013; Jourdain et al., 2013) possibly due to increased horizontal and vertical resolution in the atmosphere and ocean, parameterization development and the improved representation of Earth-system processes in CMIP5 models. However, considerable systematic errors exist, suggesting that the models are still lacking good representations of the necessary physical mechanisms involved.

AGCMs have prescribed SST; they therefore lack SST biases and could possibly have smaller errors in the large-scale circulation when compared to coupled GCMs. AMIP integrations using standardized lower boundary conditions enable the identification of atmospheric model deficiencies and common features. However, the lack of two-way air-sea coupling in AGCM experiments may also introduce new systematic biases in some regions, with further feedbacks on circulation patterns (Wu and Kirtman, 2005; Wang et al., 2005). Wang et al. (2005) show that ocean-atmosphere coupling is important to the simulation of Asian-Pacific summer monsoon rainfall variability. The comparison between coupled and atmosphere-only simulations suggests that AMIP models better simulate the wind pattern in the western Pacific monsoon (Brown et al., 2013). Li and Xie (2014) suggest that the equatorial Pacific cold tongue bias in coupled models arises from wind biases resulting from interaction with the ocean via Bjerknes feedback. However, both coupled and uncoupled model simulations fail in reproducing observed precipitation over the tropics, suggesting that the representation of convection is likely to be a key source of error (Brown et al., 2013; Li and Xie, 2014; Ackerley et al., 2015).

In this chapter, we evaluate the CMIP5 model performance in reproducing the observed seasonal climate over the Maritime Continent, focusing mainly on the AMIP experiments. We quantify the model performance using two metrics that measure the magnitude of simulation errors and the degree of similarity between the observed and simulated field. To determine what aspects of the models are most important for correctly representing the Maritime Continent precipitation, our study investigates three potential sources of model systematic errors: the role of horizontal resolution, the relationship to errors in the mean meridional circulation and global monsoon, and the impact of air-sea coupling. This reveals a possible connection between global biases and local Maritime Continent biases. Next, we performed cluster analysis on the annual cycle of precipitation in the AMIP experiment of CMIP5 in order to group together models with common systematic errors and to determine if they are connected to particular features at the large scale.

The remainder of the chapter is organized as follows. We first describe the CMIP5 models and observational (reanalysis) data used in this study in Section 2.2. In Section 2.3, we assess the atmosphere-only model simulations of seasonal precipitation and low-level wind in the Maritime Continent. Section 2.4 investigates the possible sources of model bias. In Section

2.5, we present clustering analysis on the annual cycle of precipitation. Discussion is given in Section 2.6, followed by conclusions.

2.2 Data and methods

2.2.1 Models

The 30-year period (1979-2008) of AMIP experiments from 28 CMIP5 models is analysed in this study. These AMIP experiments are forced by the same prescribed SSTs and sea ice. The original horizontal resolution of the prescribed SST boundary conditions created by the Program For Climate Model Diagnosis and Intercomparison (PCMDI) is 1° longitude × 1° latitude. These underlying SST data are interpolated by individual modelling groups to a model's own resolution to perform the AMIP experiments. A general description of the AMIP boundary condition is presented in Taylor et al. (2012). Only models that submitted precipitation, zonal (u), meridional (v) and vertical (omega) components of wind to the database were selected for this study. The Maritime Continent domain in this study is defined covering ranges of latitude 20°S-20°N and longitude 80°E-160°E.

To determine the impact of SST biases and air-sea coupling on model performance in the Maritime Continent, we make a comparison between 22 coupled CMIP5 simulations and their corresponding AMIP simulations in Section 2.4.3. We also examine the fidelity of all 46 coupled GCMs in CMIP5 in simulating the Maritime Continent mean climate from 1979-2005 (the part of the coupled experiment that overlaps AMIP). These historical runs (coupled ocean-atmosphere) are forced by observed atmospheric composition changes in both anthropogenic and natural sources, and also include land use change (Taylor et al., 2012). We consider only one ensemble member from each CMIP5 model in this study. For brevity, the coupled simulations in CMIP5 will be denoted as "CMIP5" while the AMIP simulations with prescribed SST will be denoted as "AMIP5" hereafter.

Table 2.1 lists the model name, modelling centre, experiment type and horizontal resolution of these models. Detailed documentation of the CMIP5 models and experiments can be found at `http://cmip-pcmdi.llnl.gov/cmip5`. The monthly model data were bi-linearly interpolated to a common 3.75° longitude × 3° latitude grid for comparison with each other and with respect to observations and to enable computation of error statistics.

Table 2.1: CMIP5 model name, modelling centre, atmosphere horizontal resolution, experiment type and key references. CMIP5 models analysed later in Chapter 3 are marked with an asterisk (*).

Modelling centre	**Model name**	**Atmosphere horizontal resolution (° lon. × ° lat.)**	**Experiment**	**References**
BCC	BCC-CSM1.1	2.8×2.8	AMIP5 & CMIP5*	Wu et al. (2010)
BCC	BCC-CSM1.1(m)	1.1×1.1	AMIP5 & CMIP5*	Wu et al. (2010)
BNU	BNU-ESM	2.8×2.8	AMIP5 & CMIP5	Ji et al. (2014)
CCCma	CanAM4	2.8×2.8	AMIP5	von Salzen et al. (2013)
CCCma	CanESM2	2.8×2.8	CMIP5*	von Salzen et al. (2013)
CMCC	CMCC-CESM	3.75×3.7	CMIP5*	Scoccimarro et al. (2011)
CMCC	CMCC-CM	0.75×0.7	AMIP5 & CMIP5*	Scoccimarro et al. (2011)
CMCC	CMCC-CMS	1.875×1.8	CMIP5*	Scoccimarro et al. (2011)
CNRM-CERFACS	CNRM-CM5	1.4×1.4	AMIP5 & CMIP5	Voldoire et al. (2013)
CNRM-CERFACS	CNRM-CM5-2	1.4×1.4	CMIP5*	Voldoire et al. (2013)
CSIRO-BOM	ACCESS1-0	1.875×1.25	AMIP5 & CMIP5*	Bi et al. (2013), Dix et al. (2013)
CSIRO-BOM	ACCESS1-3	1.875×1.25	AMIP5 & CMIP5*	Bi et al. (2013), Dix et al. (2013)
CSIRO-QCCCE	CSIRO-Mk3-6-0	1.9×1.9	AMIP5 & CMIP5*	Gordon et al. (2010), Rotstayn et al. (2012)
FIO	FIO-ESM	2.8×2.8	CMIP5*	
ICHEC	EC-EARTH	1.1×1.1	CMIP5*	Hazeleger et al. (2010)
INM	INM-CM4	2.0×1.5	AMIP5 & CMIP5*	Volodin et al. (2010)
IPSL	IPSL-CM5A-LR	3.75×1.875	AMIP5 & CMIP5*	Dufresne et al. (2013)
IPSL	IPSL-CM5A-MR	2.5×1.25	AMIP5 & CMIP5*	Dufresne et al. (2013)
IPSL	IPSL-CM5B-LR	3.75×1.875	AMIP5 & CMIP5*	Dufresne et al. (2013), Hourdin et al. (2013)
LASG-IAP	FGOALS-s2	2.8×1.7	AMIP5	Bao et al. (2013)
LASG-CESS	FGOALS-g2	2.8×2.8	AMIP5 & CMIP5*	Li et al. (2013)
MIROC	MIROC4h	0.56×0.56	CMIP5	Sakamoto et al. (2012)
MIROC	MIROC5	1.4×1.4	AMIP5 & CMIP5*	Watanabe et al. (2011)
MIROC	MIROC-ESM	2.8×2.8	CMIP5	Watanabe et al. (2011)
MIROC	MIROC-ESM-CHEM	2.8×2.8	CMIP5*	Watanabe et al. (2011)
MOHC	HadCM3	3.7×2.5	CMIP5*	Collins et al. (2001)
MOHC	HadGEM2-A	1.875×1.25	AMIP5	Collins et al. (2008)
MOHC	HadGEM2-ES	1.875×1.25	CMIP5*	Collins et al. (2011)
MPI-M	MPI-ESM-LR	1.9×1.9	AMIP5 & CMIP5*	Stevens et al. (2013), Raddatz et al. (2007)
MPI-M	MPI-ESM-MR	1.9×1.9	AMIP5 & CMIP5*	Stevens et al. (2013), Raddatz et al. (2007)
MPI-M	MPI-ESM-P	1.9×1.9	CMIP5*	Stevens et al. (2013), Raddatz et al. (2007)
MRI	MRI-AGCM3-2H	0.6×0.6	AMIP5	Mizuta et al. (2012)
MRI	MRI-AGCM3-2S	0.2×0.2	AMIP5	Mizuta et al. (2012)
MRI	MRI-CGCM3	1.1×1.1	AMIP5 & CMIP5*	Yukimoto et al. (2012)
MRI	MRI-ESM1	1.1×1.1	CMIP5*	Yukimoto et al. (2012)
NASA-GISS	GISS-E2-H	2.5×2.0	CMIP5*	Schmidt et al. (2006)
NASA-GISS	GISS-E2-H-CC	2.5×2.0	CMIP5*	Schmidt et al. (2006)

Table 2.1 (continued)

Modelling centre	Model name	Atmosphere horizontal resolution (° lon. × ° lat.)	Experiment	References
NASA-GISS	GISS-E2-R	2.5×2.0	AMIP5 & CMIP5*	Schmidt et al. (2006)
NASA-GISS	GISS-E2-R-CC	2.5×2.0	CMIP5*	Schmidt et al. (2006)
NCAR	CCSM4	1.25×0.9	AMIP5 & CMIP5*	Gent et al. (2011)
NCC	NorESM1-M	2.5×1.9	AMIP5 & CMIP5*	Bentsen et al. (2013)
NCC	NorESM1-ME	2.5×1.9	CMIP5*	Bentsen et al. (2013)
NIMR-KMA	HadGEM2-AO	1.875×1.25	CMIP5*	Martin et al. (2011)
NOAA-GFDL	GFDL-CM2p1	2.5×2.0	CMIP5*	Donner et al. (2011)
NOAA-GFDL	GFDL-CM3	2.5×2.0	AMIP5 & CMIP5*	Donner et al. (2011)
NOAA-GFDL	GFDL-ESM2G	2.5×2.0	CMIP5*	Donner et al. (2011)
NOAA-GFDL	GFDL-ESM2M	2.5×2.0	CMIP5*	Donner et al. (2011)
NOAA-GFDL	GFDL-HIRAM-C180	0.625×0.5	AMIP5	Zhao et al. (2009)
NOAA-GFDL	GFDL-HIRAM-C360	0.3×0.3	AMIP5	Zhao et al. (2009)
NSF-DOE-NCAR	CESM1-BGC	1.2×0.9	CMIP5*	Vertenstein et al. (2013)
NSF-DOE-NCAR	CESM1-CAM5	1.2×0.9	CMIP5*	Vertenstein et al. (2013)
NSF-DOE-NCAR	CESM1-FASTCHEM	1.2×0.9	CMIP5*	Vertenstein et al. (2013)
NSF-DOE-NCAR	CESM1-WACCM	2.5×1.9	CMIP5*	Vertenstein et al. (2013)

The multi-model mean (MMM) is obtained by taking a simple arithmetic average of climate variables among the 28 AMIP5 models. We have also calculated the 46 CMIP5 model MMM as well as the MMM of the 22 overlapping AMIP5 and CMIP5 models respectively for comparison in Section 2.4.3. The overall performance of AMIP5 and CMIP5 models is determined based on the MMM skill scores (see Section 2.2.3). In this thesis, we treat all models equally and use the unweighted multi-model mean approach. Although some of the models are different versions of the same model or share a common component and therefore might share some common biases, the interdependency of CMIP5 models is difficult to characterize and not necessarily dependent on modelling group. Models from different institutions that share common components have similar biases, while on the other hand models from the same institution but with different physics settings, for instance, could have very different model biases (Boé, 2018). Some other choice of weighting models in a multi-model mean would have to be justified by evidence, and such an exercise is beyond the scope of this thesis. While not necessarily ideal, an equally weighted multi-model approach is common in the literature analysing CMIP5 models.

2.2.2 Observations

Precipitation data from the Global Precipitation Climatology Project (GPCP) of the 30-year period from 1979 to 2008 are used in this study to validate the models. This dataset consists of a combination of rain gauges, satellites and sounding observations that have been merged to estimate monthly rainfall on a 2.5-degree global grid (Adler et al., 2003). Two additional observational precipitation datasets: 1) monthly precipitation from 1979 to 2008 on a 2.5-degree global grid from the Climate Prediction Center (CPC) merged analysis of precipitation (CMAP) dataset (Xie and Arkin, 1997) and 2) tropical rainfall measuring mission (TRMM) 3B43 monthly precipitation from 1997 to 2008 at 0.25°resolution (Huffman et al., 2007) are used to determine whether there is any sensitivity in our results to the choice of GPCP as the main observational dataset. The differences between the three precipitation datasets are small. Our analysis also shows that the results are not dependent on the choice of observational dataset. Therefore GPCP is chosen as the primary reference dataset in this study.

The zonal, meridional and vertical components of wind data on a 0.7-degree grid for the same period were obtained from the ERA-Interim reanalysis data produced by the European Centre for Medium-Range Weather Forecasts (ECMWF) (Dee et al., 2011) for validation on various pressure levels.

These monthly precipitation and wind observations (reanalysis) data were bilinearly interpolated to the common 3.75° longitude $\times$ 3° latitude grid for comparison with the model simulations.

2.2.3 Skill scores and correlation analyses

We have used two metrics to evaluate the model performance in simulating the Maritime Continent seasonal climate. The pattern correlation coefficient (PCC) is calculated to measure the degree of similarity in the spatial patterns between the observed and simulated fields. The root mean square error (RMSE) is used to measure the magnitude of simulation errors.

Correlation analyses are used to assess the relationship between different biases, for example between local (Maritime Continent) precipitation biases and biases in the global monsoon and circulation. We computed the Pearson correlation coefficient (r) to measure the strength of the association and the direction of a linear relationship between the two biases in the set of models. However, as the Pearson correlation is sensitive to outliers, we have also calculated the Spearman's rank correlation coefficient which is more robust. The Spearman's rank is the non-parametric version of the Pearson correlation calculated using the ranks of data. The correlation coefficients from the two methods show some differences. However, only results from Spearman's rank correlation are shown except in Fig. 2.3 and 2.17 where both coefficients are shown.

2.2.4 Moisture Flux Convergence (MFC)

The precipitation can be expressed as the sum of vertically-integrated MFC and evaporation. In Section 2.3, the horizontal MFC for observations and AMIP5 is calculated using the equations below:

$$MFC = -V_h \cdot \nabla q - q \nabla \cdot V_h \tag{2.1}$$

$$MFC = \underbrace{-u\frac{\partial q}{\partial x} - v\frac{\partial q}{\partial y}}_{\text{advection term}} \underbrace{- q(\frac{\partial u}{\partial x} + \frac{\partial v}{\partial y})}_{\text{convergence term}} \tag{2.2}$$

where the advection term represents the horizontal advection of specific humidity (q) and the convergence term represents the product of specific humidity and horizontal mass convergence (Banacos and Schultz, 2005). The MFC is vertically integrated over the depth of the atmosphere from the surface to 100hPa and denoted as VIMFC (vertical-integrated MFC) in this study. For observations, we use the specific humidity, zonal (u) and meridional (v) winds from ERA-interim reanalysis data to calculate the MFC.

2.2.5 Global monsoon metric

In Section 2.4.2, we will examine two annual cycle modes of the climatological monthly mean precipitation using an approach adapted from Wang and Ding (2008) (see Section 1.2.2). In their study, Wang and Ding (2008) showed that the difference between solsticial seasons (JJAS minus DJFM) and the difference between equinoctial seasons (AM minus ON) can be used as simple metrics of the seasonal cycle of global monsoon precipitation. In this study, for consistency with the seasons used in other aspect of our analyses, the solsticial mode of the annual cycle is calculated by taking the JJA mean minus DJF mean precipitation and the equinoctial mode is calculated by taking the MAM mean minus the SON mean precipitation over the domain 45°S-45°N and 0°-360°E, as in Zhou et al. (2016).

2.2.6 Cluster analysis

Hierarchical clustering analysis of Maritime Continent annual cycle precipitation was performed to characterize the model systematic biases in AMIP5 by grouping together models that are similar (Section 2.5). From the clustering analysis, we investigate the biases in groups of models to see if they pertain to common features in the large-scale atmosphere. We used the Euclidean distance metric (the square root of the sum of square distances) to measure the similarity between each model using the time-latitude mean precipitation, zonally averaged between 80°E and 160°E (refer to Fig. 2.9). The Euclidean distance between two models A

and B is defined as:

$$d(A,B) = \sqrt{\sum_i \sum_j (A_{i,j} - B_{i,j})^2} \tag{2.3}$$

where i and j are the latitude and month respectively (Wilks, 2011).

The two models with closest similarity in Maritime Continent annual cycle precipitation averaged between 80°E and 160°E are merged to form a new cluster based on a defined criterion and linkage method. The process is repeated until all models are merged into one cluster. The optimum number of clusters is chosen based on a cut-off point (threshold value) when there is a sudden increase in the distance value which reflects that the clusters that were joined were relatively far apart.

To ensure the robustness of the results, we have tested six linkage methods (not shown) to cluster the similarity between the 28 models. The six methods are single, complete, average, centroid, Ward's and weighted linkage. We chose complete linkage for our analysis in this study based on the agreement of its results with other methods, and it also produced a better cluster around the central value with smaller variance. In this method, the distance between two clusters is defined as the maximum distance between any two models when one model is chosen from each cluster and all possible pairs are compared (Wilks, 2011).

2.3 AMIP5 model evaluation

In this section, we examine the AMIP5 model performance in reproducing the seasonal climate, particularly focusing on the winter (DJF) and summer monsoons (JJA).

Seasonal mean GPCP precipitation and ERA-Interim mean 850 hPa wind over the Maritime Continent are shown in Fig. 2.1a and Fig. 2.2a. The Maritime Continent receives an abundance of rainfall throughout the year. However, there are pronounced seasonal variations in precipitation and wind patterns. The ITCZ, where the trade winds from the Northern Hemisphere converge with those from the Southern Hemisphere throughout the year, moves northward in boreal summer and shifts to the south in boreal winter. The annual cycle of monsoons are generated as part of the large-scale movement of the ITCZ in its passage from the Southern to Northern Hemisphere and back. The GPCP observed seasonal precipitation shows that the central and southern part of the Maritime Continent receives substantial precipitation during the (boreal) winter monsoon and less rainfall during the summer monsoon. In contrast, the Maritime Continent region north of 10°N (Myanmar, Thailand, Laos, Vietnam, Cambodia and the Philippines) experiences a dry season during the winter monsoon and a wet season during the summer monsoon. The seasons between the summer monsoon and winter monsoon are known as intermonsoon seasons (not shown).

In DJF, most models exhibit wet biases over the West Pacific Ocean except for four models: BCC-CSM1-1 (Fig. 2.1e), BCC-CSM1-1m (Fig. 2.1f), IPSL-CM5B-LR (Fig. 2.1w) and MRI-

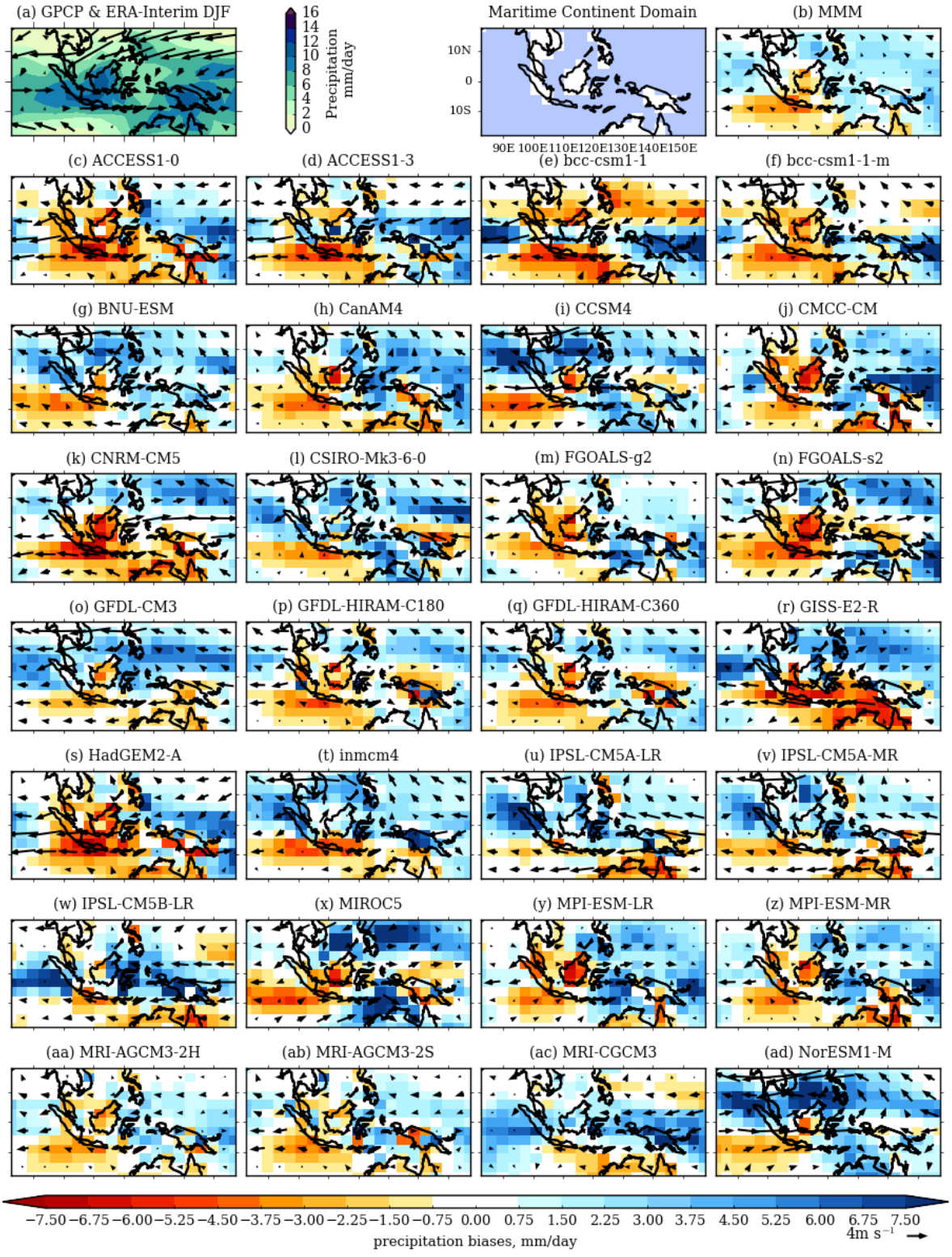

Figure 2.1: DJF precipitation (mm/day) and 850 hPa wind (m s^{-1}) for (a) GPCP and ERA-interim, (b) MMM biases and (c)-(ad) AMIP5 biases for 1979-2008 over the Maritime Continent region (20°S-20°N, 80°E-160°E). Third panel shows the Maritime Continent domain and land-sea mask.

CGCM3 (Fig. 2.1ac). About two-thirds of the models underestimate the precipitation over the land. This can be seen from the MMM (Fig. 2.1b) whereby most of the land has dry biases except for the islands of Sulawesi, New Guinea and the Philippines. The dry biases over land are associated with easterly wind biases over the region. This easterly wind bias and its associated dry bias is a common error in the atmosphere-only models. Models are able to capture the reversal of Australian monsoonal circulation from low-level westerly winds in DJF (Fig. 2.1) to easterlies in JJA (Fig. 2.2) over northern Australia. However, most of the models simulate weaker westerlies over northern Australia in DJF, while a few models such as CCSM4 (Fig. 2.1i), CSIRO-Mk3-6-0 (Fig. 2.1l), GFDL-HIRAM-360 (Fig. 2.1q), MIROC5 (Fig. 2.1x) and NorESM1-M (Fig. 2.1ad)), simulate stronger westerlies and wet biases over northern Australia.

Biases in JJA aren't very consistent, i.e. the MMM bias is small compared to individual model biases. Models are more consistent in DJF, especially over the southern Maritime Continent. A notable difference between DJF and JJA seasons is the more common presence of large biases of precipitation over the Maritime Continent north of 10°N in JJA (Fig. 2.2) as compared to DJF, indicating that the models simulate the monsoonal precipitation poorly. In JJA, BNU-ESM (Fig. 2.2g), CSIRO-Mk3-6-0 (Fig. 2.2l), IPSL-CM5A-LR (Fig. 2.2u), IPSL-CM5A-MR (Fig. 2.2v) and NorESM1-m (Fig. 2.2ad) models simulate weaker westerlies over the Maritime Continent north of 10°N whereas other models simulate overly strong westerlies that extend too far east into the West Pacific Ocean as shown in Fig. 2.2. These biases are consistent with precipitation biases, with weak westerlies associated with underestimation of the precipitation while strong westerlies increase the moisture supply and lead to overestimation of precipitation over the Maritime Continent north of 10°N and West Pacific. This also implies that stronger westerlies to the north in JJA are also a response to a stronger monsoon.

Our result agrees with Ackerley et al. (2015), who found that the austral summer precipitation biases over northern Australia in AMIP5 simulations are linked to the low-level winds. Models that overestimate the northern Australian precipitation have mean northerly flow between 120° and 150°E, which transports moisture from the ocean, whereas other models that underestimate the precipitation have mean southerly flow across the same range of longitudes. We next use correlation analyses to determine the relationship between the PCC of precipitation and 850 hPa wind across the suite of models, as well as the RMSE.

The PCC and RMSE are calculated with respect to GPCP precipitation and ERA-Interim 850 hPa winds (zonal and meridional components) over the Maritime Continent domain (20°S-20°N, 80°E-160°E) in winter and summer seasons and are listed in Table 2.2. The text in bold highlights the best performing models showing either highest PCC or lowest RMSE. Three models (MRI-AGCM3-2S, MRI-AGCM3-2H and MRI-CGCM3) from the same centre capture the spatial pattern of the precipitation in DJF with PCC higher than 0.8

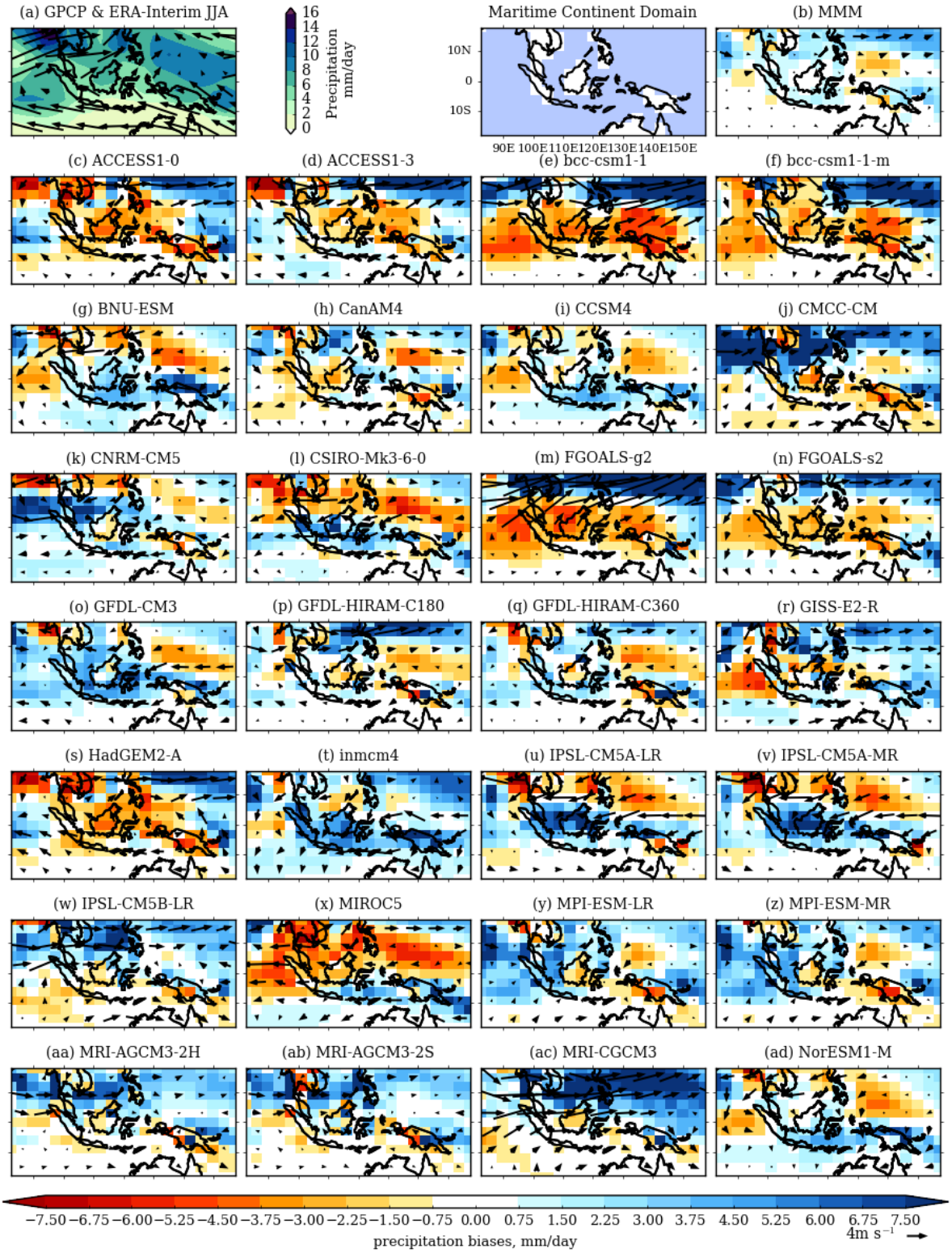

Figure 2.2: JJA precipitation (mm/day) and 850 hPa wind (m s^{-1}) for (a) GPCP and ERA-interim, (b) MMM biases and (c)-(ad) AMIP5 biases for 1979-2008 over the Maritime Continent region (20°S-20°N, 80°E-160°E). Third panel shows the Maritime Continent domain and land-sea mask.

Table 2.2: PCC and RMSE skill scores for annual cycle climatologies of precipitation, DJF and JJA seasonal mean precipitation with respect to GPCP and 850 hPa wind with respect to ERA-Interim. All PCCs are statistically significant with a p-value less than 0.01. The AMIP5 models are sorted in alphabetical order. The top 5 models with the highest PCC and lowest RMSE are highlighted in bold. The MMM is highlighted in italic bold and also has higher PCC and lower RMSE than the individual models. The models are ranked approximately in terms of horizontal resolution (from highest to lowest) as shown in the first column. PCCs and RMSEs of CMAP and TRMM with respect to GPCP are listed in the bottom two rows to indicate observational uncertainty.

Resolution ranking number	Model name / observational datasets	Annual cycle precipitation		DJF precipitation		DJF 850 hPa wind		JJA precipitation		JJA 850 hPa wind	
		PCC	RMSE	PCC	RMSE	PCC	RMSE	PCC	RMSE	PCC	RMSE
11	ACCESS1-0	0.923	**1.156**	0.678	2.888	0.885	1.705	0.715	3.316	0.914	1.680
12	ACCESS1-3	0.923	1.466	**0.764**	2.695	0.894	1.869	0.664	3.518	0.903	1.323
25	bcc-csm1-1	0.843	2.147	0.735	3.214	0.848	1.922	0.646	4.707	0.841	1.406
7	bcc-csm1-1-m	0.930	**1.174**	0.751	2.646	0.921	1.546	0.686	3.623	0.911	1.496
26	BNU-ESM	0.908	1.209	0.761	2.418	0.875	2.062	0.712	**2.480**	0.938	1.747
27	CanAM4	0.933	**1.097**	0.697	2.703	**0.941**	1.319	0.816	**2.130**	0.952	1.638
6	CCSM4	0.911	1.305	0.646	3.115	0.886	2.414	**0.818**	**2.042**	**0.969**	1.331
5	CMCC-CM	0.889	2.102	0.677	2.961	0.938	**1.069**	0.683	5.563	0.947	1.636
9	CNRM-CM5	0.811	1.720	0.487	2.801	0.820	2.168	0.683	2.802	0.938	2.311
16	CSIRO-Mk3-6-0	0.876	1.417	0.740	2.934	0.907	1.647	0.674	2.738	0.934	1.730
28	FGOALS-g2	0.770	3.231	**0.790**	**2.272**	0.928	1.357	0.612	8.062	0.855	3.019
20	FGOALS-s2	0.818	1.952	0.560	3.094	0.888	2.068	0.744	3.306	0.920	1.858
22	GFDL-CM3	0.912	1.532	0.734	2.581	0.877	2.129	0.753	**2.721**	0.962	1.521
3	GFDL-HIRAM-C180	0.937	**1.136**	0.753	**2.294**	**0.945**	1.331	0.736	3.320	0.949	1.128
2	GFDL-HIRAM-C360	**0.938**	**1.050**	0.727	2.523	**0.958**	1.195	0.727	2.961	**0.970**	**1.094**
21	GISS-E2-R	0.879	1.832	0.540	3.422	0.803	1.874	0.789	3.345	0.952	1.599
13	HadGEM2-A	0.918	1.183	0.660	3.005	0.872	1.819	0.694	3.313	0.902	1.789
14	inmcm4	0.919	2.014	0.696	2.768	0.873	1.825	0.766	3.424	0.941	1.447
23	IPSL-CM5A-LR	0.897	1.435	0.727	2.585	0.794	2.251	0.642	2.971	0.907	1.921
15	IPSL-CM5A-MR	0.893	1.349	0.724	**2.372**	0.846	1.901	0.630	2.933	0.920	1.857
24	IPSL-CM5B-LR	0.934	1.932	0.730	3.550	0.876	1.612	**0.843**	2.985	0.912	1.370
10	MIROC5	0.765	2.001	0.516	3.638	0.907	1.626	0.521	3.750	0.918	1.419
17	MPI-ESM-LR	**0.960**	1.196	0.715	2.846	0.940	**1.073**	0.780	3.083	**0.971**	**0.876**
18	MPI-ESM-MR	**0.951**	1.320	0.698	2.726	0.938	**1.052**	0.790	3.012	**0.966**	**0.934**
4	MRI-AGCM3-2H	**0.953**	1.235	**0.858**	**1.792**	**0.967**	**0.900**	**0.862**	2.987	**0.966**	**0.857**
1	MRI-AGCM3-2S	**0.953**	1.191	**0.801**	**2.134**	**0.958**	**1.027**	**0.838**	3.400	**0.976**	**0.653**
8	MRI-CGCM3	0.931	2.390	**0.816**	3.251	**0.941**	1.162	**0.824**	4.633	0.868	1.649
19	NorESM1-M	0.884	1.575	0.657	3.427	0.859	2.899	0.772	**2.243**	0.955	1.784
	MMM	***0.968***	***0.960***	***0.845***	***1.811***	***0.956***	***1.051***	***0.901***	***1.829***	***0.973***	***0.950***
	CMAP	0.987	0.962	0.934	1.405			0.911	1.872		
	TRMM	0.988	0.832	0.955	1.048			0.952	1.822		

as shown in Table 2.2. In JJA, five models (CCSM4, IPSL-CM5B-LR, MRI-AGCM3-2S, MRI-AGCM3-2H and MRI-CGCM3) capture the spatial pattern of the precipitation (PCC > 0.8). A few models such as CMCC-CM and F-GOALS-g2 have a substantial RMSE of more than 5 mm/day with particularly large precipitation errors over the region north of 10°N in JJA. For the 850 hPa wind, most models can adequately simulate the spatial pattern of low-level winds, with nearly half of the models having PCC scores higher than 0.9 in DJF and only two models (FGOALS-g2 and MRI-CGCM3) having PCC scores less than 0.9 in JJA. In terms of magnitude of simulation errors, only the MMM and MRI-AGCM3-2H have RMSE less than 2 m s^{-1} in DJF. Most models have higher RMSE in JJA compared to DJF.

The MMMs for precipitation have higher PCC and lower RMSE scores than almost all individual models for all seasons. The MMMs also have PCC above 0.8 for both precipitation and low-level wind in all seasons. The better performance of the MMM in reproducing the observed mean precipitation is in agreement with other CMIP5 studies (Colman et al., 2011; Jourdain et al., 2013; Sperber et al., 2013; Feng et al., 2014) which found that the MMM outperforms individual models at reproducing the observed monsoon climate.

To condense the information from the spatial performance skill scores of all the models and compare them for different fields, we plot scatter diagrams of precipitation PCC and 850 hPa wind PCC in Fig. 2.3a and also the RMSE skill scores for the same fields in Fig. 2.3b (in other words, we generate scatter plots using pairs of columns from Table 2). The Pearson correlation coefficients (r) and Spearman's rank correlation coefficients (sr) in the scatter plot of precipitation and 850 hPa wind in Fig. 2.3 suggest that the modeled precipitation biases are somewhat linked to the zonal and meridional circulation at 850 hPa, consistent with Sperber et al. (2013) for the Asian Monsoon region. The two correlation coefficients are comparable except for JJA and SON RMSE, as JJA and SON precipitation RMSE scores feature a number of model outliers with substantial biases of more than 4mm/day and the Pearson correlation is sensitive to outliers. We will therefore use the Spearman's rank correlation in the remaining sections. The PCC values correlate better ($>$0.45) than the RMSE except for MAM season, which is low for both. The positive linear relationship reflects the intrinsic moisture transport link between precipitation and winds in the tropics.

The PCC in Fig. 2.3a also shows that the 850 hPa wind is better simulated than the precipitation in all four seasons, as found by Brown et al. (2013) over the Western Pacific monsoon region and by Sperber et al. (2013) over the Asian monsoon region. This makes sense since one might expect the large-scale flow, which is resolved, to be represented better than rainfall, which is parameterized.

Both the RMSE and PCC in Fig. 2.3 and Table 2.2 also show that the magnitude and spatial distribution of the biases vary in each model according to season, i.e, models that perform less well in one season do not necessarily poorly represent other seasons. For example FGOALS-g2 captures the DJF precipitation but poorly simulates the JJA precipitation. GISS-E2-R

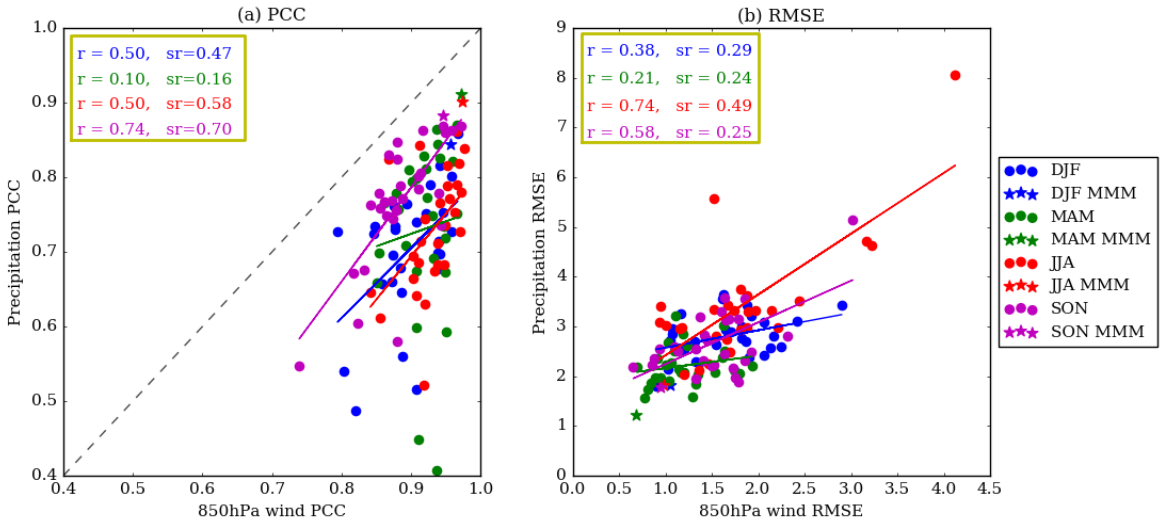

Figure 2.3: Scatter plot of the AMIP5 seasonal mean (a) PCC and (b) RMSE of Maritime Continent (20°S-20°N, 80°E-160°E) precipitation versus 850 hPa winds (u, v) for each season. The Pearson correlation coefficient (*r*) and Spearman's rank correlation coefficient (*sr*) for each season are shown in the yellow box on the top left corner. Both correlation coefficients for PCC and *r* for RMSE are statistically significant with a p-value less than 0.05 for most seasons except for MAM. For RMSE Spearman's rank correlation, only JJA *sr* is statistically significant with a p-value less than 0.05.

performs poorly in simulating DJF (PCC 0.540) precipitation over the Maritime Continent but simulates other seasons well (PCC >0.7). MRI-AGCM3-2S and MRI-AGCM3-2H capture both the precipitation and low-level winds in all seasons.

Next, we examine the AMIP5 VIMFC biases (Fig. 2.4b-ad, Fig. 2.5b-ad) over the Maritime Continent with respect to observed seasonal mean VIMFC in DJF (Fig. 2.4a) and JJA (Fig. 2.5a). Positive VIMFC are mainly found over the central and southern parts of the Maritime Continent in DJF, while during JJA, positive VIMFC are confined to the northern and central parts of the Maritime Continent, consistent with the area that receives maximum precipitation during DJF (Fig. 2.1a) and JJA (Fig. 2.2a). The 200 hPa divergent winds show upper-level divergence over the central Maritime Continent in DJF and over northern parts in JJA corresponding to the deep convection and heavy precipitation over this region.

In general, the VIMFC biases (Fig. 2.4, Fig. 2.5) over the Maritime Continent are somewhat consistent with the precipitation biases (Fig. 2.1, Fig. 2.2). In DJF, most models such as ACCESS1-3 (Fig. 2.4d), bcc-csm1-1 (Fig. 2.4e), CNRM-CM5 (Fig. 2.4k) and GISS-E2-R(Fig. 2.4r) show similar VIMFC spatial patterns with precipitation biases. However, there are some discrepancies, in particular in regions with near-zero rainfall biases or small positive precipitation biases: there are sometimes positive VIMFC biases (moisture flux divergence). For example, FGOALS-g2 (Fig. 2.4m), HadGEM2-A (Fig. 2.4s) and MRI-AGCM3-2S (Fig. 2.4ab) show positive VIMFC biases over the West Pacific, which have wet

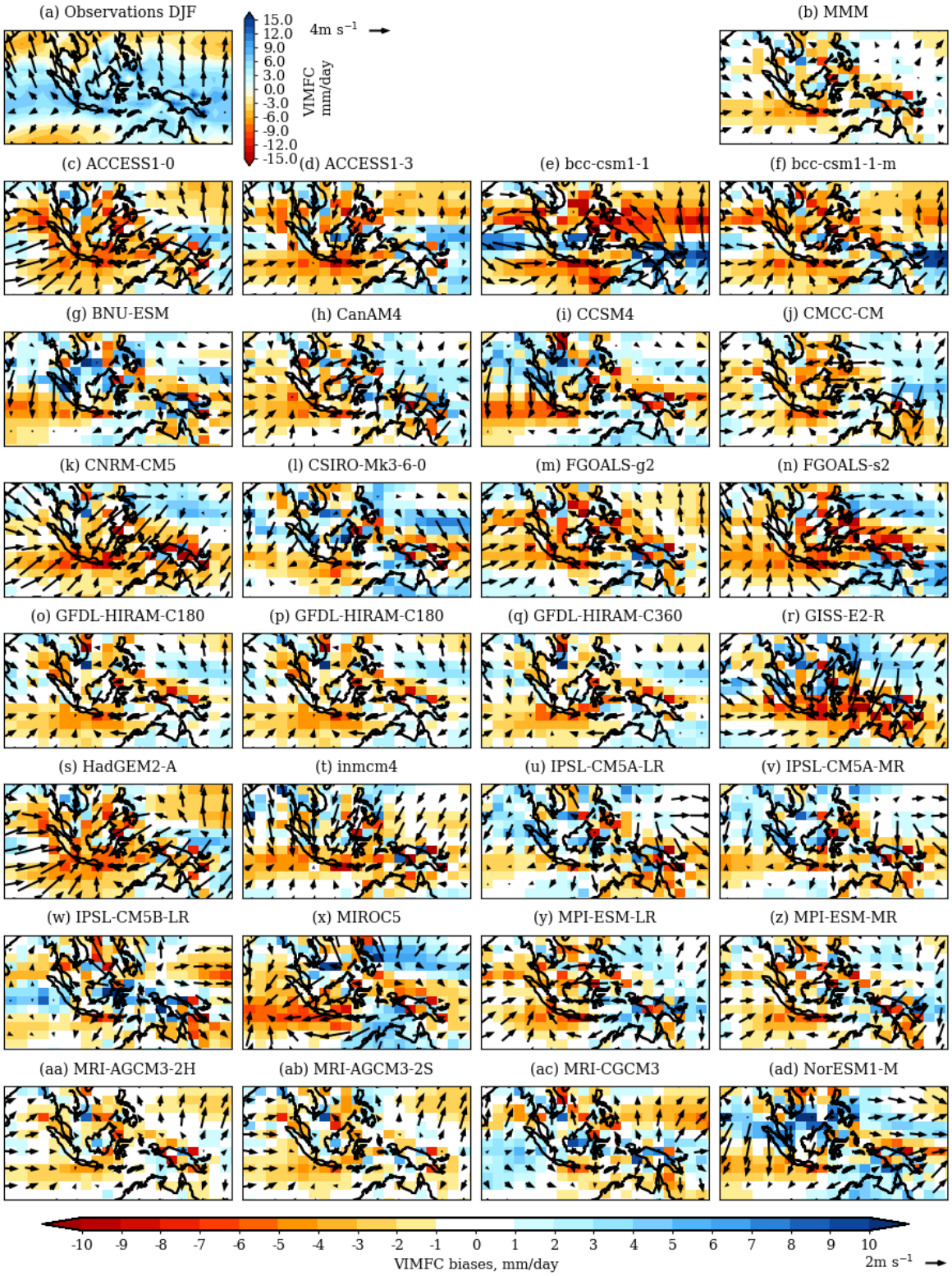

Figure 2.4: DJF VIMFC (mm/day) and 200 hPa divergent winds (vectors, m s^{-1}) for (a) observations (ERA-interim), (b) MMM biases and (c)-(ad) AMIP5 biases for 1979-2008 over the Maritime Continent region (20°S-20°N, 80°E-160°E).

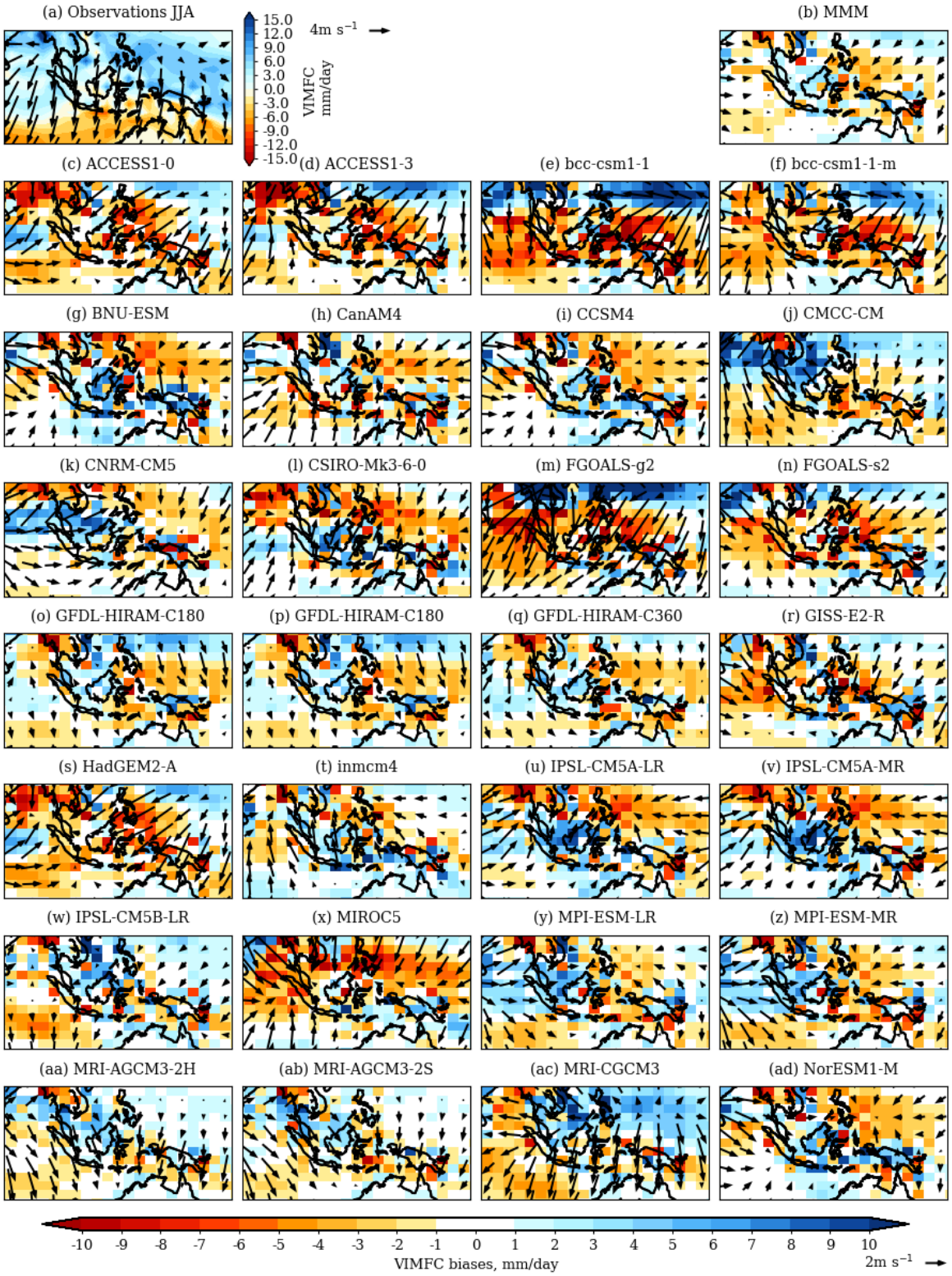

Figure 2.5: JJA VIMFC (mm/day) and 200 hPa divergent winds (vectors, m s^{-1}) for (a) observations (ERA-interim), (b) MMM biases and (c)-(ad) AMIP5 biases for 1979-2008 over the Maritime Continent region (20°S-20°N, 80°E-160°E).

biases (cf. Fig. 2.1). The divergent circulation also shows upper-level convergence over this region. This discrepancy may occur because GPCP observations are used for precipitation and ERA-Interim for calculating VIMFC in this study. We found that VIMFC biases in JJA also resemble the precipitation biases over the Maritime Continent. Our results suggest that VIMFC biases largely account for the precipitation biases over the Maritime Continent for both seasons.

2.4 Investigating potential sources of model biases

In this section, we will analyse how the performance of models over the Maritime Continent depends on model characteristics, such as resolution, or on the representation of global monsoon. This may give us insights as to what aspects of the models are most important in order to correctly represent the climate of the Maritime Continent. We focus on three possible sources of the Maritime Continent precipitation biases: the role of horizontal resolution, the relationship to biases in the local Hadley circulation and global monsoon, and the presence or lack of air-sea coupling.

2.4.1 Sensitivity of simulated mean climate to AMIP5 model resolution

In this section, we will assess the sensitivity of Maritime Continent precipitation to climate model resolution. Among the 28 AMIP5 models in this study, the highest horizontal resolution is $0.2° \times 0.2°$, while the lowest resolutions are as coarse as $3.7° \times 1.9°$ and $2.8° \times 2.8°$ (refer to Table 2.1). The monthly Maritime Continent precipitation values were bi-linearly interpolated to a common $3.75° \times 3°$grid for the calculation of model skill scores.

More than half of the highlighted top 5 models with the highest PCC and lowest RMSE scores in Table 2.2 are from the higher resolution models, which are models with ranking number 1-6 in horizontal resolution, sorted from highest to lowest in Table 2.2. This suggests that the highest resolution models have lower biases on average, although these models may also have other advantages independent of resolution.

We assess the sensitivity of Maritime Continent precipitation to climate model resolution by dividing the models into 3 categories, which are the 6 models with the highest resolutions (blue lines), the 6 models with the lowest resolutions (red lines) and the remaining 16 models at intermediate resolutions (grey lines), as shown in Fig. 2.6a. The individual model monthly precipitation PCCs in Fig. 2.6a suggest that not all high resolution models produce better precipitation simulations and vice versa. The same calculations performed over the land-only precipitation and sea-only precipitation model skill scores (both PCC and RMSE) also show no clear relationship between resolution and model performance (not shown). A comparison between model pairs from the same institution with different resolutions in Fig. 2.6b shows that only the BCC-CSM1-1m model with higher resolution performs better than its corresponding

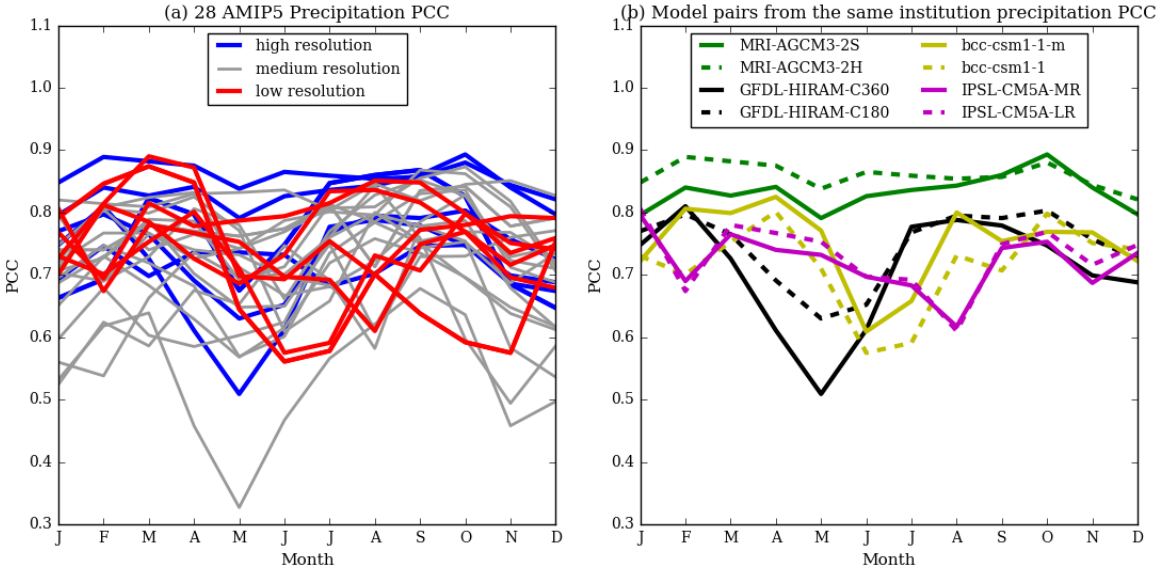

Figure 2.6: Maritime Continent monthly precipitation (a) PCC for all 28 models divided into high (blue lines), medium (grey lines) and low resolution (red lines) groups and (b) PCC for 8 models, where each pair of models belong to the same institution and solid lines represent the higher resolution versions while dashed lines represent the lower resolution versions.

lower resolution version, whereas the other lower resolution models perform better than their corresponding higher resolution versions in most months. This suggests that the cause of deficiencies is largely unrelated to resolution, although these model pairs may have other differences in addition to resolution.

To check the impact of the choice of common grid size in the re-gridding procedure, the main analysis in this section was repeated with models interpolated to a common 2.5°$\times$ 2.5°grid (intermediate resolution), consistent with that of the GPCP observational dataset. Changes to the results were small: the PCC values change by less than 0.05, while analysis of the simulated mean climate when re-gridded to this intermediate resolution (figure not shown) also reveals no resolution dependence.

This demonstrates that the choice of precipitation re-gridding is unlikely to contribute to the absence of sensitivity to the resolution of atmospheric models. If resolution were having an impact at these climate model scales, then we would expect the improvements to rectify onto the mean state, even when re-gridded to a lower resolution. For example, a newly-resolved mountain range or island at higher resolution may help to initiate convection during the diurnal cycle. Even when the output is upscaled to a coarser resolution, this would still be measurable in the mean state.

2.4.2 Mean meridional circulation and the global monsoon

Wang et al. (2014) found that ascent in the tropics also influences subsidence over the

subtropics in the Hadley circulation and suggested that remote biases are linked to regional biases. To investigate if errors in the local scale over the Maritime Continent are related to errors in the large-scale movement of the ITCZ, we will assess local Hadley circulation and the global monsoon biases and their relationship with Maritime Continent precipitation biases.

3.4.2.1 Mean meridional circulation

The ERA-Interim mean meridional circulation over the Maritime Continent in Fig. 2.7a,d shows seasonal variability in the intensities and locations of the ascending and descending branches of the local Hadley cell. In winter, the ascending branch is located around 5°S while during summer, a broader ascending branch is located around 15°N. In general, most of the models produce a similar structure and location of the local Hadley circulation with respect to ERA-Interim in all four seasons, as depicted in MMM in Figure 2.7b and 2.7f. The model with lowest RMSE, MPI-ESM-LR, is able to reproduce the Hadley Circulation with PCC above 0.9 for winter (Fig. 2.7c) and summer (Fig. 2.7g) monsoons.

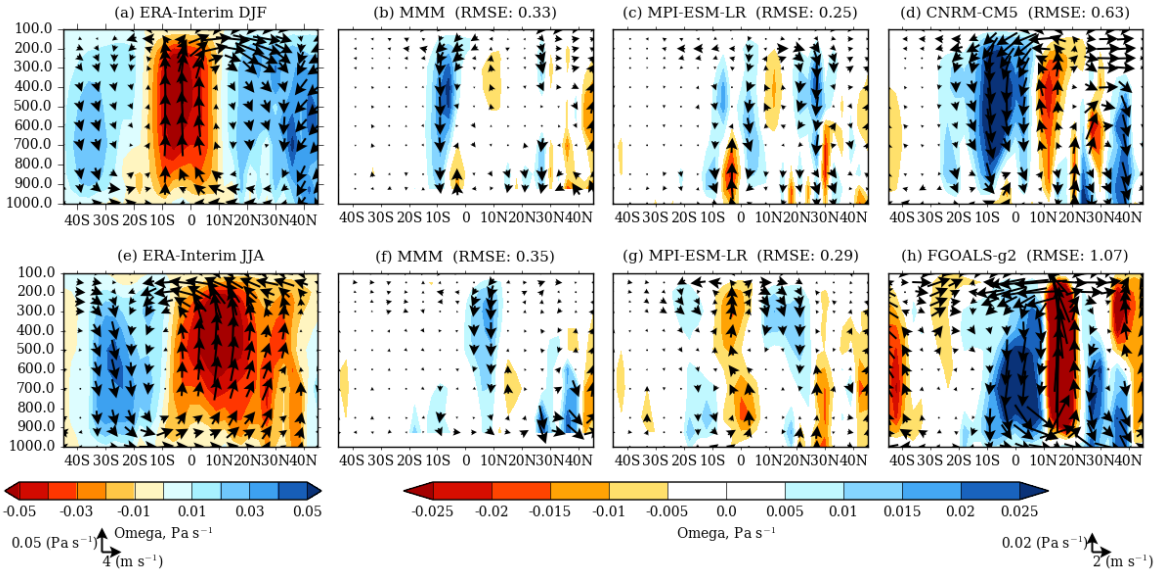

Figure 2.7: DJF mean meridional circulation averaged over the Maritime Continent region (80°E to 160°E) using omega (shading and vectors, Pa s^{-1}) and v (vectors, m s^{-1}) from (a) ERA-Interim, (b) MMM, (c) the AMIP5 model with lowest RMSE and (d) the AMIP5 model with highest RMSE. (e)-(h) are as in (a)-(d) but for JJA season. RMSE between observed and simulated local Hadley Circulation is above each panel.

The location of the ascending branch of the local Hadley circulation is consistent with the seasonal shift of the ITCZ and maximum precipitation. The reduced ascent over the Maritime Continent in CNRM-CM5 (Fig. 2.7d) and MMM (Fig. 2.7b is connected with dry biases over the Maritime Continent in DJF. The overly strong ascent around 15°N simulated in FGOALS-g2 (Fig. 2.7h) in JJA is associated with strong overestimation of rainfall over the

region.

Table 2.3: Spearman's rank correlation between AMIP5 model skill scores at simulating the local Hadley circulation and skill scores for simulation of Maritime Continent (20°S-20°N, 80°E-160°E) precipitation for the seasons indicated. A choice of PCC and RMSE skill scores is shown. Bold text indicates a statistically significant correlation with a p-value less than 0.05.

	DJF	MAM	JJA	SON
PCC	0.19	-0.1	0.23	**0.51**
RMSE	**0.39**	0.24	**0.39**	**0.53**

The correlation between RMSE skill scores of local Hadley circulation and precipitation in Table 2.3 also suggests that the seasonal mean rainfall biases over the Maritime Continent are linked to the local Hadley Circulation biases. The RMSE correlates better than the PCC except for the MAM season, which is low for both. The Spearman's rank correlation coefficients for RMSE are above 0.35 and statistically significant ($p < 0.05$) for all seasons except for MAM. Thus there is some connection between errors at the relatively small scale of the Maritime Continent and the large scale circulation.

3.4.2.2 Global monsoon

Next, we investigate if the models that have a better representation of the monsoons on the global scale (solsticial and equinoctial modes using the metrics defined in Section 2.2.5) have a better representation of the seasonal mean and annual cycle of precipitation over the Maritime Continent.

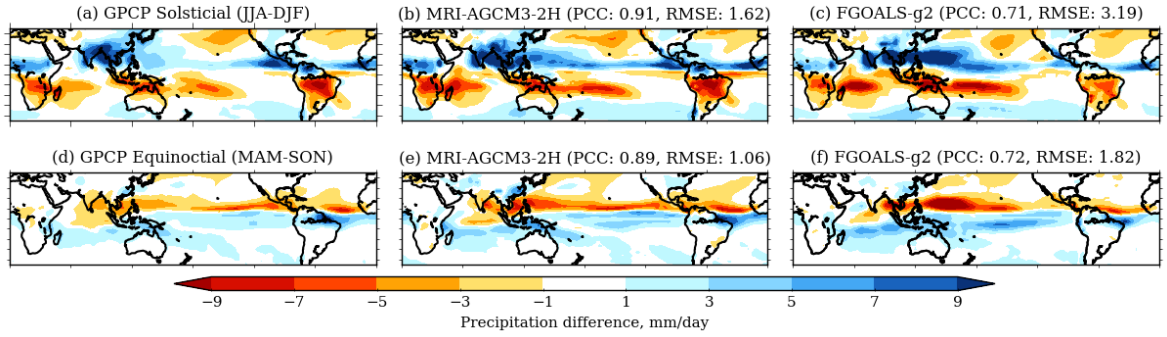

Figure 2.8: Comparison of the spatial pattern of the solsticial mode (JJA minus DJF) between (a) GPCP, (b) the AMIP5 model with the lowest RMSE and (c) the AMIP5 model with the highest RMSE. (d)-(f) are as in (a)-(c) but for equinoctial mode (MAM minus SON). The PCC and RMSE calculated between observed and simulated patterns (in the domain 45°S-45°N and 0°-360°E) are above each panel.

The global solsticial mode (JJA minus DJF) in Fig. 2.8b and equinoctial mode (MAM minus SON) in Fig. 2.8e for a selected model with the lowest RMSE (MRI-AGCM3-2H) are in good agreement with observations (Fig. 2.8a,d), but the model generally overestimates the overall amplitude of the solsticial and equinoctial precipitation signal. The PCCs are comparable for both solsticial and equinoctial modes but the RMSE scores are slightly larger for the solsticial mode. The model with the highest RMSE, FGOALs-g2, simulates an overly strong precipitation amplitude for both solsticial (Fig. 2.8c) and equinoctial (Fig. 2.8f) modes, especially over the tropical Indian and western Pacific Oceans.

Next we plot the local annual cycle of precipitation in these examples, as a time-latitude diagram averaged between 80°E and 160°E in Fig. 2.9. We can see that both MRI-AGCM3-2H and FGOALS-g2 also simulate overly strong monsoon precipitation, especially in summer and autumn seasons, which is consistent with the solsticial and equinoctial biases in Fig. 2.8. This suggests that Maritime Continent precipitation biases are related to global monsoon biases. Zonal-mean precipitation biases are dominated by biases over the Asian sector, particularly during JJA and SON. This also indicates how closely the seasonal movement of the global-scale ITCZ is related to local precipitation over the Maritime Continent. The PCC and RMSE of Maritime Continent annual cycle precipitation with respect to GPCP for all AMIP5 models are listed in Table 2.2.

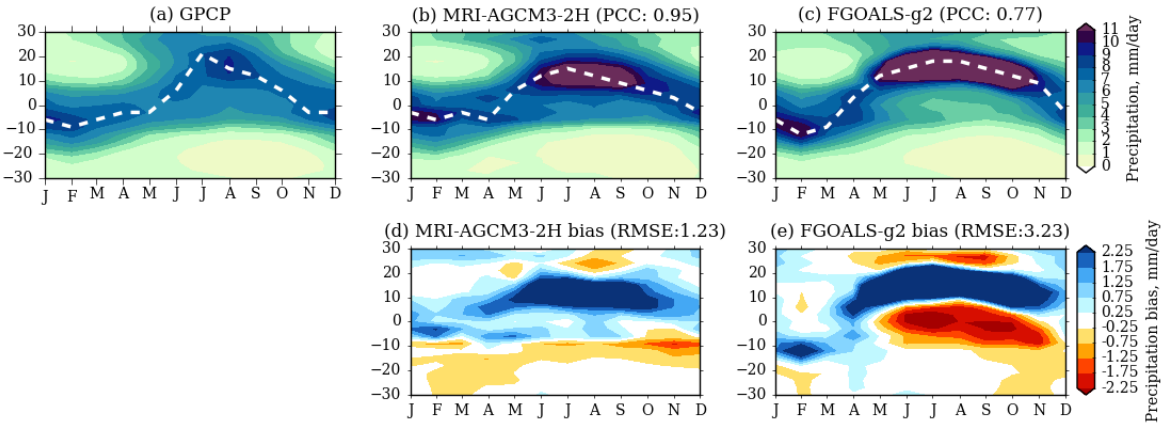

Figure 2.9: Latitude-time plot of precipitation zonally averaged between 80°E and 160°E for (a) GPCP, (b) MRI-AGCM3-2H and (c) FGOALS-g2. White dashed line shows the position of the maximum precipitation each month. Precipitation biases with respect to GPCP are shown for this same temporal-spatial averaging for (d) MRI-AGCM3-2H and (e) FGOALS-g2.

To explore this further beyond the two models shown in Fig. 2.9, Table 2.4 shows the Spearman's rank correlations of scores representing skill at simulating the solsticial mode or equinoctial mode with scores at simulating local Hadley circulation and Maritime Continent precipitation. Most of the correlation coefficient values are above 0.4 ($p < 0.05$) suggesting that those models having a better representation of the global monsoons (solsticial and equinoctial modes) will also have a better representation of the mean meridional circulation

Table 2.4: Spearman's rank correlation between skill scores at simulating the global monsoon (solsticial mode and equinoctial mode) and both the local Hadley circulation and precipitation over the Maritime Continent respectively. Bold text indicates a statistically significant correlation with a p-value less than 0.05.

	Hadley Circulation		Maritime Continent Precipitation	
Solsticial	DJF	JJA	DJF	JJA
PCC	0.30	**0.66**	0.34	**0.53**
RMSE	0.30	**0.68**	**0.55**	**0.51**
Equinoctial	MAM	SON	MAM	SON
PCC	**0.42**	**0.56**	-0.01	0.30
RMSE	0.18	**0.45**	**0.52**	**0.60**

and precipitation pattern over the Maritime Continent region. Thus our analysis demonstrates a connection all the way from the skill at simulating the global-scale circulation down to the regional scale of Maritime Continent precipitation in the AMIP5 models.

2.4.3 Sensitivity of simulated mean climate to ocean-atmosphere coupling

Ocean-atmosphere coupling is important for monsoon simulation. Song and Zhou (2014) compared the coupled and uncoupled simulations from CMIP5 and found that air-sea coupling improves the East Asian Summer Monsoon simulation in CMIP5 models. On the other hand, while many errors arise from cloud and convective parameterizations affecting coupled and atmosphere-only models alike, other errors arise through coupled feedbacks. Li and Xie (2014) attributed the double ITCZ problems in CMIP5 to cloud simulation errors in the atmospheric model, while the equatorial Pacific cold tongue errors were attributed to ocean-atmosphere feedbacks.

In this section, the analysis in Section 2.3 was first repeated for 46 coupled versions of CMIP5 models and summarised briefly: we found some similarities between CMIP5 and AMIP5. For instance, the MMM has better skill at reproducing the observed mean climate than individual models. The 850 hPa wind is better simulated than the precipitation in all four seasons in terms of its pattern correlation. The coupled versions of CMIP5 also have a significant spread in model performance. The good models in one season do not necessarily represent other seasons well.

To determine the potential impact of SST biases in simulating Maritime Continent precipitation, we made a comparison between 22 coupled CMIP5 model simulations and their corresponding AMIP simulations, which are a subset of the 28 models analysed in the previous

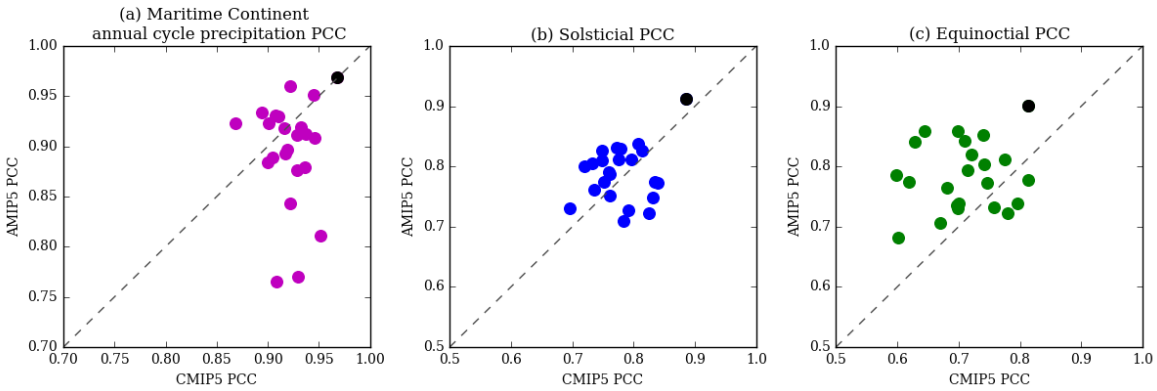

Figure 2.10: Comparison between CMIP5 and AMIP PCC of (a) Maritime Continent annual cycle precipitation averaged between 80°E and 160°E, (b) solsticial mode and (c) equinoctial mode in the domain 45°S-45°N and 0°-360°E. MMMs are plotted in black colour.

section. This is because modelling groups often run several different versions of their models, whereas not all coupled and atmosphere models from a given group are directly equivalent. The mean-state climate and biases of these 22 CMIP5 models are almost identical to the 46 CMIP5 models (not shown). The same result holds for AMIP5, whereby the 22 models have similar mean state biases to those of the 28 AMIP5 models. The MMMs shown in the remainder of this section consist of 22 corresponding CMIP5 and AMIP5 models respectively.

In Fig. 2.10a, the comparison between 22 AMIP5 and CMIP5 models PCCs in reproducing the annual cycle (time-latitude) precipitation shows that most CMIP5 models from a given modelling group perform better than their corresponding AMIP5 models. AMIP5 and CMIP5 MMMs have very similar values of PCC with observations (0.969 and 0.970) and RMSE (0.976 mm/day, Fig. 2.11b and 0.966 mm/day, Fig. 2.11d). However, the PCCs (as well as RMSE) for individual models from CMIP5 and AMIP5 vary greatly, and 14 of the 22 CMIP5 models have higher PCC scores than their corresponding AMIP5 models. This seems to suggests that air-sea coupling improves the simulation of the Maritime Continent annual cycle precipitation despite the inevitable SST biases. However, AMIP5 models generally outperform CMIP5 models in the simulation of solsticial (Fig. 2.10b) and equinoctial (Fig. 2.10c) modes. This opposite result suggests that SST biases and ocean-atmosphere feedback errors introduce larger biases in the coupled models at the large scale. Fig. 2.10 also indicates that there is a clear lack of correlation between a model's performance at simulating the annual cycle of precipitation in atmosphere-only mode and in coupled mode. This is also the case for the patterns of the equinoctial and solsticial modes.

Comparison between the spatial pattern of AMIP5 (Fig. 2.11b) and CMIP5 (Fig. 2.11d) MMM annual cycle precipitation biases shows some differences, in particular from January to March, where AMIP5 models simulate dry biases over the southern Maritime Continent, while CMIP5 shows wet biases. Four selected models, i.e. MPI-ESM-MR (AMIP5 model with highest PCC), MIROC5 (AMIP5 model with lowest PCC), CNRM-CM5 (CMIP5 model with

Table 2.5: Spearman's rank correlation of skill at simulating Maritime Continent precipitation with skill at simulating each of the four listed fields for the 22 CMIP5 models. Bold text indicates a statistically significant correlation with a p-value less than 0.05. Red text indicates a larger CMIP5 Spearman's rank correlation coefficient compared to the 28 AMIP5 model correlation coefficient scores in the previous section.

	PCC				RMSE			
	DJF	MAM	JJA	SON	DJF	MAM	JJA	SON
Low level wind	0.41	**0.44**	**0.58**	0.18	-0.11	0.19	0.39	-0.33
Hadley circulation	-0.23	-0.02	0.15	0.07	0.16	**0.54**	0.20	0.30
Solsticial	0.17		**0.60**		**0.74**		**0.79**	
Equinoctial		0.25		0.35		**0.71**		**0.56**

highest PCC) and ACCESS1-3 (CMIP5 model with lowest PCC) also show inconsistencies in the spatial pattern of precipitation biases between the model pairs of AMIP5 and CMIP5.

Although most AMIP5 models simulate the seasonal mean local Hadley circulations better than CMIP5 for all seasons (figure not shown), we also found mixed results for model skill at reproducing the seasonal precipitation and 850 hPa wind patterns over the Maritime Continent. CMIP5 better simulates both JJA and SON precipitation and low-level winds, whereas AMIP5 shows better simulation of the DJF and MAM seasonal mean climate. This suggests that air-sea coupling can be important for Maritime Continent climate simulation but its impact is complex.

CMIP5 (coupled) models show a weaker correlation between skill scores for simulating Maritime Continent precipitation and skill scores for simulating local Hadley Circulation than in AMIP5. The correlation coefficients of skill scores for simulating Maritime Continent precipitation with skill scores for simulating the low-level wind is also lower in CMIP5 than in AMIP5. However, CMIP5 skill scores for simulating Maritime Continent precipitation has stronger correlation with skill scores for simulating global monsoon solsticial mode compared with AMIP5 (see Table 2.5).

Coupling adds extra complexity, which will be a focus of next chapter when we will look at SST bias.

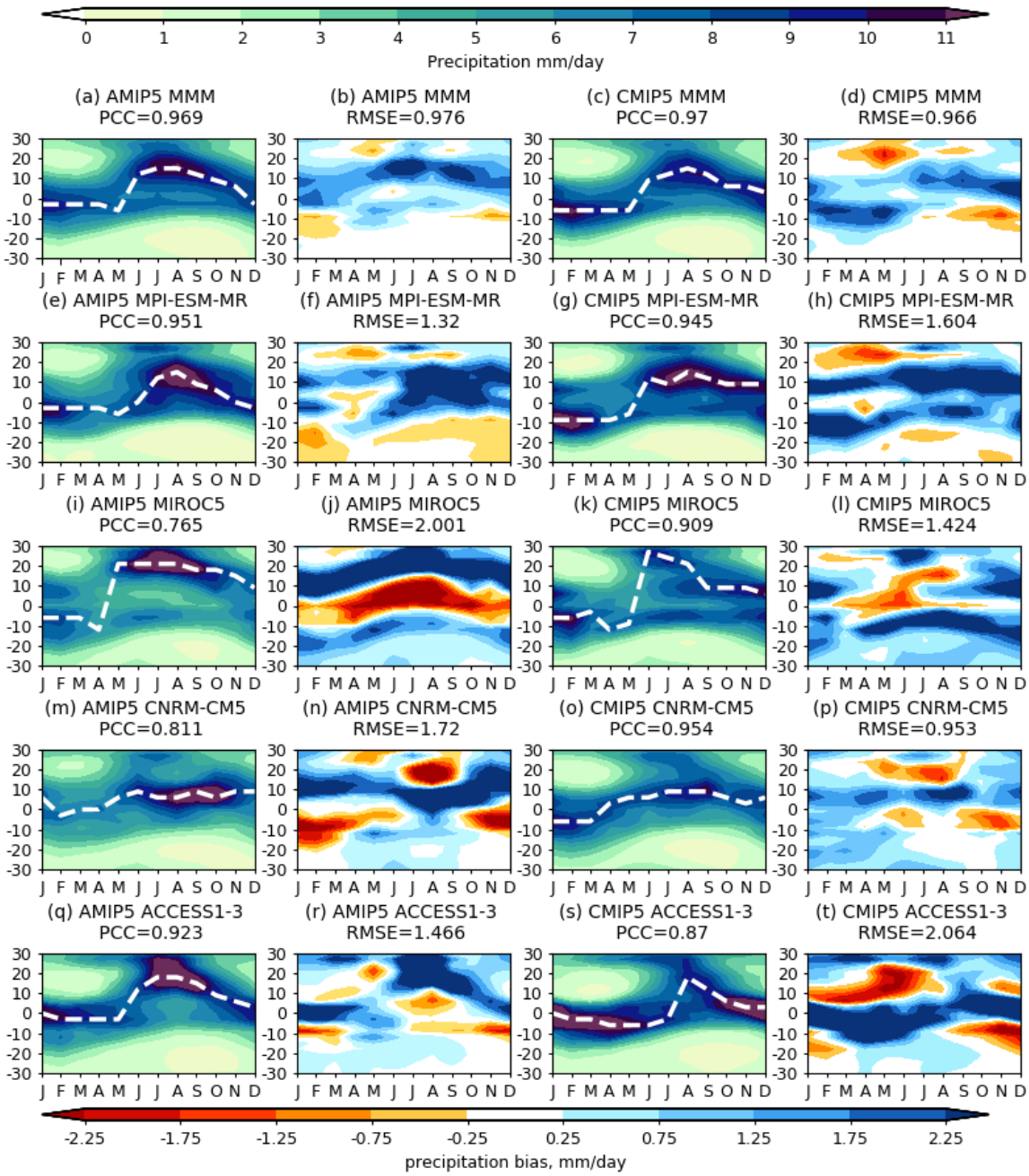

Figure 2.11: MMM (a) AMIP5 latitude-time plot of precipitation averaged between 80°E and 160°E, (b) AMIP5 precipitation biases with respect to GPCP, (c) CMIP5 latitude-time plot of precipitation averaged between 80°E and 160°E and (d) AMIP5 precipitation biases with respect to GPCP. (e)-(h) are as in (a)-(d) but for the AMIP5 model with highest PCC, (i)-(l) are for AMIP5 model with lowest PCC, (m)-(p) are for CMIP5 model with highest PCC and (q)-(t) are for CMIP5 model with lowest PCC. White dashed line shows the position of the maximum precipitation each month.

2.5 Clustering of the AMIP5 Maritime Continent annual cycle precipitation

Cluster analysis is used for classification of homogeneous climate patterns and weather regimes in climate studies (Unal et al., 2003; Bao and Wallace, 2015). Apart from that, cluster analysis can be used to group ensemble members for operational forecasting purposes (Molteni et al., 1996; Legg et al., 2002) and classifying CMIP5 climate change projections (Masson and Knutti, 2011; Mizuta et al., 2014).

In this study, hierarchical clustering analysis of Maritime Continent annual cycle precipitation was performed to characterize model systematic biases in the AMIP5 runs and determine if these biases are related to common factors elsewhere in the tropics. We chose to perform the clustering analysis on the annual cycle time latitude diagram since it is a single map which contains spatial and temporal information of precipitation from a range of seasons. The annual cycle captures the seasonal movement of the ITCZ in the Maritime Continent.

In cluster analysis, the models that are similar are grouped together based on minimizing the Euclidean distance of the Maritime Continent annual cycle precipitation between each pair of models or model clusters using the complete linkage method as described in Section 2.2.6. The dendogram in Fig. 2.12a shows that the clustering analysis resulted in five clusters with 13, 8, 4, 2 and 1 model(s) in each of the clusters.

To ensure that the clustering analysis is robust and models that are similar are grouped together, we calculated the PCCs between AMIP5 simulations and GPCP observations and plotted these in a box-and-whisker plot in Fig. 2.12b according to each cluster. Clusters I and II are quite distinct in terms of their PCC scores. Almost all of the models in Cluster I perform better than Cluster II models in simulating the annual cycle of precipitation. Cluster III only consists of four models and has a large spread in PCC values. Clusters IV and V consist of only two and one model respectively, which are also outliers from the overall sample. Consequently, for the remainder of the composite analysis in Section 2.5.1, we will only consider Clusters I and II. Although there is one outlier each in Clusters I and II, we have also examined the Euclidean distances between each of the AMIP5 simulations and the GPCP observations as well as the Euclidean distances between each of the models with other models in all clusters (figure not shown) to ensure that the models that are most similar are clustered together. We found that all the models have smaller distances between the models in the same cluster and bigger distances between models of different clusters. This shows that the clustering analysis is able to successfully group together models that are most similar.

The dendogram in Fig. 2.12a also shows that models from the same institution mostly belong to the same clusters (Masson and Knutti, 2011; Mizuta et al., 2014). For example, the models from the same institutions such as MRI (AGCM3.2 models), GFDL (HIRAM models), CSIRO-BOM (ACCESS models), IPSL (CM5A models) and MPI (ESM models)

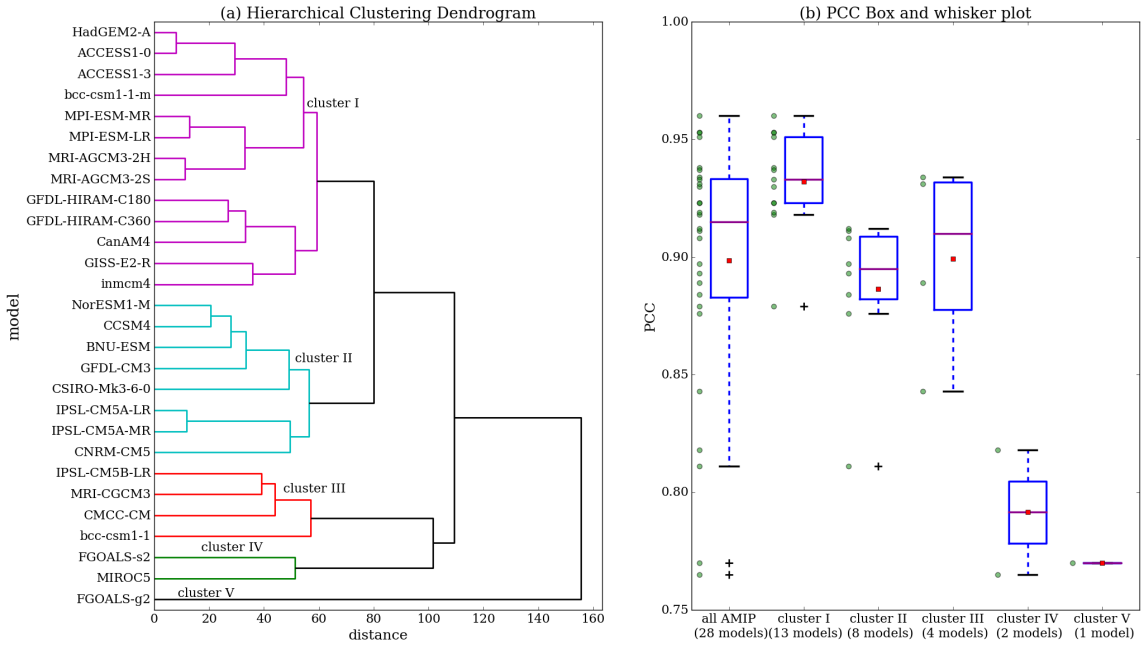

Figure 2.12: (a) Hierarchical clustering dendrogram. The models in the same colours are in the same clustering group while the distances greater than or equal to the threshold are coloured black. (b) Box-and-whisker plot of PCC between AMIP5 simulations and GPCP observations of Maritime Continent annual cycle precipitation averaged between 80°E and 160°E. Green dots are individual model's PCC; magenta lines indicate the median; red dots represent the mean and blue boxes indicate the interquartile range (IQR). The plus signs are the outliers, which are PCC scores smaller than the lower quartile by at least 1.5 times the IQR.

are in the same cluster. The models that shared the same atmospheric component also tend to cluster. The ACCESS models are based on the UK Met Office HadGEM atmospheric component and are in the same cluster with the HadGEM2-A model. The NorESM1-M model uses the same atmospheric model as CCSM4 (Bentsen et al., 2013), and BNU-ESM also uses the similar Community Atmospheric Model version 4 (CAM4) atmosphere. Both models are in the same cluster as CCSM4. On the other hand, MRI-CGCM3 is an Earth System Model, with its atmosphere component interactively coupled to an aerosol model, and it is in a different cluster from the less complex MRI-AGCM3.2H and MRI-AGCM3.2S models.

2.5.1 Composites of mean climate simulation biases for the leading two clusters of the AMIP5 models

In this section, the composites of models in Clusters I and II, obtained by taking the average of all models in each cluster are analysed. Firstly, we looked at the latitude-time plot of precipitation averaged between 80°E and 160°E in Fig. 2.13 (first column), the metric on which the models are clustered, which shows the transitions of precipitation during the course of the annual cycle. Cluster I simulates a similar seasonal migration of precipitation over

the Maritime Continent (Fig. 2.13a) to GPCP (Fig. 2.9a). Cluster I is also able to capture both the winter monsoon and summer monsoon shift and also the movement of the ITCZ, but it overestimates the precipitation, especially during the JJA and SON seasons (Fig. 2.13b). Cluster II simulates less seasonal migration and the position of maximum rainfall stays closer to the equator throughout the year (Fig. 2.13e,f). The PCC and RMSE for the composites of the two clusters show that Cluster I has better skill than Cluster II in simulating the annual cycle climatology of precipitation.

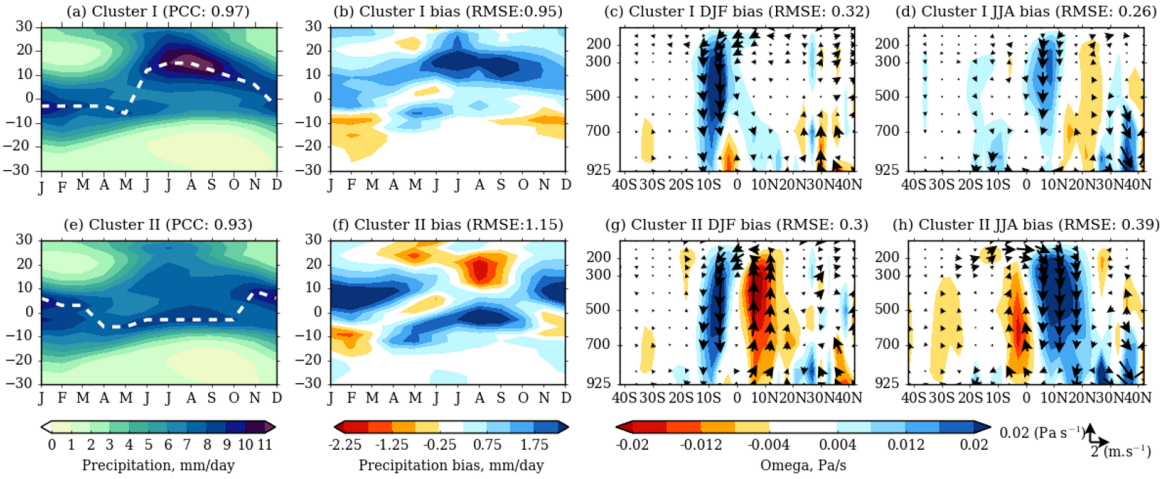

Figure 2.13: Cluster I (a) latitude-time plot of precipitation averaged between 80°E and 160°E, the white dashed line indicates the maximum precipitation for each month, roughly illustrating position of the ITCZ. (b) precipitation biases with respect to GPCP. Cluster I zonal mean meridional circulation omega (shading and arrow, Pa s^{-1}) and v (arrow, m s^{-1}) biases with respect to ERA-Interim averaged between 80°E and 160°E for (c) DJF and (d) JJA. (e)-(h) are as in (a)-(d) but for Cluster II. PCC and RMSE are shown above each panel.

To see if these errors in the position of Maritime Continent ITCZ are related to the overturning circulation, we next investigate the relationship between precipitation biases and local Hadley circulation biases during DJF and JJA seasons in the two clusters. We can see from Fig. 2.13b,f that Cluster II has larger precipitation biases than Cluster I in DJF. The Cluster I dry biases correspond to local Hadley circulation subsidence biases in the southern Maritime Continent. Cluster II wet biases over the northern Maritime Continent and dry biases over the southern Maritime Continent are consistent with the ascent and descent biases, respectively in Fig. 2.13g.

During JJA, the clusters show different biases in precipitation. Cluster I has the correct pattern but too large magnitude of precipitation in the observed wet regions of the Maritime Continent. There is a slight discrepancy between the wet biases and ascent biases. Note that, for regions with near-zero rainfall biases or small positive precipitation biases, there are sometimes downward motion biases (Fig. 2.13d, $\simeq$ 7 °N). This discrepancy may occur because GPCP observations are used for precipitation and ERA-Interim for vertical motion in

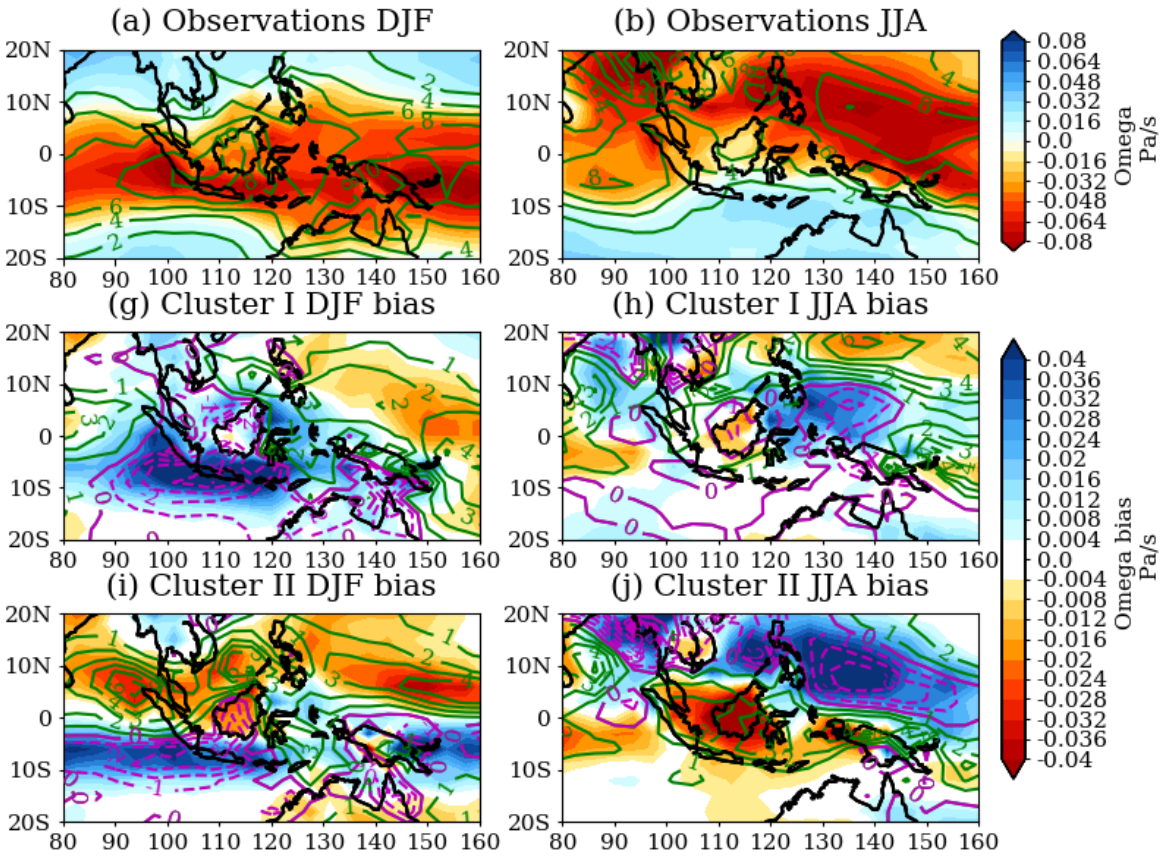

Figure 2.14: ERA-interim 500hPa omega (shaded, Pa/s) and GPCP precipitation (contour, mm/day) for (a) DJF and (b) JJA seasons, and biases for Cluster I in (c) DJF and (d) JJA seasons and Cluster II in (e) DJF and (f) JJA seasons. Green contour lines are wet biases (positive), solid magenta line represents the zero value and dashed magenta lines are dry biases.

this study. Cluster II has dry biases north of the equator and wet biases to the south, consistent with the biases in ascent and descent of the local Hadley circulations in Fig. 2.13h. Cluster II simulates the ascending branch too far south, which results in overestimation of rainfall in the southern Maritime Continent and underestimation in the northern Maritime Continent. This shows that the precipitation biases in the Maritime Continent are linked closely to the (local) Hadley circulation.

Figure 2.14(a) and (b) show the ERA-interim seasonal mean of vertical velocity (omega) at 500hPa in DJF and JJA respectively. The negative (positive) values of omega imply ascending (descending) motion. DJF and JJA show contrasting features, with negative omega over the central and southern parts of the Maritime Continent in DJF, while JJA shows strong upward motion over northern and central parts of the Maritime Continent. The deep ascent corresponds to locations of maximum precipitation. Likewise, consistent with the precipitation biases, models also show negative omega anomalies over the regions of wet bias and positive omega over dry bias regions. This shows that precipitation biases over the Maritime Continent

are related to the large-scale circulation.

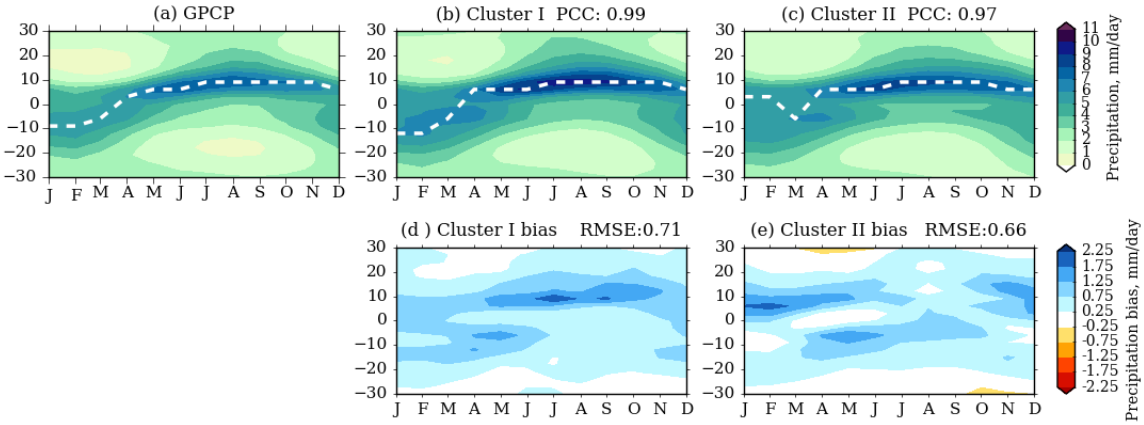

Figure 2.15: Zonal mean precipitation in the global domain (averaged between 0° and 360° E) for (a) GPCP, (b) Cluster I and (c) Cluster II, the white dashed line indicates the maximum precipitation for each month, roughly illustrating position of the ITCZ. Biases with respect to GPCP for (d) Cluster I and (e) Cluster II. PCC and RMSE are shown above each panel.

Examining the tropics-wide characteristics of the clusters, we find that the zonal mean precipitation averaged over the whole tropics between 0°and 360° E in Fig. 2.15d,e shows similar biases to the precipitation biases averaged between 80° E and 160° E in Fig. 2.13b,f when accounting for the tropics-wide mean wet biases of both clusters. This confirms what we saw earlier for individual model analysis, that Maritime Continent precipitation biases are closely related to global monsoon biases. The errors in movement of the ITCZ over the Maritime Continent are thus related to global ITCZ errors. A separation of land-only and sea-only grid points precipitation biases (figure not shown) shows that the wet biases over sea-only grid points dominate the tropics-wide errors.

Figure 2.16 shows the DJF and JJA seasonal mean GPCP precipitation and 850 hPa winds over the tropics along with Cluster I and Cluster II mean biases. Cluster I and Cluster II have somewhat similar biases over the Indian Ocean in DJF and JJA. In DJF, Cluster I (Fig. 2.16c) simulates an overly strong South Pacific Convergence Zone (SPCZ) whereas Cluster II (Fig. 2.16e) underestimates the SPCZ. In JJA, Cluster I (Fig. 2.16d) simulates an overly wet Western North Pacific (WNP) while Cluster II (Fig. 2.16f) underestimates the precipitation over the region. Bush et al. (2015) highlighted the WNP as a region with too much rainfall in the MetUM, a more recent version of the MOHC HadGEM2-A model from CMIP5, which is evident in Cluster I.

Cluster I shows wet biases over the east-central equatorial Pacific and dry biases in the Maritime Continent, Australia and northern South America in DJF and JJA (Fig. 2.16c,d). Cluster I also shows dry biases over India in JJA (Fig. 2.16d). For Cluster II, DJF biases in Fig. 2.16e are associated with a mean shift in the global monsoon whereby Cluster II simulates maximum precipitation further north than GPCP.

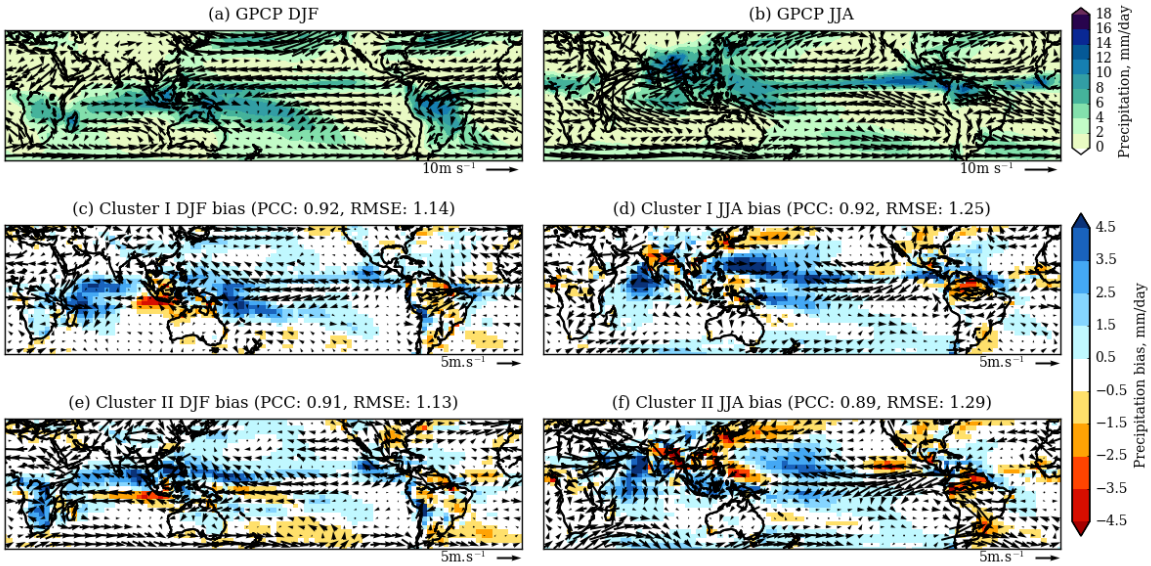

Figure 2.16: GPCP precipitation and ERA-Interim 850 hPa wind for (a) DJF and (b) JJA seasons, and biases for Cluster I in (c) DJF and (d) JJA seasons and Cluster II in (e) DJF and (f) JJA seasons. PCC and RMSE are shown above each panel.

Figure 2.17 shows scatter plots of AMIP5 Cluster I and Cluster II seasonal mean skill scores at simulating Maritime Continent precipitation versus skill scores at simulating the global monsoon solsticial and equinoctial modes. The MMMs in each cluster outperform the individual models in their cluster for all seasons. Although the individual model skill scores vary greatly, the Cluster I MMMs perform better than the Cluster II MMMs in simulating almost all of the local and global properties. This is consistent with our earlier results suggesting Cluster I simulates a realistic movement of the ITCZ, capturing the rainfall pattern but overestimating the rainfall, whereas in Cluster II, the ITCZ doesn't move as observed, giving an unrealistic pattern of rainfall which impacts both the PCC and RMSE scores. The only exception is Maritime Continent precipitation RMSE in SON, indicating that Cluster II has a slightly more realistic representation of the autumn rainfall, when the ITCZ is close to the equator anyway.

The RMSE of seasonal mean precipitation of both clusters has a strong significant correlation with the RMSE of solsticial (Fig. 2.17b,d) and equinoctial modes (Fig. 2.17f,h), except for Cluster II JJA RMSE. This indicates that the amplitude of the particular global monsoon and Maritime Continent biases singled out by these clusters are linked, just as the global monsoon biases and Maritime Continent biases are linked for all models (Section 2.4.2).

In Fig. 2.17a,c, Cluster I, which is able to capture both the winter monsoon and summer monsoon patterns, shows a significant positive correlation with the solsticial mode, whereas Cluster II, which has less similarity in the spatial patterns with GPCP and simulates the position of maximum rainfall too close to the equator, shows no correlation with the solsticial

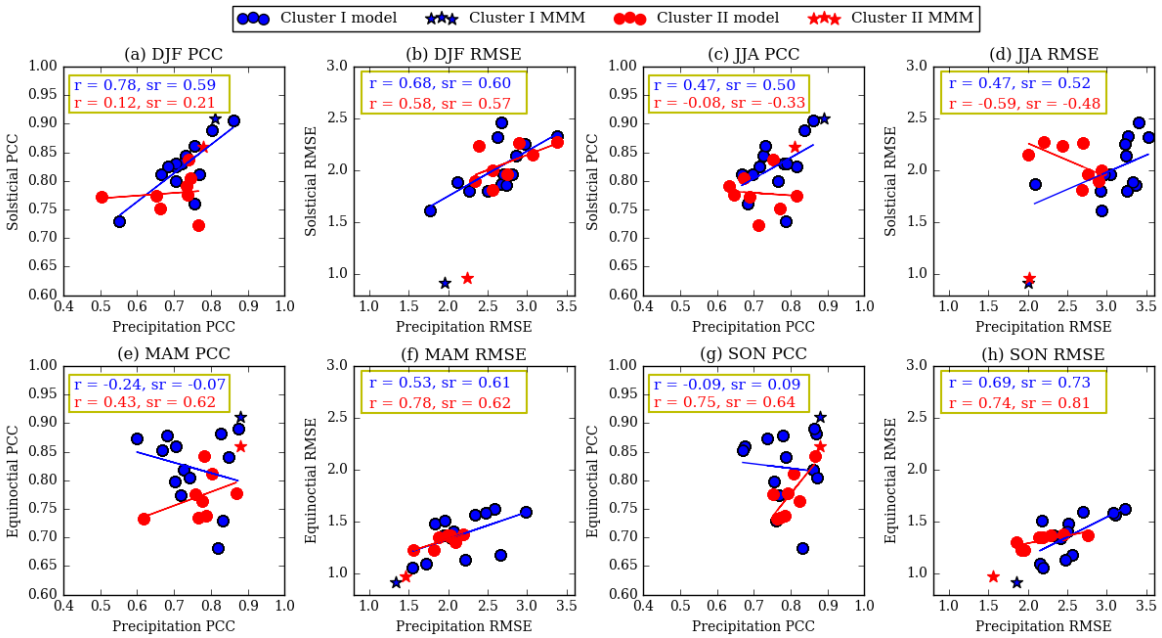

Figure 2.17: Scatter plots of the AMIP5 Cluster I (blue) and Cluster II (red) seasonal mean (a) DJF PCC, (b) DJF RMSE, (c) JJA PCC and (d) JJA RMSE of Maritime Continent precipitation versus skill scores at simulating the solsticial mode; and (e) MAM PCC, (f) MAM RMSE, (g) SON PCC and (h) SON RMSE of Maritime Continent precipitation versus skill scores at simulating the equinoctial mode. The Maritime Continent domain is 20°S-20°N and 80°E-160°E, whereas solsticial and equinoctial modes domains are 45°S-45°N and 0°-360°E. The Pearson correlation coefficient (r) and Spearman's rank correlation coefficient (sr) for each season are shown in the yellow box on the top left corner. All correlation coefficients for PCC and RMSE are statistically significant with a p-value less than 0.05 for most seasons except for Cluster II DJF PCC, Cluster I MAM PCC, Cluster II JJA PCC and Cluster I SON PCC.

mode (off-equatorial monsoon) PCCs. However, Cluster II Maritime Continent precipitation shows a stronger correlation with the equinoctial mode (Fig. 2.17e,g), perhaps because the location of the ITCZ in spring and autumn seasons is closer to the equator.

The results of the cluster analysis are in good agreement with the analysis in the previous section stating that Maritime Continent precipitation biases are closely related to local Hadley circulation biases and biases in the global monsoon. These relationship are stronger for the solsticial mode in Cluster I and the equinoctial mode in Cluster II.

2.6 Discussion

This study evaluates the AMIP5 model performance in simulating the mean climate over the Maritime Continent and investigates the model characteristics that may be potential sources of bias.

Our results in Section 2.4.1 agree with Neale and Slingo (2003) that model performance is largely unrelated to resolution. Although the range of resolutions in AMIP5 is compa-

rable to the size of several typical Maritime Continent islands, even the higher resolution AMIP5 models insufficiently resolve some of the smaller islands and steeper orography in the Maritime Continent. The model performance perhaps does not improve as resolution is increased because these models all still rely on convective parameterizations. Ogata et al. (2017) showed that increasing resolution of both the MRI-AGCM and MetUM models decreased the precipitation biases over the western Pacific. However, MRI-AGCM showed no clear resolution dependency in the simulation of precipitation over the southern Maritime Continent (0-10S, 90E-160E). They suggested that the different result of the resolution sensitivity over the Maritime Continent in MetUM and MRI-AGCM is likely due to the differences in the models physics scheme. On the other hand, the lack of correlation between CMIP5 model skill and resolution is also evident in the mean climate simulation over other regions such as East Asian summer monsoon (Song and Zhou, 2014).

Our analysis of the relationship between local Hadley circulation biases and precipitation biases in the Maritime Continent suggests that the seasonal mean biases in the region are linked to the local Hadley Circulation biases. The correlations between the global monsoon (solsticial and equinoctial modes) and the Maritime Continent precipitation show some connection between errors at the regional scale of the Maritime Continent and errors at the larger global circulation scale. The same results hold for both Cluster I and Cluster II in Section 2.5.

On the other hand, the impact of ocean-atmosphere coupling impacts is complex. We found that CMIP5 performs better than AMIP5 model in the simulation of Maritime Continent annual cycle precipitation, which suggest that air-sea coupling improves the simulation despite the inevitable SST biases. However, we also found that CMIP5 perform less well at simulation of the global monsoon modes which suggest that SST biases and ocean-atmosphere feedback errors introduce larger biases in the coupled models at larger scales. Hendon (2003) suggests that the SST changes feed back on the surface winds and thus affect the Walker circulation and precipitation. The next chapter will look at SST biases over the Maritime Continent and investigate their relationship with precipitation and circulation biases.

Apart from the three potential sources of bias discussed in Section 2.4, i.e. the role of horizontal resolution, the relationship to biases in the local Hadley circulation and global monsoon, and the presence or lack of two way air-sea coupling, there are also other factors. One possible source of common error between global monsoon biases and local Maritime Continent biases are errors associated with the parameterization of cumulus convection. Studies have shown that the simulation of tropical precipitation is highly sensitive to the convection scheme (Sherwood et al., 2014; Bush et al., 2015). Ackerley et al. (2015) suggested that wet biases over Australia in summer in the BNU-ESM, NorESM1-M and CCSM4 models might be related to the convection schemes that are used in these models. Here we briefly examine the relationship between the convection scheme and the model biases. Table

Table 2.6: AMIP5 models convection scheme and closure.

Cluster	Model	Convection scheme	Closure
I	MRI-AGCM3.2H	Yoshimura (Yukimoto et al., 2011); Tiedtke (1993)	CAPE
	MRI-AGCM3.2S		
	GFDL-HIRAM-C180	Moorthi and Suarez (1992)	CAPE
	GFDL-HIRAM-C360		
	BCC-CSM1.1(m)	modified Zhang and McFarlane (1995); Zhang and Mu (2005)	CAPE
	ACCESS1.0	Modified Gregory and Rowntree (1990)	CAPE
	ACCESS1.3		
	HadGEM2-A	Modified Gregory and Rowntree (1990); Adaptive Detrainment (Derbyshire et al., 2011)	CAPE
	INM-CM4	Betts (1986)	CAPE
	MPI-ESM-MR	Tiedtke (1989); Nordeng (1994)	CAPE
	MPI-ESM-LR		
	GISS-E2-R	DelGenio and Yao (1993)	A cloud base neutral buoyancy
	CanAM4	Zhang and McFarlane (1995)	CAPE
II	CCSM4	modified Zhang and McFarlane (1995); Richter and Rasch (2008); Neale et al. (2008)	CAPE
	CNRM-CM5	Bougeault (1985)	Kuo
	IPSL-CM5A-LR	Modified Emanuel (1991); Bony and Emanuel (2001)	CAPE
	IPSL-CM5A-MR		
	CSIRO-Mk3.6.0	Modified Gregory and Rowntree (1990)	Stability-dependent mass-flux
	NorESM1-M	Zhang and McFarlane (1995)	CAPE
	GFDL-CM3	Donner (1993); Donner et al. (2001); Wilcox and Donner (2007)	CAPE
	BNU-ESM	modified Zhang and McFarlane (1995); Zhang (2002); Zhang and Mu (2005)	Closure scheme couples convection to the large-scale forcing in the free troposphere
III	CMCC-CM	Tiedtke (1989); Nordeng (1994)	CAPE
	MRI-CGCM3	Yoshimura (Yukimoto et al., 2011), Tiedtke (1993)	CAPE
	IPSL-CM5B-LR	Modified Emanuel (1991); Bony and Emanuel (2001); Grandpeix et al. (2004)	Available lifting power
	BCC-CSM1.1(m)	modified Zhang and McFarlane (1995); Zhang and Mu (2005)	CAPE
IV	MIROC5	Chikira and Sugiyama (2010)	Prognostic convective kinetic energy
	FGOALS-s2	Tiedtke (1989); Nordeng (1994)	CAPE
V	FGOALS-g2	Zhang and McFarlane (1995); Zhang and Mu (2005)	CAPE

2.6 shows the convection scheme and type of convective closure for each of the AMIP5 models, arranged by cluster group. Although the members in the same cluster use different convection schemes and closures, the models from the same institution that use different convection schemes do not cluster. This includes GFDL-HIRAM and GFDL-CM3; IPSL-CM5A and IPSL-CM5B; FGOALS-s2 and FGOALS-g2. The IPSL-5A-LR and IPSL-5A-MR atmospheric models, which differ only in resolution, are in the same cluster, whereas the IPSL-CM5B models that involved substantial changes in the atmospheric model including convection scheme and closure (Dufresne et al., 2013) are in different clusters. On the other hand, the BCC-CSM models are the only ones which use the same convection scheme, and differ only in resolution, but are not in the same cluster.

These results suggest that the convection scheme can be important for model simulation of the annual cycle precipitation in the Maritime Continent, but further work would be necessary to characterize the biases according to convection scheme, which is beyond the scope of this thesis.

2.7 Conclusions

This chapter examines the fidelity of CMIP5 models in simulating mean climate over the Maritime Continent, focusing mainly on the uncoupled versions of the models. The 28 CMIP5 model simulations for the 30-year period (1979-2008) in AMIP configuration with prescribed SSTs and sea ice (AMIP5) are compared with observational datasets. We quantify the model performance based on the pattern correlation coefficient (PCC) and root mean square error (RMSE) skill scores. We find that there is a considerable spread in the performance of the 28 AMIP5 models in reproducing the seasonal mean climate and seasonal cycle over the Maritime Continent region. Model performance is not necessarily consistent across seasons. A model with high skill in one season does not necessarily represent other seasons well. The multi-model mean (MMM) has better skill at reproducing the observed climate than individual models, in common with other studies of monsoon regions (e.g. Colman et al., 2011; Jourdain et al., 2013; Sperber et al., 2013; Feng et al., 2014). The PCC comparison also shows that models have higher skill at simulating the Maritime Continent 850 hPa winds than precipitation in all four seasons. Our results also suggest that VIMFC biases largely account for the precipitation biases over the Maritime Continent.

We also investigated the possible sources of the model biases. Our assessment of the sensitivity of Maritime Continent precipitation to climate model resolution suggests that, at the resolutions typical of AMIP5, the model performance is largely unrelated to model horizontal resolution. Instead, our analyses show that the local Maritime Continent biases are somewhat related to global circulation and global monsoon biases. The models that have a better representation of the local Hadley Circulation and global monsoons have a better

representation of the seasonal means of precipitation and winds over the Maritime Continent.

The analysis was repeated for 46 coupled versions of CMIP5 models, which we called "CMIP5", and we found similar results as in AMIP5. For instance, the MMM has better skill at reproducing the observed mean climate than the individual CMIP5 models. The 850 hPa wind is better simulated than the precipitation in all four seasons. CMIP5 models also showed significant spread in model performance. The comparison between 22 pairs of CMIP5-AMIP5 simulations shows that most CMIP5 models perform better than their AMIP5 counterpart in reproducing the annual cycle of Maritime Continent precipitation. However, AMIP5 models generally outperform CMIP5 models in simulating the global monsoon. Although most AMIP5 models simulate the seasonal mean local Hadley circulation better for all seasons compared to CMIP5, we found mixed results for model skill at reproducing the seasonal mean precipitation and 850 hPa winds over the Maritime Continent. Besides that, CMIP5 models show weaker correlation between the Maritime Continent precipitation biases and both the local Hadley Circulation biases and the low-level wind biases but stronger correlation with the global monsoon solsticial mode biases compared to AMIP5.

Hierarchical clustering analysis of Maritime Continent annual cycle precipitation was performed to characterize model systematic biases in the AMIP5 runs and determine if these biases are related to common factors elsewhere in the tropics. Our analysis resulted in two distinct clusters. Cluster I is able to reproduce the observed seasonal migration of Maritime Continent precipitation, but it overestimates precipitation amount, especially during the JJA and SON seasons. On the other hand, in Cluster II the maximum rainfall position too close to the equator throughout the year. The tropics-wide properties of these clusters also indicate a connection all the way from the skill of simulating the global properties down to skill at simulating the regional scale of Maritime Continent precipitation.

This chapter therefore highlights the importance of global monsoon and local Hadley circulation simulations in AMIP5, which are significantly associated with the mean climate simulation biases at Maritime Continent. On the other hand, ocean-atmosphere coupling impacts are more complex, and these will be the focus of next chapter to look at SST biases over the Maritime Continent and investigate their relationship with precipitation and circulation biases.

Chapter 3

Large-scale interactions between Maritime Continent precipitation and tropical sea surface temperature in CMIP5 models

3.1 Introduction

The previous chapter evaluated the fidelity of CMIP5 atmosphere-only models in simulating the mean climate over the Maritime Continent and the role of model horizontal resolution, inclusion of atmosphere-ocean coupling etc. The preliminary comparison with coupled models showed that air-sea coupling yielded complex impacts on Maritime Continent precipitation biases that warrants further investigation. This chapter will further examine the relationship between Maritime Continent mean state precipitation biases and tropical seas surface temperature (SST) biases in coupled CMIP5 models. Furthermore, the behaviour of Maritime Continent precipitation variability, its teleconnection to the El Niño-Southern Oscillation (ENSO) and Indian Ocean Dipole (IOD) in atmosphere-only and coupled CMIP5 models will be assessed.

One of the outstanding problems in the coupled CMIP5 models is the presence of significant SST biases in tropical ocean basins, including cold biases in the equatorial Pacific cold tongue (Li et al., 2015a; Zheng et al., 2012), warm biases over the southeastern Pacific and Atlantic Oceans (Hourdin et al., 2015; Wang et al., 2014) and seasonally dependent biases over the western Indian Ocean (Li et al., 2015b). These biases in the Indo-Pacific region affect the model skill at simulating the mean climate and its variability in this region such as ENSO and IOD, and their teleconnections.

Models tend to simulate excessively cold SST with inter-model difference up to 3°C over the Pacific cold tongue that extends too far west into the western Pacific (Li et al., 2015a; Zheng et al., 2012). Associated with the cold SST biases are dry biases and surface

easterly biases over the Pacific cold tongue region, arising from misrepresentation of ocean-atmosphere interactions via Bjerknes feedback (Li and Xie, 2014). Taschetto et al. (2014) showed that mean state biases in the equatorial Pacific SST induced the ENSO SST anomaly biases and zonal wind stress anomalies extending too far west across the equatorial Pacific. The anomalous westward Pacific cold tongue produces a significant positive correlation with rainfall over Papua in DJF, opposite to observations, and thus affect the ENSO-rainfall teleconnection simulated by the CMIP models (Cai et al., 2009; Jourdain et al., 2013).

In order to examine the impact of modelled cold tongue cold biases, Inness et al. (2003) applied heat flux-adjustments in the 20-year coupled HadCM3 model run with the SSTs between 10°N and 10°S in the Pacific and Indian Ocean being relaxed back to climatology on a timescale of approximately 14 days. Their study found that the anomalous heat flux reduced the cold SST biases of up to 3 °C and changed the low-level mean zonal wind from easterly to westerly in the western Pacific, resulting in a better agreement with observations. Using the same flux-adjusted integration of HadCM3, Turner et al. (2005) showed that the improved mean state of the tropical Pacific led to improved ENSO simulation, that in turn also improved the Asian summer monsoon-ENSO teleconnection. The analysis of Annamalai et al. (2007) in the CMIP3 models arrives at the same conclusion: models that better represent the basic state and Walker circulation are able to simulate the ENSO-monsoon teleconnection better. Achuta Rao and Sperber (2006) showed that the fidelity of CMIP2 and CMIP3 models at reproducing the ENSO-related precipitation anomaly over the tropics is linked to the model skill at simulating the climatology of boreal winter precipitation.

On the other hand, Langenbrunner and Neelin (2013) showed that an AMIP model with specified observed SSTs, also struggles to simulate ENSO precipitation teleconnections, with only a slight improvement from CMIP3 to CMIP5.

In the Indian Ocean, Levine and Turner (2012) showed that the mean state of Indian monsoon rainfall in the coupled HadGEM3 model is significantly underestimated due to cold SST biases in the northern Indian Ocean. Many CMIP5 models also exhibit systematic cold biases in the northern Arabian Sea and simulate weaker monsoon rainfall (Levine et al., 2013). Li et al. (2015b) showed that the weak southwest summer monsoon over the Arabian Sea in coupled CMIP5 models induced warm SST biases over the western equatorial Indian Ocean, which resulted in an easterly wind bias and precipitation bias that resembles the positive IOD mode via Bjerknes feedback. Their study showed that these mean state biases result in an overly large amplitude of interannual IOD variability simulated in CMIP5 models. Cai et al. (2009) showed that the CMIP3 models that simulate larger IOD amplitude had a stronger IOD teleconnection to southeast Australia, Sumatra and Java rainfall. However, Jourdain et al. (2013) found that the Maritime Continent-IOD relationship is weak in the CMIP3 and CMIP5 models.

In this chapter, we investigate the large-scale interactions between Maritime Continent

precipitation and tropical SSTs in CMIP5 models. We examine the influence of both local and remote air-sea interactions in the tropical oceans on the simulation of Maritime Continent precipitation. This chapter is organised as follows. We first describe the CMIP5 models and observational (reanalysis) datasets used in this chapter in Section 3.2. Section 3.3 build on the results of the previous chapter to assess the relationship between climatological seasonal SST biases in the tropical ocean and climatological seasonal precipitation in the Maritime Continent in CMIP5. Section 3.4 focuses on two dominant modes of variability influencing the climate of the Maritime Continent on interannual time-scales (i.e. ENSO and IOD in both AMIP and coupled experiments of CMIP5). In other words, we will assess Pacific and Indian Ocean teleconnections to the Maritime Continent in experiments using accurate, observed SSTs, followed by experiments that generated their own SST, with inherent biases. A comparison is made between AMIP and coupled CMIP5 models to investigate whether ocean-atmosphere coupling improves these teleconnections. Discussion and conclusions are given in Section 3.5.

3.2 Datasets and analysis

3.2.1 Models

Historical experiments from 1979 to 2005 of 42 fully coupled ocean-atmosphere CMIP5 are analysed in this chapter. The 42 models are marked with an asterisk (*) in Table 2.1 in Chapter 2. CMIP5 models' SST data on a already interpolated to a common $1^\circ \times 1^\circ$ regular grid spacing is obtained from the Asia-Pacific Data-Research Center (APDRC) at University of Hawaii (`http://apdrc.soest.hawaii.edu/`).

The 28 CMIP5 atmosphere-only models (AMIP5) discussed in the previous chapter are also analysed in this chapter for the simulation of interannual variability from 1979 to 2008. In addition to making general ensemble-mean comparisons, we also compare directly between 20 pairs of AMIP and coupled simulations to assess the extent and impact of SST biases on the teleconnections in coupled CMIP5 models.

To compare the models, all the models' atmospheric data are bi-linearly interpolated to a common 3.75° longitude $\times$ 3° latitude grid. We calculate the interannual anomalies by removing the long-term seasonal climatology over the entire period, 1979-2008 for AMIP5 and 1979-2005 for CMIP5. The multimodel mean (MMM) in this chapter is the average of 42 CMIP5 models and 28 AMIP5 models, unless otherwise specified.

3.2.2 Observations

The monthly mean SST data at $1^\circ \times 1^\circ$ from AMIP5 (Taylor et al., 2000) based on the monthly mean Hadley Centre sea ice and SST dataset version 1 (HadISST1) and version 2 of the

National Oceanic and Atmospheric Administration (NOAA) weekly optimum interpolation (OI) SST analysis is used for evaluating the CMIP5 model's ability at simulating the seasonal mean SST climatology and its interannual variability.

3.2.3 Index definition

To represent the ENSO and IOD in this study, we use the standard SST area-averaged indices. We select the Niño 3.4 (5°S-5°N, 120°W-170°W) SST anomalies to represent ENSO (Bamston et al., 1997). We identify an El Niño event when the 3-month running mean SST anomalies in the Niño 3.4 region are greater than 0.5°C for at least five consecutive months as defined by the Climate Prediction Center (CPC). A La Niña event is defined when the 3-month running mean SST anomalies in the Niño 3.4 region are less than -0.5°C for at least five consecutive months.

We calculate the Dipole Mode Index (DMI) as defined in Saji et al. (1999) to represent IOD in this study. DMI is the difference between western Indian Ocean (IODW, 10°S-10°N, 50°E -70°E) and eastern Indian Ocean (IODE, 0°-10°S, 90°E-110°E) SST anomalies. Positive and negative IOD phases are defined when the SON DMI exceeds a threshold of +/- 0.5°C.

The analysis of interannual variability related to ENSO focuses on the DJF season when ENSO typically peaks and analysis of the IOD focuses on SON, when the IOD signal is strongest. Since they are forced by the same prescribed SST, all AMIP5 models have the same Niño 3.4 index and DMI while the CMIP5 models generate their own SST and have different Niño 3.4 and DMI values.

3.2.4 Statistical analyses

In Section 4.2, we perform linear regression analysis to determine the relationship between Maritime Continent precipitation and tropical SST. Note that this is not a standard time-series regression, instead we use different climate models in place of the time dimension, as in Li et al. (2017). We regress climatological precipitation averaged over the Maritime Continent domain (20°S-20°N, 80°E-160°E) in 42 models onto the seasonal mean SST climatologies of those models. In other words, the independent variable is the climatological seasonal mean SST of each model and the dependent variable is the climatological seasonal mean of precipitation averaged over Maritime Continent of each model. In this way, we hope to determine how Maritime Continent precipitation biases will vary in response to SST biases in different regions. We refer to this regression analysis among the models as multimodel regression. Analogous correlation analysis using different climate models as the time dimension is refers to as multimodel correlation.

The correlation method used in this chapter is the Pearson linear correlation. We compute the Pearson correlation coefficient (r) to measure the strength of the association and the

direction of a linear relationship between two variables. We refer to the Pearson correlation coefficients computed according to time series as temporal correlation.

3.3 Relationship between tropical SST biases and the Maritime Continent mean state precipitation biases

Studies have shown that CMIP5 models exhibit significant SST biases. Biases in models' SSTs have a large impact on the simulation of the atmospheric mean state and other errors also arise through coupled feedbacks in the coupled GCMs. However, how these SST biases influence the simulated climate in the Maritime Continent is not well understood.

3.3.1 Seasonal coupled SST biases

In this section, we will first analyse the spatial pattern of SST biases averaged from 1979-2005 in CMIP5 models. The magnitude, sign and spatial pattern of SST biases are somewhat similar in all four seasons, apart from the western Indian Ocean where the biases change sign in different seasons. Some models including the MMM simulate colder than observed SST in DJF and MAM seasons but warmer than observed SST in JJA and SON seasons in the western Indian Ocean (figure not shown). Li et al. (2015b) showed that these seasonally dependent biases over the western Indian Ocean are related to the weaker South Asian summer monsoon simulated over the Arabian Sea in most CMIP5 models. For brevity, we only show the spatial pattern of CMIP5 climatological SST biases in DJF.

The MMM in Fig. 3.1(b) shows the typical SST biases in CMIP5 models in DJF: a cold biases over the central and western Pacific Ocean as well as the central and eastern Indian Ocean; and a warm biases over southeastern Pacific Ocean and equatorial Atlantic Ocean. These biases are also present in the other seasons (figure not shown). However, Fig. 3.1(c-ar) show that there are significant inter-model differences in the CMIP5 DJF SST mean state biases. Although most models simulate colder SSTs than observed over the western and central Pacific Ocean (e.g. CSIRO Mk3-6-0, MIROC5, HadGEM2-ES), as well as the Indian Ocean, some models such as bcc-csm1-1-m (Fig. 3.1d), GISS-E2-R-CC (Fig. 3.1af), CCSM4 (Fig. 3.1ag) and CESM1-FASTCHEM (Fig. 3.1aq) simulate warmer SSTs. The excessive cold bias over the Pacific cold tongue is a persistent bias in CMIP models but there is some improvement in the cold tongue simulation in CMIP5 compared to CMIP3 (Flato et al., 2013). Li and Xie (2012) showed that cold biases over the Pacific and Atlantic cold tongue are due to shallow thermocline biases in ocean models. Fig. 3.1 also shows that most models tend to simulate warmer SST in the Atlantic Ocean and over the eastern Pacific Ocean, with some even extending towards the central Pacific. Hourdin et al. (2015) showed that the warm SST biases over the eastern Pacific and Atlantic Oceans are related to biases in surface humidity

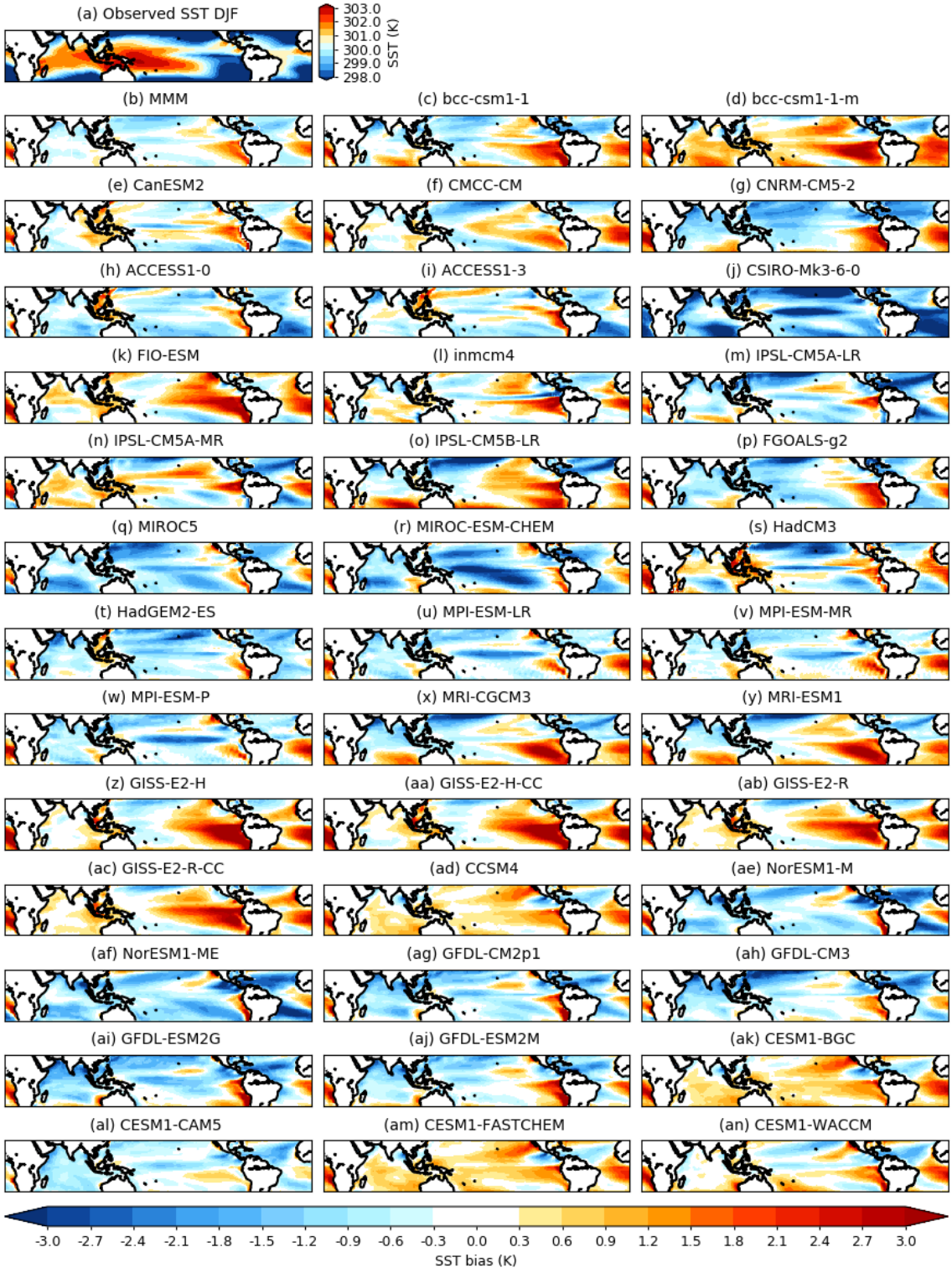

Figure 3.1: Seasonal climatological mean DJF SST (K) for (a) Observation, (b) MMM biases and (c)-(ar) individual CMIP5 model biases averaged from 1979 - 2005.

and underestimation of stratocumulus clouds in the CMIP5 models.

3.3.2 Multimodel regression: relating SST bias and 850 hPa wind bias to Maritime Continent precipitation

To examine the relationships between these seasonal mean climatological SST biases over the tropical oceans and Maritime Continent precipitation, we performed multimodel regression of 42 CMIP5 models' climatological seasonal mean precipitation averaged over the Maritime Continent domain (20°S - 20°N, 80°E - 160°E) onto climatological seasonal mean SSTs in Fig. 3.2 as described in Section 4.2.4. The multimodel regression coefficient represents the Maritime Continent precipitation rate per Kelvin change of SST (mm day^{-1} K^{-1}).

Apart from DJF, when the Maritime Continent mean-state precipitation is largely unrelated to local SSTs, the other seasons (MAM, JJA and SON) show some relationship between local SST and Maritime Continent precipitation. SON, in particular, shows a strong positive correlation over the western Pacific and the SPCZ.

For all four seasons, the Maritime Continent precipitation shows a negative association with central and eastern Pacific Ocean SSTs; the relationship is strongest in DJF (Fig. 3.2a). This resembles the ENSO pattern: that is, reduced rainfall (dry biases) over the Maritime Continent are associated with warmer SST over the central and eastern Pacific, while the colder SST over the central and eastern Pacific are linked to enhancement of rainfall (wet biases) over the Maritime Continent. To investigate the relationship between low-level circulation biases and Maritime Continent precipitation biases, we also performed the same multimodel regression of 38 CMIP5 models climatological seasonal mean precipitation averaged over the Maritime Continent domain (20°S - 20°N, 80°E - 160°E) onto the climatological seasonal mean 850hPa wind (zonal and meridional components) in Fig. 3.3. The multimodel regression shows that the Maritime Continent precipitation increases (wet biases) when model simulates stronger easterly wind over central and eastern Pacific, and vice versa, resembling the La Niña pattern. Fig. 3.3 shows that the Maritime Continent precipitation wet biases are also associated with stronger northerly winds over northwestern Pacific and southern Indian Ocean and southerly wind over the southeastern Pacific in all seasons.

While the region of large correlations remains relatively stationary in space with the seasons over the equatorial Pacific, this is not observed over the Indian Ocean. Thus, the multi-model regression results are seasonally dependent, in particular over the Indian Ocean. Figure 3.2(d) shows that the regression between Maritime Continent precipitation and SST over the Indian Ocean resembles an IOD-like pattern in the Indian Ocean in autumn season (SON) that is not evident in other seasons. The eastern Indian Ocean SSTs show positive regression coefficients, whereas the western Indian Ocean SSTs show a negative regression relationship with Maritime Continent mean-state precipitation. This shows that models which

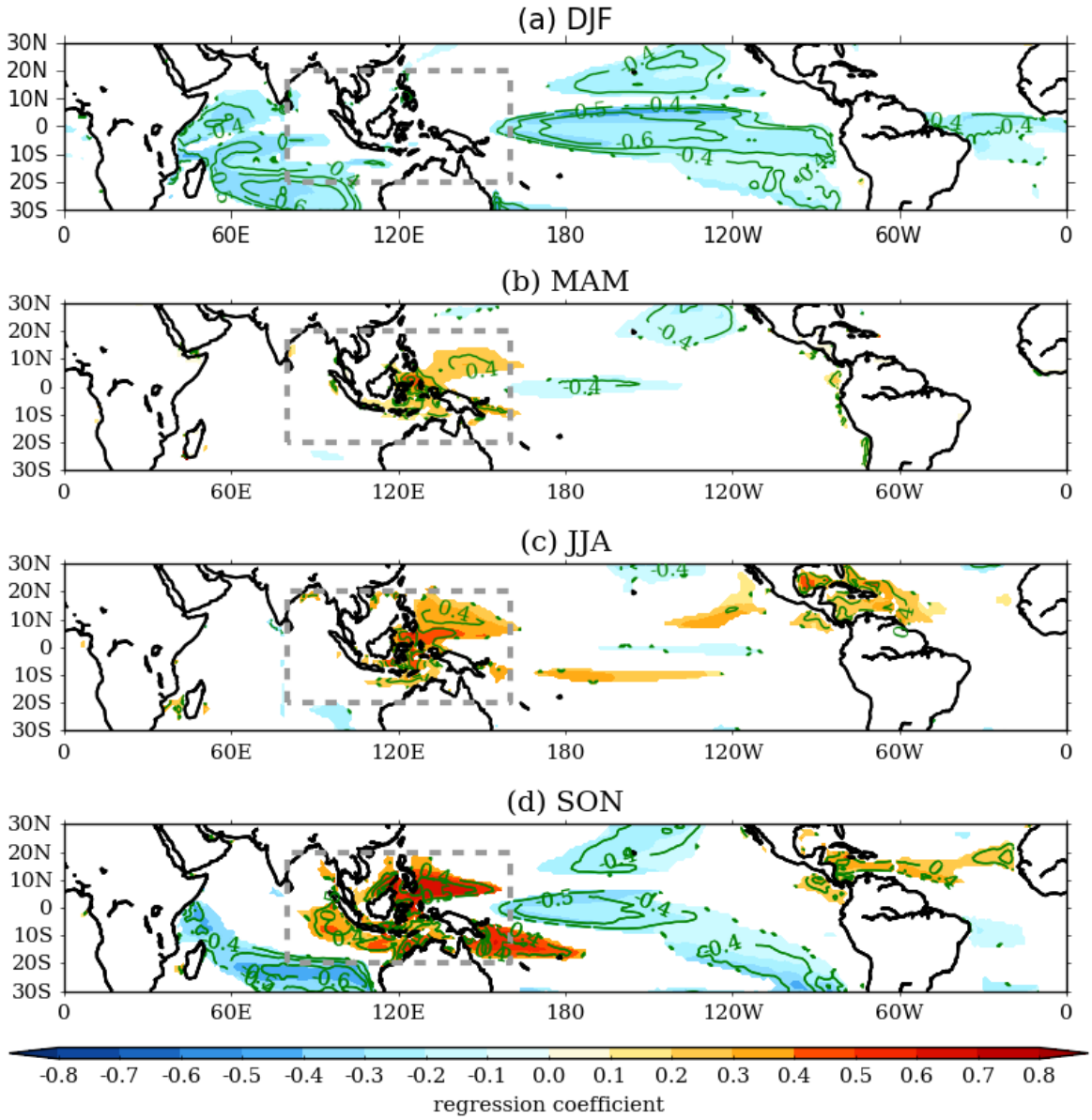

Figure 3.2: Multimodel regression coefficients (mm day^{-1} / K, colour shading) of climatological seasonal mean precipitation in 42 CMIP5 models averaged over the Maritime Continent domain (20°S - 20°N, 80°E - 160°E) regressed onto climatological seasonal mean SSTs for (a) DJF, (b) MAM, (c) JJA and (d) SON. Only regressions that are statistically significant at the 95% confidence interval are shown. Green contour lines represent the multimodel correlation coefficients. The period used for computing the climatology is 1979 - 2005.

simulate colder eastern and warmer western Indian Ocean SST will have wet biases over the Maritime Continent and vice versa. Fig. 3.3(d) shows that wet biases over the Maritime Continent are associated with strengthened westerlies over the Indian Ocean. Figure 3.2 also shows that Maritime Continent precipitation has some relationship with Atlantic Ocean SST in DJF, JJA and SON seasons. However, this will not be further discussed in this study.

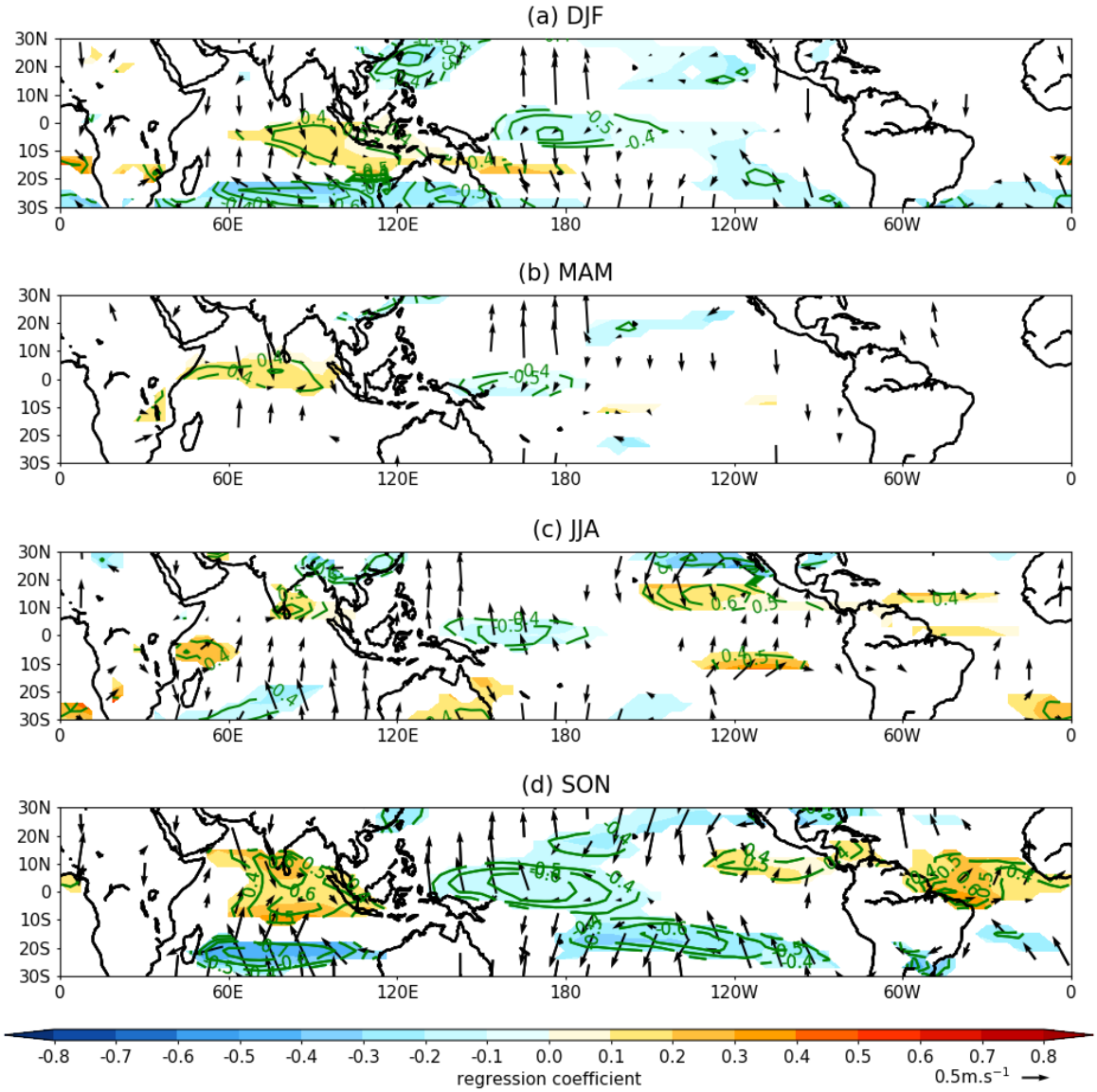

Figure 3.3: Multimodel regression coefficients (mm day^{-1}/m s^{-1}, color shading) of climatological seasonal mean precipitation in 38 CMIP5 models averaged over the Maritime Continent domain (20°S - 20°N, 80°E - 160°E) regressed onto climatological seasonal mean 850hPa zonal winds (u) for (a) DJF, (b) MAM, (c) JJA and (d) SON. Green contour lines represent the multimodel correlation coefficients for zonal winds (u). Vectors represent the multimodel regression coefficients for 850hPa winds (zonal and meridional components). The period used for computing the climatology is 1979 - 2005. Only regression coefficients statistically significant at the 95% confidence interval for the zonal and/or meridional wind components are shown.

3.3.3 Correlations with evaporation

In this section, we examine the relationships between seasonal mean climatological evaporation over the tropical oceans and Maritime Continent precipitation. We performed multimodel regression of 38 CMIP5 models climatological seasonal mean precipitation averaged over the

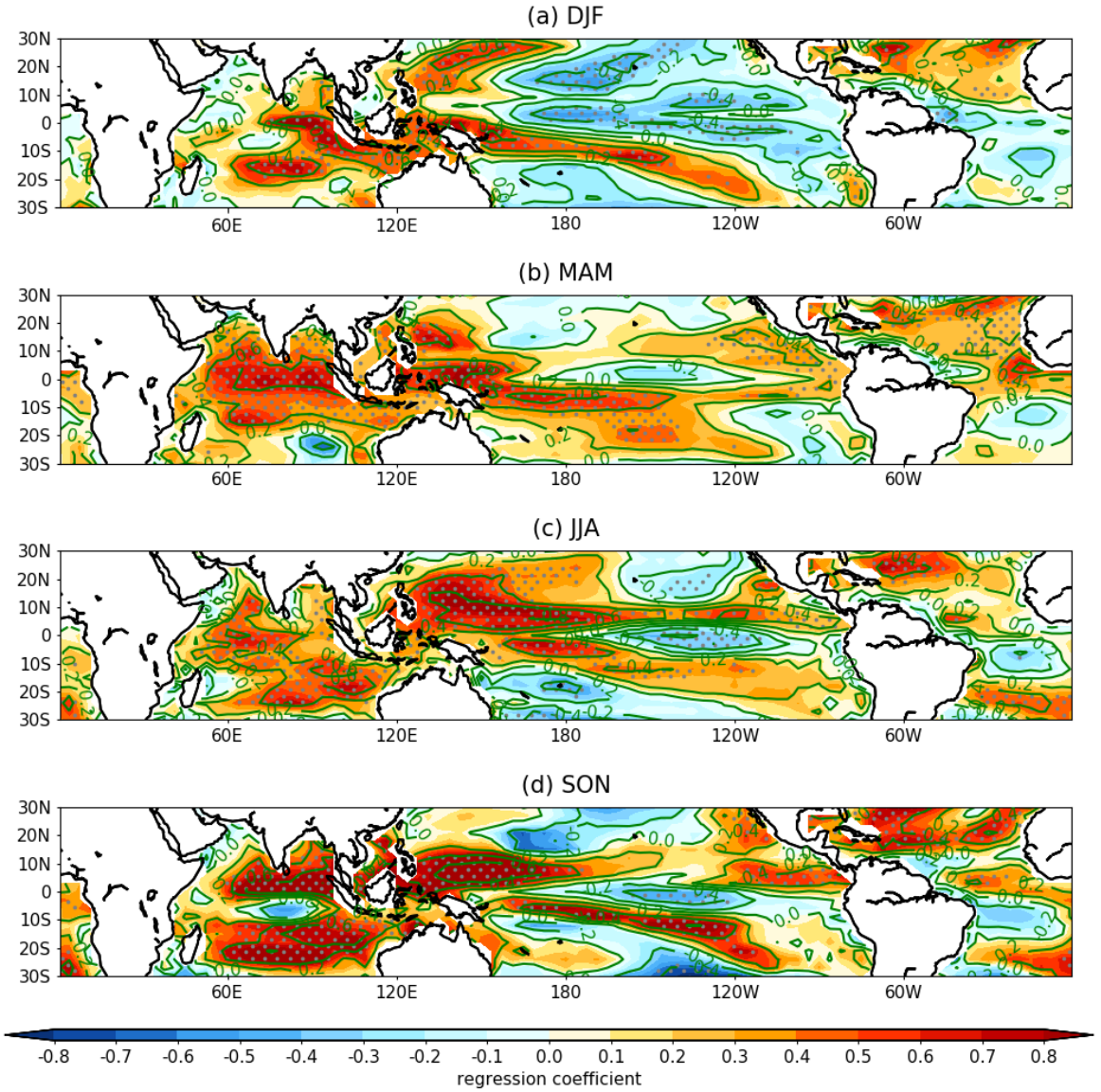

Figure 3.4: Multimodel regression coefficients (colour shading) of climatological seasonal mean precipitation in 38 CMIP5 models averaged over the Maritime Continent domain (20°S - 20°N, 80°E - 160°E) regressed onto climatological seasonal mean evaporation for (a) DJF, (b) MAM, (c) JJA and (d) SON. Regressions that are statistically significant at the 95% confidence interval are stippled. Green contour lines represent the multimodel correlation coefficients. The period used for computing the climatology is 1979 - 2005.

Maritime Continent domain (20°S - 20°N, 80°E - 160°E) onto climatological seasonal mean evaporation in Fig. 3.4. The evaporation and precipitation generally show positive regression coefficients over the Maritime Continent, suggesting that the precipitation biases are related to moisture biases through evaporation. The regression between evaporation and Maritime Continent precipitation has negative coefficients over the central and eastern Pacific, which is somewhat consistent with the negative regressions between SST and Maritime Continent precipitation over this region (Fig. 3.4). On the other hand, in the Indian Ocean there is

generally a positive relationship between evaporation and Maritime Continent precipitation apart from in SON and DJF, which has negative coefficients over the eastern and central Indian Ocean (0 to 10°S).

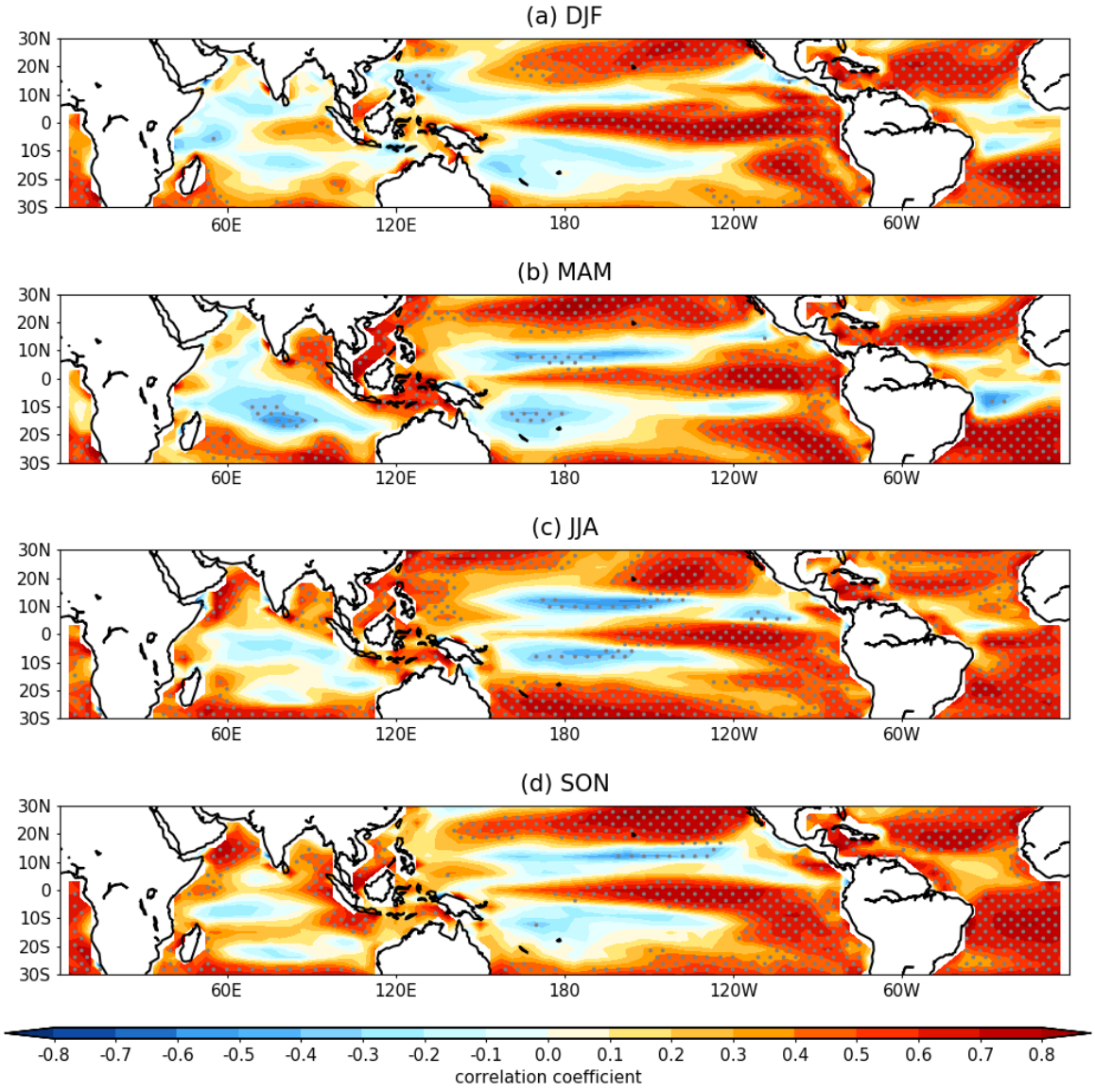

Figure 3.5: Pointwise correlations (colour shading) between climatological seasonal mean evaporation of 38 CMIP5 models and climatological seasonal mean SST for (a) DJF, (b) MAM, (c) JJA and (d) SON. Correlations that are statistically significant at the 95% confidence interval are stippled. The period used for computing the climatology is 1979 - 2005.

Next, we investigate the relationship between local SST and evaporation. Figure 3.5 shows the pointwise correlation between climatological seasonal mean evaporation of 38 CMIP5 models and climatological seasonal mean SST, for each season. Over the Pacific Ocean, the region of strong significant correlations remains relatively stationary in space with the seasons, whereas the correlations are weaker and the coefficients change sign in different season

over the Indian Ocean and Maritime Continent. The evaporation and SST are strongly and positively correlated in the Niño 3 and 3.4 regions for all seasons indicating SST influence on evaporation. Over the Maritime Continent, only DJF shows weak and insignificant correlation, while the other seasons generally show significant positive correlations.

3.3.4 Composites of wettest models minus driest model: connection to biases in lower tropospheric winds and the Walker Circulation

The multimodel regression shows that the Maritime Continent mean-state precipitation bias is strongly related to the SST biases and low-level wind biases in two dominant regions over the central Pacific and western Indian Oceans. To investigate the wind biases associated with the precipitation biases in the coupled models and their relationship with SST biases, we show the seasonal mean Walker circulation, low-level wind and SST difference between the five wettest and driest models in Fig. 3.6. We calculate the area-averaged precipitation biases over the Maritime Continent with respect to observations and select five models with the largest positive (negative) bias to be identified as the wettest (driest) models respectively. For consistency with the analysis in the next section, we only show the DJF and SON seasons. The driest and wettest models are listed in Table 3.1.

Table 3.1: Five driest and five wettest models based on the area-averaged precipitation biases over the Maritime Continent domain in DJF and SON seasons compared to GPCP observations.

DJF		SON	
Driest models	Wettest models	Driest models	Wettest models
bcc-csm1-1	CSIRO-Mk3-6-0	bcc-csm1-1-m	HadCM3
bcc-csm1-1-m	HadCM3	CMCC-CM	MPI-ESM-MR
CMCC-CM	MPI-ESM-LR	IPSL-CM5B-LR	MPI-ESM-P
IPSL-CM5A-LR	GFDL-CM2p1	MRI-CGCM3	GFDL-CM2p1
IPSL-CM5B-LR	GFDL-ESM2G	MRI-ESM1	GFDL-ESM2G

The SST difference between the five wettest and driest models in Fig. 3.6 shows a somewhat similar patterns to the multimodel regression. This demonstrates that the multimodel regression analysis is robust. There are little differences between the SSTs of the wettest and driest models over the Maritime Continent in DJF season (Fig. 3.6a), whereas the increase of Maritime Continent precipitation in SON season is related to warmer SSTs over the Maritime Continent (Fig. 3.6c), consistent with the earlier regression analysis.

Both the winter and autumn seasons are significantly affected by the cold SST biases over the Pacific and Indian Oceans. The wet conditions over the Maritime Continent are related to easterly winds over the equatorial Pacific Ocean and westerly winds over the equatorial Indian Ocean converging towards the Maritime Continent. This is consistent with the findings of Li and Xie (2014) that the surface easterly biases over the Pacific cold tongue region arise

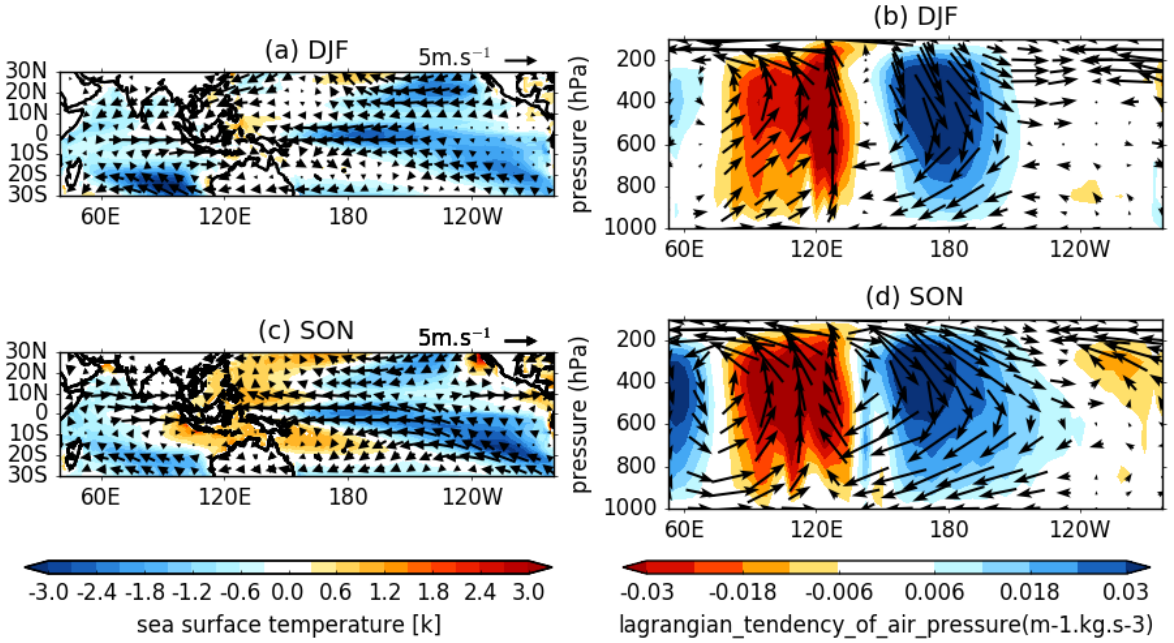

Figure 3.6: Difference between the composite of the 5 wettest models and 5 driest models for (a) SST (K) and 850 hPa wind (m s^{-1}) and (b) mean zonal circulation averaged over 10°N to 10°S using omega (shading and arrow, Pa s^{-1}) and u (arrow, m s^{-1}) for DJF seasons from 1979 - 2005. (c) - (d) are as in (a) - (b) but for SON.

from misrepresentation of ocean-atmosphere interactions via Bjerknes feedback in coupled models. These zonal wind anomalies indicate the strengthening of the Indo-Pacific Walker circulation. These wind anomalies can also cause cooling of SSTs in the equatorial Pacific and Indian Oceans. The SST zonal asymmetry enhances the Walker circulation as shown in Fig. 3.6. The positive precipitation anomalies in the Maritime Continent are associated with strong ascent over the Maritime Continent and descent over the Pacific and Indian Oceans. The descending branch of the Indian Ocean Walker circulation is stronger in SON (Fig. 3.6d) than in DJF (Fig. 3.6b). The SST anomaly pattern over the Indian Ocean in SON season is reminiscent of the positive IOD. Just as in the Pacific Ocean, it appears that mean-state model biases in the Indian Ocean that are reminiscent of an IOD SST pattern yield similar impacts on the Maritime Continent.

3.3.5 SST gradients and Maritime Continent biases

Based on the findings from the above analysis, we next investigate the impact of climatological SST biases in the tropical Pacific and Indian Oceans, their combination, and their connections with the precipitation averaged over the Maritime Continent. We focus on two regions: the Central Tropical Pacific Ocean (CTPO) region (5°S-5°N, 120°W-170°W) and Western Tropical Indian Ocean (WTIO) region (10°S-10°N, 50°E-70°E). Note that the CTPO region is the same as the Niño 3.4 region and the WTIO region is the same as the western Indian

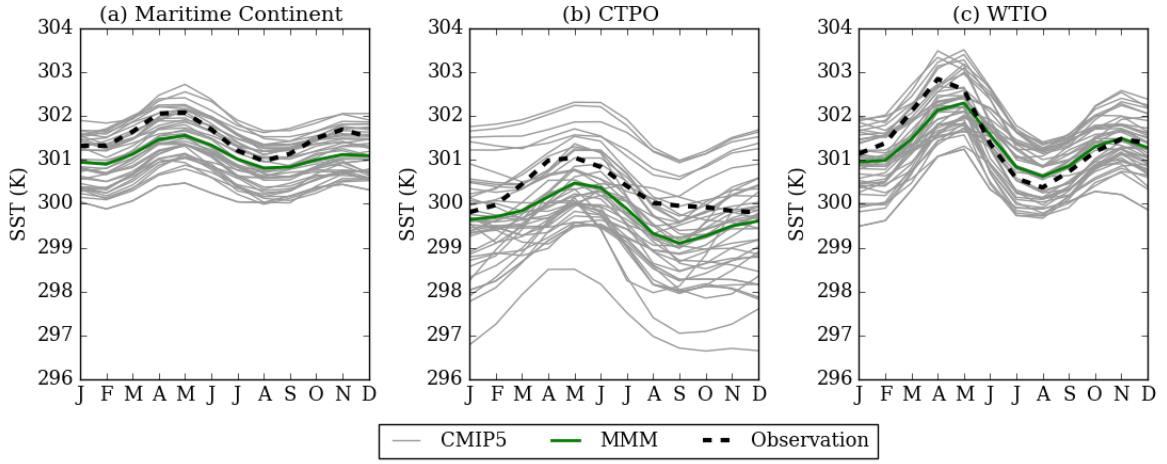

Figure 3.7: Climatological monthly mean SST from 1979 to 2005 averaged over (a) Maritime Continent domain (20°S-20°N and 80°E-160°E), (b) CTPO region (5°S-5°N and 120°W-170°W), and (c) WTIO (10°S-10°N and 50°E-70°E) of individual coupled CMIP5 models (grey lines). The black dashed line represents the observation while the green line represents the MMM.

Ocean Dipole region (IODW) defined in the Saji et al. (1999) paper. However, we first look at climatological mean biases in these boxes, not interannual variability. To avoid confusion, we use CTPO and WTIO when referring to these two regions on climatological time scales in this chapter. When later discussing the interannual variability (ENSO and IOD), we refer these two regions as Niño 3.4 and IODW.

The climatological monthly mean SST simulated by CMIP5 coupled models over the regions of interest are plotted in Fig. 3.7. Most models generally simulate colder climatological monthly mean SST than observed in the Maritime Continent and CTPO regions. However, some models simulate warmer SST than observed in WTIO (Fig. 3.7c) during JJA and SON. The SST climatological mean biases are between -1.5K to 1K over the Maritime Continent, between -3K to 2K over the CTPO and between -2K to 1K over the WTIO. Models perform less well at simulating the annual cycle SSTs over CTPO compared to the other regions and show a considerable inter-model spread of up to 5K for this region. This motivates us to understand how these SST biases may interact with the mean state climatology of the Maritime Continent and its teleconnections, which we will explore in the next section.

To quantify the interaction between SST biases in each of the three oceanic regions and Maritime Continent precipitation, in Fig. 3.8 shows the scatterplots of seasonal-mean precipitation in 42 CMIP5 models versus the SST climatology. The SST and precipitation over the Maritime Continent are weakly correlated (Fig. 3.8a) in all four seasons. However, Maritime Continent precipitation is strongly negatively correlated with CTPO SST (Fig. 3.8b) indicating that remote SST has a stronger relationship with the Maritime Continent on climatological time scales than the local SST. Those models featuring warmer CTPO SST

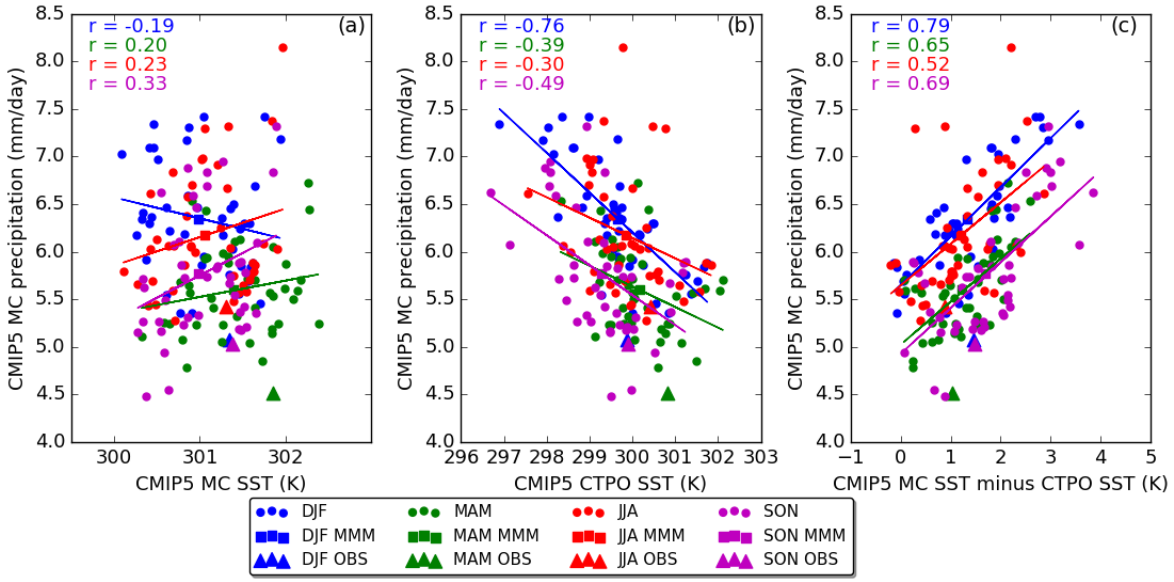

Figure 3.8: Scatterplot of CMIP5 Maritime Continent seasonal mean precipitation climatology versus (a) Maritime Continent seasonal mean SST climatology, (b) CTPO seasonal mean SST climatology and (c) Maritime Continent seasonal mean SST climatology minus CTPO seasonal mean SST climatology. The period used for computing the climatology is 1979 - 2008. The Pearson correlation coefficient (r) for each season is shown in the top left corner. The Pearson correlation coefficients ± 0.4 are significant at the 5% level.

in the mean state generally feature reduced precipitation in the Maritime Continent and vice versa, especially during DJF. Fig. 3.8c shows that the mean-state zonal temperature gradient between the Maritime Continent and the central Pacific is significantly correlated with Maritime Continent precipitation, suggesting an association with the mean-state of Walker Circulation. These correlation coefficients are larger in magnitude than the CTPO correlation coefficients alone, apart from during DJF when a similar magnitude is found.

We perform the same correlation analysis for SSTs and their zonal gradient in the Indian Ocean (Fig. 3.9). We find that the Maritime Continent mean-state precipitation is negatively correlated with model SSTs in the WTIO (Fig. 3.9a), as in the CTPO but with weaker magnitude for all seasons. The mean-state zonal temperature gradient between the Maritime Continent and the WTIO is significantly correlated with Maritime Continent precipitation and the negative correlation is strongest during SON which is the peak phase of IOD (Fig. 3.9b). In other words, as depicted in Fig. 3.2, a negative-IOD-like mean state is associated with excess precipitation over the Maritime Continent.

To investigate the Maritime Continent-Pacific Ocean-Indian Ocean interactions in more detail, we performed the correlation between Maritime Continent mean-state precipitation and Maritime Continent SST minus the CTPO and WTIO SST as shown in Fig. 3.9c using the equation:

$$P_{\mathrm{MC}} = 2 \times T_{\mathrm{MC}} - T_{\mathrm{CTPO}} - T_{\mathrm{WTIO}} \tag{3.1}$$

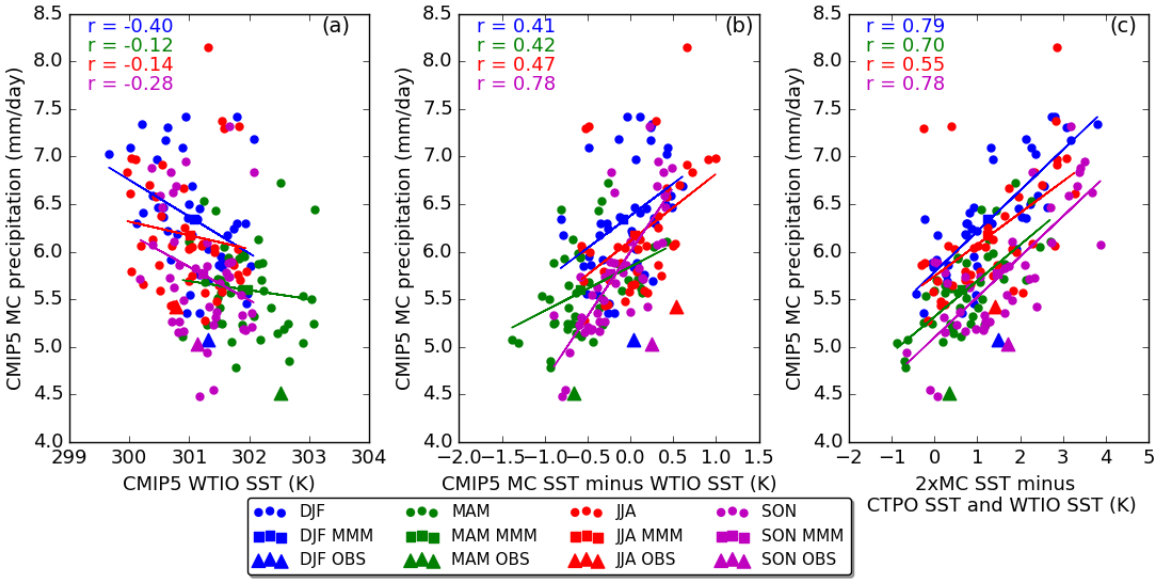

Figure 3.9: Scatterplot of CMIP5 Maritime Continent seasonal mean precipitation climatology versus (a) WTIO seasonal mean SST climatology and (b) Maritime Continent seasonal mean SST climatology minus WTIO seasonal mean SST climatology; and (c) two times Maritime Continent seasonal mean SST climatology minus CTPO and WTIO seasonal mean SST climatology ($P_{\mathrm{MC}} = 2 \times T_{\mathrm{MC}} - T_{\mathrm{CTPO}} - T_{\mathrm{WTIO}}$). The period used for computing the climatology is 1979 - 2008. The Pearson correlation coefficient (r) for each season is shown in the top left corner. The Pearson correlation coefficients ± 0.4 are significant at the 5% level.

where P and T represent the precipitation and SST in the specified regions.

This combination of both CTPO and WTIO seasonal mean SST climatology also shows a significantly strong relationship with Maritime Continent seasonal mean precipitation climatology. This suggests the combined interactions between the climatological Walker cells over the Indian and Pacific Oceans with Maritime Continent mean-state precipitation and circulation. Molteni et al. (2015) showed a tri-polar feature of teleconnection between Maritime Continent, central Pacific Ocean and western Indian Ocean. They found a positive correlation between central Pacific Ocean and western Indian Ocean; and SSTs in both of these regions are negatively correlated with the Maritime Continent on interannual time scales. Our results show that the SST gradients in coupled GCMs are also tightly coupled to the Walker circulations in the climatological mean-state. This correlation in Fig. 3.9 is consistent with the multimodel regression (Fig. 3.2) that showed the Maritime Continent mean-state precipitation is significantly correlated with central Pacific and western Indian Oceans SSTs.

Having established the clear link between Maritime Continent climatological precipitation and the representation of the Indian and Pacific Oceans mean states in coupled GCMs, next, we investigate the interannual variability of Pacific Ocean and Indian Ocean SST and its teleconnection toward the Maritime Continent, and later determine if mean state biases impact this teleconnection.

3.4 Pacific and Indian Ocean teleconnections to the Maritime Continent in AMIP5 and CMIP5 models

This section is divided into two parts. The first part investigates the ENSO teleconnections to the Maritime Continent while the second part assesses the IOD teleconnections to the Maritime Continent.

3.4.1 ENSO-Maritime Continent teleconnections

In this section, we first analyse relationship between the Maritime Continent precipitation and ENSO at interannual scale in AMIP5. We then analyse these relationships in the CMIP5 models. In the coupled model, the biases in simulating ENSO and its teleconnection involves ocean-atmosphere feedbacks, that can come either from the ocean driving the atmosphere or the atmosphere forcing the ocean. Before we can understand the impact of SST biases on teleconnections to Maritime Continent rainfall, we must first analyse how these models perform in prescribed SST mode.

3.4.1.1 AMIP5

In this section, we analyse the interannual variability of precipitation over the Maritime Continent during ENSO events simulated in AMIP5 experiments, run with prescribed SSTs. El Niño events were chosen using the SST anomalies in the Niño-3.4 region (5°S-5°N, 120°W-170°W) which had an amplitude of greater than 0.5°C for at least five consecutive 3-month running mean periods. Similarly, values below -0.5°C were used to define La Niña. The El Niño and La Niña years in the AMIP5 are listed in Table 3.2. The nine El Niño events and the eight La Niña events are composited and compared to the 1979 - 2008 climatology in observations (GPCP rainfall and ERA-Interim reanalysis winds).

Table 3.2: The El Niño and La Niña years between 1979 to 2008 in AMIP5 as defined by SSTs in the Niño 3.4 region and exceeding the ±0.5 °C threshold for at least five consecutive 3-month running mean periods. The 1979 refers to the DJF of 1979/80 winter, i.e. December of the given year and January and February of the following year.

ENSO	**Year**								
El Niño	1982	1986	1987	1991	1994	1997	2002	2004	2006
La Niña	1983	1984	1988	1995	1998	1999	2000	2007	

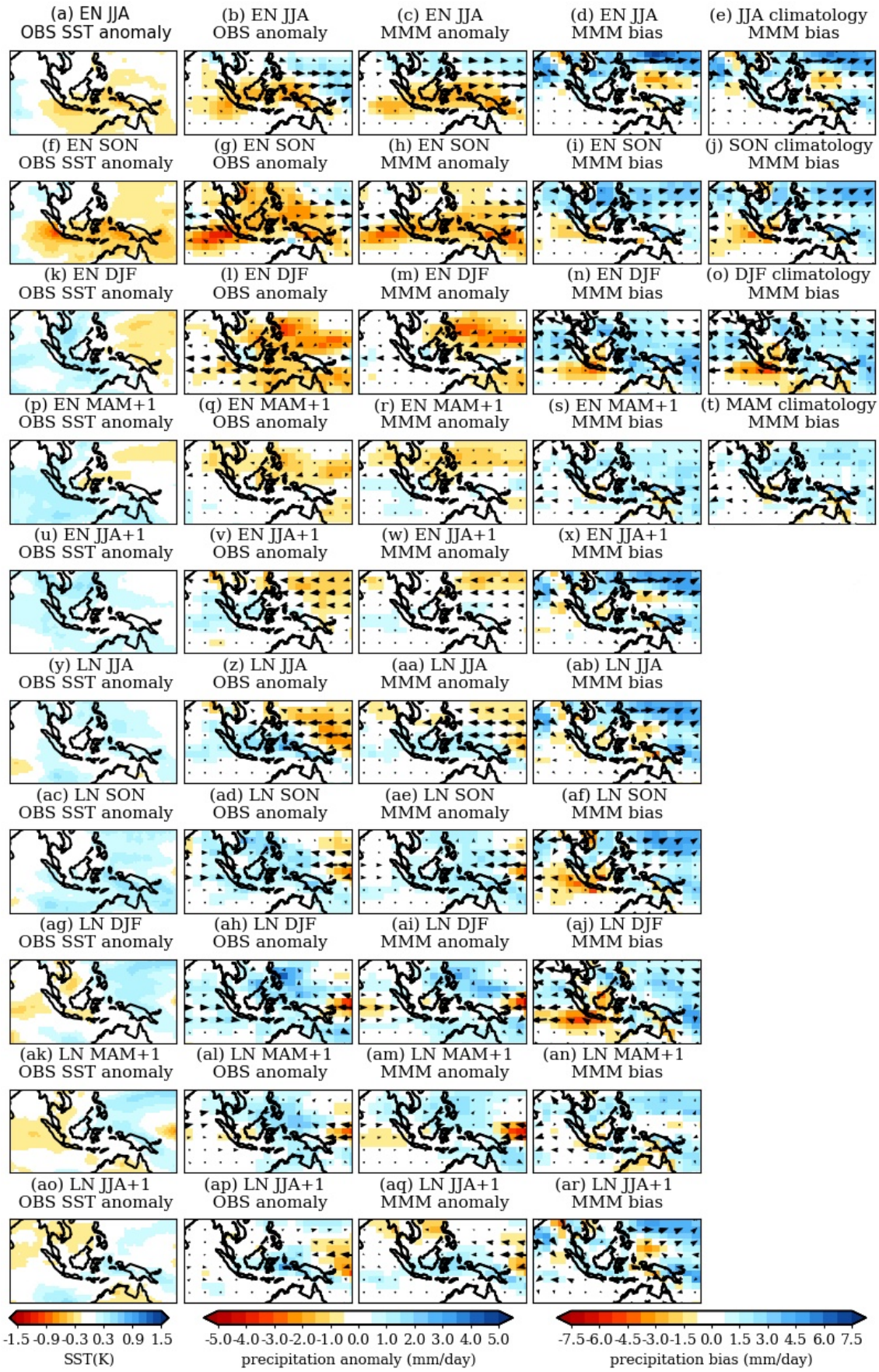
(a) EN JJA OBS SST anomaly
(b) EN JJA OBS anomaly
(c) EN JJA MMM anomaly
(d) EN JJA MMM bias
(e) JJA climatology MMM bias
(f) EN SON OBS SST anomaly
(g) EN SON OBS anomaly
(h) EN SON MMM anomaly
(i) EN SON MMM bias
(j) SON climatology MMM bias
(k) EN DJF OBS SST anomaly
(l) EN DJF OBS anomaly
(m) EN DJF MMM anomaly
(n) EN DJF MMM bias
(o) DJF climatology MMM bias
(p) EN MAM+1 OBS SST anomaly
(q) EN MAM+1 OBS anomaly
(r) EN MAM+1 MMM anomaly
(s) EN MAM+1 MMM bias
(t) MAM climatology MMM bias
(u) EN JJA+1 OBS SST anomaly
(v) EN JJA+1 OBS anomaly
(w) EN JJA+1 MMM anomaly
(x) EN JJA+1 MMM bias
(y) LN JJA OBS SST anomaly
(z) LN JJA OBS anomaly
(aa) LN JJA MMM anomaly
(ab) LN JJA MMM bias
(ac) LN SON OBS SST anomaly
(ad) LN SON OBS anomaly
(ae) LN SON MMM anomaly
(af) LN SON MMM bias
(ag) LN DJF OBS SST anomaly
(ah) LN DJF OBS anomaly
(ai) LN DJF MMM anomaly
(aj) LN DJF MMM bias
(ak) LN MAM+1 OBS SST anomaly
(al) LN MAM+1 OBS anomaly
(am) LN MAM+1 MMM anomaly
(an) LN MAM+1 MMM bias
(ao) LN JJA+1 OBS SST anomaly
(ap) LN JJA+1 OBS anomaly
(aq) LN JJA+1 MMM anomaly
(ar) LN JJA+1 MMM bias
-1.5 -0.9 -0.3 0.3 0.9 1.5
SST(K)
-5.0 -4.0 -3.0 -2.0 -1.0 0.0 1.0 2.0 3.0 4.0 5.0
precipitation anomaly (mm/day)
-7.5 -6.0 -4.5 -3.0 -1.5 0.0 1.5 3.0 4.5 6.0 7.5
precipitation bias (mm/day)

Figure 3.10: Maritime Continent JJA (in onset phase) (a) composites of El Niño observed SST anomaly, (c) composites of El Niño observed precipitation and 850 hPa wind anomaly, (c) AMIP5 MMM composites of El Niño precipitation and 850 hPa wind anomaly, (d) AMIP5 MMM composites of El Niño precipitation and 850 hPa wind biases with respect to observations, and (e) AMIP5 MMM climatological seasonal mean precipitation and 850 hPa wind biases with respect to observations. (f)-(j) are the same as (a)-(e) but for SON, (k)-(o) for DJF, (p)-(l) for MAM and (u)-(x) for JJA (in decay phase). (u)-(ar) are same as (a)-(x) but for the La Niña phase. The period used for computing the climatology is 1979 - 2008.

An ENSO event usually begins to develop in JJA and SON seasons and reaches its peak in DJF. It then slowly decays in the MAM and JJA seasons of the following year. First, we look at the composite of observed El Niño SST anomalies in the first column of Fig. 3.10. The Maritime Continent SST shows negative anomalies during the onset phase in JJA (Fig. 3.10a) and SON (Fig. 3.10f) and more positive anomalies over the eastern part of Maritime Continent in DJF (Fig. 3.10k) and MAM (Fig. 3.10p) and most of Maritime Continent in JJA (Fig. 3.10u). Maritime Continent observed precipitation generally shows negative anomalies between the previous summer and the following spring: El Niño onset phase, i.e JJA (Fig. 3.10b) and SON (Fig. 3.10g); peak phase, i.e DJF (Fig. 3.10l); and decay phase, i.e MAM (Fig. 3.10q). However, the El Niño decay phase in JJA (Fig. 3.10v), which begins the transition into La Niña, shows more positive anomalies over the Maritime Continent. The dry conditions are generally more confined over the equatorial region in JJA (onset phase), and spread towards the off-equatorial region from autumn to spring season as described by Kubota et al. (2011). The MMM El Niño shows few differences in precipitation and 850 hPa wind anomalies for all three phases (Fig. 3.10, third column) compared to observed anomalies (Fig. 3.10, second column). The MMM simulates slightly stronger winds in JJA (onset phase), SON, DJF and MAM than observed. The area of simulated dry anomalies is slightly smaller than observed in all phases. During La Niña the SST and precipitation anomalies are opposite to the El Niño whereby negative SST anomalies and wetter than normal conditions occur over the Maritime Continent.

The MMM precipitation and 850 hPa wind biases over the Maritime Continent with respect to observations are similar for the seasonal climatology (Fig. 3.10e, j, o, t) and El Niño events (Fig. 3.10d, i, n, s, x). This implies that the MMM is able to capture the El Niño anomaly. The same result holds for La Niña events (Fig. 3.10ab, af, aj, an, ar). This suggests that biases in precipitation and circulation during ENSO events result from the climatological mean state biases. This is consistent with the Achuta Rao and Sperber (2006) study on CMIP3 and CMIP2 models which showed that the model skill at reproducing the El Niño precipitation composite over the tropics depends on the model fidelity at simulating the boreal winter precipitation climatology.

To examine the ability of the AMIP5 models to reproduce the wintertime interannual variability in the Maritime Continent precipitation, the box-and-whisker plot in Fig. 3.11

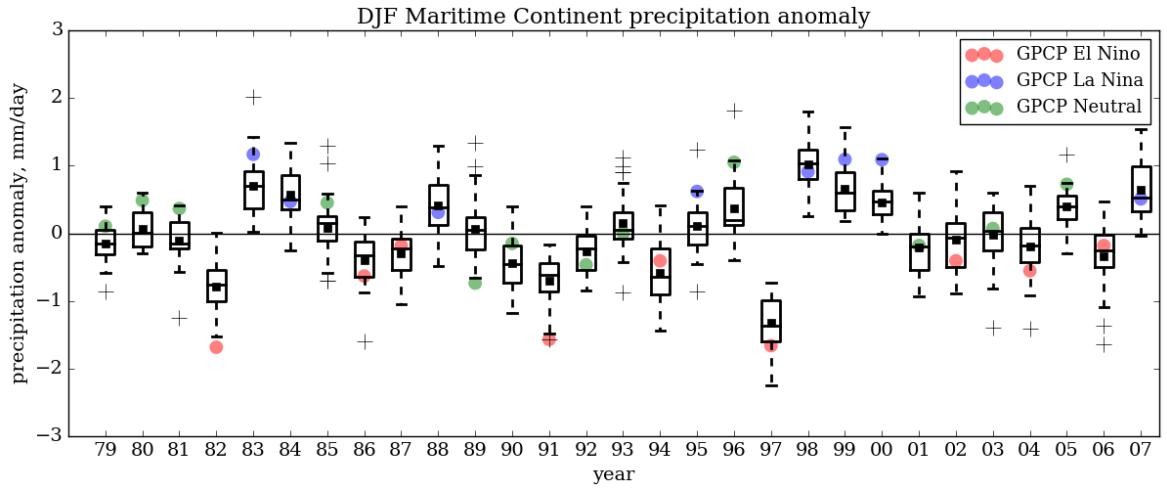

Figure 3.11: Box-and-whisker plot of AMIP5 DJF interannual precipitation anomaly averaged over the Maritime Continent domain (20°S-20°N and 80°E-160°E) from 1979 to 2007. Black boxes indicate the interquartile range (IQR), black lines in the boxes indicate the median; black squares represent the mean. The plus signs are the outliers, which are anomalies smaller than the lower quartile or larger than the upper quartile by at least 1.5 times the IQR. The dots are the GPCP DJF precipitation anomaly for El Niño (red), neutral (green) and La Niña (blue) years. The DJF of 1979 refers to the 1979/80 winter, December of the given year and January and February of the following year.

shows the spread of AMIP5 DJF precipitation anomalies averaged over the Maritime Continent domain (refer to Fig. 3.10k, l) from 1979-2008. Without exception, the mean DJF GPCP precipitation anomalies over the Maritime Continent are negative anomalies for El Niño (red dots), whereas La Niña (blue dots) shows positive anomalies. The MMM of AMIP5 is able to capture the anomalies for most years, demonstrating a reasonably consistent relationship between El Niño (La Niña) and dry (wet) DJF periods. However, there are some inter-model differences between the precipitation anomalies for certain years. Most models overestimate the Maritime Continent precipitation for 1982 and 1991 which are both El Niño years.

To further investigate the skill of AMIP5 at simulating the relationship between Maritime Continent precipitation anomalies and ENSO, we plot another box-and-whisker plot according to the Niño 3.4 index that classified ENSO events by strength in Fig. 3.12. Forced by prescribed SST, all the AMIP5 models have the same Niño 3.4 index but with different atmospheric responses. Consistent with the observations, the models simulate an inverse relationship between Maritime Continent precipitation anomalies and the Niño 3.4 index. For strong El Niño events exceeding 1 °C, most models are able to simulate negative precipitation anomalies over the Maritime Continent. And vice versa for La Niña: models simulate positive precipitation anomalies over the Maritime Continent.

While the performance shown above for the relationship between ENSO and Maritime Continent precipitation in AMIP5 models looks good, coupled models feature SST biases that

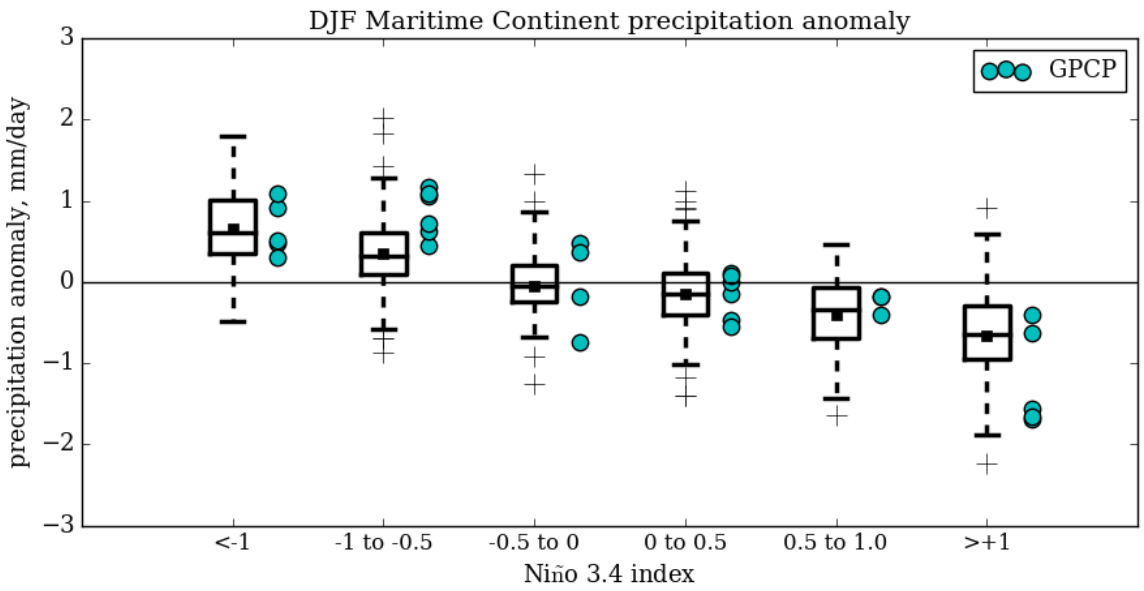

Figure 3.12: Box-and-whisker plot of AMIP5 DJF precipitation anomaly averaged over the Maritime Continent domain (20°S-20°N and 80°E-160°E) according to the Niño 3.4 index. Black boxes indicate the interquartile range (IQR), black lines in the boxes indicate the median; black squares represent the mean. The plus signs are the outliers, which are anomalies smaller than the lower quartile or larger than upper quartile by at least 1.5 times the IQR. The green dots are the GPCP DJF precipitation anomalies from 1979 to 2008.

may affect these teleconnections. Next, we examine these SST biases and their relationship to precipitation biases on interannual time-scales in CMIP5.

3.4.1.2 CMIP5

To investigate the relationship between Maritime Continent precipitation and local as well as remote SSTs, we calculate the Pearson correlation coefficient (r) between the DJF interannual precipitation and SST for observations and CMIP5 models and plot these temporal correlations in Fig. 3.13. The observational datasets suggest an insignificant local SST correlation (Fig. 3.13a, green bar), whereas certain models such as inmcm4, CCSM4, GFDL-ESM2M and CESM1-CAM5 suggest a significant relationship. The coupled models show larger variations of the temporal correlation between local SST and Maritime Continent precipitation compared to AMIP5, for which all models simulate insignificant temporal correlation (figure not shown).

Most coupled models are able to capture the observed remote Niño 3.4 SST and Maritime Continent precipitation relationship (Fig. 3.13b) as well as the east-west SST gradient and Maritime Continent relationship (Fig. 3.13c). Only three models simulate negative correlation between SST gradient and Maritime Continent precipitation, opposite from observations, while six models simulate positive correlation but not statistically significant at 95% level. The rest of the models are capable of capturing the relationship between zonal SST gradient

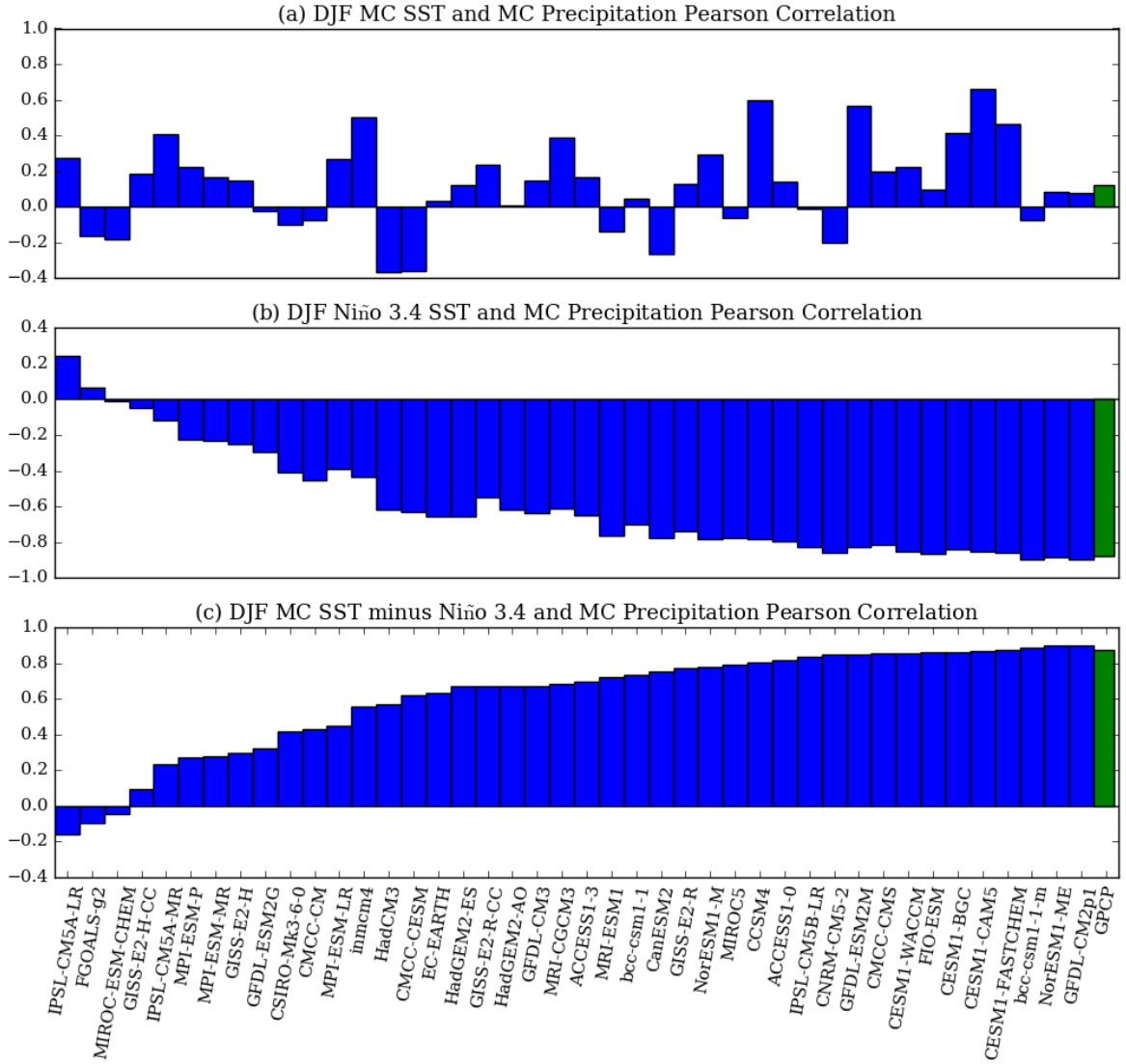

Figure 3.13: Temporal correlation between DJF CMIP5 Maritime Continent precipitation and (a) Maritime Continent SST, (b) Niño 3.4 SST and (c) Maritime Continent SST minus Niño 3.4 SST. The panels are arranged showing models in order from lowest to highest Pearson correlation coefficients in (c). The green bars show the observed correlation using GPCP precipitation.

and Maritime Continent precipitation. This shows that CMIP5 models are in general able to simulate the zonal SST gradient between Maritime Continent and Pacific Ocean and the associated precipitation anomalies over the Maritime Continent (i.e. the ENSO teleconnection). When SSTs over the Maritime Continent (western Pacific) are cooler than normal and SSTs over the Niño 3.4 region (central Pacific) are warmer than normal, models simulate less rainfall over the Maritime Continent, and vice versa.

Studies have shown that models with a better representation of the basic state are able to capture well the ENSO-monsoon teleconnection (Turner et al., 2005; Annamalai et al., 2007). Here, we show the scatter plot of the 42 CMIP5 models' DJF temporal correlation

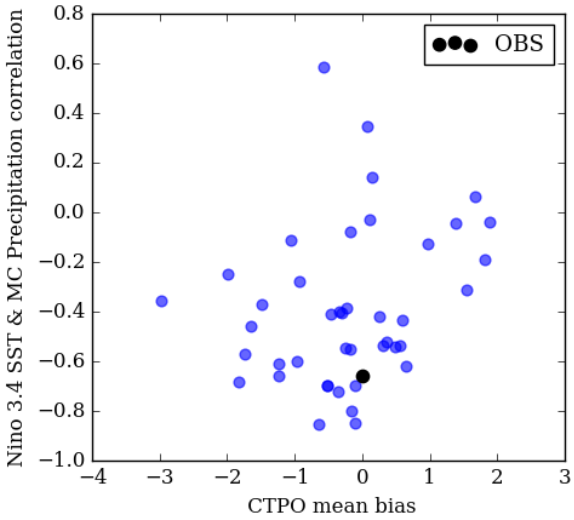

Figure 3.14: Scatter plot of the 42 CMIP5 models' DJF temporal correlation coefficient between Niño 3.4 SST and the Maritime Continent precipitation versus the CTPO mean bias. The black dot represents the observed relationship.

coefficient between Niño 3.4 SST and the Maritime Continent precipitation versus the absolute value of the CTPO mean bias in Fig. 3.14. As depicted in Fig. 3.14, models with smaller CTPO SST mean bias have a better representation of ENSO-Maritime Continent precipitation teleconnection. The Pearson correlation for the 42 model points shown in the scatterplot in Fig. 3.14 is 0.27. This is statistically significant at the 90% level suggesting some relationship between the CTPO SST mean-state biases and ENSO-Maritime Continent teleconnection.

Apart from ENSO's temporal evolution, inaccuracies in the representation of ENSO also include its spatial structure of the variability. As there is some spatial variation of dry conditions over the Maritime Continent during El Niño years (see Fig. 3.10l), we plot the map of temporal correlation between gridpoint precipitation and Niño 3.4 index in DJF season for AMIP5 and CMIP5 models in Fig. 3.15.

The spatial map of observed temporal correlations (Fig. 3.15a) shows that Maritime Continent precipitation is generally negatively correlated with the Niño 3.4 index, apart from a small area in southwestern Borneo which is positively correlated with Niño 3.4 index as described in Qian et al. (2013). The increase of rainfall over southwestern Borneo during El Niño events in DJF, in contrast to decreases over the rest of the region is related to the inverse relationship between monsoonal wind speed and the diurnal cycle of land-sea breezes (Qian et al., 2013).

The PCC of the ENSO teleconnection pattern with respect to observations is depicted at the top of each panel in Fig. 3.15. The MMM ENSO teleconnection spatial map is obtained by taking the average of Pearson correlation coefficients among the 20 AMIP5 and CMIP5 models respectively. The AMIP5 MMM is able to simulate the observed ENSO teleconnection

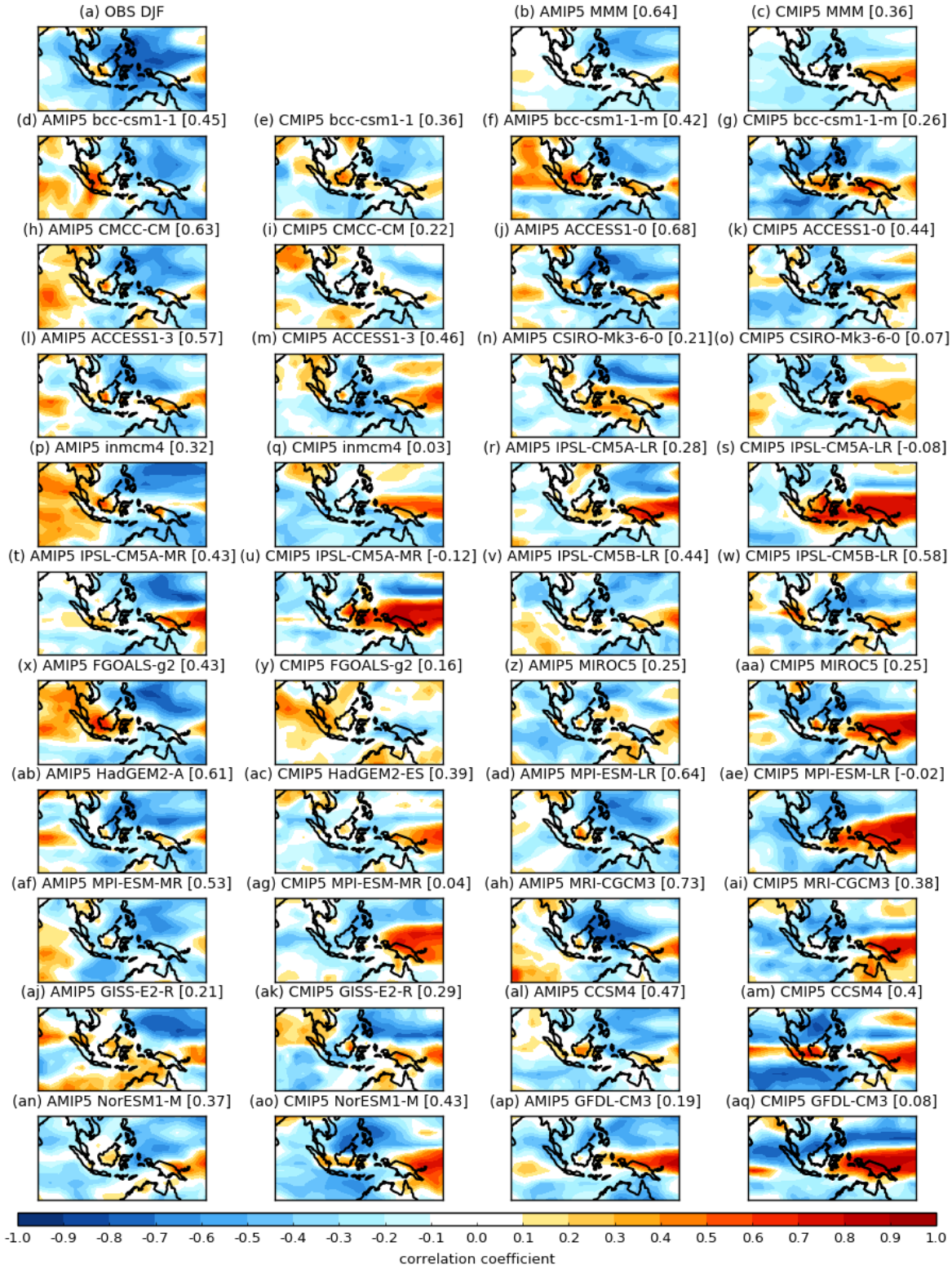

Figure 3.15: Spatial maps of temporal correlation between gridpoint precipitation and Niño 3.4 index in DJF for (a) Observations, AMIP5 (first and third column) and CMIP5 (second and fourth column). The PCC calculated between the observed and simulated teleconnection pattern over the Maritime Continent is in square brackets above each panel.

pattern over the Maritime Continent (Fig. 3.15b, PCC=0.64) but the correlation is weaker. On the other hand, the CMIP5 MMM has larger discrepancies compared to observations (Fig. 3.15c, PCC=0.36), with a positive correlation over Papua opposite to observations and a much weaker negative correlation over the rest of the Maritime Continent region.

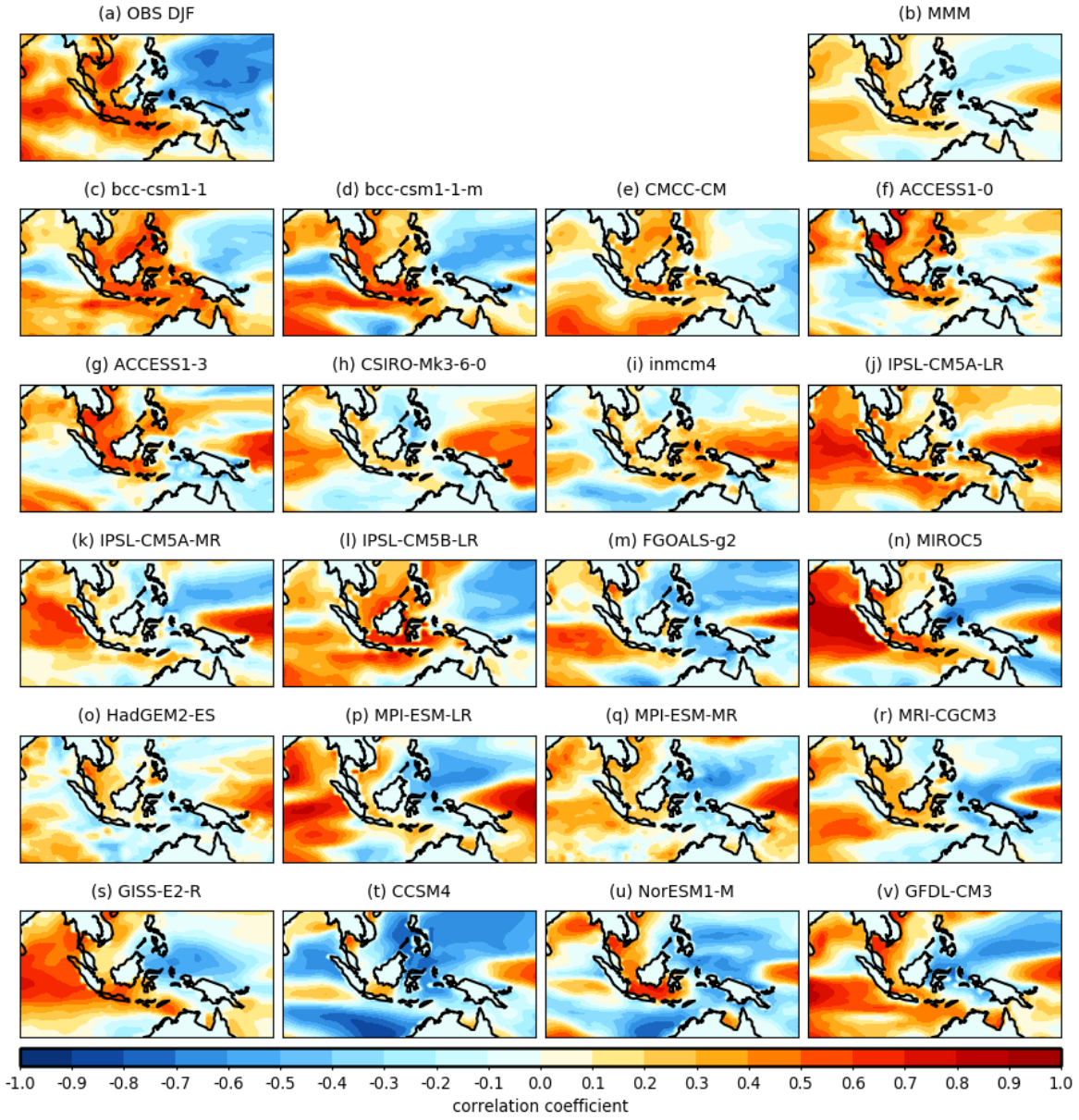

Figure 3.16: Spatial maps of temporal correlation between gridpoint SST and Niño 3.4 index in DJF for (a) Observations, (b) MMM and (c)-(v) CMIP5 models.

Comparison between AMIP5 and CMIP5 individual model PCCs show that most of the AMIP5 models perform better than CMIP5 models at simulating the spatial patterns of the temporal correlation between the Niño 3.4 index and precipitation over the Maritime Continent

except for three models (IPSL-CM5B-LR, GISS-E2-R and NorESM1-M). Coupled CMIP5 models such as IPSL-CM5A-LR (Fig. 3.15s), MIROC5 (Fig. 3.15aa) and MPI-ESM-LR (Fig. 3.15ae) simulate positive correlations that are too strong, extending too far westwards from the central Pacific to Papua compared to observations and AMIP5. This error was also found in previous versions of CMIP models, for example in CMIP2 (Achuta Rao and Sperber, 2006) and CMIP3 (Annamalai et al., 2007; Cai et al., 2009). This systematic error in ENSO is related to the mean-state SST cold biases over the Pacific cold tongue that extend too far westward into the western Pacific. The positive correlation over the Maritime Continent is opposite to observations which show a negative correlation, i.e. warm anomalies over the Niño 3.4 region are associated with reduced rainfall over the Maritime Continent and vice versa. The RMSE of teleconnection pattern of CMIP5 is also larger than AMIP5 suggesting that SST and coupling biases degraded the ENSO-Maritime Continent teleconnection in CMIP5.

Figure 3.16 shows the spatial maps of temporal correlation between gridpoint SST over the Maritime Continent and the Niño 3.4 index in DJF. The observed SST over the western Pacific is negatively correlated with the Niño 3.4 index while the SSTs in the Indian Ocean are positively correlated with the Niño 3.4 index. MMM shows weaker correlations and a positive correlation that extend westward into the western Pacific indicating a mean-sate SST cold biases over this region. However, IPSL-CM5B-LR (Fig. 3.15w), i.e. the model with the highest PCC value (0.58) at simulating the spatial patterns of the temporal correlation between the Niño 3.4 index and precipitation over the Maritime Continent, is able to capture the correlations between SST and the Niño 3.4 index. Figure 3.16 shows that most CMIP5 models simulate positive correlation over the western Pacific indicating systematic error of ENSO response extending westward into the west Pacific.

3.4.2 IOD-Maritime Continent teleconnections

SST variability in the tropical Indian Ocean significantly modulates Maritime Continent climate, in particular through the IOD teleconnection. In this section, we first analyse the IOD and its relationship with Maritime Continent precipitation in AMIP5, followed by CMIP5 and then determine if mean state biases impact this teleconnection.

3.4.2.1 AMIP5

First, we calculate the Dipole Mode Index (DMI) based on the difference between IODW (10°S-10°N, 50°E-70°E) and IODE (0°S-10°S, 90°E-110°E) SST anomalies as defined in Saji et al. (1999). IOD typically develops in JJA, reaches its peak in SON and then slowly decays in DJF. The life cycle of the IOD is shorter than ENSO. The five positive IOD events and four negative IOD events listed in Table 3.3 are composited and compared to the 1979-2008

climatology in observations (GPCP rainfall and ERA-Interim reanalysis winds). All of the positive IOD years are also the El Niño years while 1998 is also both a La Niña and negative IOD year.

Table 3.3: Positive IOD and negative IOD years between 1979 to 2008 as defined by the SON DMI exceeding the ±0.5 °C threshold.

IOD	**Year**				
Negative IOD	1980	1992	1996	1998	
Positive IOD	1982	1991	1994	1997	2006

The first column of Figure 3.17 shows the observed SST anomalies while the second columns show the observed precipitation and wind anomalies over the Maritime Continent during positive IOD and negative IOD events. During positive IOD events, negative SST anomalies are generally observed over the Maritime Continent in JJA (Figure 3.17a) and SON (Figure 3.17f) and over the west Pacific in DJF (Figure 3.17k). On the other hand, the dry anomalies are generally more confined over the equatorial region in JJA (onset phase), and spread toward the off-equatorial region from SON to DJF seasons. The negative IOD composites show opposite condition to positive IOD composites but with weaker magnitude. The MMM (Fig. 3.17, third column) simulates weaker dry anomalies for all three seasons than the observations and stronger westerlies over the western Pacific in JJA and SON during positive IOD events.

The spatial patterns in precipitation and 850 hPa wind biases over the Maritime Continent during positive IOD events (Fig. 3.17d, i, n) and negative IOD events (Fig. 3.17s, w, aa) are similar to the seasonal climatological biases (Fig. 3.17e, j, o) for the onset, peak and decay phases. This suggests that biases in AMIP5 precipitation and circulation over the Maritime Continent during IOD events result from the climatological mean-state biases.

To investigate the interannual Maritime Continent precipitation simulated by AMIP5, we plot the box-and-whisker plot as in Fig. 3.11 but using the DMI and SON season in Fig. 3.18. The SON GPCP precipitation anomalies over the Maritime Continent are negative anomalies for positive IOD (red dots) and positive anomalies for negative IOD (blue dots) except 1980 and 1992. The MMM of AMIP5 did fairly well at capturing the interannual variations of SON precipitation anomalies for most years compared to individual models.

Next, we plot the box-and-whisker plot according to DMI in Fig. 3.19 to investigate the skill of AMIP5 models at simulating the negative relationship between Maritime Continent precipitation anomalies and the IOD. Consistent with observations, AMIP5 models are able to simulate the inverse relationship between the Maritime Continent precipitation anomalies and DMI. During positive IOD events when SSTs over the eastern Indian Ocean are colder than normal, and SSTs in the western Indian Ocean are warmer than normal, most models simulate negative precipitation anomalies over the Maritime Continent. Conversely, positive

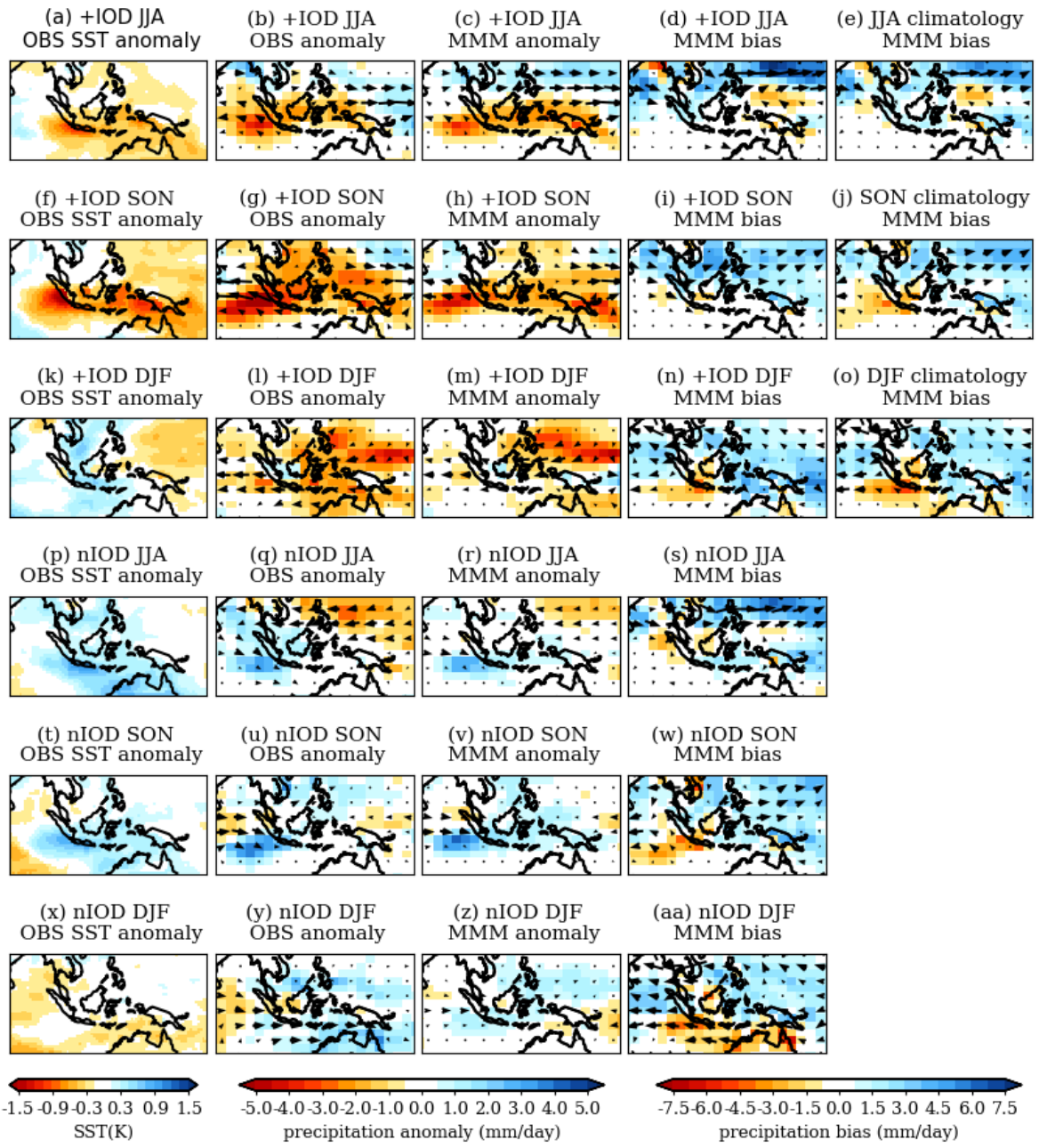

Figure 3.17: Maritime Continent JJA composites of (a) positive IOD observed SST anomaly, (b) positive IOD observed precipitation and 850 hPa wind anomaly, (c) AMIP5 MMM positive IOD precipitation and 850 hPa wind anomaly, (d) AMIP5 MMM positive IOD precipitation and 850 hPa wind biases with respect to observations. In (e) we show AMIP5 MMM climatological seasonal mean precipitation and 850 hPa wind biases with respect to observations. (f)-(j) are same as (a)-(e) but for SON and (k)-(o) for DJF. (p)-(aa) are same as (a)-(o) but for the composites of negative IOD. The period used for computing the climatology is 1979 - 2008.

precipitation anomalies are simulated during negative IOD events. Next, we examine the skill of CMIP5 coupled models at simulating Maritime Continent precipitation on interannual

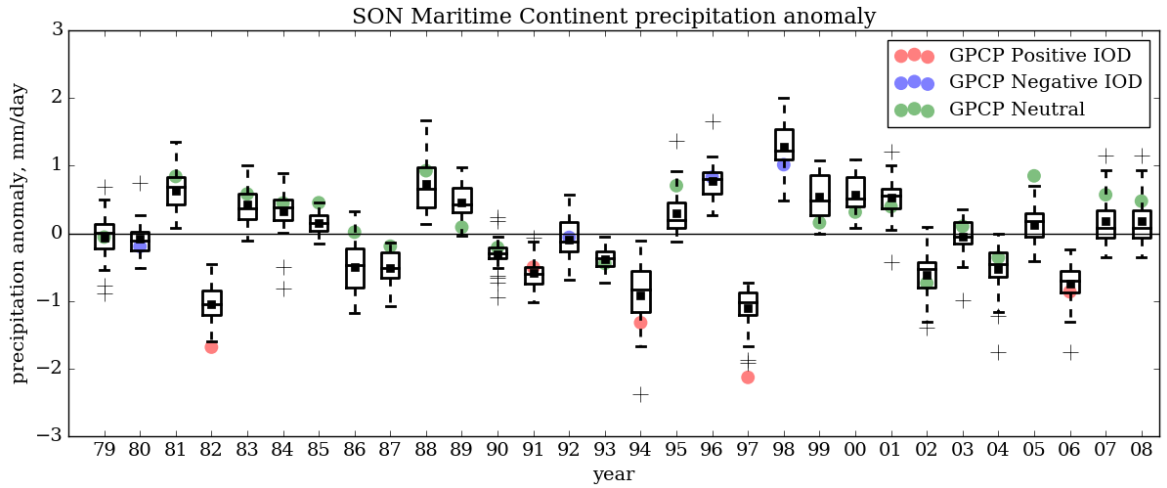

Figure 3.18: Box-and-whisker plot of AMIP5 SON precipitation anomaly averaged over the Maritime Continent domain (20°S-20°N and 80°E-160°E). Black boxes indicate the interquartile range (IQR), black lines in the boxes indicate the median; black squares represent the mean. The plus signs are the outliers, which are anomalies smaller than the lower quartile or larger than the upper quartile by at least 1.5 times the IQR. The dots are the GPCP SON mean SST anomaly for positive IOD (red), neutral (green) and negative IOD (blue) years.

timescales in CMIP5 during SON.

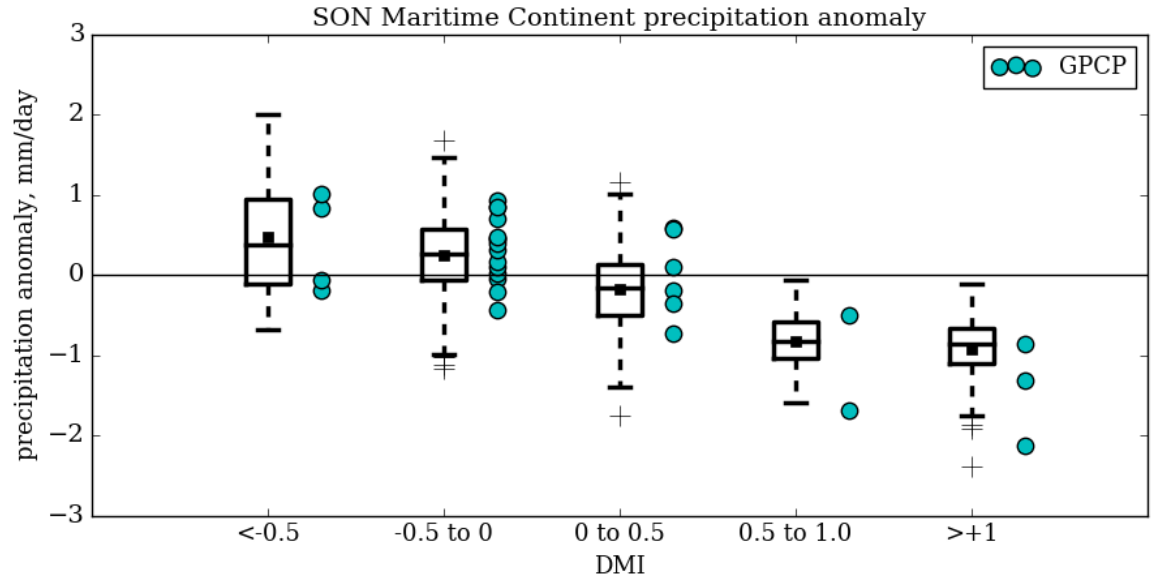

Figure 3.19: Box-and-whisker plot of AMIP5 SON mean precipitation anomaly averaged over the Maritime Continent domain (20°S-20°N and 80°E-160°E) according to DMI. Black boxes indicate the interquartile range (IQR), black lines in the boxes indicate the median; black squares represent the mean. The plus signs are the outliers, which are anomalies smaller than the lower quartile or larger than the upper quartile by at least 1.5 times the IQR. The dots are the GPCP SON precipitation anomaly from 1979 to 2008.

3.4.2.2 CMIP5

The SST biases in a coupled model may affect the IOD teleconnections in the CMIP5 experiment. To verify the relationship between IODW SST and tropical precipitation, we calculated the Pearson correlation coefficient (r) between the SON interannual precipitation and SST for GPCP and CMIP5 models. Although for interannual time-scales, the observed SON local SST and local precipitation shows a slightly stronger relationship compared to IODW SST, however, the largest temporal correlation is between Maritime Continent precipitation and zonal SST gradient of Maritime Continent and IODW (green bars in Fig. 3.20).

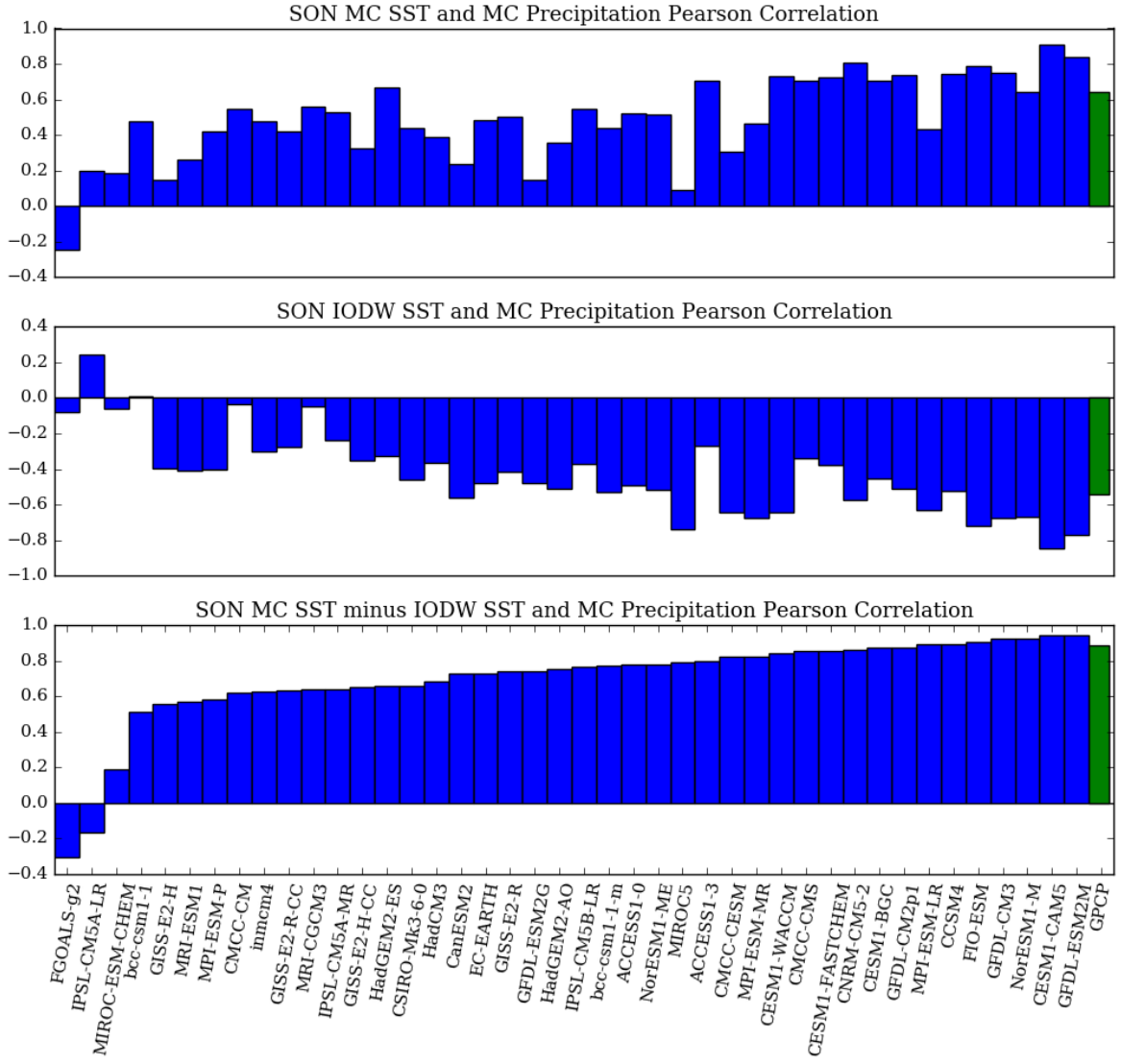

Figure 3.20: Temporal correlations between SON CMIP5 Maritime Continent precipitation and (a) Maritime Continent SST, (b) IODW SST and (c) Maritime Continent SST minus IODW SST. The panels are arranged showing models in order from lowest to highest Pearson correlation coefficients in (c). The green bars show the observed correlation using GPCP precipitation.

CMIP5 models simulate larger variations of temporal correlation coefficients between Maritime Continent precipitation and local SST (Fig. 3.20) as well as IODW SST than to the zonal SST gradient between Maritime Continent and IODW. Most models are able to capture the significant positive temporal correlation between Maritime Continent precipitation and the zonal SST gradient between Maritime Continent and IODW except for three models (FGOALS-g2, IPSL-CM5A-LR and MIROC-ESM-CHEM). This shows that most models are able to simulate more rainfall over Maritime Continent when SSTs are anomalously colder over the western Indian Ocean relative to the eastern Indian ocean, and vice versa.

The relationship between the CMIP5 models' WTIO mean state biases and the IOD-Maritime Continent teleconnection was also investigated. However, we found no significant correlation between the WTIO mean state biases and the IOD-Maritime Continent teleconnection strength (figure not shown).

To compare the AMIP5 and CMIP5 model performance at reproducing the spatial pattern of teleconnection between IOD and SON precipitation in the Maritime Continent, we compute the temporal correlation between gridpoint precipitation and DMI in SON and plot the spatial maps of temporal correlations in Fig. 3.21. In general, both AMIP5 and CMIP5 models simulate much weaker Maritime Continent precipitation-IOD teleconnections compared to observations. Observations show a negative correlation with the DMI apart from certain areas over the western Pacific and Indian Ocean. However, most models simulate a positive correlation, in particular spurious positive correlations around Papua are more prominent in the CMIP5 models, suggesting the influence of SST biases over this region. Most of the AMIP5 models perform better than CMIP5 models in simulating the IOD-Maritime Continent teleconnections based on the PCC and RMSE skill scores.

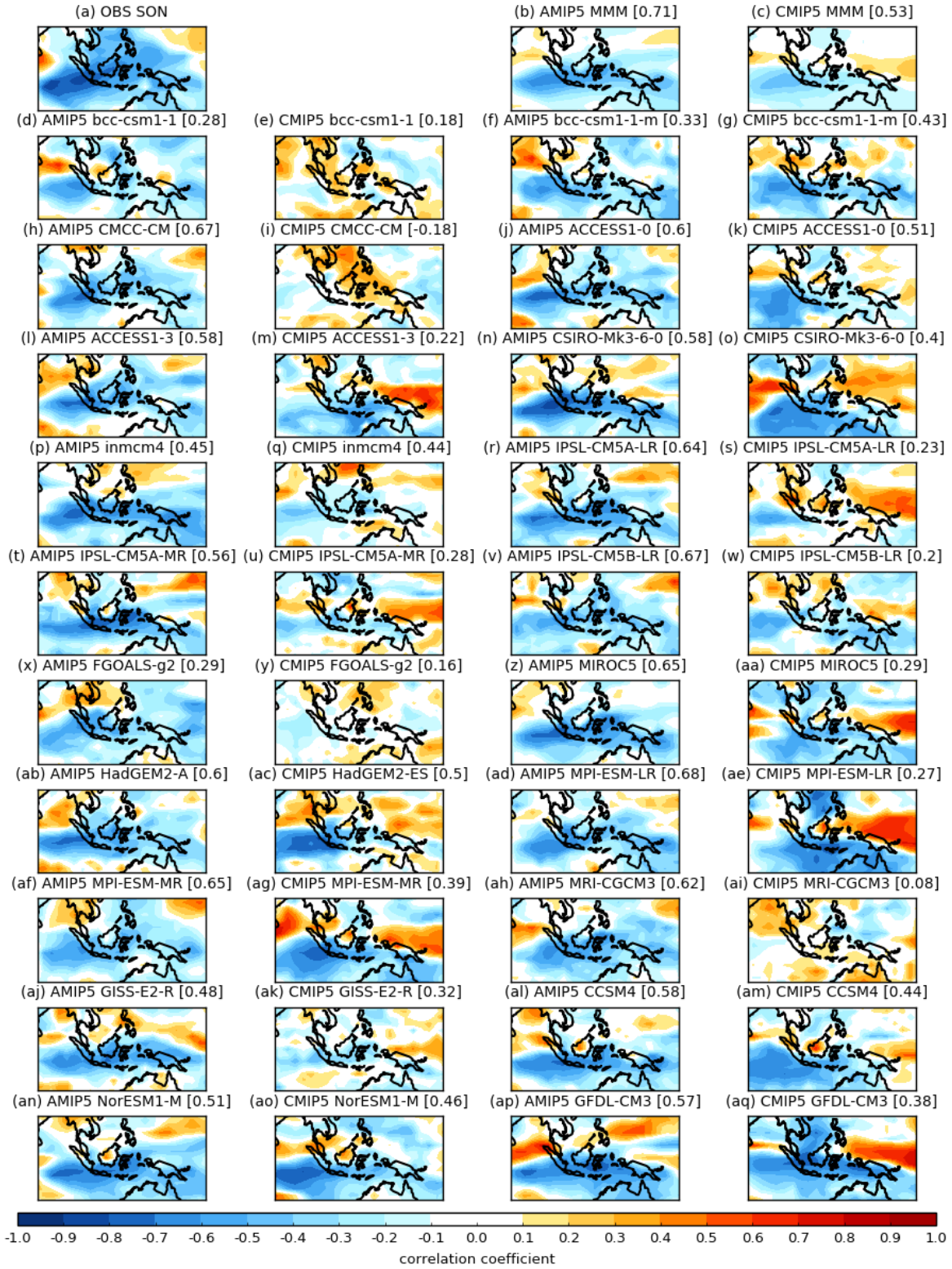

Figure 3.21: Spatial map of temporal correlation between gridpoint precipitation and DMI in SON for (a) Observations, AMIP5 (first and third column) and CMIP5 (second and fourth column) from 1979 - 2008.

3.5 Discussion and Conclusions

Our analysis suggests that SST plays an important role in modulating the Maritime Continent precipitation in CMIP5 models, both at the level of the model climatology and on interannual time scales in a given model. Using multimodel regression, we highlighted the central Pacific and western Indian Ocean as the key regions which exhibit the most surface temperature correlation with Maritime Continent mean-state precipitation in the coupled CMIP5 models. Remote ocean-atmosphere interactions play an important role in affecting the circulation and precipitation over the Maritime Continent and resultant underlying SST, and forming the inverse SST-precipitation relationship over the Maritime Continent, especially during the DJF and SON seasons. On the other hand, local SSTs play an active role in affecting precipitation and circulation and result in a positive SST-precipitation correlation during JJA and SON seasons.

On interannual timescales, the MMM of AMIP5 simulates a reasonably consistent relationship in which El Niño years show below-average Maritime Continent rainfall and La Niña years show above-average Maritime Continent rainfall. However, there are some inter-model differences in the precipitation anomalies for certain years in AMIP5. The striking similarity of precipitation and wind biases for seasonal mean and ENSO events suggests that biases in precipitation and circulation during ENSO events mainly result from the climatological mean-state biases.

On the other hand, most of the coupled CMIP5 models are able to capture the relationship between ENSO and area-averaged Maritime Continent precipitation but are less able to simulate the spatial pattern of precipitation anomalies over the Maritime Continent. Our analysis suggests that there is some relationship between SST mean-state biases and the ENSO-Maritime Continent teleconnection. Comparison between AMIP and coupled CMIP5 models show that AMIP models perform better than coupled CMIP5 models at simulating the spatial pattern of teleconnection between ENSO and the Maritime Continent precipitation in DJF. The low PCCs between teleconnection pattern in CMIP5 models and observations are mainly related to the spurious positive correlations around Papua. Coupled CMIP5 models which have a positive correlation over Papua (unlike the observations which have a negative correlation), tend to poorly simulate the ENSO-Maritime Continent teleconnection.

For the IOD-Maritime Continent teleconnections, AMIP5 MMM is able to capture the drier than normal conditions in precipitation and 850 hPa wind anomalies for the positive IOD events. Model performance at simulating the teleconnection is related to the mean-state representation of the Maritime Continent precipitation. Observation shows strong correlation between Maritime Continent precipitation and local SST compared to correlation with IODW SST, however, the largest correlation is between Maritime Continent precipitation and the zonal temperature gradient to the west between the Maritime Continent and the IODW.

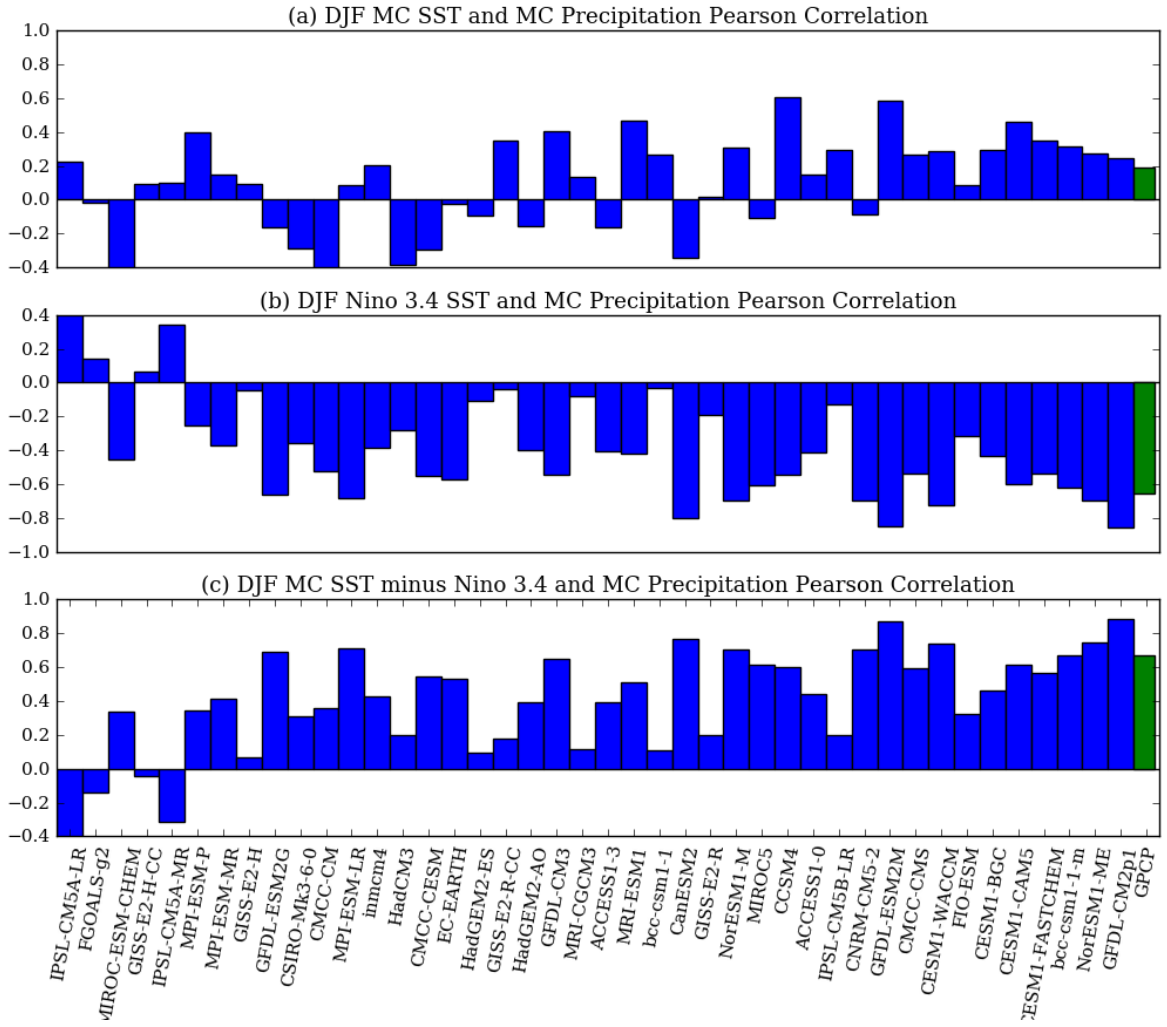

Figure 3.22: Temporal correlation between DJF CMIP5 Maritime Continent land-only precipitation and (a) Maritime Continent SST, (b) Niño 3.4 SST and (c) Maritime Continent SST minus Niño 3.4 SST. The panels are arranged following the order as in Fig. 3.13. The green bars show the observed correlation using GPCP precipitation.

The area-averaged IOD-Maritime Continent teleconnection is well simulated by both AMIP and coupled models but not the spatial pattern of the teleconnection. Comparison between AMIP5 and CMIP5 models showed that AMIP5 models perform better than CMIP5 models at simulating the spatial pattern of temporal correlation between IOD and the Maritime Continent precipitation in SON. Both AMIP5 and CMIP5 models simulate weaker IOD-Maritime Continent teleconnections than observed, as found in previous studies (Jourdain et al., 2013). We found no significant correlation between WTIO mean-state SST biases and the IOD-Maritime Continent teleconnection.

In this study, we investigated the relationship between tropical ocean SST and Maritime Continent precipitation over both land and sea. However, this relationship may be different when considering land-only and sea-only parts of the region. Figure 3.22 shows a similar temporal correlation figure as Fig. 3.13 but for land-only precipitation over the Maritime

Continent using the original resolution data. The sea-only correlation dominates (figure not shown) when considering the Maritime Continent land and sea as a whole. However, CMIP5 models behave differently when considering only the land precipitation over the Maritime Continent. Most of the CMIP5 models simulate weaker temporal correlation between DJF Niño 3.4 SST and Maritime Continent land-only precipitation compared to the overall Maritime Continent. Further investigation on the Maritime Continent land-only precipitation teleconnection to ENSO and IOD is recommended for societal benefit, but is beyond the scope of this study.

Chapter 4

Investigating the role of the Indo-Pacific on Maritime Continent precipitation using AGCM sensitivity experiments

4.1 Introduction

In the previous chapter, we investigated large-scale interactions between Maritime Continent precipitation and tropical sea surface temperature (SST) in CMIP5. Our analysis showed that central Pacific and western Indian Ocean climatological SSTs are significantly negatively correlated with Maritime Continent climatological mean state precipitation in the coupled CMIP5 models, while local SST demonstrates seasonally-dependent correlations. This motivates us to test causality in the relationships between SST and precipitation anomalies and better understand the mechanism underlying these relationships.

As one of the principal heat sources driving the global circulation (Ramage, 1968), Maritime Continent biases affect the tropics and extratropics by perturbing the Walker and Hadley Circulations and exciting planetary waves (Neale and Slingo, 2003; Zhang et al., 2016). Previous studies (Qu et al., 2005; Strachan, 2007) showed that adding a 1°C anomaly over the Maritime Continent SST in their SST sensitivity experiment using the atmosphere-only MetUM HadGAM1 model resulted in an increase of precipitation over the Maritime Continent and reduced precipitation over the western Pacific and western Indian Oceans. This reduced the model's systematic dry biases over the Maritime Continent and wet biases over the western Pacific and western Indian Ocean via a response in the Walker Circulation. Strachan (2007) also performed SST sensitivity experiments over targeted areas in the west Pacific and west Indian Oceans which produced a localised precipitation response and relatively weak remote responses across the Indo-Pacific region.

Neale and Slingo (2003) suggested that the surface air temperature cold bias over the Maritime Continent islands might contribute to the dry biases local in the MetUM HadAM3 model. They replaced land grid points over the Maritime Continent with ocean grid points

and found that a warmer surface increased the precipitation over the Maritime Continent and resulted in better representation of precipitation over the equatorial Indian Ocean and the South Pacific Convergence Zone (SPCZ).

These previous studies (Neale and Slingo, 2003; Qu et al., 2005; Strachan, 2007) mainly focused on improving the model simulations over the Maritime Continent. Our study instead considers the effect of Indo-Pacific SST perturbations on the Maritime Continent climate mean state, interannual variability and teleconnections to El Niño-Southern Oscillation (ENSO) and the Indian Ocean Dipole (IOD). As it is difficult to separate cause and effect in the coupled atmosphere-ocean system, we perform SST sensitivity experiments using an atmosphere-only model to test causality in atmosphere-ocean interactions by removing the ocean feedbacks in the model simulation.

Dado and Takahashi (2017) performed SST sensitivity experiments using the Advanced Research Weather Research and Forecasting (WRF) regional climate model to investigate the relationship between rainfall over the western Philippines and interannual variations in local SST during the summer monsoon. The rainfall over the northwestern Philippines shows a positive linear interannual relationship with area-averaged local SST anomalies.

Annamalai et al. (2005), using ECHAM5 AGCM, showed that positive SST anomalies over the southwest Indian Ocean enhance local precipitation and lead to a reduction of precipitation over the Maritime Continent and tropical west Pacific through an anomalous Walker circulation over the Indian Ocean.

Spencer et al. (2004) imposed composite cycles of El Niño and La Niña SST in different regions (i.e: (1) Pacific Ocean only, (2) Indian and Pacific Oceans, (3) the whole tropical ocean and (4) global ocean) and climatological SST elsewhere to investigate remote SST influence on ENSO teleconnections using the MetUM HadAM3 atmospheric model. Their study found that the Maritime Continent and Indian Ocean SST anomalies induced a tropospheric circulation response that damped the ENSO teleconnection response.

In this chapter, we present two sets of sensitivity experiments using the UK MetUM HadGEM3-GA6 atmosphere-only model. The first set of sensitivity experiments examines the effect of Maritime Continent SST perturbations on the tropical mean state, variability and teleconnections. The second set of experiments investigates the influence of SST perturbations elsewhere in the tropics (i.e. the equatorial Pacific and Indian Oceans) on climate mean state and variability within the Maritime Continent. Our study will also investigate how SST perturbations over different regions in the Indo-Pacific alter the atmospheric response to ENSO and the IOD over the Maritime Continent, looking at both local and remote responses to these drivers.

This chapter is structured as follows. In Section 5.2, we describe the model experimental design and the observational datasets used for comparison. Section 5.3 presents the mean state biases in the control experiment compared to observations. Section 5.4 examines the Maritime

Continent SST perturbation experiments seasonal mean responses, followed by analysis of the Pacific and Indian Oceans SST perturbation experiments in Section 5.5 and 5.6. The impact of SST changes on interannual variability, the Maritime Continent-ENSO teleconnection, and the Maritime Continent-IOD teleconnection will be investigated in Section 5.7. Lastly, the discussion and conclusions are given in Section 5.8.

4.2 Model and observational datasets

4.2.1 Model description

In this chapter, we performed global atmosphere-only experiments using the MetUM HadGEM3-GA6 model (Walters et al., 2017). The model simulations were run at horizontal resolution of N96 (1.875° longitude and 1.25° latitude) with 85 vertical levels. We chose to run the model at N96 resolution because it is computationally inexpensive and suitable for running multiple experiments.

HadGEM3-GA6 employs the ENDGame (Even Newer Dynamics for General atmospheric modelling of the environment) dynamical core. This dynamical core is formulated based on a semi-implicit semi-Lagrangian method to solve the non-hydrostatic, fully compressible deep-atmosphere equations of motion. The prognostic fields are discretised on a latitude-longitude grid with a C-grid staggering in the horizontal and Charney-Phillips staggering in the vertical.

The Edwards and Slingo (1996) radiation scheme, configured based on the Cusack et al. (1999) correlated-k distribution method, is used to calculate surface fluxes and heating rates. Convection is parameterized by the Gregory and Rowntree (1990) mass flux convection scheme. The deep convection scheme employs a convective available potential energy (CAPE) closure. Adaptive detrainment (Derbyshire et al., 2011) is implemented as an extension to the Gregory-Rowntree convection scheme. Mixing detrainment rates are based on relative humidity and forced detrainment rates adapt to the buoyancy of the convective plume. The configuration of HadGEM3-GA6 is described in detail in Walters et al. (2017).

4.2.2 Experimental set-up

We performed 10 experiments in this study. Each experiment is run for 30 years from 1982 to 2011. This 30-year period allow us to investigate the impact of SST perturbations on mean climate as well as interannual climate variability and teleconnections.

The control run was forced by prescribed daily varying observed SST used in the AMIP-type experimental design of CMIP5. The prescribed SST data at a spatial resolution of 1° × 1° is based on the monthly mean Hadley Centre sea ice and SST dataset version 1 (HadISST1) and version 2 of the National Oceanic and Atmospheric Administration (NOAA) weekly optimum interpolation (OI) SST analysis. The AMIP SST boundary conditions are described

Table 4.1: A list of the sensitivity experiments performed with HadGEM3-GA6 from 1982 to 2011. Perturbations are applied only over sea points.

Simulation abbreviation	**Perturbation to daily SST**
Control	None
MC+1K	Adding 1K to the Maritime Continent
MC-1K	Removing 1K from the Maritime Continent
MC+0.5K	Adding 0.5K to the Maritime Continent
CTPO+1K	Adding 1K to CTPO
CTPO-1K	Removing 1K from CTPO
CTPO+2K	Adding 2K to CTPO
WTIO+1K	Adding 1K to WTIO
WTIO-1K	Removing 1K from WTIO
WTIO+2K	Adding 2K to WTIO

in Taylor et al. (2000).

The control experiment is equivalent to the HadGEM2-A AMIP experiment in CMIP5 discussed in Chapter 3, but using a newer version of the MetUM HadGEM model with a completely new dynamical core for the atmosphere. The changes to the physics and dynamics from HadGEM2 to HadGEM3 are described in Walters et al. (2017). Our analysis shows that the HadGEM3-GA6 control run performs better than HadGEM2-A at simulating the Maritime Continent seasonal mean precipitation and 850 hPa winds compared to HadGEM2-A for all four seasons. However, the current version of the model still suffers from common systematic biases, which will be discussed in Section 4.3.

The purpose of performing SST perturbation experiments in this chapter is not to improve the model, but to test the model sensitivity to SST errors. For the Maritime Continent SST sensitivity experiments, three runs are performed with SST perturbations to sea points in the Maritime Continent domain (20°S-20°N and 80°E-160°E). This is the same Maritime Continent domain that was defined in the previous chapter. For the tropical Indian and Pacific Oceans SST sensitivity experiments, three runs are performed with perturbations to the CTPO domain (5°S-5°N and 120°W-170°W) SST and the WTIO domain (10°S-10°N and 50°E-70°E) SST respectively. The CTPO and WTIO domains are the same regions as defined in Section 4.3 and are chosen based on Fig. 3.2 of the multimodel regression. Note that the CTPO is also the Niño 3.4 region and the WTIO is the western Indian Ocean Dipole region (IODW) defined in Saji et al. (1999). However, to distinguish our mean climate analyses from the interannual time scale associated with ENSO and IOD analyses, we refer to the central Pacific perturbation region as CTPO and western Indian Ocean perturbation region as WTIO. The SST sensitivity experiments performed in this study are outlined in Table 4.1 along with the abbreviations used.

The magnitude of SST anomalies for the sensitivity experiments is chosen based on the maximum and mean magnitude of biases over each region in the coupled CMIP5 models,

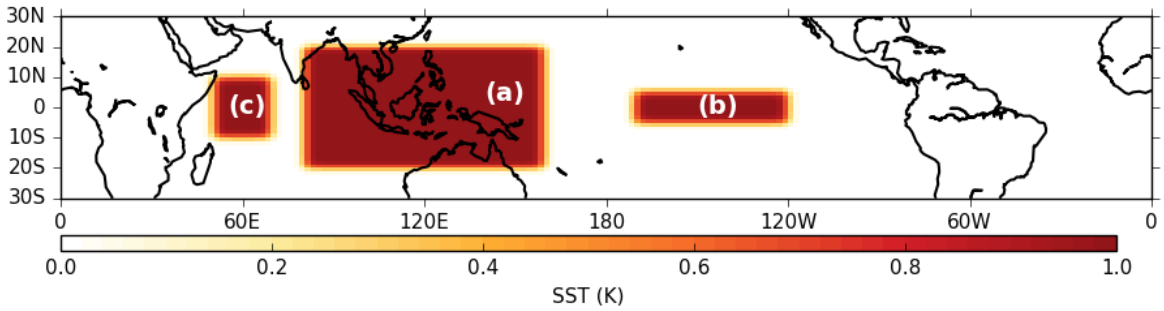

Figure 4.1: Domains and magnitudes of SST perturbation experiments with Gaussian smoothing over (a) Maritime Continent, (b) CTPO and (c) WTIO. Note that perturbations are applied only over sea points.

as depicted in Fig. 3.7 in the previous chapter. Note that the perturbations do not vary with year or season, so for instance, interannual variability of SST still follows AMIP (except for the effects of the uniform perturbations). A Gaussian spatial filter is applied to smooth the edges of the perturbation domains in order to avoid potential discontinuities. Gaussian smoothing uses a kernel that represents the shape of a Gaussian (normal distribution) curve. The Gaussian equation is as below:

$$G(x,y) = \frac{1}{\sigma\sqrt{2\pi}} e^{-\left(x^2+y^2\right)\Big/2\sigma^2} \tag{4.1}$$

In this study, we use $\sigma = 1$ for the standard deviation of the Gaussian kernel. Figure 4.1 shows the domain of (a) the Maritime Continent, (b) the CTPO and (c) the WTIO regions in the plus 1K experiments with Gaussian smoothing.

The SST distribution and magnitude play an important role for convection over the tropics. The Maritime Continent is located within the Indo-Pacific Warm Pool (IPWP), which is one of the warmest ocean regions. Relatively small changes to the SST over this warm region can lead to large impacts on atmospheric convection and circulation as dictated by the Clausius-Clapeyron relationship:

$$\frac{de_s}{dT} = \frac{Le_s}{R_v T^2} \tag{4.2}$$

where e_s is the saturation vapour pressure, T is the absolute temperature, L is the latent heat of vaporisation (2.5×10^6 J kg^{-1}), and R_v is the gas constant for water vapour (461.5 J kg^{-1} K $^{-1}$). The Clausius-Clapeyron equation relates saturation vapour pressure of a parcel of air to its temperature. Equation 4.2 shows that saturation vapour pressure increases exponentially with temperature. Increasing the SST over a warm region will result in a large increase of water vapour in the atmosphere and will provide more moisture for convection and precipitation. Therefore, the rate of change in precipitation depends on the magnitude of the SST perturbation as well as the existing temperature over the region. This is one possible

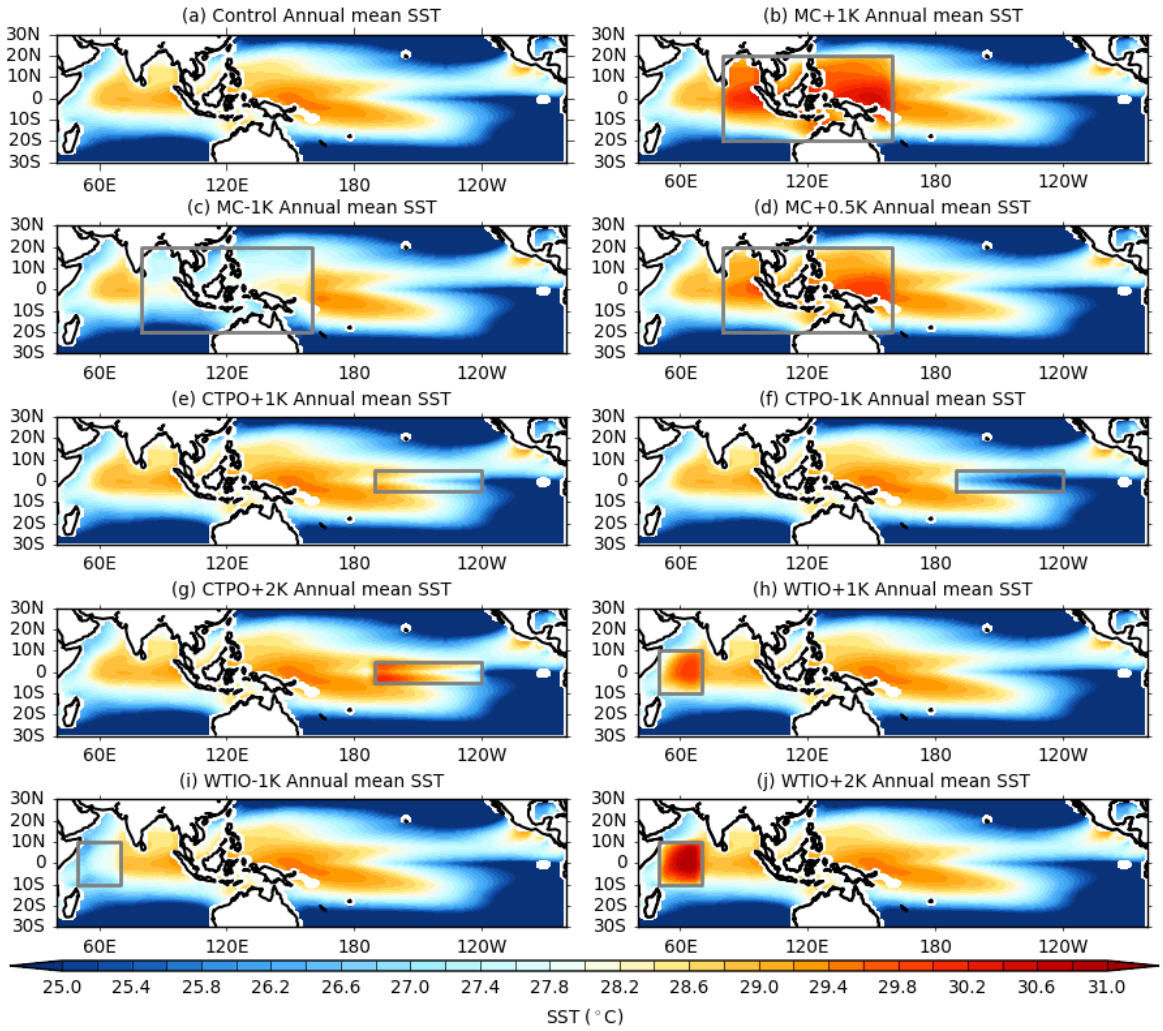

Figure 4.2: Annual mean SST (°C) from 1982-2012 for each experiment: (a) control, (b) MC+1K, (c) MC-1K, (d) MC+0.5K, (e) CTPO+1K, (f) CTPO-1K, (g) CTPO+2K, (h) WTIO+1K, (i) WTIO-1K and (j) WTIO+2K experiments. Grey box shows the domain of SST perturbation region in each experiment.

reason for non-linear behaviour of precipitation responses. Another possible reason is due to the weak SST gradient, whereby a small change in relative SST can lead to significant shifts in rainfall to relatively warmer regions.

To examine the distribution of SST after the anomalies are applied in each experiment, Fig. 4.2 shows the annual mean SST over the tropics for the control run and the SST perturbation experiments. In the control run (Fig. 4.2a), the Maritime Continent is located within the warmest ocean region. Meanwhile, for the MC-1K experiment (Fig. 4.2c), the warmest SSTs are now over the SPCZ and the western and central Indian Ocean regions. We expect to see reduced rainfall over the Maritime Continent and rainfall increases over the warmer SST regions in the Indian Ocean and the Pacific Ocean in this MC-1K experiment. In the CTPO+1K experiment (Fig. 4.2e), the warmest SSTs are still over the Maritime Continent,

whereas the CTPO+2K experiment (Fig. 4.2g) has extended the warmest region towards the central Pacific Ocean. The Maritime Continent is the warmest SST region in both the CTPO-1K and WTIO-1K experiment, while the WTIO is the warmest SST region in the WTIO+2K and WTIO+1K experiments.

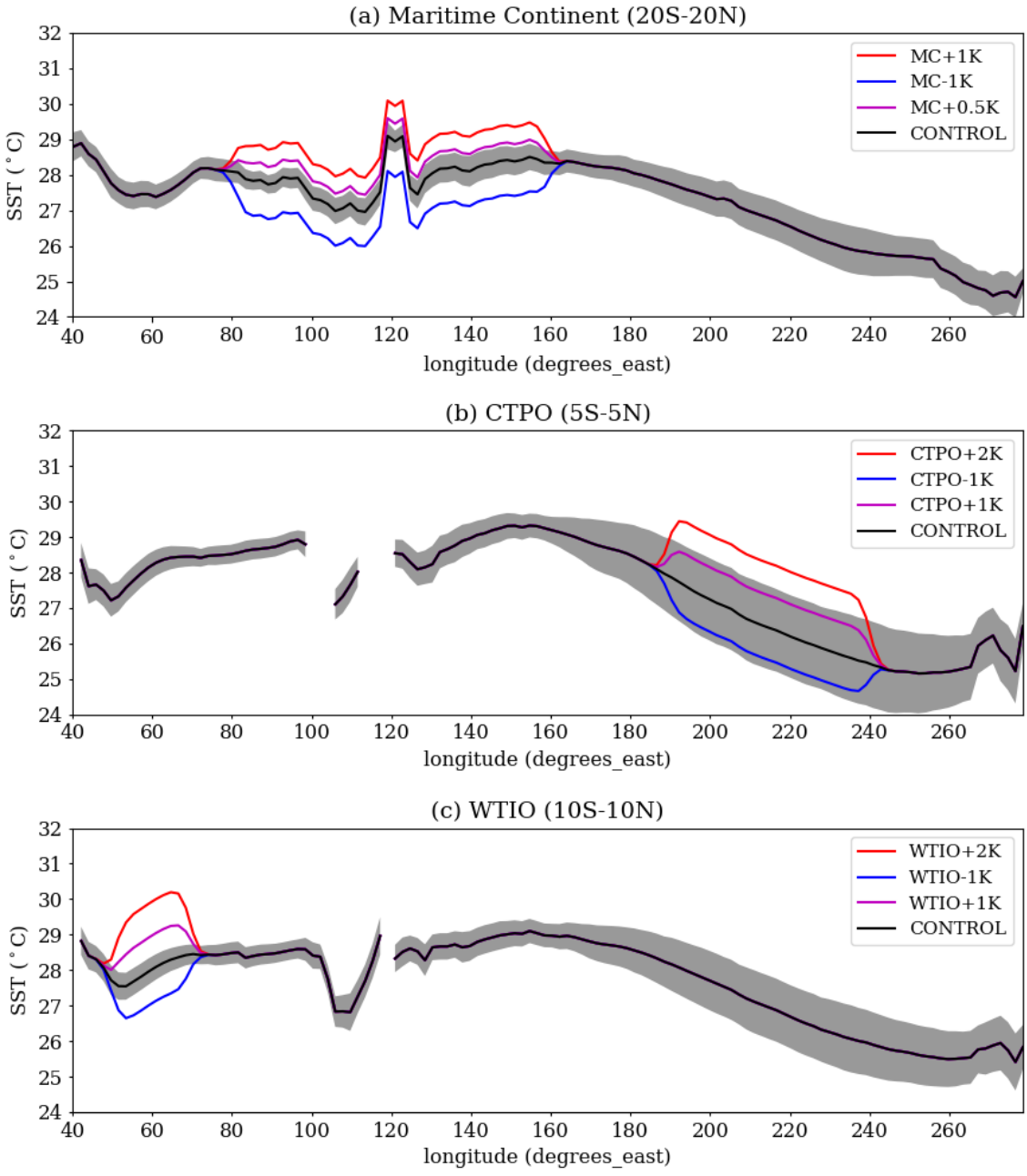

Figure 4.3: DJF climatological mean longitudinal SST (°C) from 1982-2011 meridionally averaged over: (a) Maritime Continent (20°S - 20°N), (b) CTPO (5°S - 5°N) and (c) WTIO (10°S - 10°N) in the control experiment (black line) and sensitivity experiments (coloured lines). The grey shaded area is the interannual standard deviation of DJF seasonal-mean SST in the control experiment.

Figure 4.3 shows the DJF climatological mean longitudinal distribution of SST (°C)

from 1982-2011 averaged over the perturbation latitude ranges in the sensitivity experiments. There are some differences when averaging over different latitude ranges, however the SST is generally between 27-29°C over the Indian Ocean and Maritime Continent and decreases from west to east over the Pacific Ocean. The zonal SST gradient is approximately 4°C over the Pacific Ocean and is the largest gradient compared to the other ocean basins. The perturbation magnitudes are outside the range of the standard deviation (interannual variability) over all of the respective perturbation regions except the CTPO. Figure 4.3 also shows the location of the SST maximum during DJF in each experiment, which corresponds to the location of the SST maximum in annual mean SST as depicted in Figure 4.2.

From these experiments, we expect the increase in the magnitude of local rainfall over the perturbed area to be larger in the MC+0.5K, MC+1K, WTIO+1K and WTIO+2K experiments than in the CTPO+1K and CTPO+2K experiments following the Clausius-Clapeyron relation. Based on the negative relationship between Maritime Continent precipitation and CTPO as well as WTIO found in Chapter 3.3.5, the Maritime Continent is expected to show precipitation responses in opposite sign to the SST perturbations in the CTPO and WTIO.

4.2.3 Observational datasets

Two observational/reanalysis datasets are used for model validation: 1) 2.5°$\times$ 2.5° monthly precipitation data from the GPCP (Adler et al., 2003); and 2) monthly wind data at approximately 0.7° resolution from the ERA-Interim reanalysis data (Dee et al., 2011) for the period 1982 - 2011. The datasets are interpolated to the N96 grid using bi-linear-interpolation for comparison with the model.

The seasonal mean, standard deviation and anomaly values in this chapter are calculated with respect to the 1982 - 2011 baseline period.

4.3 Control Experiment

Before investigating the sensitivity of the simulated climate to SST perturbations, we will first examine the biases in the HadGEM-GA6 control run and identify systematic biases in the model simulation.

Fig. 4.4 shows the control run seasonal mean precipitation and 850 hPa winds and its biases with respect to GPCP and ERA-interim in DJF and JJA. HadGEM3-GA6 exhibits systematic dry biases over the Maritime Continent and wet biases especially over the Indian Ocean, Western Pacific and South Pacific Convergence Zone (SPCZ) in DJF. Other studies also noted dry precipitation biases over the Maritime Continent in different versions of the HadGEM model (Neale and Slingo, 2003; Schiemann et al., 2014; Johnson et al., 2015). In JJA, there are significant dry biases over India and wet biases are even more prominent over the Indian Ocean and Western Pacific Ocean (Fig. 4.4d).

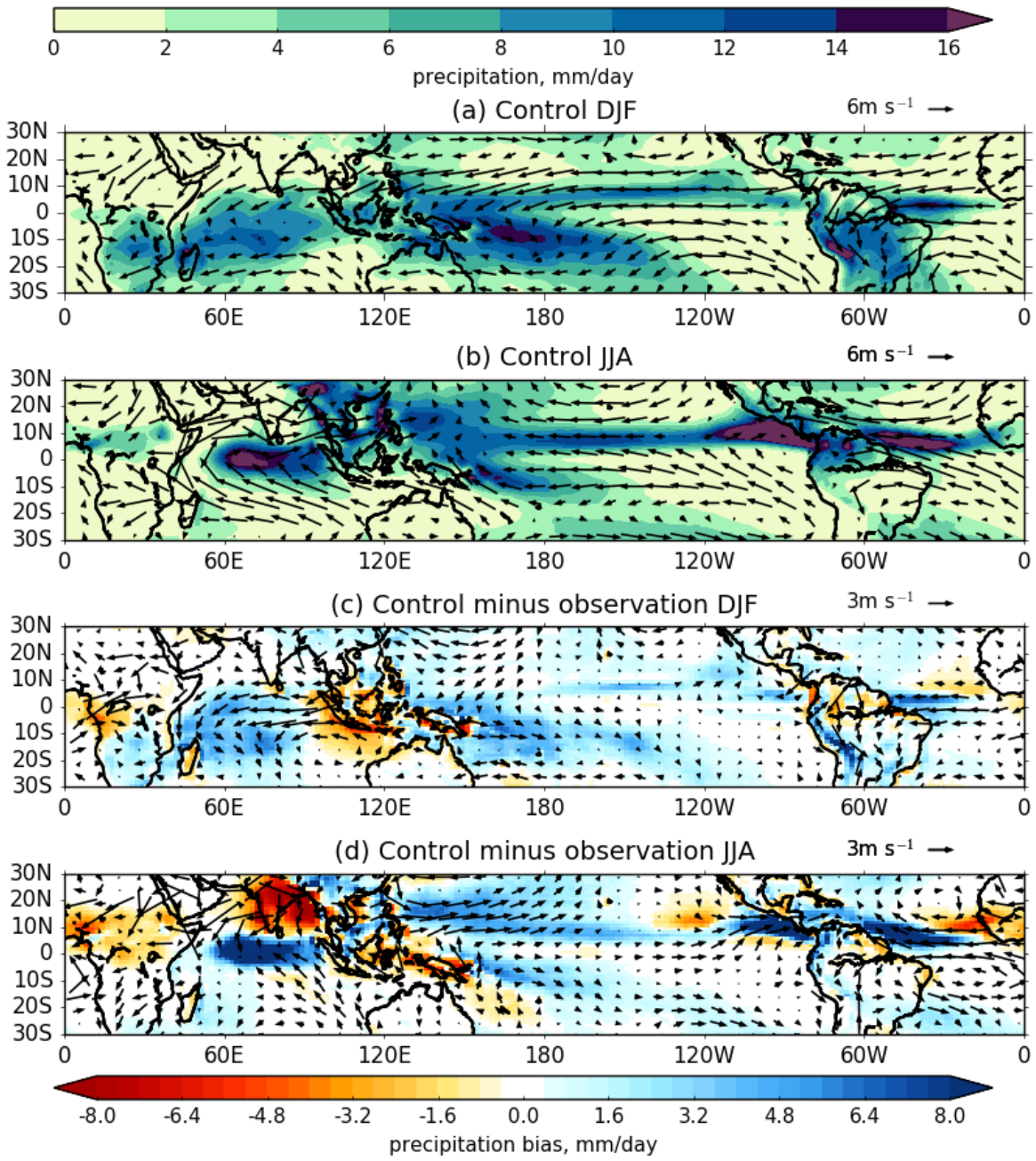

Figure 4.4: Control experiment seasonal mean precipitation (shading, mm day^{-1}) and 850 hPa wind (vectors, m s^{-1}) for (a) DJF and (b) JJA seasons, and biases with respect to GPCP and ERA-Interim in (c) DJF and (d) JJA seasons.

In DJF, the precipitation biases are associated with significant easterly wind biases driving moisture from the Maritime Continent towards the Indian Ocean. The westerly biases over the equatorial Pacific Ocean show a weakening of the trade winds over this region. Figure 4.5 shows the DJF and JJA seasonal mean omega biases at 500 hPa in the control experiment with respect to ERA-interim. The model simulates too little ascent over the Maritime Continent and excessive ascent over the Pacific and Indian Oceans. The omega biases at 500 hPa are

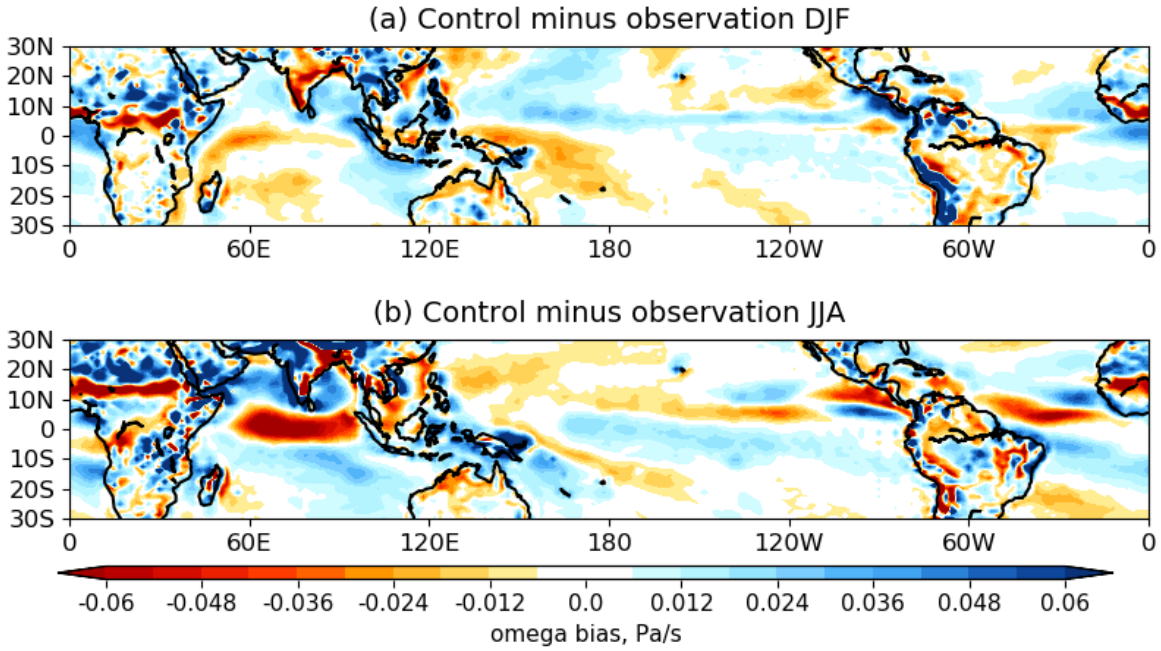

Figure 4.5: Control experiment seasonal mean omega biases at 500 hPa (shading, Pa s^{-1}) with respect to ERA-interim for (a) DJF and (b) JJA.

consistent with the dry biases over the Maritime Continent and wet biases over the Pacific and Indian Ocean. However, the biases are less coherent over the other continents.

4.4 Maritime Continent SST perturbation experiments

In this section, we investigate the impact of SST perturbations over the Maritime Continent on the tropical Indo-Pacific mean climate. We focus on DJF and JJA seasons which are the Australian summer monsoon and Asian Summer monsoon seasons.

Figure 4.6a,d shows that the MC+1K experiment produces more precipitation over the Maritime Continent. The precipitation and circulation of the MC+1K experiment produced a Matsuno-Gill like response (Matsuno, 1966; Gill, 1980) to diabatic heating over the Maritime Continent. The increased precipitation over the Maritime Continent is associated with the strengthening of the easterly trade winds with a Kelvin wave response over the Pacific Ocean, and a Rossby wave response with twin cyclonic circulation over the Indian Ocean (Gill, 1980). Warmer SSTs increase convective activity and enhance local precipitation.

However, this experiment also produces even less precipitation over some land areas, especially over Sumatra and Borneo (Fig. 4.7). This may be because of reduced land-sea contrast over this region in this experiment. Figure 4.8 shows the surface temperature changes over the Maritime Continent in the MC+1K experiment with respect to control run. While the surface temperature increases over the Maritime Continent islands (but not Australia and mainland Southeast Asia) with respect to the control run, the increase over land is generally

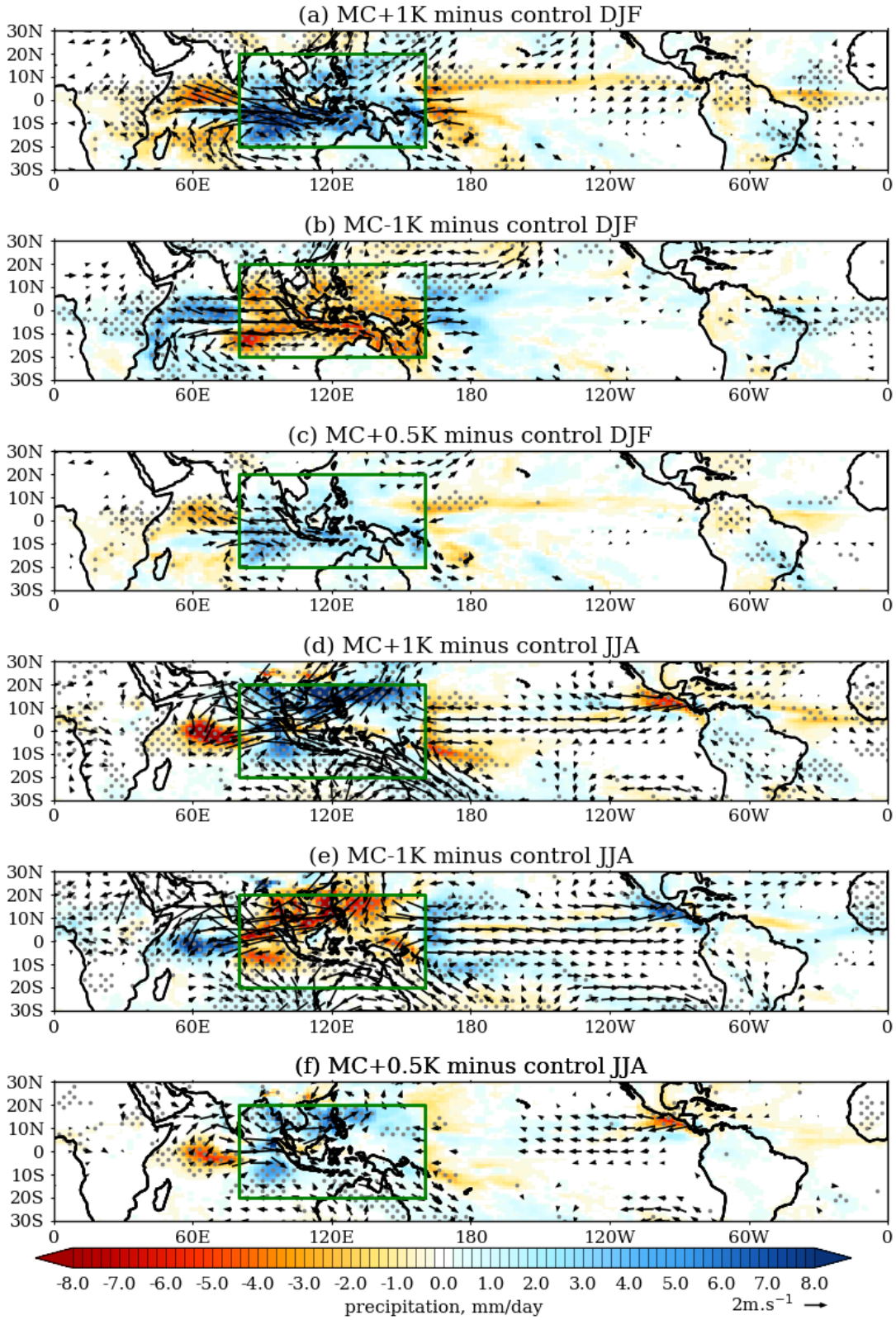

Figure 4.6: DJF precipitation (shading, mm day^{-1}) and 850 hPa wind (vectors, m s^{-1}) changes with respect to the control run in (a) MC+1K experiment, (b) MC-1K experiment and (c) MC+0.5K experiment. (d)-(f) are as in (a)-(c) but for JJA. Changes that are statistically significant at the 95% confidence level are stippled. Green box shows the domain of the SST perturbation region.

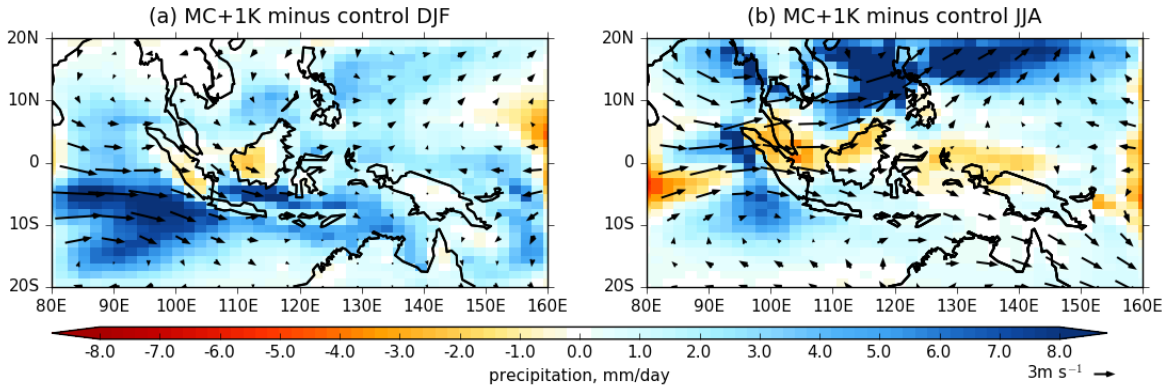

Figure 4.7: DJF precipitation (shading, mm day^{-1}) and 850 hPa wind (vectors, m s^{-1}) changes with respect to the control run in (a) MC+1K experiment, (b) MC-1K experiment and (c) MC+0.5K experiment. (d)-(f) are as in (a)-(c) but for JJA. This is as in Fig. 4.6 but zoomed in over the Maritime Continent.

smaller than the increase over the surrounding sea except for Peninsular Malaysia. This shows that by applying 1K warm anomalies over the Maritime Continent, the thermal land-sea contrast between the Maritime Continent islands and surrounding seas are reduced, and can lead to weaker sea breezes and reduced rainfall over the land.

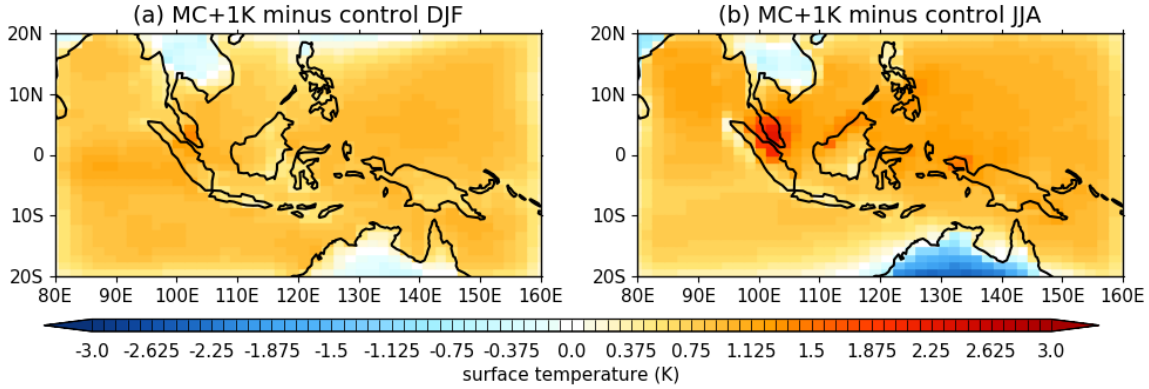

Figure 4.8: The MC+1K experiment surface temperature changes (K) with respect to the control run for (a) DJF and (b) JJA.

The warmer SST over the Maritime Continent also results in remote responses over the Pacific and Indian Oceans, with precipitation decreasing over these regions (Fig. 4.6a,d). This is consistent with findings from previous studies (Neale and Slingo, 2003; Qu et al., 2005; Strachan, 2007) which showed that the Maritime Continent precipitation biases are linked to those over the Indo-Pacific region. The remote responses also extend over the Atlantic Ocean. However, we regard the Atlantic Ocean as outside the scope of this study.

The MC+0.5K experiment shows similar results but with much weaker responses (Fig. 4.6c, f). The westerlies from the Indian Ocean and easterlies from the Pacific Ocean converge over the Maritime Continent, corresponding to increased precipitation there.

On the other hand, the MC-1K experiment shows approximately opposite results to the MC+1K experiment with precipitation decreasing over the Maritime Continent and increasing over the Pacific and Indian Oceans (Fig. 4.6b,e). Larger responses of the 850 hPa wind are simulated during JJA than in DJF, at least over the Pacific. The imposed cold SST anomalies over the Maritime Continent in the MC-1K experiments produce low-level wind divergence anomalies over the Maritime Continent. Westerly anomalies blowing towards the Pacific Ocean suggesting a weakening of the Walker circulation.

Next, we examine Fig. 4.9 which shows the changes in seasonal mean of omega at 500hPa for each of the sensitivity experiment with respect to control experiment. Figure 4.9 a,c,d,f shows that warm anomalies in the Maritime Continent generate stronger anomalous ascent over the Maritime Continent and anomalous descent over the Indian Ocean and the central Pacific Ocean. The MC+1K and MC+0.5K experiments increase the intensity of the Walker Circulation ascending branch over the Maritime Continent as well as the local Hadley Circulation.

Figure 4.9b,e shows that the MC-1K experiment simulates anomalous descent over the Maritime Continent and ascent over the Indian Ocean and the central Pacific Ocean, coinciding with precipitation anomalies that result in an even drier Maritime Continent and wetter Indian and Pacific Oceans. The displacement of ascending branches of the Walker circulation also correspond to the locations of the warmest SST in the MC-1K experiment (Fig. 4.2b), which are now over the Indian and Pacific Oceans and not the Maritime Continent.

Moreover, the strengthening or weakening of ascent over the Maritime Continent is also associated with corresponding vertical motion changes of opposite sign associated with changes in the local Hadley circulation over India, China, southern Australia and the southern Indian Ocean.

4.4.1 Moisture budget analysis

Next, we performed an analysis of the moisture budget to better understand the model's precipitation responses to SST changes in the Maritime Continent. The precipitation (P) has to be balanced by the sum of evaporation (E) and vertically integrated moisture flux convergence (VIMFC). Figure 4.10a shows that the evaporation in HadGEM3-GA6 generally exhibits a positive bias except over mainland Southeast Asia, India and central Africa (Fig. 4.10a). The difference between precipitation and evaporation (P-E, Fig. 4.4b) shows the ITCZ region with positive P-E (i.e. precipitation exceeds evaporation) in DJF as expected. The VIMFC (Fig. 4.10c) largely resembles the P-E (Fig. 4.10b) but is less coherent over the land area. The model moisture budget is balanced. The VIMFC biases (Fig. 4.10d) are somewhat similar to the precipitation biases (cf. Fig. 4.4c) but the spatial pattern is noisier. However, there is some discrepancy over the Pacific Ocean, whereby HadGEM3-GA6

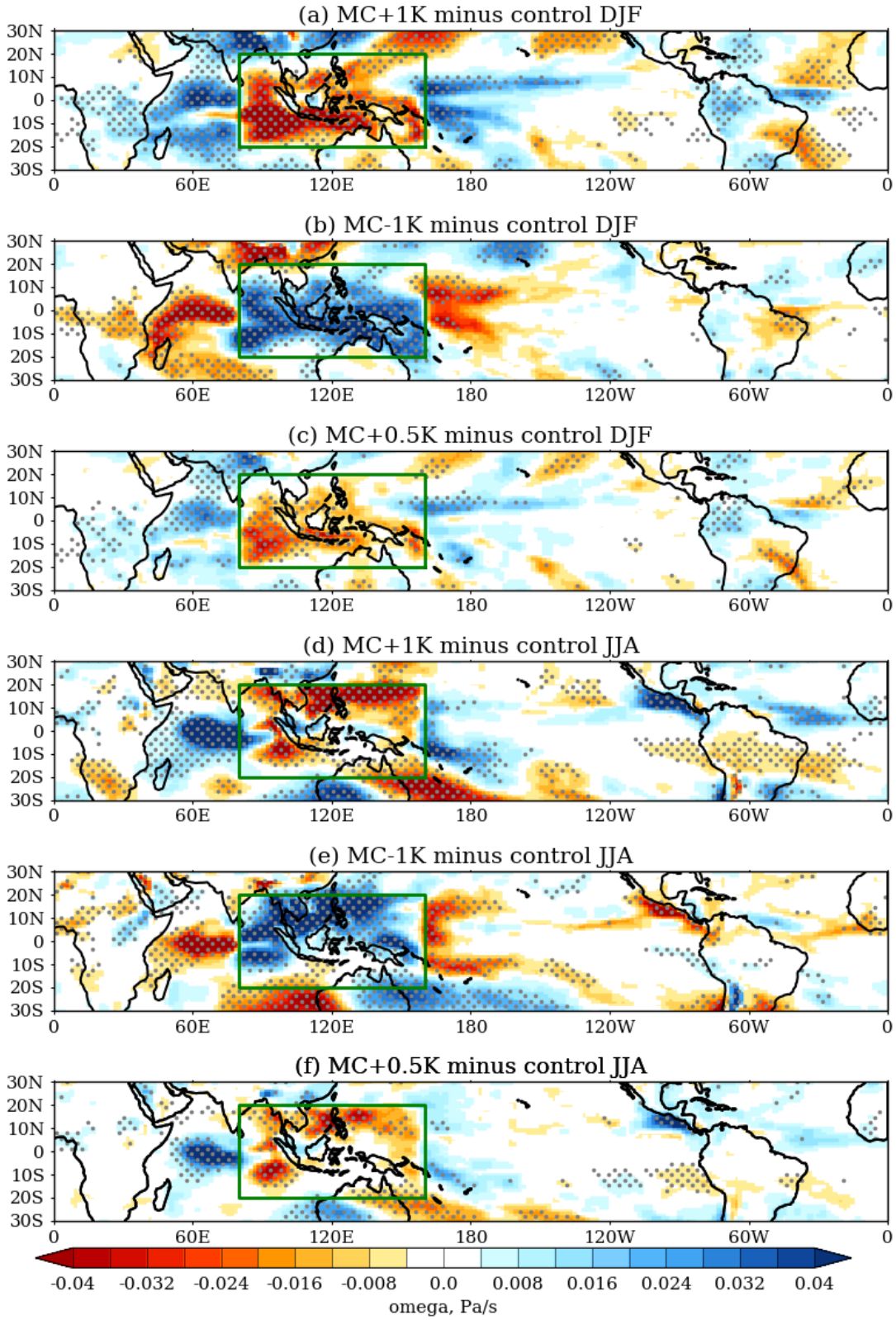

Figure 4.9: DJF seasonal mean 500hPa omega changes (shading, Pa s^{-1}) with respect to control run for: (a) MC+1K experiment, (b) MC-1K experiment and (c) MC+0.5K experiment. (d)-(f) are as in (a)-(c) but for JJA. Changes that are statistically significant at the 95% confidence level are stippled. Green box shows the domain of the SST perturbation region.

generally simulates moisture flux divergence over the regions with near-zero precipitation biases or small positive precipitation biases.

For brevity, only the moisture budget analysis for the MC+1K experiment in DJF is shown in Figure 4.10. Imposing SST anomalies over Maritime Continent has resulted in a slight decrease of evaporation over the Maritime Continent and a small increase of evaporation over the Pacific Ocean (Fig. 4.10e). The changes in VIMFC (Fig. 4.10f) are similar to changes in P-E (Fig. 4.10g), as well as to changes in precipitation (Fig. 4.1a).

To further investigate the sensitivity of Maritime Continent precipitation to local SST, we calculated the area-averaged precipitation difference over the Maritime Continent between each experiment and the control run. The area-averaged seasonal mean precipitation response associated with the local SST change is approximately 2 mm day^{-1} K $^{-1}$ for both the MC+1K (Fig. 4.6a, d) and MC-1K experiments (Fig. 4.6b, e). The magnitude of local response is reduced to half in the MC+0.5K experiment (Fig. 4.6c, f). This suggests that the local responses of mean precipitation to SST changes over the Maritime Continent are linear.

We also calculated the regression coefficients between Maritime Continent mean-state precipitation and Maritime Continent mean-state SST in the coupled CMIP5 runs analysed in Section 3.3.5 (slopes of the regression lines in Fig. 3.8a) and compared them to the local responses of mean precipitation in this section. DJF shows a negative regression coefficient (-0.23 mm day^{-1} K^{-1}) while other seasons show positive regression coefficients between 0.20 to 0.45 mm day^{-1} K^{-1}. These regression coefficients are ten times smaller than the area-averaged local precipitation responses in the Maritime Continent perturbation experiments. The discrepancies between these two fields might be related to the lacking of P-SST feedbacks in the sensitivity experiments.

Next, we quantify the Indian Ocean and Pacific Ocean responses to SST changes in the Maritime Continent, respectively. As expected, the remote precipitation responses to SST perturbations in the Maritime Continent are non-linear over the Pacific Ocean. However, the seasonal precipitation responses do not vary much across seasons. We found a reduction of precipitation of up to 6 mm day^{-1} in the MC+1K experiment and up to 4 mm day^{-1} in the MC+0.5K experiment and an increase of rainfall of up to 5mm day^{-1} in the MC-1K experiment around the SPCZ region. In the Indian Ocean, a larger response is induced during the JJA season with the MC+1K experiment producing precipitation increases of up to 10 mm day^{-1} compared to 5 mm day^{-1} in other seasons. The larger response during JJA may be related to the underlying pattern of precipitation bias which is larger over the Indian Ocean during JJA, leading to amplification of the remote responses. The remote responses to perturbing Maritime Continent SST are not linear in the Indian Ocean, as expected. For example in JJA, precipitation over the Indian Ocean (around 5° S - 5° N, 60°- 80° E) increases up to 6 mm day^{-1} in the MC+0.5K experiment while the MC-1K experiment reduces Indian Ocean precipitation by up to 8 mm day^{-1}. The difference between CMIP5 and perturbation

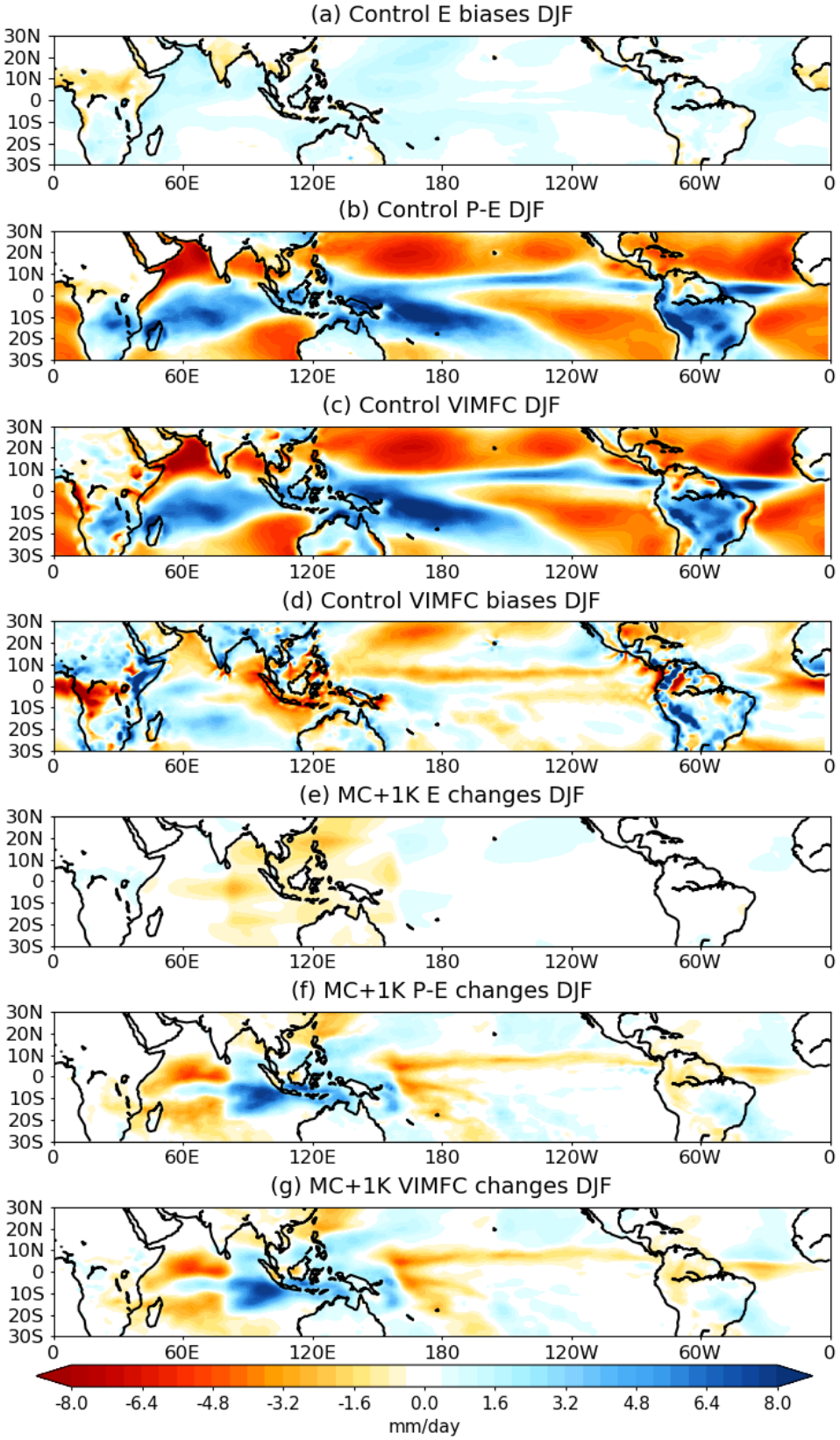

Figure 4.10: DJF seasonal mean control experiment (a) evaporation biases, (b) P-E, (c) VIMFC, and (d) VIMFC biases. MC+1K experiment changes with respect to control run for: (e) evaporation, (f) P-E and (g) VIMFC. Units are in mm/day.

experiments suggests that P-SST feedbacks are important.

Next, we will investigate the sensitivity of the Maritime Continent climate mean state to changes in the Pacific Ocean and Indian Ocean SST.

4.5 Pacific Ocean SST perturbation experiments

We next present three sensitivity experiments to SST changes over the CTPO. When an increase of SST over CTPO is prescribed in HadGEM-GA6 simulations, the CTPO+1K (Fig. 4.11a, d) and CTPO+2K (Fig. 4.11c, f) experiments produce a localised response over the central Pacific Ocean. The anomalous westerly flow from the west Pacific and anomalous easterly flow from the eastern Pacific Ocean converge towards the warm CTPO domain when the SST is increased, which resembles an El Niño event on interannual time scales. Figure 4.12a,c,d,f) show anomalous ascent over CTPO and anomalous descent over the Maritime Continent and the regions north of and south of CTPO. This shows that perturbation over CTPO induces changes in meridional and zonal circulations.

On the other hand, the CTPO-1K experiment, which resembles La Niña conditions, simulates a decrease of rainfall over the CTPO and an increase of rainfall over the Maritime Continent as shown in Fig. 4.11b, e. The cold anomalies imposed over the CTPO lead to a greater zonal SST gradient across the Pacific Ocean, with stronger easterlies blowing towards the Maritime Continent associated with strengthening of the Walker circulation (Fig. 4.12b, e). The anomalous ascent over the Maritime Continent correspond to the increase in rainfall.

Localised precipitation responses in the CTPO perturbation experiments are not linear. In the CTPO+1K experiment, area-averaged precipitation increased by around 2 mm day^{-1} over the CTPO, whereas in the CTPO+2K experiment, the precipitation increased by around 7 mm day^{-1}. This is more than triple the amount for 1K responses in DJF and JJA. Despite applying the same magnitude of anomalies, the cold anomalies in the CTPO-1K experiment produce only half of the magnitude of mean local precipitation response compared to the CTPO+1K experiment. The nonlinearity of the local rainfall response may be due to the Clausius-Clapeyron relationship (Section 5.2.2) as well as the shift of precipitation away from, or towards other tropical regions depending on changes in relative SSTs. In the CTPO+2K experiment, larger SST induces larger changes in atmospheric moisture and anomalies in precipitation and surface winds, compared to CTPO+1K and CTPO-1K experiments that have relatively low SST.

The precipitation remote response over the Maritime Continent in the CTPO experiments are somewhat comparable to the multimodel regression in Chapter 3.3.5. To quantify the remote responses, we calculated the regression coefficients (gradient of the best-fit lines, mm day^{-1}K^{-1}) between the Maritime Continent mean-state rainfall and CTPO mean-state SST in the coupled CMIP5 models from Fig. 3.8b in Chapter 3.3.5 and area-averaged precipitation

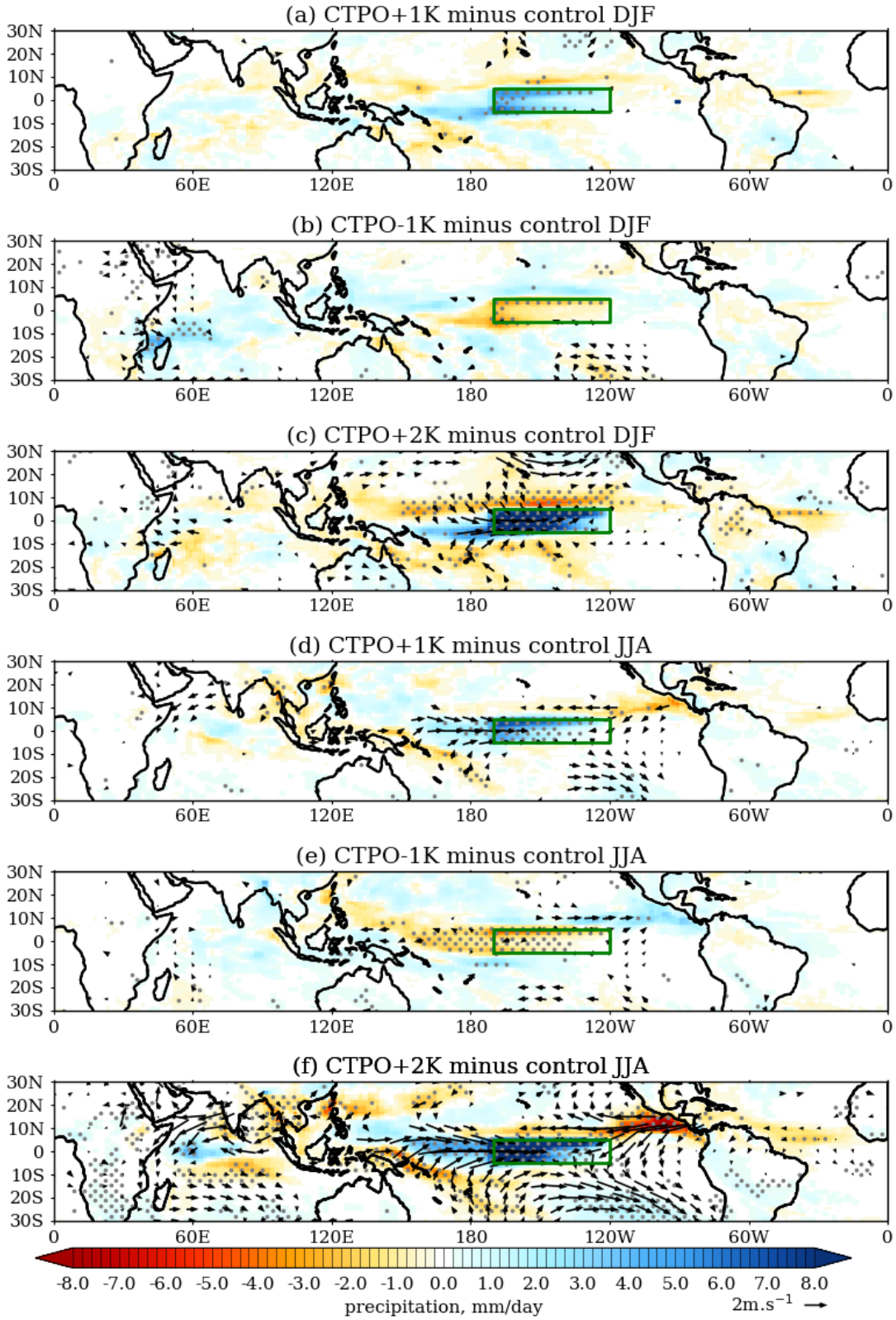

Figure 4.11: DJF precipitation (shading, mm day^{-1}) and 850 hPa wind (vectors, m s^{-1}) changes with respect to the control run in (a) CTPO+1K experiment, (b) CTPO-1K experiment and (c) CTPO+2K experiment. (d)-(f) are as in (a)-(c) but for JJA. Changes that are statistically significant at the 95% confidence level are stippled. Green box shows the domain of the SST perturbation region.

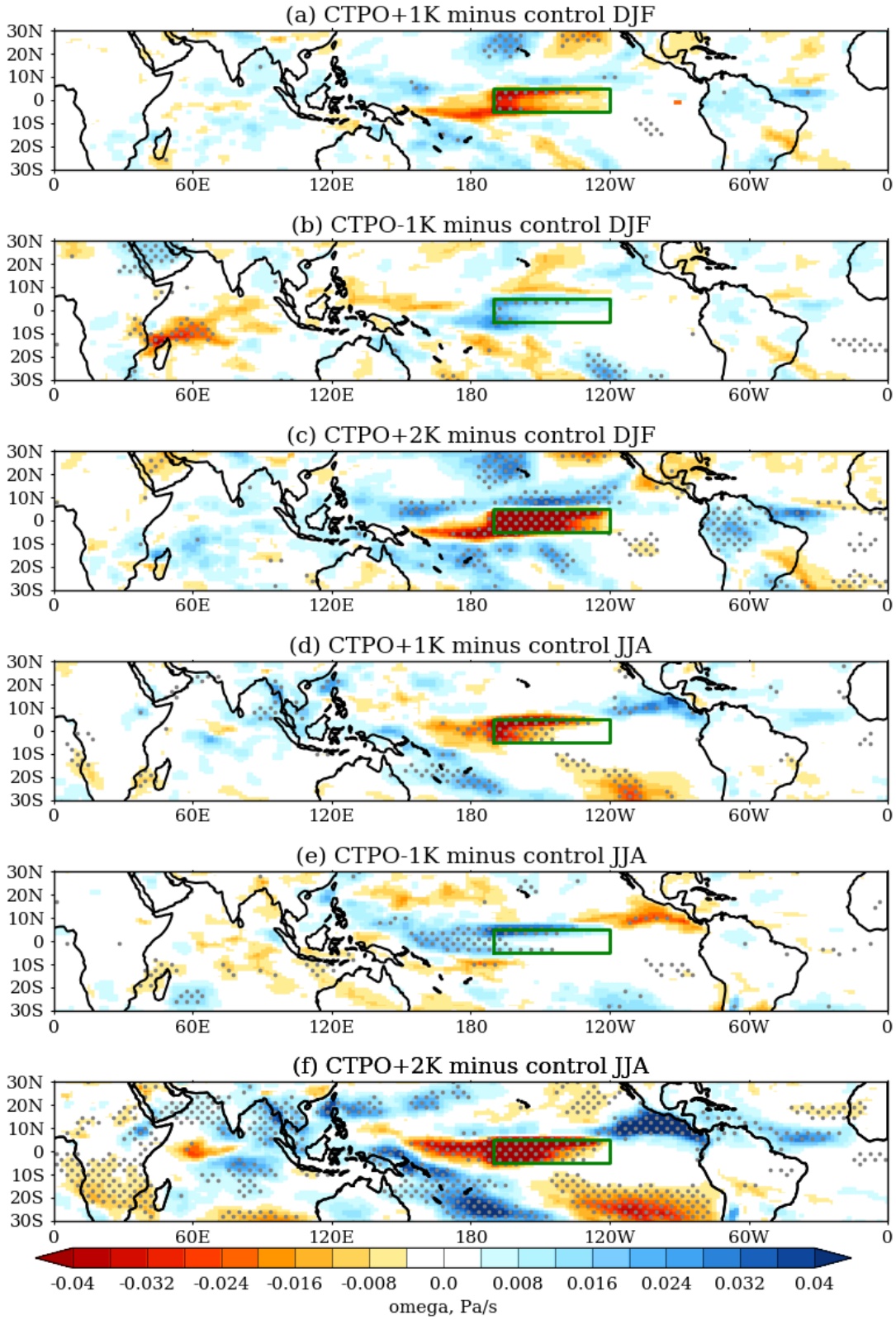

Figure 4.12: DJF seasonal mean 500hPa omega changes (shading, Pa s^{-1}) with respect to control run for: (a) CTPO+1K experiment, (b) CTPO-1K experiment and (c) CTPO+2K experiment. (d)-(f) are as in (a)-(c) but for JJA. Changes that are statistically significant at the 95% confidence level are stippled. Green box shows the domain of the SST perturbation region.

response over the Maritime Continent in CTPO perturbation experiments in Fig. 4.11 as listed in Table 4.2. The mean precipitation response over the Maritime Continent is weaker in the CTPO-1K than the CTPO+1K experiment. However, the normalised magnitude of precipitation responses over the Maritime Continent in CTPO+2K is similar to the response in CTPO+1K. The magnitude of normalised mean rainfall responses over the Maritime Continent is between -0.1 to -0.3 mm day^{-1} in CTPO+1K and CTPO+2K experiments. These values are consistent with the regression coefficients showing the rate of change in the Maritime Continent precipitation per Kelvin SST change in CTPO (mm day^{-1}K^{-1}) from the analyses of the coupled CMIP5 runs in Chapter 4.

Table 4.2: The first row shows the regression coefficients (mm day^{-1}K^{-1}) between the Maritime Continent rainfall and CTPO SST from the coupled CMIP5 run analyses shown in Fig. 3.8b (gradient of the best-fit lines) in Chapter 3.3.5. The second to fourth rows are the normalised area-averaged precipitation responses (mm day^{-1}) over the Maritime Continent in the CTPO perturbation experiments.

Season	DJF	MAM	JJA	SON
Regression coefficient	-0.32	-0.14	-0.16	-0.25
CTPO-1K	0.12	0.17	0.01	0.01
CTPO+1K	-0.21	-0.36	-0.22	-0.14
CTPO+2K	-0.20	-0.31	-0.26	-0.14

The results in this section suggest that models featuring a warm SST biases in the central Pacific will simulate reduced rainfall over the Maritime Continent (and vice versa, to a lesser extent), in agreement with Chapter 4. The area-averaged precipitation response over the Maritime Continent in CTPO perturbation experiments shows a similar magnitude to the regression coefficients between the Maritime Continent rainfall and CTPO SST in Chapter 3.3.5. This indicates that the remote CTPO SST biases in the CMIP5 coupled models contribute to, and possibly cause, the precipitation biases over the Maritime Continent.

4.6 Indian Ocean SST perturbations experiments

In this section, we present experiments with SST perturbations over the WTIO. Fig. 4.13 shows the DJF and JJA seasonal mean precipitation (mm day^{-1}) and 850 hPa wind (m s^{-1}) for each WTIO perturbation experiment minus the control run. Compared to the control run, the precipitation is reduced over the WTIO and increased over the Maritime Continent in the WTIO-1K experiment. The colder SSTs over the WTIO produce a larger east-west SST gradient over the Indian Ocean, driving stronger low level westerlies towards the warmer Maritime Continent and increased precipitation over the Maritime Continent, which resembles a negative IOD phase. The omega at 500hPa shows anomalous descent over WTIO Fig. 4.14, coinciding with decreased rainfall over the WTIO.

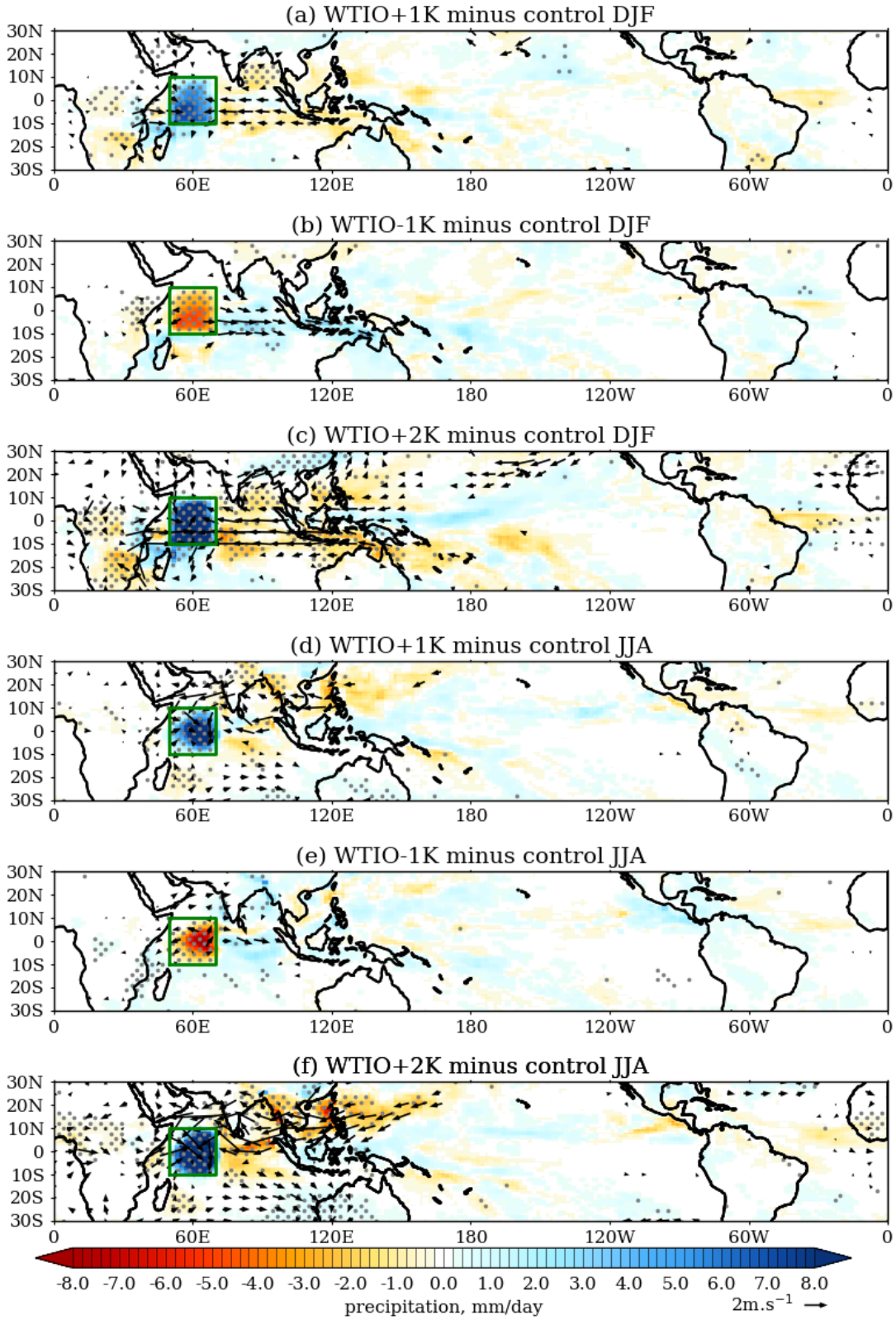

Figure 4.13: DJF precipitation (shading, mm day^{-1}) and 850 hPa wind (vectors, m s^{-1}) changes with respect to the control run in (a) WTIO+1K experiment, (b) WTIO-1K experiment and (c) WTIO+2K experiment. (d)-(f) are as in (a)-(c) but for JJA. Changes that are statistically significant at the 95% confidence level are stippled. Green box shows the domain of the SST perturbation region.

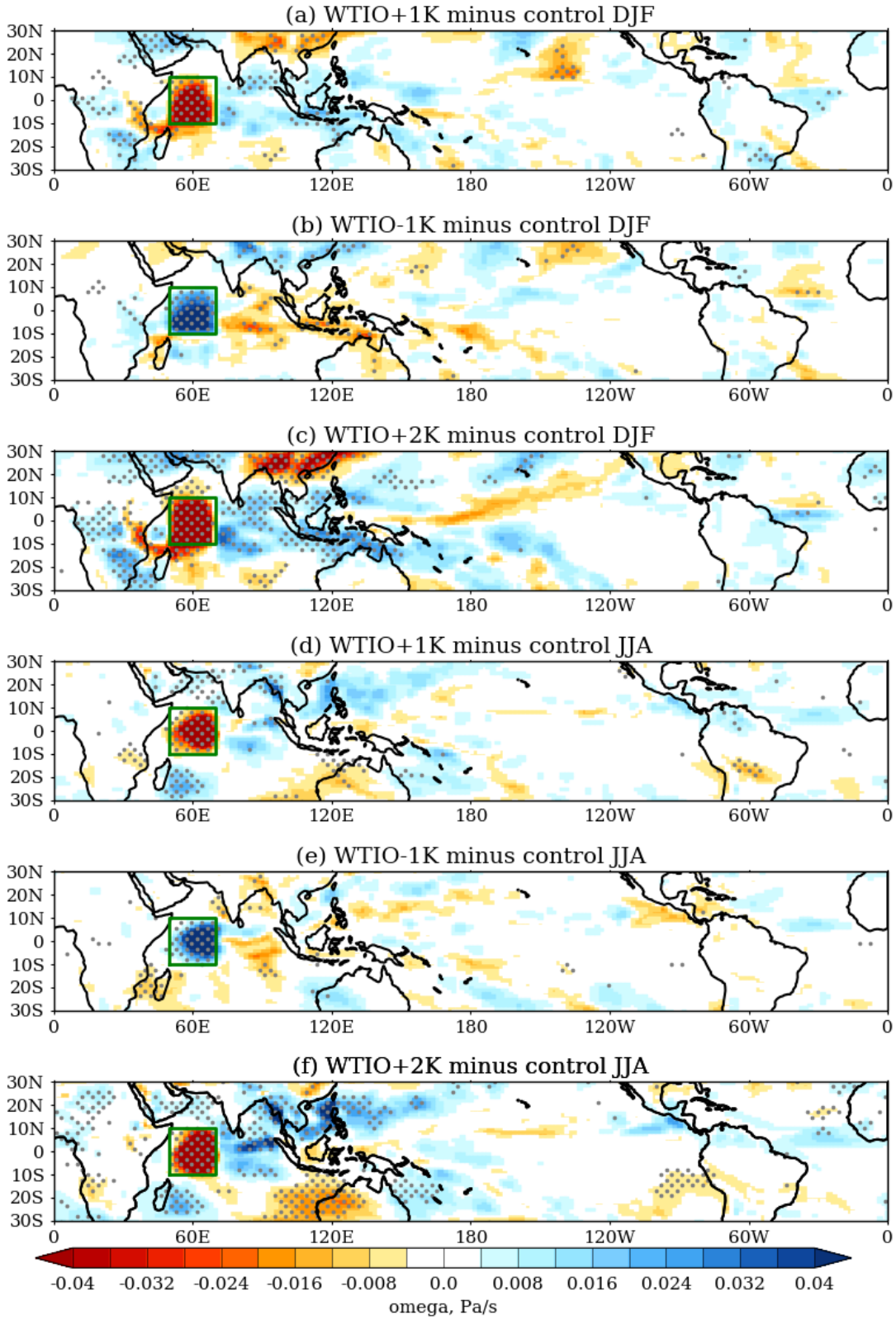

Figure 4.14: DJF seasonal mean 500hPa omega changes (shading, Pa s^{-1}) with respect to control run for: (a) WTIO+1K experiment, (b) WTIO-1K experiment and (c) WTIO+2K experiment. (d)-(f) are as in (a)-(c) but for JJA. Changes that are statistically significant at the 95% confidence level are stippled. Green box shows the domain of the SST perturbation region.

Table 4.3: The first row shows the regression coefficients (mm day^{-1}K^{-1}) between the Maritime Continent mean rainfall and WTIO SST in coupled CMIP5 models from Fig. 3.9a (gradient of the best-fit lines) in Chapter 3.3.5. The second to fourth rows are the normalised area-averaged precipitation responses (mm day^{-1}) over the Maritime Continent in WTIO perturbation experiments.

Season	DJF	MAM	JJA	SON
Regression coefficient	-0.36	-0.09	-0.09	-0.29
WTIO-1K	0.40	0.04	0.20	0.22
WTIO+1K	-0.37	-0.22	-0.28	-0.29
WTIO+2K	-0.30	-0.18	-0.28	-0.32

In contrast, the WTIO+1K and WTIO+2K experiments show an opposite response. The warm anomalies prescribed over the WTIO mean that the WTIO is warmer than the Maritime Continent (Fig. 4.2h, j in Section 5.2.2). The SST gradient between the western and eastern Indian Ocean leads to easterly anomalies from the eastern Indian Ocean and westerly anomalies from Africa converging towards the warmer WTIO at low-levels (Fig. 4.13c, f). The pattern agrees with the Gill (1980) response to heating. The warm anomalies over WTIO drive the easterly anomalies over the Indian Ocean through the Kelvin wave and induce twin cyclonic circulations over Africa through a Rossby wave response.

The vertical velocity (omega at 500hPa) in Fig. 4.14a,c shows anomalous ascent over the warmer WTIO coinciding with increased rainfall, and anomalous descent over the Maritime Continent, eastern Indian Ocean, Middle East and southern Indian Ocean, associated with changes in zonal and meridional overturning circulations.

The WTIO also shows similar results as in CTPO experiments for the local precipitation responses to the SST perturbation: the precipitation amounts are reduced over the WTIO in the negative perturbation experiments and increased in the positive perturbation experiments. The area-averaged precipitation response with respect to the control run over the WTIO shows that the local response is slightly weaker in the WTIO-1K experiment ($\sim$3mm day^{-1}) compared to the WTIO+1K experiment ($\sim$4mm day^{-1}), while the area-averaged local precipitation response in the WTIO+2K experiment is around 8mm day^{-1}, twice that of the WTIO+1K experiment response.

For the remote responses, seasonal area-averaged precipitation responses over the Maritime Continent in the WTIO perturbation experiments are listed in Table 4.3 and compared with the regression coefficients (mm day^{-1}K^{-1}) for the corresponding Maritime Continent rainfall and the WTIO SST mean bias relationship from Fig. 3.9a (gradient of the best-fit lines) in Chapter 3.3.5. The DJF and SON show comparable magnitudes of remote precipitation response over the Maritime Continent and the regression coefficients. In addition, our analysis in Chapter 4 also shows that SON and DJF are the two seasons in which the WTIO shows a significant relationship with the Maritime Continent mean state precipitation. The remote

responses are linear in DJF and SON.

The results in this section suggest that models featuring a warm SST bias in the western Indian Ocean will simulate reduced rainfall over the Maritime Continent while models featuring a cold SST bias in the western Indian Ocean will simulate excess rainfall over the Maritime Continent, in agreement with the results of Chapter 3.3.5. The area-averaged precipitation responses over the Maritime Continent in the WTIO perturbation experiments in DJF and SON show similar magnitudes to the regression coefficients (mm $day^{-1}K^{-1}$) between the Maritime Continent rainfall and WTIO SST from Fig. 3.9a (gradient of the best-fit lines) in Chapter 3.3.5. This indicates that the remote WTIO SST biases in the CMIP5 coupled models could potentially cause those models' precipitation biases over the Maritime Continent.

4.7 Interannual variability of the Maritime Continent precipitation

In the previous section, we investigated the impact of SST perturbations on seasonal mean climatology. Our results showed that SST perturbations not only influence local atmospheric circulation but also have a substantial large-scale impact on the circulation. In this section, we will investigate the impact of SST perturbations on the interannual variability of the Maritime Continent precipitation in DJF and SON seasons, which are the peak phases of ENSO and IOD events respectively.

4.7.1 ENSO teleconnection to the Maritime Continent

All the experiments in this chapter are forced by the same AMIP SST (except for the effects of the uniform perturbations), hence SST interannual variability in all experiments still follows the AMIP control run. Figure 4.15(a) shows a time series of DJF precipitation (mm day^{-1}) averaged over the Maritime Continent from 1982 to 2010 in the observations and SST perturbation experiments. This figure shows that the control run is able to simulate the observed interannual variability over the Maritime Continent region with reasonable skill. The interannual DJF seasonal mean correlation coefficient between GPCP and control run Maritime Continent precipitation is 0.83, which is statistically significant at the 99.5% confidence limit as shown in Table 4.4. This indicates that the control run captures the interannual seasonal variations in precipitation over the Maritime Continent.

Table 4.4 shows that interannual variations of precipitation in the Maritime Continent region in the CTPO and MC perturbation experiments are less correlated to observations compared to the control experiment. The MC+0.5K experiment shows the lowest interannual correlation of Maritime Continent precipitation with observations. Whereas, the Maritime

Table 4.4: Interannual correlation coefficient between observed and simulated Maritime Continent precipitation in various experiments during DJF, arranged in descending order.

Experiment	control	MC-1K	CTPO-1K	CTPO+2K	CTPO+1K	MC+1K	MC+0.5K
Correlation coefficient	0.83	0.78	0.76	0.74	0.73	0.73	0.61

Continent precipitation in the MC-1K experiment has higher correlation with the observations than the MC+0.5K and MC+1K experiments.

To classify the DJF seasons according to the occurrence of ENSO events, we use the Niño 3.4 index as defined in Section 3.2.3. The El Niño events and La Niña events are listed in Table 4.5 by year of the "December" in DJF.

Table 4.5: The El Niño and La Niña years between 1982 to 2011 as defined by DJF SSTs in the Niño 3.4 region and exceeding ± 0.5 °C threshold. The DJF of 1982 refers to the 1982/83 winter, December of the given year and January and February of the following year.

ENSO	**Years**									
El Niño	1982	1986	1987	1991	1994	1997	2002	2004	2006	2009
La Niña	1983	1984	1988	1995	1998	1999	2000	2007	2010	

Figure 4.15 shows the DJF precipitation (mm day^{-1}) averaged over the Maritime Continent from 1982-2011. As anticipated, in the MC+1K and MC+0.5K experiments, the localised response over the perturbation regions is consistent with the climatological mean shown in the previous section, whereby an increase in local SST will increase convection. Hence precipitation increases over the Maritime Continent for all years. The MC-1K experiment also shows a reduction in rainfall compared to the control run over the perturbation regions for all years. For the MC+1K and MC+0.5K experiments, El Niño events show the biggest increment in precipitation with respect to the control run than other years (eg. 1991 and 2002). On the other hand, El Niño years have a smaller reduction in rainfall with respect to the control run, compared to other years in the MC-1K experiment. During El Niño the SST is warmer than normal over the Niño 3.4 region and colder than normal over the Maritime Continent. By adding 1K over the Maritime Continent in the MC+1K experiment, the zonal temperature gradient between the east and west Pacific is reduced. The small change in SST can lead to a larger shift in rainfall to the relatively warmer Maritime Continent. Whereas in the MC-1K experiment, the zonal temperature gradient over the Pacific is increased, hence less rainfall is induced in this experiment.

On the other hand, the remote responses are more complicated. It is anticipated that through the area-averaged mean state precipitation responses in Chapter 4.5, an increase of SST over the CTPO will reduce rainfall over the Maritime Continent, and conversely, reducing SST over the CTPO will increase rainfall over the Maritime Continent. The CTPO+2K experiment simulates less precipitation over the Maritime Continent compared to the control

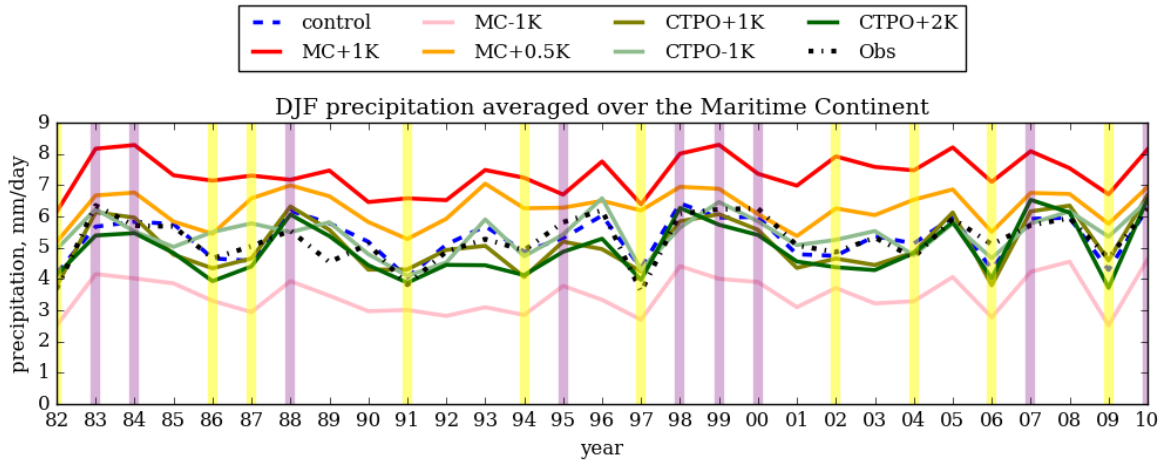

Figure 4.15: DJF precipitation (mm day^{-1}) averaged over the Maritime Continent from 1982-2011. The yellow vertical lines show the El Niño years and purple vertical lines show the La Niña years.

run, consistent with Chapter 5.5 results, apart from 3 years (2007, 2008 and 2010). 2007 and 2010 are La Niña years, during which the Maritime Continent generally receives above normal rainfall. For neutral years preceding El Niño years, all three experiments tend to simulate less rainfall than the control run (e.g. 1985 and 1990). This suggests that ENSO variability has a substantial impact on the Maritime Continent precipitation and the SST perturbation impacts vary according to ENSO phase.

Figure 4.16 shows the SST (shading, K) and precipitation (contour, mm/day) evolution across the equatorial Pacific during a two-year period of composite La Niña or El Niño events adapted from Turner et al. (2005). In the control run, the composite evolution of El Niño events shows that the warmest absolute SSTs extend eastwards towards the central and eastern Pacific and reach their peak in December, while during La Niña events, the warm SST is more confined over the western Pacific, as expected. Convection also follows the migration of the warm SST, with positive anomalies moving eastward to the central Pacific and negative anomalies forming over the Maritime Continent. The CTPO+1K experiment produces a larger region of warm SST. The black contour lines in Fig. 4.16 are the precipitation (mm day^{-1}). Heavier precipitation occurs over the warm SST region, however the maximum precipitation is not located over the warmest SST. The figure shows that the spatial distribution of rainfall shows some difference from the SST distribution in the IPWP region, in agreement with Chen and Houze (1997) that stronger deep convection does not colocate exactly with warmest SST over the IPWP region.

Next, we investigate the impact of SST perturbations on the spatial distribution of rainfall and 850 hPa winds during El Niño and La Niña. First, looking at the control experiment precipitation biases with respect to observations, the composites of both the El Niño (Fig. 4.17a) and La Niña (Fig. 4.18a) phases have somewhat similar biases, but La Niña features a larger

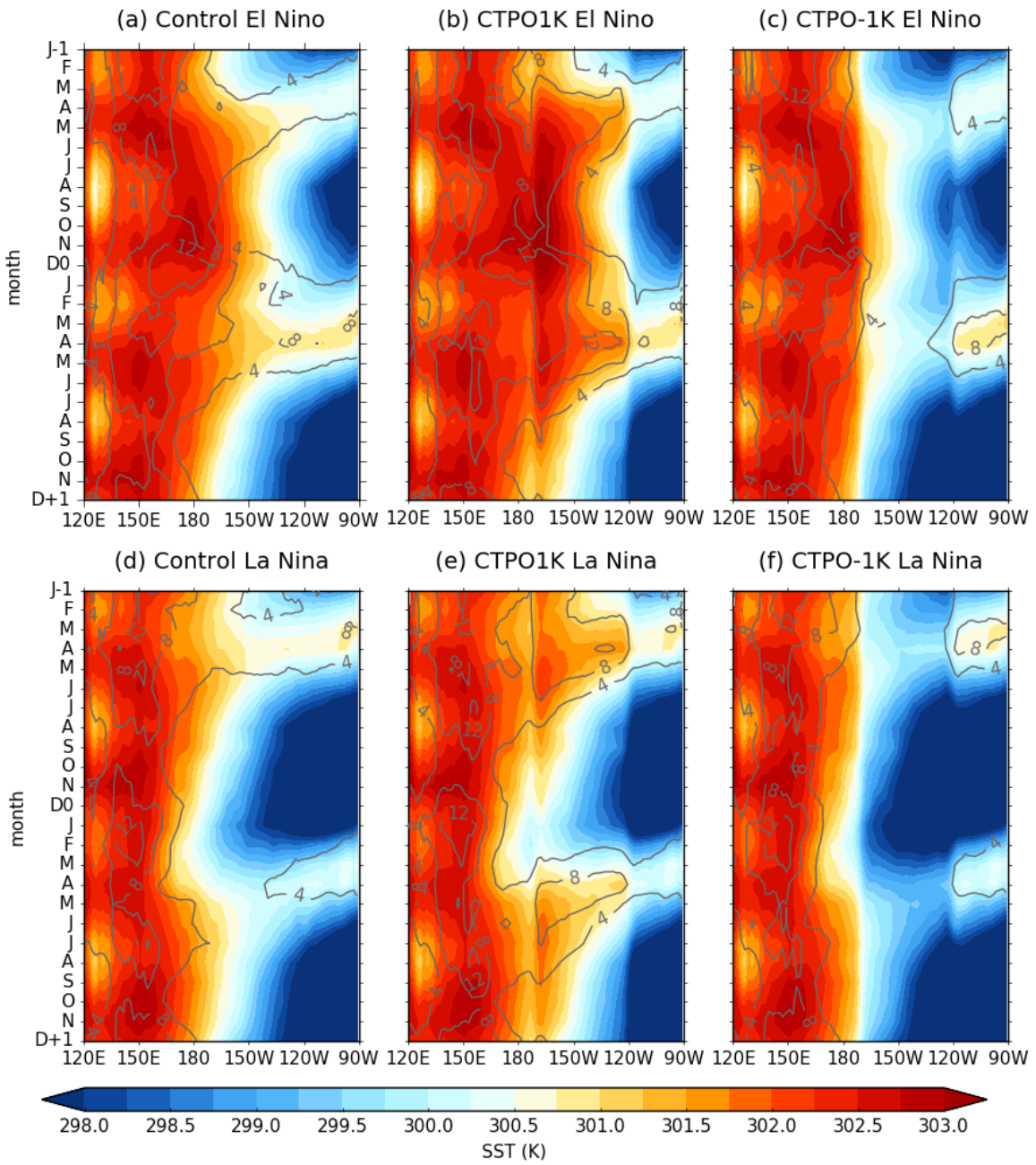

Figure 4.16: Evolution of mean equatorial (5°S-5°N) SST (K, shading) and precipitation (mm day^{-1}, contour) in a composite of ten El Niño events in two-year period for (a) control, (b) CTPO+1K and (c) CTPO-1K experiments. (d)-(f) are as in (a)-(c) but for La Niña.

area of wet biases over the Pacific Ocean. We also investigate the precipitation and 850 hPa wind biases in the Maritime Continent during El Niño and La Niña (zoomed figure not shown). We found a striking similarity between the biases in mean state climatology and biases in composited El Niño and La Niña events over the Maritime Continent. The PCC values are above 0.9 and the RMSE is less than 1 mm day^{-1} between mean state climatology biases and El Niño biases in Maritime Continent precipitation. This result is in agreement with our

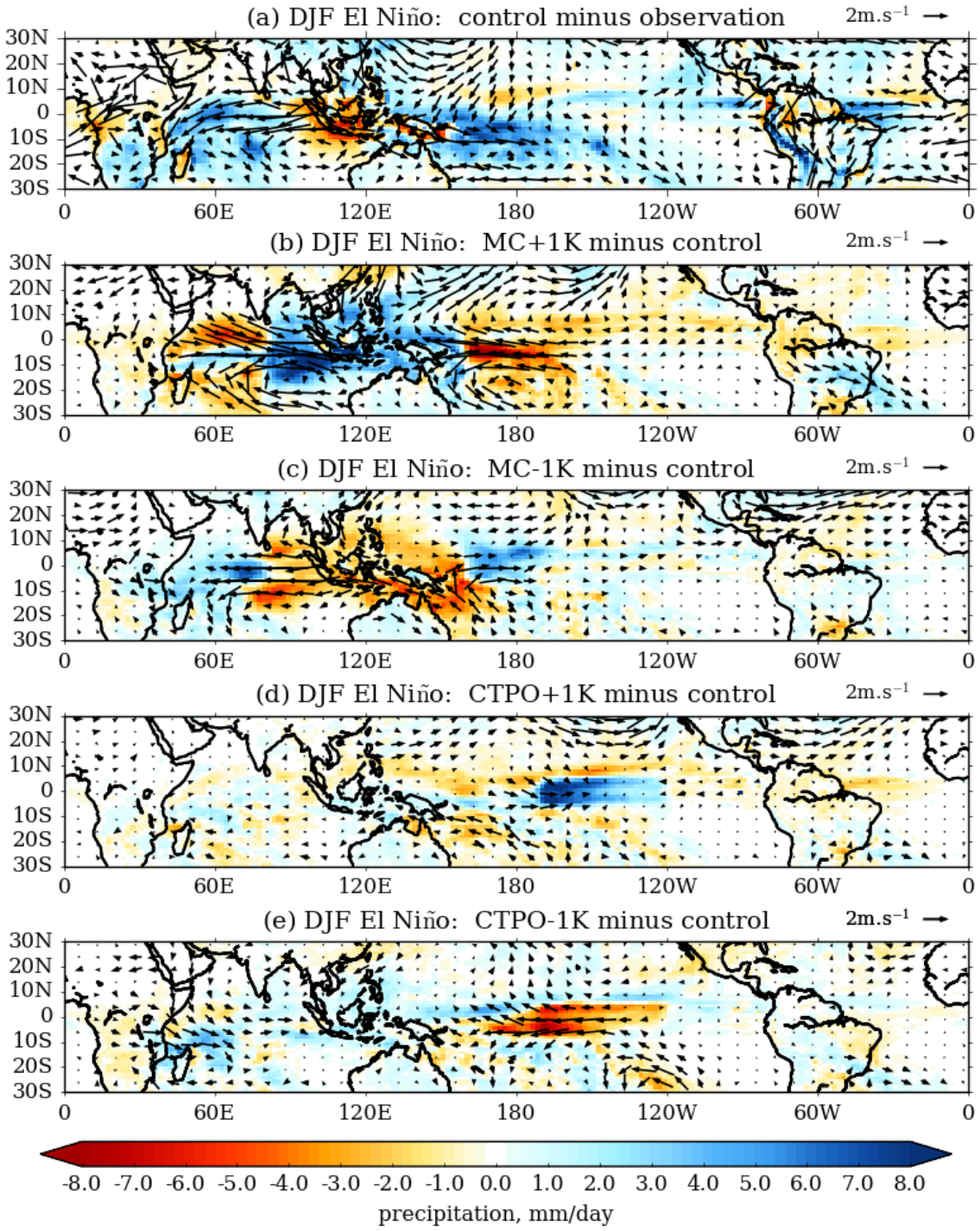

Figure 4.17: DJF seasonal mean precipitation (shading, mm day^{-1}) and 850 hPa wind (vectors, m s^{-1}) for El Niño composite of (a) control minus observations (b) MC+1K minus control, (c) MC-1K minus control, (d) CTPO+1K minus control and (e) CTPO-1K minus control.

finding in Chapter 4 that biases in precipitation and circulation over the Maritime Continent during ENSO and IOD events mainly result from the climatological mean state biases in the control AMIP experiment.

In the MC+1K experiment, easterlies from the Pacific Ocean converge towards the warmer

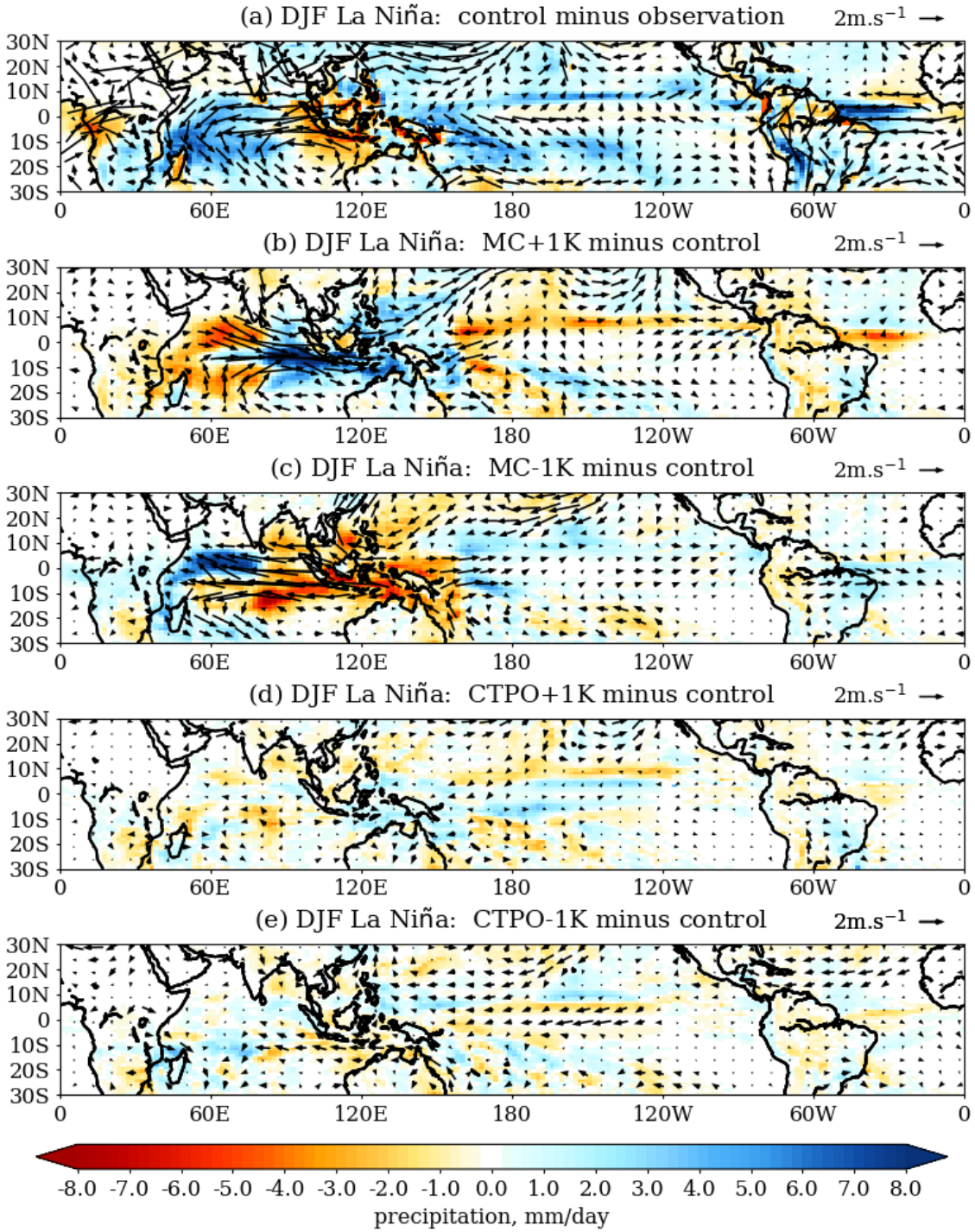

Figure 4.18: DJF seasonal mean precipitation (shading, mm day^{-1}) and 850 hPa wind (vectors, m s^{-1}) for La Niña composite of (a) control minus observations (b) MC+1K minus control, (c) MC-1K minus control, (d) CTPO+1K minus control and (e) CTPO-1K minus control.

SST. A weaker response in wind and precipitation is found in La Niña (Fig. 4.18b) compared to El Niño (Fig. 4.17b). The area-averaged precipitation over the Maritime Continent in Fig. 4.15(b) also shows that the changes in El Niño events are larger than La Niña events. This may be due to the asymmetry of ENSO, where El Niño events are often stronger than La

Niña events.

In the CTPO perturbation experiments, the local precipitation response shows different results in La Niña and El Niño events. In the El Niño composite, the CTPO+1K experiment shows an increase of rainfall over the CTPO (Fig. 4.17d), while the CTPO-1K experiment simulates a decrease of rainfall in CTPO (Fig. 4.17e) with respect to observations. On the other hand, CTPO local precipitation and wind patterns responses are small during La Niña events. This might be because the SST over the CTPO after perturbation is less than the threshold for convection (Johnson and Xie, 2010), consistent with Fig. 4.16, which shows that CTPO SST is much colder in the La Niña phase even for the CTPO+1K experiment.

4.7.2 IOD teleconnection to the Maritime Continent

Following on from the previous section, we discuss the impact of mean-state SST perturbation experiments on the teleconnection of Maritime Continent rainfall to the IOD. Fig. 4.19(a) shows the SON precipitation (mm day^{-1}) averaged over the Maritime Continent and IODW regions from 1982 to 2010. In the Maritime Continent region, the control run is able to capture the interannual variability of precipitation as observed (r=0.83). However, unlike in DJF, for which the control run has the highest interannual correlation to GPCP, the perturbation experiments are better correlated to GPCP in SON except for the WTIO-1K experiment.

Table 4.6: Interannual correlation between observed SON precipitation and simulated SON precipitation over the Maritime Continent in SST perturbation experiments, arranged in descending order.

Experiment	MC+1K	WTIO+1K	MC-1K	WTIO+2K	MC+0.5K	control	WTIO-1K
Correlation coefficient	0.91	0.86	0.85	0.84	0.84	0.83	0.82

To further investigate how do these sensitivity experiments alter the Maritime Continent atmospheric response to IOD, we classify the SON seasons according to the occurrence of IOD events. Table 4.7 lists the positive IOD and negative IOD years between 1982 to 2011. The IOD events are selected based on the DMI, as defined in Section 3.2.3.

Table 4.7: Positive IOD and negative IOD years between 1982 to 2011 as defined by SON DMI exceeding the $\pm$0.5 °C threshold.

IOD	**Years**			
Negative IOD	1992	1996	1998	2010
Positive IOD	1991	1994	1997	2006

The MC experiment local response shows that adding 1K to the SST here increases the precipitation, while reducing the SST by 1K decreases the precipitation over the Maritime Continent (Fig. 4.19), as indicated by the area-averaged mean state precipitation responses in

Section 4.6. The local responses are mainly linear in the Maritime Continent SST perturbation experiments, which is consistent with the findings of Section 4.6.

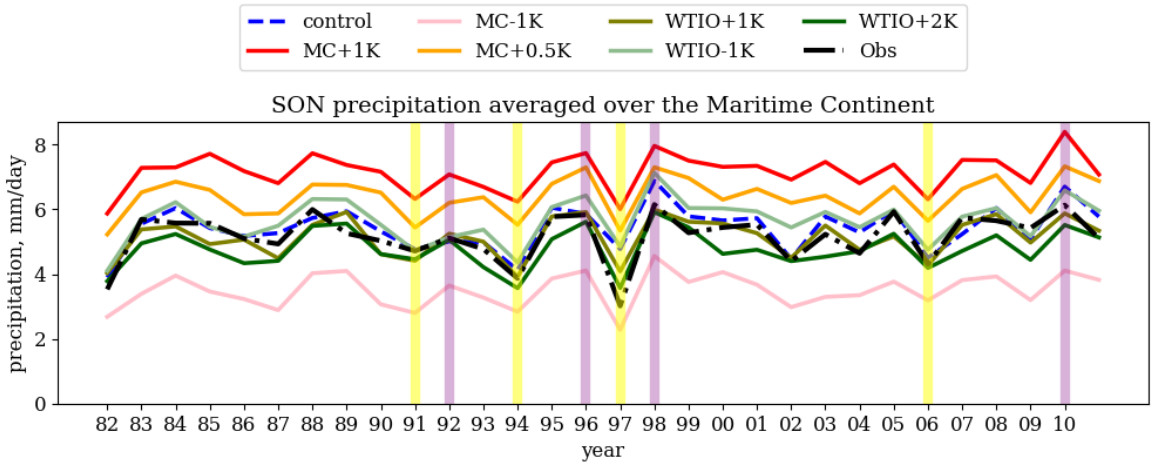

Figure 4.19: SON precipitation (mm day^{-1}) averaged over the Maritime Continent from 1982-2011. The yellow vertical lines show the positive IOD years and purple vertical lines show the negative IOD years.

The remote responses over the Maritime Continent in the WTIO experiment show that warmer SST in the WTIO leads to reduced rainfall over the Maritime Continent and colder SST in the WTIO increases the rainfall over the Maritime Continent in most years (Fig. 4.19a). In the WTIO-1K experiment, only four years show negative precipitation anomalies and these four years are IOD-neutral years. Only 1992, which is a negative IOD year, shows an increase of rainfall in all three WTIO experiments.

Figure 4.20(a) shows the composite of positive IOD for precipitation and 850 hPa winds in the control experiment and its biases with respect to observation, while Fig. 4.21(a) shows the composite for the negative IOD. Both positive and negative IOD composites have similar biases, for example the dry biases in India and the Maritime Continent, the wet biases in the SPCZ, west Pacific (westerly biases) and Indian Ocean (easterly biases). In the Maritime Continent, the biases in IOD composites are similar to the climatological biases (figure not shown), suggesting that biases in the precipitation and 850 hPa wind during the IOD events mainly result from climatology biases, consistent with the results of Chapter 3.4.

Figure 4.20 also shows the positive IOD SON precipitation and 850 hPa wind anomalies minus the control in each experiment. In the MC+1K experiment, wet anomalies are observed over the perturbation region, Maritime Continent and dry anomalies over the western Indian and Pacific Oceans. Anomalous easterlies from the Pacific Ocean and anomalous westerlies from the Indian Ocean converge over the Maritime Continent in both positive IOD (Fig. 4.20b) and negative IOD (Fig. 4.21b) events. The MC-1K experiment shows an opposite response (Fig. 4.20c, Fig. 4.21c).

In the WTIO+1K and WTIO-1K experiments, the local precipitation response is generally

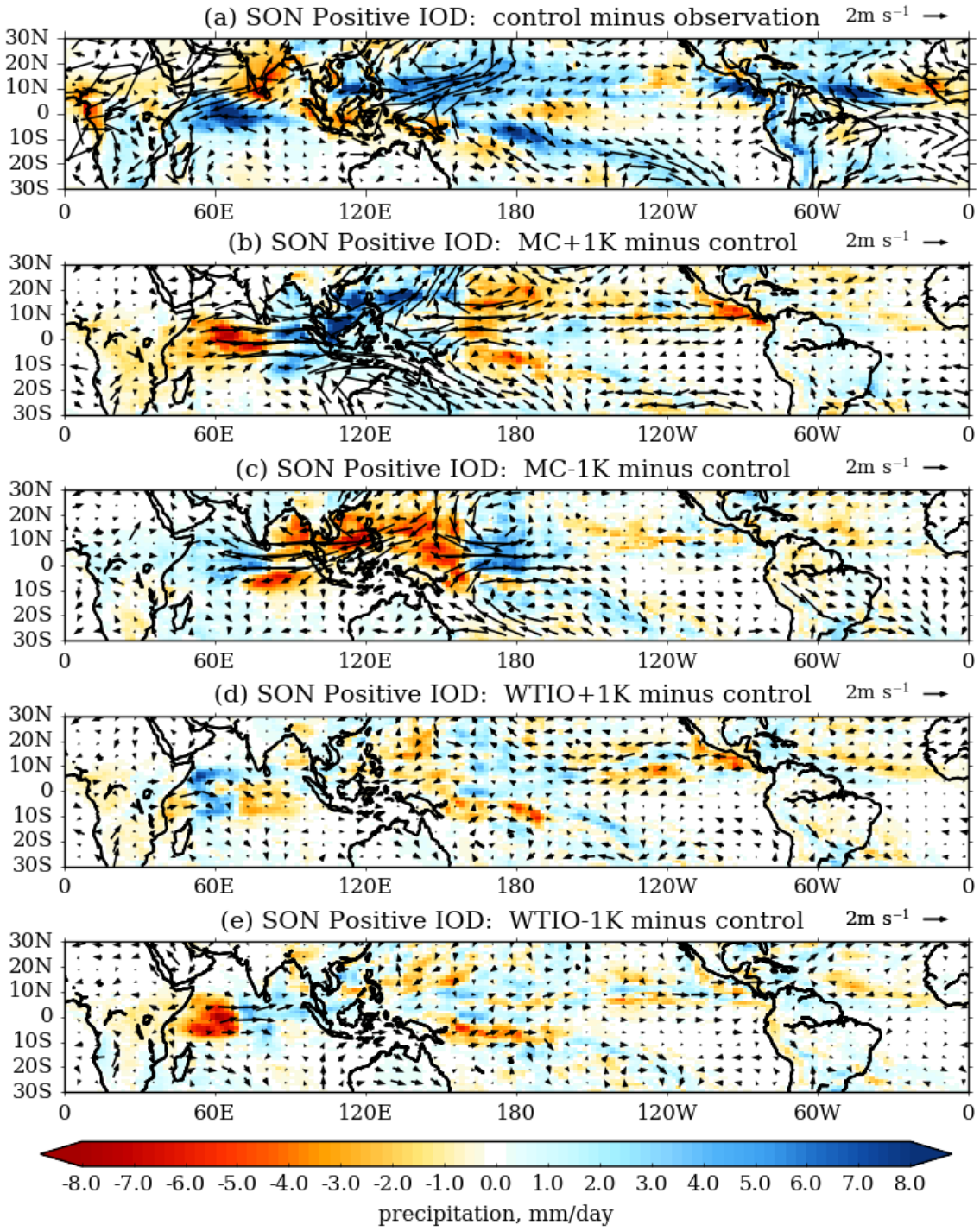

Figure 4.20: SON seasonal mean precipitation (shading, mm day^{-1}) and 850 hPa wind (vectors, m s^{-1}) for positive IOD composite of (a) control minus observations (b) MC+1K minus control, (c) MC-1K minus control, (d) WTIO+1K minus control and (e) WTIO-1K minus control.

of the same sign as the SST perturbations, whereas in the Maritime Continent the remote precipitation response is generally opposite in sign in both phases of IOD. This shows that in general, the WTIO-1K experiment results in reduced precipitation over the WTIO and

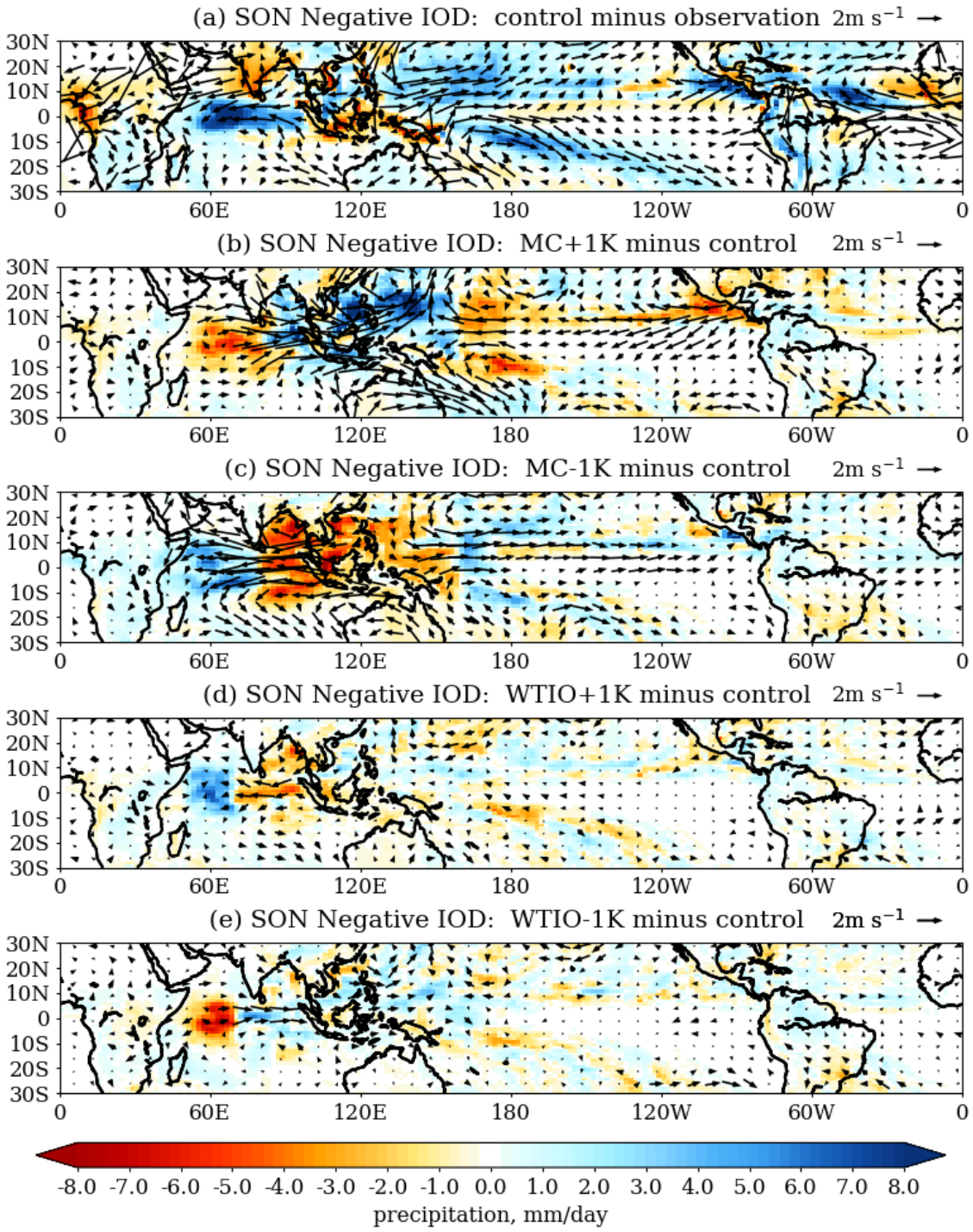

Figure 4.21: SON seasonal mean precipitation (shading, mm day^{-1}) and 850 hPa wind (vectors, m s^{-1}) for negative IOD composite of (a) control minus observations (b) MC+1K minus control, (c) MC-1K minus control, (d) WTIO+1K minus control and (e) WTIO-1K minus control.

increased precipitation over the Maritime Continent compared to the control run in positive IOD (Fig. 4.20e) and negative IOD events (Fig. 4.21e). Opposite local and remote precipitation responses are produced in WTIO+1K experiments (Fig. 4.20d, 4.21d).

4.8 Discussion and conclusions

In this chapter, we analysed a suite of sensitivity experiments to examine the effect of Maritime Continent SST perturbations on tropical variability and teleconnections, and to investigate the influence of SST perturbations elsewhere in the tropics (i.e. the Pacific and Indian Oceans) on climate variability within the Maritime Continent.

The perturbations to SST produce local and remote responses. For the mean state analysis, we focused on DJF and JJA. Our results show that when SST is increased over the Maritime Continent, the increased westerlies from the Indian Ocean and increased easterlies from the Pacific Ocean converge towards the Maritime Continent, corresponding to increased precipitation there. The MC-1K experiment shows opposite results with anomalous wind divergence from the Maritime Continent and weakening of the Walker circulation, leading to a decrease in Maritime Continent rainfall. The seasonal mean precipitation local responses to SST changes are linear in the Maritime Continent perturbation experiments.

Seasonal area-averaged mean precipitation responses over the Maritime Continent to local SST perturbations are of the same sign as the regression coefficient between Maritime Continent precipitation and Maritime Continent SST in the coupled CMIP5 runs analysed in Chapter 4 apart from DJF, which had a negative regression coefficient. However, the magnitude of local precipitation responses is ten-times larger than the regression coefficients.

However, the MC+1K experiment also produces even less precipitation over some land areas, especially over Sumatra and Borneo. This suggests that warm SST anomalies provide greater moisture supply over the ocean, however, it also reduces the temperature difference between the land and the sea which can lead to weaker sea breezes and reduced rainfall over the land.

The Maritime Continent SST perturbation experiments also affect the circulation and precipitation over the Pacific and Indian Oceans, in agreement with previous studies showing that precipitation biases over the Maritime Continent contribute to other systematic biases over the tropics (Neale and Slingo, 2003; Zhang et al., 2016). The precipitation in the Pacific and Indian Oceans shows non-linear negative responses to SST changes in the Maritime Continent. Seasonal precipitation responses are up to 5 to 6 mm day^{-1} K^{-1} apart from during JJA, where SST change in the Maritime Continent can induce remote precipitation responses over the Indian Ocean of up to 10 mm day^{-1}.

The moisture budget analysis shows that the control experiment VIMFC is similar to the difference between precipitation and evaporation (P-E). The evaporation biases are modest over the Maritime Continent (less than 2 mm day^{-1}). Therefore, the VIMFC biases also largely resemble the precipitation biases in the control run. In the sensitivity experiments, we found that the changes in VIMFC are again similar to the changes in P-E, as well as to the changes in precipitation.

On the other hand, the CTPO+1K and CTPO+2K experiments resulted in anomalous ascent over CTPO and less rainfall over the Maritime Continent. The CTPO-1K experiment showed an opposite response, with rainfall increasing over the Maritime Continent. The localised precipitation responses in the CTPO perturbation experiments are not linear, which may be explained by the Clausius-Clapeyron relationship. The warmer SST in the CTPO+2K experiment induces larger changes in atmospheric moisture and anomalies in precipitation and surface winds, compared to the CTPO+1K and CTPO-1K experiments that have relatively low SST. Another possible reason for nonlinearity of the local rainfall response over the CTPO is the shift of precipitation away from other tropical regions. The precipitation remote responses over the Maritime Continent in the CTPO experiments are somewhat comparable to the regression coefficients between the Maritime Continent mean-state rainfall and the CTPO mean-state SST for the CMIP5 coupled models in Chapter 3.3.5. These results show that models featuring warm SST biases in the central Pacific will simulate reduced rainfall over the Maritime Continent and vice versa. This suggests that the SST biases over the CTPO causes precipitation biases over the Maritime Continent for the CMIP5 coupled models in Chapter 4 as well.

In the WTIO-1K experiment, colder SSTs over the WTIO produce a larger east-west SST gradient over the Indian Ocean, driving stronger low-level westerlies towards the warmer Maritime Continent. Precipitation increases over the Maritime Continent and decreases over WTIO. The positive perturbation of WTIO SST shows an opposite precipitation and circulation response. The area-averaged precipitation responses with respect to the control run show that the local precipitation response is slightly weaker in the WTIO-1K experiment compared to the WTIO+1K experiment, while the WTIO+2K experiment precipitation response to local SST perturbation is twice that of the WTIO+1K experiment precipitation response. The area-averaged precipitation responses over the Maritime Continent in the WTIO perturbation experiments in DJF and SON show similar magnitudes to the regression coefficients between the Maritime Continent rainfall and WTIO SST for the coupled CMIP5 models in Chapter 3.3.5. This indicates that the remote WTIO SST biases in the CMIP5 coupled model contribute to, and possibly cause, the precipitation biases over the Maritime Continent.

For the analysis on interannual variability, we focused on the winter season (DJF) when ENSO events peak for the Pacific Ocean perturbation experiments and autumn (SON) season for the Indian Ocean experiments, since SON is the peak season for IOD events. The control run is able to capture the interannual variability of precipitation represented by these modes. The localised response over the perturbation regions is consistent with the climatological mean response, whereby an increase in local SST will increase the precipitation here. The precipitation responses over the Maritime Continent during El Niño events are stronger in the MC+1K experiment than the MC-1K experiment. The remote responses over the Maritime Continent are more complicated, particularly those relating to ENSO variability in the CTPO

experiments.

For the IOD analyses, there are only four positive IOD and negative IOD events from 1982 to 2011, limiting the sample size, hence no significant changes are identified in the interannual variability of the Maritime Continent precipitation relating to IOD events. On the other hand, all of the positive IOD years are also the El Niño years, while 1998 is also both a La Niña and negative IOD year. While previous studies (Saji et al., 1999; Webster et al., 1999) suggested that the IOD is an independent mode of variability in the Indian Ocean, Allan et al. (2001) argued that the IOD is related to the ENSO. Nur'utami and Hidayat (2016) showed that an individual IOD event, individual ENSO event and combinations of both ENSO and IOD events have different impacts on Indonesian rainfall. Hence it is hard to separate the variability associated with ENSO and the IOD.

We found that biases in precipitation and circulation over the Maritime Continent during ENSO and IOD events mainly result from the climatological mean state biases, in agreement with the results of Chapter 4.

In this study, we have only considered the impact of Indo-Pacific SST biases on Maritime Continent precipitation and circulation. However, as shown in Fig. 3.1 and Fig. 3.2, there are also biases in other parts of the ocean basins that may play a role, which are beyond the scope of this study. Furthermore, the interaction between the Pacific Ocean and Indian Ocean also warrants further investigation.

Our results highlight the importance of the Maritime Continent on the Indo-Pacific climate. The perturbation over the Maritime Continent SST induced significant opposite remote precipitation responses over the Indo-Pacific and the magnitude of remote precipitation responses are larger compared to the CTPO and WTIO perturbation experiments. This suggests that the influence of the Maritime Continent on the large-scale circulation and precipitation across the Indo-Pacific is significant. The CTPO and WTIO experiments produce area-averaged seasonal mean precipitation remote responses over the Maritime Continent of a comparable magnitude to the regression coefficients (mm day^{-1}K^{-1}) between the Maritime Continent rainfall and the CTPO and WTIO SSTs for coupled CMIP5 models shown in Chapter 3.3.5. Our SST sensitivity experiments suggest that SST biases in the CTPO and WTIO could possibly be the cause of coupled model precipitation biases over the Maritime Continent. Further work could extend this experiment by running the MC-KPP type (Multi-Column K Profile Parameterization ocean) mixed-layer ocean model(MetUM-GOML) or coupled version of the HadGEM3 model.

Chapter 5

Conclusions and Future Work

In this chapter, we summarize the key findings of the thesis in Section 5.1. The limitations of the work are discussed in Section 5.2, and suggestions for future work are given in Section 5.3.

5.1 Summary of key findings

Variations in rainfall have significant implications for societies in the Maritime Continent, who depend on monsoon rainfall for their water supply and agricultural purposes. This in turn has an effect on the overall economies of the countries in the Maritime Continent. Better understanding of the climate mean state and its variability in the Maritime Continent region and its representation in General Circulation Models (GCMs) is crucial from both a socio-economic and climate perspective. The Maritime Continent is one of the principal heat sources that drive the global circulation (Ramage, 1968). Despite its importance in the global climate system, the ability of General Circulation Models (GCMs) to simulate the mean climate and climate variability over the Maritime Continent remains a modelling challenge. In this section, we will revisit the principal aims of this thesis and the specific questions based around the main aims posed in Chapter 1.

The first aim of this thesis is to investigate the fidelity of current state-of-the-art climate models at simulating the climate mean state and its variability in the Maritime Continent as stated in Section 1.9. Chapter 3 focuses mainly on the Atmospheric Model Intercomparison Project (AMIP) experiments of the Coupled Model Intercomparison Project Phase 5 (CMIP5) and the results are published in Climate Dynamics (Toh et al., 2018). We addressed the following questions in Chapter 3:

How well do CMIP5 models simulate the mean seasonal climate over the Maritime Continent?

We find that AMIP models suffer from systematic biases and there is a considerable spread of skill at simulating the seasonal mean climate over the Maritime Continent region. The

magnitude and spatial pattern of the biases vary in each model according to season, i.e, a model with high skill in one season does not necessarily represent other seasons well.

The multimodel mean (MMM) has better skill at reproducing the observed mean climate than the individual models, in agreement with other CMIP5 studies (Colman et al., 2011; Jourdain et al., 2013; Sperber et al., 2013; Feng et al., 2014) which found that the MMM outperforms individual models at reproducing the observed monsoon climate.

The spatial pattern of 850 hPa wind is better simulated than the precipitation over the Maritime Continent in all four seasons, as found by Brown et al. (2013) over the Western Pacific monsoon region and Sperber et al. (2013) over the Asian monsoon region.

The comparison with coupled models in CMIP5 shows that AMIP models generally performed better than coupled models in the simulation of the global monsoon and local Hadley circulation but less well at simulating the Maritime Continent annual cycle of precipitation. There is a clear lack of correlation between a model's performance at simulating the annual cycle of precipitation in atmosphere-only mode and in coupled mode. This is also the case for the equinoctial and solsticial modes.

What are the model systematic biases in the Maritime Continent?

In DJF, most AMIP models overestimate the precipitation over the West Pacific Ocean and underestimate the precipitation over the land. The dry biases over land are associated with easterly wind biases over the region and these precipitation and wind biases are common errors in the atmosphere-only models. A notable difference between DJF and JJA seasons is the more common presence of large biases of precipitation over the Maritime Continent north of 10°N in JJA compared to DJF, indicating that the models simulate the monsoonal precipitation poorly.

Furthermore, there are systematic discrepancies among the AMIP models in simulating the annual cycle of precipitation over the Maritime Continent. Cluster analysis performed in this study to characterize model systematic biases resulted in two clusters with distinct fidelity at representing the annual cycle of precipitation over the Maritime Continent. Cluster I models perform better than Cluster II models at simulating the seasonal migration of precipitation over the Maritime Continent, but they overestimate the precipitation, especially during the JJA and SON seasons. Cluster II models simulate less seasonal movement of the Intertropical Convergence Zone (ITCZ) over the Maritime Continent than observed, and the maximum rainfall position stays closer to the equator throughout the year.

What are the possible sources of model systematic biases?

To better understand the causes of the Maritime Continent precipitation biases and what aspects of the models are most important for correctly representing the climate of the Maritime Continent, we focus on three possible sources of bias: the role of horizontal resolution, the

relationship to biases in the local Hadley circulation and global monsoon, and the impact of air-sea coupling.

We find that AMIP model performance is largely unrelated to resolution, in agreement with Neale and Slingo (2003). Instead, our results show that models' local Maritime Continent biases are related to their biases in the local Hadley circulation and global monsoon, and these same results hold for both Cluster I and Cluster II. Models that better represent the global monsoons and local Hadley circulation will also have a better representation of the precipitation pattern over the Maritime Continent region. This also indicates that the biases in seasonal migration of the ITCZ over the Maritime Continent are thus related to the global-scale ITCZ movement biases.

The comparison between AMIP and coupled models in CMIP5 shows that AMIP models generally perform better than coupled models at simulating the global monsoon and local Hadley circulation. However, coupled models better capture the Maritime Continent annual cycle of precipitation. This opposite result suggests that air-sea coupling improves the simulation of the Maritime Continent annual cycle precipitation despite the inevitable sea surface temperature (SST) biases. However, SST biases and ocean-atmosphere feedback errors introduce larger biases in the coupled models at the large scale. We also found mixed results for model skill at reproducing the seasonal precipitation and 850 hPa wind patterns over the Maritime Continent. These comparisons between AMIP-coupled pairs showed that air-sea coupling yields complex impacts on Maritime Continent precipitation biases. The relationship between SST and the Maritime Continent precipitation is further investigated in Chapter 4.

Chapters 4 and 5 address the second and third aims of this thesis: (2) to explore the impact of model biases in the Maritime Continent on tropical variability and teleconnections; and (3) to determine the relationship between SST in the tropics and climate variability within the Maritime Continent. The specific research questions that were raised in the Introduction chapter of this thesis are addressed below.

How well do CMIP5 coupled models simulate the tropical ocean SST?

The performance of coupled CMIP5 models varies greatly at reproducing the seasonal mean SST and the annual cycle. In general, most CMIP5 models exhibit cold biases over the central and western Pacific Ocean as well as the central and eastern Indian Ocean while simulating warm biases over the southeastern Pacific Ocean and equatorial Atlantic Ocean. The magnitude, sign and spatial pattern of SST biases are somewhat similar in all four seasons, apart from the western Indian Ocean where the biases change sign in different seasons. Some models including the MMM simulate colder than observed SST in DJF and MAM seasons but warmer than observed SST in JJA and SON seasons in the western Indian Ocean.

Models perform less well at simulating the central tropical Pacific Ocean (CTPO) annual

cycle SSTs compared to the Maritime Continent and western tropical Indian Ocean (WTIO) and show a considerable inter-model spread of up to 5 °C for this region.

What is the relationship between Maritime Continent mean-state precipitation biases and tropical SST biases?

Our analysis shows that Maritime Continent mean-state precipitation biases in coupled models are largely unrelated to local mean-state SST biases, apart from during SON which shows a statistically significant positive correlation. On the other hand, remote SSTs are significantly correlated with the Maritime Continent mean-state precipitation. For all four seasons, the Maritime Continent mean-state precipitation shows negative association with the central and eastern Pacific Ocean SSTs. The relationship is strongest in DJF. This shows that those models featuring warmer central tropical Pacific ocean (CTPO, 5°S-5°N and 120°W-170°W) SST in the mean state generally feature reduced precipitation in the Maritime Continent and vice versa. We also found that the mean-state zonal temperature gradient between the Maritime Continent and the central Pacific is significantly correlated with the Maritime Continent precipitation, suggesting an association with the mean-state Walker Circulation.

In the Indian Ocean, there is an IOD-like bias pattern in mean-state precipitation, wind and SST during SON that is not evident in other seasons. The eastern tropical Indian Ocean SSTs show a positive correlation to the Maritime Continent precipitation in SON. In contrast, the western tropical Indian Ocean (WTIO, 10°S-10°N and 50°E-70°E) SSTs show a negative relationship to the Maritime Continent precipitation, as in the central Pacific Ocean but with weaker magnitude for all seasons. The mean-state zonal temperature gradient between the Maritime Continent and the western Indian Ocean is significantly correlated with Maritime Continent precipitation, suggesting an association with the mean-state Indian Ocean Walker Circulation. The relationship is strongest during SON which is the peak phase of the IOD.

We also found that wet biases in the Maritime Continent are associated with warm SST biases over the Maritime Continent and cold SST biases over the CTPO and WTIO concurrently. This suggests the combined interactions between the climatological Walker cells over the Indian and Pacific Oceans with the Maritime Continent mean-state precipitation and circulation.

How well do CMIP5 atmosphere-only and coupled models simulate teleconnections between ENSO/IOD and the Maritime Continent?

The El Niño-Southern Oscillation (ENSO) and the Indian Ocean Dipole (IOD) are modes of variability that significantly affect the climate over the Maritime Continent on interannual timescales. The observed Maritime Continent precipitation generally shows negative precipitation anomalies during El Niño and positive precipitation anomalies during La Niña in DJF. Most of the AMIP and coupled CMIP5 models capture the relationship between Niño

3.4 SST and area-averaged Maritime Continent precipitation but not the spatial pattern of precipitation anomalies over the Maritime Continent. The AMIP and coupled CMIP5 models simulate weaker grid-point temporal correlations compared to the observation. The coupled models tend to have a positive correlation over Papua and surrounding sea (opposite to the observed correlation), and a much weaker negative correlation over the rest of the Maritime Continent region.

For the IOD, most of the AMIP models are able to simulate the inverse relationship between the area-averaged Maritime Continent precipitation anomalies and Dipole Mode Index (DMI). During positive IOD events (when SSTs over the eastern Indian Ocean are colder than normal and SSTs in the western Indian Ocean are warmer than normal), most models simulate negative precipitation anomalies over the Maritime Continent. Likewise, most of the coupled CMIP5 models are able to simulate the interannual temporal correlation between area-averaged Maritime Continent precipitation and zonal SST gradient of the Maritime Continent and western Indian Ocean. However, most of the AMIP and coupled models perform less well at capturing the spatial pattern of IOD teleconnection with the Maritime Continent precipitation in SON.

Does ocean-atmosphere coupling improve these teleconnections?

Most of the coupled models have larger discrepancies compared to observations than their respective AMIP counterpart at simulating the spatial pattern of ENSO-Maritime Continent teleconnection in DJF.

Comparison between AMIP and coupled CMIP5 models show that AMIP models also perform better than coupled CMIP5 models at simulating the spatial pattern of teleconnection between IOD and Maritime Continent in SON. The RMSE of the Maritime Continent-IOD teleconnection pattern in coupled models is also larger than AMIP models suggesting that SST and coupling biases degraded the IOD-Maritime Continent teleconnection in CMIP5.

How are these teleconnections influenced by the mean state SST biases?

CMIP5 coupled models with smaller CTPO SST mean bias have a better representation of the ENSO-Maritime Continent teleconnection, i.e. their temporal correlation coefficients between Niño3.4 SST and the Maritime Continent precipitation are closer to the observed value. This suggests some relationship between the CTPO SST mean-state biases and ENSO-Maritime Continent teleconnection. The poor performance of coupled models at simulating the spatial pattern of ENSO-Maritime Continent teleconnection is mainly related to a spurious positive ENSO response that extends westwards into the West Pacific. This systematic error in ENSO is related to the mean state SST cold biases over the Pacific cold tongue that extend too far westward into the western Pacific.

The relationship between the CMIP5 models' WTIO mean state biases and the IOD-Maritime Continent teleconnection was also investigated. However, we find no significant correlation between the WTIO mean state biases and the IOD-Maritime Continent teleconnection.

On the other hand, we show that a model's skill at simulating the ENSO teleconnection to the Maritime Continent in DJF is related to model fidelity at simulating the Maritime Continent DJF precipitation climatology. The IOD teleconnection to the Maritime Continent in SON is dependent on model fidelity at simulating the Maritime Continent SON precipitation climatology. This highlights the importance of reducing model systematic errors for model fidelity in simulating the ENSO and IOD teleconnections to the Maritime Continent.

Our analysis of coupled historical runs in Chapter 4 highlights the central Pacific and western Indian Ocean as key regions that exhibit the most surface temperature correlation with the Maritime Continent mean state precipitation in the coupled CMIP5 models, while local SST exhibits seasonally-dependent correlations. To test causality in the relationships between SST anomalies and precipitation anomalies and better understand the mechanism underlying these relationships, a suite of sensitivity experiments to perturb the SST over the Maritime Continent, CTPO and WTIO regions are performed using the MetUM HadGEM3-GA6 atmosphere-only model to address the following questions in Chapter 5.

What are the systematic biases in HadGEM3-GA6?

In the control run, the seasonal mean precipitation biases when compared to GPCP show that the model exhibits systematic dry biases over the Maritime Continent and wet biases especially over the Indian Ocean, Western Pacific and South Pacific Convergence Zone (SPCZ). In JJA, there are significant dry biases over India, and wet biases are even more prominent over the Indian Ocean and Western Pacific Ocean. Other studies also noted the systematic dry precipitation biases over the Maritime Continent in different versions of the HadGEM model (Neale and Slingo, 2003; Schiemann et al., 2014; Johnson et al., 2015).

How sensitive is the tropical Indo-Pacific circulation and precipitation in the model to SST changes in the Maritime Continent, the Pacific Ocean and the Indian Ocean?

In the Maritime Continent SST perturbation experiments, we find that area-averaged local precipitation responses are linear for all seasons. In the MC+1K and MC+0.5K experiments, warmer SST over the Maritime Continent enhance the local precipitation and reduce the precipitation over the western Pacific and western Indian Oceans, consistent with Walker Circulation responses. The MC-1K experiments shows opposite local and remote precipitation responses compared to the MC+1K experiment. The remote precipitation responses to perturbing Maritime Continent SST are not linear in the Pacific and Indian Ocean. The seasonal mean remote precipitation responses do not vary much across seasons in the Pacific

Ocean. Whereas in the Indian Ocean, a perturbation of the Maritime Continent SST results in a larger remote precipitation response during the JJA season than in other seasons.

On the other hand, the MC+1K experiment also produces even less precipitation over some land areas in the Maritime Continent, especially over Sumatra and Borneo. This may be because of reduced land-sea contrast over this region in this experiment.

The CTPO perturbation experiments result in a non-linear local precipitation response. In terms of remote responses over the Maritime Continent in these experiments, the results show that warm SST anomalies in the central Pacific resulted in reduced rainfall over the Maritime Continent (and vice versa, to a lesser extent).

In the WTIO perturbation experiments, local precipitation response is of the same sign as the SST perturbations, whereas the remote precipitation response in the Maritime Continent is opposite in sign. This shows that the WTIO-1K experiments results in reduced precipitation over the WTIO and increased precipitation over the Maritime Continent compared to the control run.

The local and remote precipitation responses to SST perturbations in these experiments mainly result via a response in the Walker Circulation. We also find that these experiments also alter the local Hadley Circulations over the Maritime Continent and the global Hadley circulation.

The non-linear precipitation responses in the Maritime Continent, CTPO and WTIO perturbation experiments may be due to the non-linearity in the Clausius-Clapeyron relationship as well as the shift of precipitation between different tropical regions depending on changes in relative SSTs.

How do these sensitivity experiments alter the atmospheric response to ENSO and IOD?

The interannual localised precipitation response over the perturbation regions is consistent with the sign of climatological mean precipitation response, whereby an increase in local SST will increase the local precipitation. For the MC+1K experiment, El Niño years show the biggest increment in precipitation with respect to the control run, while conversely MC-1K experiment have a smaller reduction in rainfall with respect to the control run in El Niño years.

However, the remote precipitation responses over the Maritime Continent in the CTPO perturbation experiments are more complicated with some years showing opposite-signed responses compared to the climatological mean precipitation response. The CTPO+2K experiment simulates less precipitation over the Maritime Continent compared to the control run, consistent with the climatological mean precipitation response, apart from 3 years (2007, 2008 and 2010). 2007 and 2010 are La Niña years, during which the Maritime Continent generally receives above normal rainfall. This suggests that ENSO variability has some impact

on the Maritime Continent precipitation and the SST perturbation impacts vary according to ENSO phase.

Both positive and negative IOD composites have similar biases, for example the dry biases in India and the Maritime Continent, and the wet biases in the SPCZ, west Pacific (westerly biases) and Indian Ocean (easterly biases). In the WTIO+1K and WTIO-1K experiments, the local precipitation response is of the same sign as the SST perturbations, whereas in the Maritime Continent the remote precipitation response is of the opposite sign in both phases of the IOD, consistent with climatological local and remote precipitation responses. In these experiments, there are only four positive IOD and negative IOD events, limiting the sample size, hence no significant changes are identified in the interannual variability of the Maritime Continent precipitation responses relating to IOD events.

How does the sensitivity of the seasonal mean climate and climate variability in the tropics to SST perturbations compare to the relationships found in the coupled models in Chapter 4?

The area-averaged precipitation remote responses over the Maritime Continent in the CTPO and WTIO warm anomalies experiments are somewhat comparable to the regression coefficients between the Maritime Continent mean-state rainfall and CTPO and WTIO SSTs in Chapter 4. This indicates that the remote CTPO and WTIO SST biases in the CMIP5 coupled models contribute to, and could plausibly cause, the precipitation biases over the Maritime Continent.

5.2 Limitations

In Chapter 3, we show that the CMIP5 AMIP model performance at simulating the mean climate over the Maritime Continent is largely unrelated to the resolution of atmospheric models. As these 28 AMIP models are diverse GCMs in many ways, we further compare between model pairs from the same institution with different resolution. The model pairs comparison shows that three out of four models with lower resolution perform better than their corresponding higher resolution models in most months. The remaining 20 models lack a different resolution simulation for comparison which may change the relative percentage of this comparison result if all models are considered. Running more versions of the same model with different resolutions in the next CMIP6, for example in High Resolution Model Intercomparison Project (HighResMIP), will account for this limitation.

We performed hierarchical clustering analysis of the Maritime Continent annual cycle precipitation to characterize model systematic biases in the AMIP runs. The cluster analysis is robust when the biases are distinct as found in the AMIP runs, however when performed on the coupled historical runs, all clusters have a large spread in PCC values and no distinct

systematic biases are found from the hierarchical clustering analysis (not shown). This may be due to coupled runs' Maritime Continent annual cycle precipitation having a more diverse range of biases. There are also alternative methods to characterize model systematic bias such as Empirical Orthogonal Functions (EOF) analysis. While cluster analysis only allows models to be grouped into only one cluster which is advantageous when we want to identify model characteristics, EOF analysis is efficient in retaining as much as possible of the variation present in the dataset with the fewest possible degrees of freedom.

We briefly discussed the parameterization of cumulus convection as a possible source of common error between global monsoon biases and local Maritime Continent biases in Section 2.6. Our results suggested that the convection scheme can be important for CMIP5 AMIP model simulation of the annual cycle of precipitation in the Maritime Continent. However, it is difficult to disentangle effects of different convection schemes and the biases they impose on rainfall; in particular, model systems tend not to be designed to allow easy swapping of different convection schemes in the model code.

The CMIP5 nominal period for AMIP simulations is 30 years from 1979 to 2008. Although 30-year simulations are sufficient for seasonal climatology analyses, there were only four negative IOD and five positive IOD events identified from 1979 to 2008. This limitation is also relevant to the teleconnection study in the SST sensitivity experiments where there were only four negative IOD and four positive IOD events from 1982 to 2012. Increasing the length of integration would allow a greater sample of IOD events in positive and negative phases to test the robustness of our composite analysis.

In exploring the relationship between the Maritime Continent precipitation biases and remote SST biases, we have considered only the WTIO and CTPO regions as the locations of the SST biases. However, as shown in Fig. 3.1 and Fig. 3.2, there are also biases in other parts of the ocean basins that may impact on or be impacted by the precipitation anomalies over the Maritime Continent. Neale and Slingo (2003) showed that warm anomalies over the Maritime Continent affects the stationary waves over the Euro-Atlantic region via response of the global circulation to La Niña.

In Chapter 5, we performed a suite of SST sensitivity experiments using the HadGEM3-GA6 atmosphere-only model to investigate the impact of SST changes on seasonal mean climate and interannual variability. For the Maritime Continent perturbation experiments, we had performed it on the domain from 20°S to 20°N and 80°E to 160°E to be consistent with the domain of the Maritime Continent defined in previous chapters. A caveat for these experiments is the Maritime Continent perturbation domain is relatively larger compared to the WTIO and CTPO region. Apart from that, the Gaussian spatial filter that was applied to smooth the edges of the perturbation domains needs some modification as the responses are crude over the sharp edges of the perturbation domains.

For the SST sensitivity experiments, we chose to run these experiments using an atmosphere-

only framework with prescribed SSTs, because an AMIP experiment is suitable for testing causality in the relationships between SST anomalies and precipitation anomalies. While an AMIP experiment is advantageous in this respect, the AMIP experiment design neglects feedbacks between the atmosphere and ocean. The SST-forced response in the AMIP framework can be different from the coupled response in coupled model simulations. For example in the coupled model, during cloud free conditions or when there is large scale subsidence, the solar fluxes will warm the ocean, whereas, precipitation accompanied by cloud cover reduces shortwave solar radiation and cools the SST. These feedbacks are missing in the AMIP framework.

5.3 Future work

Cluster analysis performed in Chapter 3 to characterize model systematic biases resulted in two clusters with distinct fidelity at representing the annual cycle of precipitation over the Maritime Continent for the AMIP experiment. Although there are limitations to this method as stated in Section 5.2, this method is also robust and suitable for characterizing the SST biases in Chapter 4. Cluster analysis of the seasonal mean SST could be performed to compare if the resulting clusters produce similar precipitation and low-level wind biases as in Chapter 4.

As stated in Section 5.2, an extension to this work could include expanding the analysis in this study to other parts of the ocean basins such as the Atlantic Ocean. While we have assessed the remote responses over the tropical Indo-Pacific to changes over the Maritime Continent, the assessment on the impact of model biases in the Maritime Continent on extratropical variability and teleconnections would be a good addition to the current study.

The focus of this study is to investigate the seasonal climate, annual cycle and interannual variability over the Maritime Continent. The interactions between different time-scales of variability show that diurnal and intraseasonal timescales affect the seasonal timescale and vice versa (Moron et al., 2015; Slingo et al., 2003). There is much scope in the future work for further understanding of the interactions between different timescales of variability over the Maritime Continent in the CMIP5 and HadGEM3-GA6.

As stated in Section 5.2, the Maritime Continent perturbation domain in this study is relatively large compared to the CTPO and WTIO regions. The same experiment could be performed over a smaller region of the Maritime Continent (for example a rectangular area of 10°S-10°N and 90°E-150°E) to compare if the perturbation over a smaller region produces similar results to the simulation in this thesis. Gaussian smoothing with $\sigma = 3$ could be applied over the Maritime Continent to reduce the crudeness over the edges of the perturbation domain. In addition to experiments in this thesis, further experimentation to perturb the CTPO and WTIO simultaneously in HadGEM3-GA6 could provide more insight

on the influence of SSTs in these different regions on Maritime Continent precipitation.

As noted in Section 5.2, running longer simulations of the control run and SST sensitivity experiments mean that there will be a larger number of different phases of IOD events as well as ENSO events. With the increasing number of ENSO events, further analysis of the ENSO teleconnection to the Maritime Continent could be divided into El Niño Modoki and the conventional El Niño, since other studies have found that these two types of ENSO have different impacts on the Maritime Continent (As-Syakur et al., 2016; Salimun et al., 2014; Feng et al., 2010). We could also divide the IOD and ENSO events to pure IOD and pure ENSO events and the years where both IOD and ENSO occurred concurrently. Alternatively, other Niño region indices could be used to classify the ENSO events as a comparison to the Niño 3.4 indices used in this study. It would also be beneficial to separate the land-only and sea-only impacts as there are spatial differences over the Maritime Continent and the sea-only teleconnection dominates the total responses as shown in Section 3.5. These differences in the land-only and sea-only teleconnections are related to land breezes and sea breezes.

As stated in Section 5.2, performing the same SST perturbation experiment using the MC-KPP type (Multi-Column K Profile Parameterization ocean) mixed-layer ocean model (MetUM-GOML) or coupled version of the HadGEM3 model will complement the current study. The impacts of air-sea coupling could be further investigated by assessing the relationship between Maritime Continent precipitation biases and tropical SST biases using the atmosphere-ocean mixed layer coupled model and a fully coupled version of the HadGEM3 model, and compare those experiments to the AMIP experiments. The main advantage of MetUM-GOML over a fully dynamically coupled ocean model is that it can be run much faster and has a higher vertical resolution (Hirons et al., 2015). These experiments will shed greater light into the relationship between Maritime Continent precipitation anomalies and tropical SST anomalies.

Possible improvement to the climate model simulation of the Maritime Continent

Reflecting on the work done in this thesis, a few recommendations are given to improve model simulations over the Maritime Continent.

Our analyses on AMIP models in Chapter 3 highlights the importance of global monsoon and circulation simulations, which are significantly associated with the mean climate simulation biases at Maritime Continent. This result shows that models that better capture the global monsoon and local Hadley circulation will also have a better representation of the precipitation pattern over the Maritime Continent region. Therefore, we recommend to focus efforts on improving the simulation of global monsoon and circulation in GCMs to improve simulation of the Maritime Continent mean climate. As our study also shows that biases in precipitation and circulation during ENSO and IOD events mainly result from the climatological mean state biases, better representation of global monsoon and circulation is

also expected to improve the simulation of ENSO and IOD teleconnections with the Maritime Continent, in addition to improving the seasonal mean climate.

Furthermore, one possible source of common error between global monsoon biases and local Maritime Continent biases are errors associated with the parameterization of cumulus convection. As noted in Section 5.2, it is difficult to disentangle effects of different convection schemes and the biases they impose on rainfall when examining the multimodel framework. Therefore, we recommend performing experiments with the control run, and experimenting with modifying the convection scheme, and switching off convective parameterization, e.g. at suitably high horizontal resolution using the same model for comparison.

In Chapter 4, we identified the central Pacific and western Indian Ocean as the key regions that exhibit the most surface temperature correlation with the Maritime Continent mean-state precipitation in the coupled CMIP5 models. We then performed SST perturbation experiments in Chapter 5 to test the model sensitivity to SST anomalies in these regions. Although we do not examine the improvement of simulation over the Maritime Continent in these perturbation experiments, the results from these experiments suggest that remote SST biases over the central Pacific and western Indian Ocean in the CMIP5 coupled models could plausibly cause the precipitation biases over the Maritime Continent. This result shows that cold SST biases in the central Pacific and western Indian Ocean lead to strengthening of the easterly trade winds and Walker circulation, resulting in anomalous ascent and thus enhanced rainfall over the Maritime Continent. Enhanced rainfall over the Maritime Continent will also lead to stronger low-level convergence. This is consistent with Sperber et al. (2013) study that most of the CMIP3 and CMIP5 coupled models tend to overestimate the mean precipitation in the Maritime Continent. Our result suggests that the precipitation bias over the Maritime Continent is more likely due to SST biases over these remote regions. Thus, reducing SST biases in coupled models will likely lead to improvement in the simulation of the Maritime Continent climate.

Bibliography

Achuta Rao K, Sperber KR (2006) ENSO simulation in coupled ocean-atmosphere models: Are the current models better? *Climate Dynamics* 27(1):1–15

Ackerley D, Berry G, Jakob C, Reeder MJ, Schwendike J (2015) Summertime precipitation over northern Australia in AMIP simulations from CMIP5. *Quarterly Journal of the Royal Meteorological Society* 141(690):1753–1768, DOI 10.1002/qj.2476

Adler RF, Huffman GJ, Chang A, Ferraro R, Xie PP, Janowiak J, Rudolf B, Schneider U, Curtis S, Bolvin D, Gruber A, Susskind J, Arkin P, Nelkin E (2003) The Version-2 Global Precipitation Climatology Project (GPCP) Monthly Precipitation Analysis (1979-Present). *Journal of Hydrometeorology* 4(6):1147–1167

Allan R, Chambers D, Drosdowsky W (2001) Is there an Indian Ocean dipole and is it independent of the El Niño-Southern Oscillation. *Clivar Exchanges* 6(3):18–22

Annamalai H, Liu P, Xie SP (2005) Southwest Indian Ocean SST variability: Its local effect and remote influence on Asian monsoons. *Journal of Climate* 18:4150–4167

Annamalai H, Hamilton K, Sperber KR (2007) The South Asian summer monsoon and its relationship with ENSO in the IPCC AR4 simulations. *Journal of Climate* 20(6):1071–1092

Arakawa O, Kitoh A (2005) Rainfall Diurnal Variation over the Indonesian Maritime Continent Simulated by 20 km-mesh GCM. *Sola* 1:109–112

As-syakur AR, Adnyana IWS, Mahendra MS, Arthana IW, Merit IN, Kasa IW, Ekayanti NW, Nuarsa IW, Sunarta IN (2014) Observation of spatial patterns on the rainfall response to ENSO and IOD over Indonesia using TRMM Multisatellite Precipitation Analysis (TMPA). *International Journal of Climatology* 34(15):3825–3839

As-Syakur AR, Osawa T, Miura F, Nuarsa IW, Ekayanti NW, Dharma IGBS, Adnyana IWS, Arthana IW, Tanaka T (2016) Maritime Continent rainfall variability during the TRMM era: The role of monsoon, topography and El Niño Modoki. *Dynamics of Atmospheres and Oceans* 75:58–77

Bamston AG, Chelliah M, Goldenberg SB (1997) Documentation of a highly enso-related sst region in the equatorial pacific: Research note. *Atmosphere - Ocean* 35:367–383

Banacos PC, Schultz DM (2005) The Use of Moisture Flux Convergence in Forecasting Convective Initiation: Historical and Operational Perspectives. *Weather and Forecasting* 20(3):351–366

Bao M, Wallace JM (2015) Cluster Analysis of Northern Hemisphere Wintertime 500-hPa Flow Regimes 1920-2014. *Journal of the Atmospheric Sciences* 72(9):3597–3608

Bao Q, Lin P, Zhou T, Liu Y, Yu Y, Wu G, He B, He J, Li L, Li J, Li Y, Liu H, Qiao F, Song Z, Wang B, Wang J, Wang P, Wang X, Wang Z, Wu B, Wu T, Xu Y, Yu H, Zhao W, Zheng W, Zhou L (2013) The Flexible Global Ocean-Atmosphere-Land system model, Spectral Version 2: FGOALS-s2. *Advances in Atmospheric Sciences* 30(3):561–576

Bentsen M, Bethke I, Debernard JB, Iversen T, Kirkevåg A, Seland Ø, Drange H, Roelandt C, Seierstad Ia, Hoose C, Kristjánsson JE (2013) The Norwegian Earth System Model, NorESM1-M - Part 1: Description and basic evaluation of the physical climate. *Geoscientific Model Development* 6:687–720

Betts A (1986) A new convective adjustment scheme. Part I: Observational and theoretical basis. *Quarterly Journal of the Royal Meteorological Society* 112:677–691

Bi D, Dix M, Marsland SJ, O'Farrell S, Rashid HA, Uotila P, Hirst AC, Kowalczyk E, Golebiewski M, Sullivan A, Yan H, Hannah N, Franklin C, Sun Z, Vohralik P, Watterson I, Zhou X, Fiedler R, Collier M, Ma Y, Noonan J, Stevens L, Uhe P, Zhu H, Griffies SM, Hill R, Harris C, Puri K (2013) The ACCESS coupled model: description, control climate and evaluation. *Australian Meteorological and Oceanographic Journal* 63:41–64

Birch CE, Roberts MJ, Garcia-Carreras L, Ackerley D, Reeder MJ, Lock AP, Schiemann R (2015) Sea-breeze dynamics and convection initiation: The influence of convective parameterization in weather and climate model biases. *Journal of Climate* 28:8093–8108

Bjerknes J (1969) Atmospheric Teleconnections from the Equatorial Pacific. *Monthly Weather Review* 97(3):163–172

Boé J (2018) Interdependency in Multimodel Climate Projections: Component Replication and Result Similarity. *Geophysical Research Letters* 45:2771–2779

Bony S, Emanuel KA (2001) A Parameterization of the Cloudiness Associated with Cumulus Convection; Evaluation Using TOGA COARE Data. *Journal of the Atmospheric Sciences* 58(21):3158–3183

Bougeault P (1985) A simple Parameterization of the Large-Scale Effect of Cumulus Convection. *Monthly Weather Review* 113:2108–2121

Brown JR, Colman Ra, Moise AF, Smith IN (2013) The western Pacific monsoon in CMIP5 models: Model evaluation and projections. *Journal of Geophysical Research: Atmospheres* 118(22):12,458–12,475

Bush SJ, Turner AG, Woolnough SJ, Martin GM, Klingaman NP (2015) The effect of increased convective entrainment on Asian monsoon biases in the MetUM general circulation model. *Quarterly Journal of the Royal Meteorological Society* 141(686):311–326

Cai W, Sullivan A, Cowan T (2009) Rainfall teleconnections with Indo-Pacific variability in the WCRP CMIP3 models. *Journal of Climate* 22(19):5046–5071

Chang CP, Wang Z, McBride J, Liu CH (2005) Annual cycle of Southeast Asia - Maritime Continent rainfall and the asymmetric monsoon transition. *Journal of Climate* 18:287–301

Chen SS, Houze RA (1997) Interannual variability of deep convection over the tropical warm pool. *Journal of Geophysical Research* 102:25,783–25,795

Chikira M, Sugiyama M (2010) A Cumulus Parameterization with State-Dependent Entrainment Rate. Part I: Description and Sensitivity to Temperature and Humidity Profiles. *Journal of the Atmospheric Sciences* 67:2171–2193

Collins M, Tett SFB, Cooper C (2001) The internal climate variability of HadCM3, a version of the Hadley Centre coupled model without flux adjustments. *Climate Dynamics* 17(1):61–81

Collins W, Bellouin N, Doutriaux-Boucher M, Gedney N, Hinton T, Jones CD, Liddicoat S, Martin G, O'Connor F, Rae J, Senior C, Totterdell I, Woodward S, Reichler T, Kim J (2008) Evaluation of HadGEM2 model. *Meteorological Office Hadley Centre, Technical Note 74*

Collins WJ, Bellouin N, Doutriaux-Boucher M, Gedney N, Halloran P, Hinton T, Hughes J, Jones CD, Joshi M, Liddicoat S, Martin G, O'Connor F, Rae J, Senior C, Sitch S, Totterdell I, Wiltshire A, Woodward S (2011) Development and evaluation of an Earth-system model HadGEM2. *Geoscientific Model Development* 4:1051–1075

Colman RA, Moise AF, Hanson LI (2011) Tropical Australian climate and the Australian monsoon as simulated by 23 CMIP3 models. *Journal of Geophysical Research: Atmospheres* 116, d10116

Cusack S, Edwards JM, Crowther JM (1999) Investigating k distribution methods for parameterizing gaseous absorption in the hadley centre climate model. *Journal of Geophysical Research* 104:2051–2057

Dado JMB, Takahashi HG (2017) Potential impact of sea surface temperature on rainfall over the western Philippines. *Progress in Earth and Planetary Science* 4:1–12

Dee DP, Uppala SM, Simmons AJ, Berrisford P, Poli P, Kobayashi S, Andrae U, Balmaseda MA, Balsamo G, Bauer P, Bechtold P, Beljaars ACM, van de Berg L, Bidlot J, Bormann N, Delsol C, Dragani R, Fuentes M, Geer AJ, Haimberger L, Healy SB, Hersbach H, Hólm EV, Isaksen L, Kållberg P, Köhler M, Matricardi M, McNally AP, Monge-Sanz BM, Morcrette JJ, Park BK, Peubey C, de Rosnay P, Tavolato C, Thépaut JN, Vitart F (2011) The ERA-Interim reanalysis: Configuration and performance of the data assimilation system. *Quarterly Journal of the Royal Meteorological Society* 137(656):553–597

DelGenio AD, Yao MS (1993) Efficient Cumulus Parameterization for Long-Term Climate Studies: The GISS Scheme. In: Emanuel KA, Raymond DJ (eds) The Representation of Cumulus Convection in Numerical Models, American Meteorological Society, Boston, MA, pp 181–184

Derbyshire SH, Maidens AV, Milton SF, Stratton RA, Willett MR (2011) Adaptive detrainment in a convective parametrization. *Quarterly Journal of the Royal Meteorological Society* 137(660):1856–1871

Dix M, Vohralik P, Bi D, Rashid H, Marsland S, O'Farrell S, Uotila P, Hirst T, Kowalczyk E, Sullivan A, Yan H, Franklin C, Sun Z, Watterson I, Collier M, Noonan J, Rotstayn L, Stevens L, Uhe P, Puri K (2013) The ACCESS coupled model: documentation of core CMIP5 simulations and initial results. *Australian Meteorological and Oceanographic Journal* 63(1):83–99

Donner LJ (1993) A cumulus parameterization including mass fluxes, vertical momentum dynamics, and mesoscale effects. *Journal of the Atmospheric Sciences* 50(6):889–906

Donner LJ, Seman CJ, Hemler RS, Fan S (2001) A Cumulus Parameterization Including Mass Fluxes, Convective Vertical Velocities, and Mesoscale Effects: Thermodynamic and Hydrological Aspects in a General Circulation Model. *Journal of Climate* 14(16):3444–3463

Donner LJ, Wyman BL, Hemler RS, Horowitz LW, Ming Y, Zhao M, Golaz JC, Ginoux P, Lin SJ, Schwarzkopf MD, Austin J, Alaka G, Cooke WF, Delworth TL, Freidenreich SM, Gordon CT, Griffies SM, Held IM, Hurlin WJ, Klein SA, Knutson TR, Langenhorst AR, Lee HC, Lin Y, Magi BI, Malyshev SL, Milly PCD, Naik V, Nath MJ, Pincus R, Ploshay JJ, Ramaswamy V, Seman CJ, Shevliakova E, Sirutis JJ, Stern WF, Stouffer RJ, Wilson RJ, Winton M, Wittenberg AT, Zeng F (2011) The Dynamical Core, Physical Parameterizations, and Basic Simulation Characteristics of the Atmospheric Component AM3 of the GFDL Global Coupled Model CM3. *Journal of Climate* 24(13):3484–3519

Dufresne J, Foujols M, Denvil S, Caubel A, Marti O, Aumont O, Balkanski Y, Bekki S, Bellenger H, Benshila R, Bony S, Bopp L, Braconnot P, Brockmann P, Cadule P, Cheruy F, Codron F, Cozic A, Cugnet D, de Noblet N, Duvel J, Ethé C, Fairhead L, Fichefet T, Flavoni S, Friedlingstein P, Grandpeix J, Guez L, Guilyardi E, Hauglustaine D, Hourdin F, Idelkadi A, Ghattas J, Joussaume S, Kageyama M, Krinner G, Labetoulle S, Lahellec A, Lefebvre M, Lefevre F, Levy C, Li ZX, Lloyd J, Lott F, Madec G, Mancip M, Marchand M, Masson S, Meurdesoif Y, Mignot J, Musat I, Parouty S, Polcher J, Rio C, Schulz M, Swingedouw D, Szopa S, Talandier C, Terray P, Viovy N, Vuichard N (2013) Climate change projections using the IPSL-CM5 Earth System Model: from CMIP3 to CMIP5. *Climate Dynamics* 40(9-10):2123–2165

Edwards JM, Slingo A (1996) Studies with a flexible new radiation code. I: Choosing a configuration for a large-scale model. *Quarterly Journal of the Royal Meteorological Society* 122:689–719

Emanuel KA (1991) A Scheme for Representing Cumulus Convection in Large-Scale Models. *Journal of the Atmospheric Sciences* 48(21):2313–2329

Feng J, Wang L, Chen W, Fong SK, Leong KC (2010) Different impacts of two types of Pacific Ocean warming on Southeast Asian rainfall during boreal winter. *Journal of Geophysical Research Atmospheres* 115:1–9

Feng J, Wei T, Dong W, Wu Q, Wang Y (2014) CMIP5 / AMIP GCM Simulations of East Asian Summer Monsoon. *Advances in Atmospheric Sciences* 31(4):836–850

Flato G, Marotzke J, Abiodun B, Braconnot P, Chou S, Collins W, Cox P, Driouech F, Emori S, Eyring V, Forest C, Gleckler P, Guilyardi E, Jakob C, Kattsov V, Reason C, Rummukainen M (2013) Evaluation of Climate Models. *Climate Change 2013: The Physical Science Basis Contribution of Working Group I to the Fifth Assessment Report of the Intergovernmental Panel on Climate Change* pp 741–866

Gent PR, Danabasoglu G, Donner LJ, Holland MM, Hunke EC, Jayne SR, Lawrence DM, Neale RB, Rasch PJ, Vertenstein M, Worley PH, Yang ZL, Zhang M (2011) The Community Climate System Model Version 4. *Journal of Climate* 24(19):4973–4991

Gill AE (1980) Some simple solutions for heat-induced tropical circulation. *Quarterly Journal of the Royal Meteorological Society* 106:447–462

Glauber AJ, Moyer S, Adriani M, Gunawan I (2016) The Cost of Fire : An Economic Analysis of Indonesia's 2015 Fire Crisis. Indonesia Sustainable Landscapes Knowledge Note No. 1. Tech. rep., World Bank, Jakarta, URL `https://openknowledge.worldbank.org/handle/10986/23840License:CCBY3.0IGO`

Gordon H, Farrell SO, Collier M, Dix M, Rotstayn L, Kowalczyk E, Hirst T, Watterson I (2010) The CSIRO Mk3 . 5 Climate Model. Tech. Rep. 021, CAWCR

Grandpeix JY, Phillips V, Tailleux R (2004) Improved Mixing Representation in Emanuel's Convection Scheme. *Quarterly Journal Of The Royal Meteorological Society* 130:3207–3222

Gregory D, Rowntree PR (1990) A Mass Flux Convection Scheme with Representation of Cloud Ensemble Characteristics and Stability-Dependent Closure. *Monthly Weather Review* 118(7):1483–1506

HAII (2011) 2011 Thailand Flood Executive Summary. *Thailand Integrated Water Resource Management* pp 1–7, URL `http://www.thaiwater.net/web/index.php`

Hazeleger W, Severijns C, Semmler T, Ştefănescu S, Yang S, Wang X, Wyser K, Dutra E, Baldasano JM, Bintanja R, Bougeault P, Caballero R, Ekman AML, Christensen JH, Van Den Hurk B, Jimenez P, Jones C, Kållberg P, Koenigk T, McGrath R, Miranda P, Van Noije T, Palmer T, Parodi JA, Schmith T, Selten F, Storelvmo T, Sterl A, Tapamo H, Vancoppenolle M, Viterbo P, Willén U (2010) EC-Earth: A seamless Earth-system prediction approach in action. *Bulletin of the American Meteorological Society* 91(10):1357–1363

Hendon HH (2003) Indonesian rainfall variability: Impacts of ENSO and local air-sea interaction. *Journal of Climate* 16(11):1775–1790

Hirons LC, Klingaman NP, Woolnough SJ (2015) MetUM-GOML1: A near-globally coupled atmosphere-ocean-mixed-layer model. *Geoscientific Model Development* 8:363–379

Holloway CE, Woolnough SJ, Lister GMS (2012) Precipitation distributions for explicit versus parametrized convection in a large-domain high-resolution tropical case study. *Quarterly Journal of the Royal Meteorological Society* 138:1692–1708

Hourdin F, Grandpeix JY, Rio C, Bony S, Jam A, Cheruy F, Rochetin N, Fairhead L, Idelkadi A, Musat I, Dufresne JL, Lahellec A, Lefebvre MP, Roehrig R (2013) LMDZ5B: The atmospheric component of the IPSL climate model with revisited parameterizations for clouds and convection. *Climate Dynamics* 40(9-10):2193–2222

Hourdin F, Ginus-Bogdan A, Braconnot P, Dufresne JL, Traore AK, Rio C (2015) Air moisture control on ocean surface temperature, hidden key to the warm bias enigma. *Geophysical Research Letters* 42:10,885–10,893

Huffman GJ, Bolvin DT, Nelkin EJ, Wolff DB, Adler RF, Gu G, Hong Y, Bowman KP, Stocker EF (2007) The TRMM Multisatellite Precipitation Analysis (TMPA): Quasi-

Global, Multiyear, Combined-Sensor Precipitation Estimates at Fine Scales. *Journal of Hydrometeorology* 8:38–55

Ichikawa H, Yasunari T (2006) Time-space characteristics of diurnal rainfall over Borneo and surrounding oceans as observed by TRMM-PR. *Journal of Climate* 19(7):1238–1260

Inness PM, Slingo JM (2003) Simulation of the Madden-Julian oscillation in a coupled general circulation model. Part I: Comparison with observations and an atmosphere-only GCM. *Journal of Climate* 16:345–364

Inness PM, Slingo JM, Guilyardi E, Cole J (2003) Simulation of the Madden-Julian oscillation in a coupled general circulation model. Part II: The role of the basic state. *Journal of Climate* 16(3):365–382

Jha B, Kumar A (2009) A Comparison of the Atmospheric Response to ENSO in Coupled and Uncoupled Model Simulations. *Monthly Weather Review* 137(1):479–487

Ji D, Wang L, Feng J, Wu Q, Cheng H, Zhang Q, Yang J, Dong W, Dai Y, Gong D, Zhang RH, Wang X, Liu J, Moore JC, Chen D, Zhou M (2014) Description and basic evaluation of Beijing Normal University Earth System Model (BNU-ESM) version 1. *Geoscientific Model Development* 7(5):2039–2064

Johnson NC, Xie SP (2010) Changes in the sea surface temperature threshold for tropical convection. *Nature Geoscience* 3(12):842–845

Johnson SJ, Levine RC, Turner AG, Martin GM, Woolnough SJ, Schiemann R, Mizielinski MS, Roberts MJ, Vidale PL, Demory ME, Strachan J (2015) The resolution sensitivity of the South Asian monsoon and Indo-Pacific in a global 0.35°AGCM. *Climate Dynamics* 46(3):807–831

Jourdain NC, Gupta AS, Taschetto AS, Ummenhofer CC, Moise AF, Ashok K (2013) The Indo-Australian monsoon and its relationship to ENSO and IOD in reanalysis data and the CMIP3/CMIP5 simulations. *Climate Dynamics* 41(11-12):3073–3102

Kubota H, Shirooka R, Hamada JI, Syamsudin F (2011) Interannual Rainfall Variability over the Eastern Maritime Continent. *Journal of the Meteorological Society of Japan* 89A:111–122

Langenbrunner B, Neelin JD (2013) Analyzing ENSO teleconnections in CMIP models as a measure of model fidelity in simulating precipitation. *Journal of Climate* 26(13):4431–4446

Legg TP, Mylne KR, Woolcock C (2002) Use of medium-range ensembles at the Met Office I: PREVIN - a system for the production of probabilistic forecast information from the ECMWF EPS. *Meteorological Applications* 9(3):255–271

Levine RC, Turner AG (2012) Dependence of Indian monsoon rainfall on moisture fluxes across the Arabian Sea and the impact of coupled model sea surface temperature biases. *Climate Dynamics* 38:2167–2190

Levine RC, Turner AG, Marathayil D, Martin GM (2013) The role of northern Arabian Sea surface temperature biases in CMIP5 model simulations and future projections of Indian summer monsoon rainfall. *Climate Dynamics* 41:155–172

Li G, Xie SP (2012) Origins of tropical-wide SST biases in CMIP multi-model ensembles. *Geophysical Research Letters* 39, l22703

Li G, Xie SP (2014) Tropical Biases in CMIP5 Multimodel Ensemble : The Excessive Equatorial Pacific Cold Tongue and Double ITCZ Problems. *Journal of Climate* 27(4):1765–1780

Li G, Du Y, Xu H, Ren B (2015a) An intermodel approach to identify the source of excessive equatorial pacific cold tongue in CMIP5 models and uncertainty in observational datasets. *Journal of Climate* 28:7630–7640

Li G, Xie SP, Du Y (2015b) Monsoon-induced biases of climate models over the tropical Indian Ocean. *Journal of Climate* 28(8):3058–3072

Li G, Xie SP, He C, Chen Z (2017) Western Pacific emergent constraint lowers projected increase in Indian summer monsoon rainfall. *Nature Climate Change* 7(10):708–712

Li L, Lin P, Yu Y, Wang B, Zhou T, Liu L, Liu J, Bao Q, Xu S, Huang W, Xia K, Pu Y, Dong L, Shen S, Liu Y, Hu N, Liu M, Sun W, Shi X, Zheng W, Wu B, Song M, Liu H, Zhang X, Wu G, Xue W, Huang X, Yang G, Song Z, Qiao F (2013) The Flexible Global Ocean-Atmosphere-Land System Model , Grid-point Version 2: FGOALS-g2. *Advances in Atmospheric Sciences* 30(3):543–560

Madden Ra, Julian PR (1972) Description of Global-Scale Circulation Cells in the Tropics with a 4050 Day Period. *Journal of the Atmospheric Sciences* 29:1109–1123

Martin GM, Bellouin N, Collins WJ, Culverwell ID, Halloran PR, Hardiman SC, Hinton TJ, Jones CD, McDonald RE, McLaren AJ, O'Connor FM, Roberts MJ, Rodriguez JM, Woodward S, Best MJ, Brooks ME, Brown AR, Butchart N, Dearden C, Derbyshire SH, Dharssi I, Doutriaux-Boucher M, Edwards JM, Falloon PD, Gedney N, Gray LJ, Hewitt HT, Hobson M, Huddleston MR, Hughes J, Ineson S, Ingram WJ, James PM, Johns TC, Johnson CE, Jones A, Jones CP, Joshi MM, Keen AB, Liddicoat S, Lock AP, Maidens AV, Manners JC, Milton SF, Rae JGL, Ridley JK, Sellar A, Senior CA, Totterdell IJ, Verhoef A, Vidale PL, Wiltshire A (2011) The HadGEM2 family of Met Office Unified Model climate configurations. *Geoscientific Model Development* 4(3):723–757

Masson D, Knutti R (2011) Climate model genealogy. *Geophysical Research Letters* 38

Matsuno T (1966) Quasi-Geostrophic Motions in the Equatorial Area. *Journal of the Meteorological Society of Japan Ser II* pp 25–43

McBride JL, Haylock MR, Nicholls N (2003) Relationships between the maritime continent heat source and the El Niño-Southern oscillation phenomenon. *Journal of Climate* 16:2905–2914

Meehl GA (1987) The Annual Cycle and Interannual Variability in the Tropical Pacific and Indian Ocean Regions. *Monthly Weather Review* 115:27–50

Meehl GA, Boer GJ, Covey C, Latif M, Stouffer RJ (2000) The Coupled Model Intercomparison Project (CMIP). *Bulletin of the American Meteorological Society* 81:313–318

Mizuta R, Yoshimura H, Murakami H, Matsueda M, Endo H, Ose T, Kamiguchi K, Hosaka M, Sugi M, Yukimoto S, Kusunoki S, Kitoh A (2012) Climate Simulations Using MRI-AGCM3.2 with 20-km Grid. *Journal of the Meteorological Society of Japan* 90A:233–258

Mizuta R, Arakawa O, Ose T, Kusunoki S, Endo H, Kitoh A (2014) Classification of CMIP5 Future Climate Responses by the Tropical Sea Surface Temperature Changes. *SOLA* 10:167–171

Molteni F, Buizza R, Palmer TN, Petroliagis T (1996) The ECMWF Ensemble Prediction System: Methodology and validation. *Quarterly Journal of the Royal Meteorological Society* 122(529):73–119

Molteni F, Stockdale TN, Vitart F (2015) Understanding and modelling extra-tropical teleconnections with the Indo-Pacific region during the northern winter. *Climate Dynamics* 45:3119–3140

Moorthi S, Suarez MJ (1992) Relaxed Arakawa-Schubert. A Parameterization of Moist Convection for General Circulation Models. *Monthly Weather Review* 120(6):978–1002

Moron V, Robertson AW, Qian JH, Ghil M (2015) Weather types across the Maritime Continent: from the diurnal cycle to interannual variations. *Frontiers in Environmental Science* 2:1–19

Neale R, Slingo J (2003) The Maritime Continent and its role in the global climate: A GCM study. *Journal of Climate* 16:834–848

Neale RB, Richter JH, Jochum M (2008) The impact of convection on ENSO: From a delayed oscillator to a series of events. *Journal of Climate* 21(22):5904–5924

Nordeng T (1994) Extended versions of the convective parametrization scheme at ECMWF and their impact on the mean and transient activity of the model in the tropics. Technical memorandum European Center for Medium-Range Weather Forecasts, ECMWF

Nur'utami MN, Hidayat R (2016) Influences of IOD and ENSO to Indonesian Rainfall Variability: Role of Atmosphere-ocean Interaction in the Indo-pacific Sector. *Procedia Environmental Sciences* 33:196–203

Ogata T, Johnson SJ, Schiemann R, Demory ME, Mizuta R, Yoshida K, Arakawa O (2017) The resolution sensitivity of the Asian Summer Monsoon and its Inter-Model Comparison between MRI-AGCM and MetUM. *Climate Dynamics* p 33453361

Ooi SH, Samah AA, Braesicke P (2011) A case study of the Borneo Vortex genesis and its interactions with the global circulation. *Journal of Geophysical Research Atmospheres* 116

Oueslati B, Bellon G (2015) The double ITCZ bias in CMIP5 models: interaction between SST, large-scale circulation and precipitation. *Climate Dynamics* 44:585–607

Peatman SC, Matthews AJ, Stevens DP (2014) Propagation of the Madden-Julian Oscillation through the Maritime Continent and scale interaction with the diurnal cycle of precipitation. *Quarterly Journal of the Royal Meteorological Society* 140:814–825

Qian JH (2008) Why Precipitation Is Mostly Concentrated over Islands in the Maritime Continent. *Journal of the Atmospheric Sciences* 65(4):1428–1441

Qian JH, Robertson AW, Moron V (2013) Diurnal cycle in different weather regimes and rainfall variability over borneo associated with ENSO. *Journal of Climate* 26:1772–1790

Qu T, Du Y, Strachan J, Meyers G, Slingo J (2005) Sea Surface Temperature and its Variability in the Indonesian Region. *Oceanography* 18(4):50–61

Raddatz TJ, Reick CH, Knorr W, Kattge J, Roeckner E, Schnur R, Schnitzler KG, Wetzel P, Jungclaus J (2007) Will the tropical land biosphere dominate the climate-carbon cycle feedback during the twenty-first century? *Climate Dynamics* 29(6):565–574

Ramage CS (1968) Role of a tropical Maritime Continent in the atmospheric circulation. *Monthly Weather Review* 96(6):365–370

Richter JH, Rasch PJ (2008) Effects of Convective Momentum Transport on the Atmospheric Circulation in the Community Atmosphere Model, Version 3. *Journal of Climate* 21(7):1487–1499

Rotstayn LD, Jeffrey SJ, Collier MA, Dravitzki SM, Hirst AC, Syktus JI, Wong KK (2012) Aerosol- and greenhouse gas-induced changes in summer rainfall and circulation in the Australasian region: A study using single-forcing climate simulations. *Atmospheric Chemistry and Physics* 12(14):6377–6404

Saji NH, Goswami BN, Vinayachandran PN, Yamagata T (1999) A dipole mode in the tropical Indian Ocean. *Nature* 401(6751):360–363

Saji NH, Xie SP, Yamagata T (2006) Tropical Indian Ocean variability in the IPCC twentieth-century climate simulations. *Journal of Climate* 19(17):4397–4417

Sakamoto TT, Komuro Y, Nishimura T, Ishii M, Tatebe H, Shiogama H, Hasegawa A, Toyoda T, Mori M, Suzuki T, Imada Y, Nozawa T, Takata K, Mochizuki T, Ogochi K, Emori S, Hasumi H, Kimoto M (2012) MIROC4h - A New High-Resolution Atmosphere-Ocean Coupled General Circulation Model. *Journal of the Meteorological Society of Japan* 90(3):325–359

Salimun E, Tangang F, Juneng L, Behera SK, Yu W (2014) Differential impacts of conventional El Niño versus El Niño Modoki on Malaysian rainfall anomaly during winter monsoon. *International Journal of Climatology* 34:2763–2774

von Salzen K, Scinocca JF, McFarlane NA, Li J, Cole JNS, Plummer D, Verseghy D, Reader MC, Ma X, Lazare M, Solheim L (2013) The Canadian Fourth Generation Atmospheric Global Climate Model (CanAM4). Part I: Representation of Physical Processes. *Atmosphere-Ocean* 51(1):104–125

Schiemann R, Demory ME, Mizielinski MS, Roberts MJ, Shaffrey LC, Strachan J, Vidale PL (2014) The sensitivity of the tropical circulation and Maritime Continent precipitation to climate model resolution. *Climate Dynamics* 42(9-10):2455–2468

Schmidt GA, Ruedy R, Hansen JE, Aleinov I, Bell N, Bauer M, Bauer S, Cairns B, Canuto V, Cheng Y, Del Genio A, Faluvegi G, Friend AD, Hall TM, Hu Y, Kelley M, Kiang NY, Koch D, Lacis AA, Lerner J, Lo KK, Miller RL, Nazarenko L, Oinas V, Perlwitz J, Perlwitz J, Rind D, Romanou A, Russell GL, Sato M, Shindell DT, Stone PH, Sun S, Tausnev N, Thresher D, Yao MS (2006) Present-day atmospheric simulations using GISS Model: Comparison to in situ, satellite, and reanalysis data. *Journal of Climate* 19:153–192

Schneider T, Bischoff T, Haug GH (2014) Migrations and dynamics of the intertropical convergence zone. *Nature* 513:45–53

Scoccimarro E, Gualdi S, Bellucci A, Sanna A, Fogli PG, Manzini E, Vichi M, Oddo P, Navarra A (2011) Effects of tropical cyclones on ocean heat transport in a high-resolution coupled general circulation model. *Journal of Climate* 24(16):4368–4384

Sherwood SC, Bony S, Dufresne JL (2014) Spread in model climate sensitivity traced to atmospheric convective mixing. *Nature* 505(7481):37–42

Slingo J, Inness P, Neale R, Woolnough S, Yang GY (2003) Scale interactions on diurnal to seasonal timescales and their relevance to model systematic errors. *Annals of Geophysics* 46:139–156

Song F, Zhou T (2014) The climatology and interannual variability of east Asian summer monsoon in CMIP5 coupled models: Does air-sea coupling improve the simulations? *Journal of Climate* 27(23):8761–8777

Song ZY, Liu HL, Wang CZ, Zhang LP, Qiao FL (2014) Evaluation of the eastern equatorial Pacific SST seasonal cycle in CMIP5 models. *Ocean Science* 10(5):837–843

Spencer H, Slingo JM, Davey MK (2004) Seasonal predictability of ENSO teleconnections: the role of the remote ocean response. *Climate Dynamics* 22(5):511–526

Sperber KR, Annamalai H, Kang IS, Kitoh A, Moise A, Turner A, Wang B, Zhou T (2013) The Asian summer monsoon: an intercomparison of CMIP5 vs. CMIP3 simulations of the late 20th century. *Climate Dynamics* 41(9-10):2711–2744

Stevens B, Giorgetta M, Esch M, Mauritsen T, Crueger T, Rast S, Salzmann M, Schmidt H, Bader J, Block K, Brokopf R, Fast I, Kinne S, Kornblueh L, Lohmann U, Pincus R, Reichler T, Roeckner E (2013) Atmospheric component of the MPI-M Earth System Model: ECHAM6. *Journal of Advances in Modeling Earth Systems* 5(2):146–172

Strachan J (2007) Understanding and Modelling the Climate of the Maritime Continent. PhD thesis, University of Reading

Taschetto AS, Gupta AS, Jourdain NC, Santoso A, Ummenhofer CC, England MH (2014) Cold tongue and warm pool ENSO Events in CMIP5: Mean state and future projections. *Journal of Climate* 27(8):2861–2885

Taylor KE, Williamson DL, Zwiers F (2000) The Sea Surface Temperature and Sea-Ice Concentration Boundary Conditions for AMIP II Simulations. *PCMDI Report 60, Program for Climate Model Diagnosis and Intercomparison, Lawrence Livermore National Laboratory*

Taylor KE, Stouffer RJ, Meehl GA (2012) An overview of CMIP5 and the experiment design. *Bulletin of the American Meteorological Society* 93(4):485–498

Tiedtke M (1989) A comprehensive mass flux scheme for cumulus parameterization in large-scale models. *Monthly Weather Review* 117(8):1179–1800

Tiedtke M (1993) Representation of Clouds in Large-Scale Models. *Monthly Weather Review* 121:3040–3061

Toh YY, Turner AG, Johnson SJ, Holloway CE (2018) Maritime Continent seasonal climate biases in AMIP experiments of the CMIP5 multimodel ensemble. *Climate Dynamics* 50:777–800

Turner AG, Inness PM, Slingo JM (2005) The role of the basic state in the ENSOmonsoon relationship and implications for predictability. *Quarterly Journal of the Royal Meteorological Society* 131(607):781–804

Unal Y, Kindap T, Karaca M (2003) Redefining the climate zones of Turkey using cluster analysis. *International Journal of Climatology* 23(9):1045–1055

Vertenstein M, Craig T, Middleton A, Feddema D, Fischer C (2013) CESM1.0.4 Users Guide. Tech. rep., NCAR

Voldoire A, Sanchez-Gomez E, Salas y Mélia D, Decharme B, Cassou C, Sénési S, Valcke S, Beau I, Alias A, Chevallier M, Déqué M, Deshayes J, Douville H, Fernandez E, Madec G, Maisonnave E, Moine MP, Planton S, Saint-Martin D, Szopa S, Tyteca S, Alkama R, Belamari S, Braun A, Coquart L, Chauvin F (2013) The CNRM-CM5.1 global climate model: Description and basic evaluation. *Climate Dynamics* 40(9-10):2091–2121

Volodin EM, Dianskii NA, Gusev AV (2010) Simulating present-day climate with the INMCM4.0 coupled model of the atmospheric and oceanic general circulations. *Izvestiya, Atmospheric and Oceanic Physics* 46(4):414–431

Walters D, Boutle I, Brooks M, Melvin T, Stratton R, Vosper S, Wells H, Williams K, Wood N, Allen T, Bushell A, Copsey D, Earnshaw P, Edwards J, Gross M, Hardiman S, Harris C, Heming J, Klingaman N, Levine R, Manners J, Martin G, Milton S, Mittermaier M, Morcrette C, Riddick T, Roberts M, Sanchez C, Selwood P, Stirling A, Smith C, Suri D, Tennant W, Luigi Vidale P, Wilkinson J, Willett M, Woolnough S, Xavier P (2017) The Met Office Unified Model Global Atmosphere 6.0/6.1 and JULES Global Land 6.0/6.1 configurations. *Geoscientific Model Development* 10(4):1487–1520

Wang B, Ding Q (2008) Global monsoon: Dominant mode of annual variation in the tropics. *Dynamics of Atmospheres and Oceans* 44(3-4):165–183

Wang B, Ding Q, Fu X, Kang IS, Jin K, Shukla J, Doblas-Reyes F (2005) Fundamental challenge in simulation and prediction of summer monsoon rainfall. *Geophysical Research Letters* 32

Wang C, Zhang L, Lee SK, Wu L, Mechoso CR (2014) A global perspective on CMIP5 climate model biases. *Nature Climate Change* 4(3):201–205

Watanabe S, Hajima T, Sudo K, Nagashima T, Takemura T, Okajima H, Nozawa T, Kawase H, Abe M, Yokohata T, Ise T, Sato H, Kato E, Takata K, Emori S, Kawamiya M (2011) MIROC-ESM 2010: model description and basic results of CMIP5-20c3m experiments. *Geoscientific Model Development Discussions* 4:1063–1128

Webster PJ, Moore AM, Loschnigg JP, Leben RR (1999) Coupled oceanatmosphere dynamics in the Indian Ocean during 199798. *Nature* 401:356–360

Weller E, Cai W (2013) Realism of the indian ocean dipole in CMIP5 models: The implications for climate projections. *Journal of Climate* 26(17):6649–6659

Wheeler MC, Hendon HH (2004) An All-Season Real-Time Multivariate MJO Index: Development of an Index for Monitoring and Prediction. *Monthly Weather Review* pp 1917–1932

Wilcox EM, Donner LJ (2007) The frequency of extreme rain events in satellite rain-rate estimates and an atmospheric general circulation model. *Journal of Climate* 20(1):53–69

Wilks DS (2011) Statistical Methods in the Atmospheric Sciences. Academic Press

Wu CH, Hsu HH (2009) Topographic influence on the MJO in the maritime continent. *Journal of Climate* 22(20):5433–5448

Wu P, Hara M, Hamada JI, Yamanaka MD, Kimura F (2009) Why a large amount of rain falls over the sea in the vicinity of western Sumatra Island during nighttime. *Journal of Applied Meteorology and Climatology* 48(7):1345–1361

Wu R, Kirtman BP (2005) Roles of Indian and Pacific Ocean air-sea coupling in tropical atmospheric variability. *Climate Dynamics* 25(2-3):155–170

Wu T, Yu R, Zhang F, Wang Z, Dong M, Wang L, Jin X, Chen D, Li L (2010) The Beijing Climate Center atmospheric general circulation model: Description and its performance for the present-day climate. *Climate Dynamics* 34(1):123–147

Xie P, Arkin PA (1997) Global Precipitation : A 17-Year Monthly Analysis Based on Gauge Observations, Satellite Estimates, and Numerical Model Outputs. *Bulletin of the American Meteorological Society* 78(11):2539–2558

Yang GY, Slingo J (2001) The diurnal cycle in the tropics. *Monthly Weather Review* 129(4):784–801

Yukimoto S, Yoshimura H, Hosaka M, Sakami T, Tsujino H, Hirabara M, Tanaka TY, Deushi M, Obata A, Nakano H, Adachi Y, Shindo E, Yabu S, Ose T, Kitoh A (2011) Meteorological Research Institute-Earth System Model Version 1 (MRI-ESM1) -Model Description. *Technical Reports* 64(64):88

Yukimoto S, Adachi Y, Hosaka M, Sakami T, Yoshimura H, Hirabara M, Tanaka TY, Shindo E, Tsujina H, Deushi M, Mizuta R, Yabu S, Obata A, Nakano H, Koshiro T, Ose T, Kitoh A (2012) A New Global Climate Model of the Meteorological Research Institute: MRI-CGCM3 - Model Description and Basic Performance;. *Journal of the Meteorological Society of Japan* 90A(0):23–64

Zhang GJ (2002) Convective quasi-equilibrium in midlatitude continental environment and its effect on convective parameterization. *Journal of Geophysical Research Atmospheres* 107(14):1–16

Zhang GJ, McFarlane NA (1995) Sensitivity of climate simulations to the parameterization of cumulus convection in the Canadian climate centre general circulation model. *Atmosphere-Ocean* 33(3):407–446

Zhang GJ, Mu M (2005) Effects of modifications to the Zhang-McFarlane convection parameterization on the simulation of the tropical precipitation in the National Center for Atmospheric Research Community Climate Model, version 3. *Journal of Geophysical Research D: Atmospheres* 110(9):1–12

Zhang T, Yang S, Jiang X, Zhao P (2016) Seasonal-interannual variation and prediction of wet and dry season rainfall over the maritime continent: Roles of ENSO and monsoon circulation. *Journal of Climate* 29(10):3675

Zhao M, Held IM, Lin SJ, Vecchi GA (2009) Simulations of global hurricane climatology, interannual variability, and response to global warming using a 50-km resolution GCM. *Journal of Climate* 22(24):6653–6678

Zheng Y, Lin JL, Shinoda T (2012) The equatorial Pacific cold tongue simulated by IPCC AR4 coupled GCMs: Upper ocean heat budget and feedback analysis. *Journal of Geophysical Research: Oceans* 117(5)

Zhou T, Turner AG, Kinter JL, Wang B, Qian Y, Chen X, Wu B, Liu B, Zou L, He B (2016) GMMIP (v1.0) contribution to CMIP6: Global Monsoons Model Inter-comparison Project. *Geoscientific Model Development* 9:3589–3604